Université catholique de Louvain (UCL)

de Duve Institute
CELL unit

Nephropathic cystinosis : pathophysiology, adaptations and investigations towards a new rationale treatment.

Janssens Virginie

Décembre 2019

Promotor : Prof. Pierre J. COURTOY
Co-promotor : Prof. Christophe E. PIERREUX

Thèse présentée en vue de l'obtention du grade
de docteur en sciences biomédicales et pharmaceutiques

Secteur des sciences de la santé

Cover legend. Extended view of a whole kidney sagittal section from a cystinotic mouse in which the *megalin* gene has been efficiently excised specifically in kidneys (“double knock-out”). Triple labelling for NaPi-IIa (green), LT-lectin (red) and nuclei (Hoechst, blue) shows a preserved overall structure, comparable to a wild-type mouse. Whereas NaPi-IIa signal is uniformly limited to cortex (together with LT-lectin, thus generating a yellow emission), LT-lectin labeling encompasses both cortex and the entire outer stripe of the outer medulla (which thus appears in red). For further explanations, see supplementary Figure 6B of Janssens et al., 2019.

Members of the jury

Prof. Frédéric LEMAIGRE
(President) UCLouvain

Prof. Francesco EMMA
(External member) Ospedale Pediatrico Bambino Gesù, Roma

Prof. François JOURET
(External member) Université de Liège

Prof. Sandrine HORMAN
(Internal member) UCLouvain

Prof. Isabelle LECLERCQ
(Internal member) UCLouvain

Prof. Etienne MARBAIX
(Internal member) UCLouvain

Prof. Pierre J. COURTOY
(Promotor) UCLouvain

Prof. Christophe E. PIERREUX
(Co-promotor) UCLouvain

Remerciements

Au terme de cette thèse, j'aimerais remercier toutes les personnes qui m'ont aidée et soutenue de près ou de loin dans sa réalisation.

En premier lieu, je remercie mon promoteur, le Professeur Pierre Courtoy, de m'avoir tout d'abord permis de travailler dans son unité en tant qu'assistante de recherche et ensuite, de m'avoir donné la chance de réaliser ma thèse sur un projet aussi passionnant. Je le remercie pour son immense savoir qu'il partage ardemment ainsi que pour sa confiance. Merci à vous qui, malgré votre éméritat, avez consacré du temps pour m'encadrer et ce parfois au détriment du temps passé avec votre famille. Merci aussi à Chantal pour ces sacrifices.

Je remercie mon co-promoteur, le Professeur Christophe Pierreux, pour sa disponibilité, ses conseils avisés, sa gentillesse et sa patience mais aussi d'avoir été un soutien très important pour moi. Je le remercie aussi d'être toujours à l'écoute et de nous guider parfaitement tout au long de la thèse, scientifiquement et humainement. C'est un réel plaisir de travailler et d'évoluer à ses côtés.

Mes remerciements vont aussi aux membres de mon jury qui m'ont guidée et encouragée durant ma thèse. Je les remercie pour leurs nombreux conseils qui ont permis d'améliorer significativement ce manuscrit. Merci au Professeur Frédéric Lemaigre d'avoir accepté d'être président de mon jury de thèse et d'être toujours disponible et à l'écoute. Je remercie aussi les Professeurs Sandrine Horman, Isabelle Leclercq et Etienne Marbaix pour leur extrême gentillesse, leur bienveillance et la pertinence de leurs remarques. Un grand merci aussi aux

Professeurs Francesco Emma et François Jouret, membres externes, d'avoir été présents lors ma défense de thèse privée et pour leur implication enthousiaste dans mon projet.

Je souhaite aussi exprimer toute ma gratitude à la Cystinosis Research Foundation (CRF) pour leur soutien et leur confiance en ce projet.

Merci au Professeur Marie-Françoise Vincent d'avoir accepté de réaliser les dosages de cystine et plus particulièrement, merci au Docteur Sandrine Marie avec qui c'est un réel plaisir de collaborer.

Un tout grand merci à Patrick Van Der Smissen pour sa gentillesse et son aide mais surtout pour la microscopie électronique et les images magnifiques obtenues grâce à lui.

Je remercie les Professeurs Donatienne Tyteca et Patrick Henriet d'avoir toujours pris le temps de répondre à mes questions ou de discuter de mes résultats. Un énorme merci aussi pour leur aide au quotidien dans le laboratoire et pour la bonne humeur qu'ils y apportent.

Je tiens à remercier Héloïse qui était chargée de recherche sur ce projet à mon arrivée au laboratoire. Travailler avec elle a été une source d'inspiration et de motivation. J'ai énormément appris à ses côtés et les moments partagés avec elle font partie de mes meilleurs souvenirs au laboratoire. D'un point de vue humain, je la remercie d'être une personne exceptionnelle et d'être devenue une amie qui déborde de qualités, son humour étant l'une de celles que je préfère.

Je remercie Pascale de partager son expérience et d'apporter une aide tellement précieuse dans les manips qui nous posent problème. Mais surtout, je la remercie pour son écoute et son soutien dans les moments plus difficiles.

Merci à Charlotte T, ce petit énergumène un peu froid au premier abord (disons le premier jour) mais tellement attachant ensuite. Je la remercie pour sa joie de vivre, les fous-rires, sa positivité, pour les discussions scientifiques ou non mais aussi pour sa sensibilité, son écoute et sa gentillesse.

Je remercie aussi le « groupe de Christophe » : Catherine, Charlotte H, Ophélie, Léolo, Laura, Manon et Siam. Merci pour votre aide, votre bonne humeur (et vos grimaces en tout genre pour certains), pour votre implication dans la vie au sein du laboratoire (rangement, organisation et évènements hors labo) et pour votre superbe esprit d'entraide. Pour leur grain de folie, merci aussi au « groupe de Dona » : Hélène, Louise, Anne-Sophie, Maumau, Amaury et Maxime.

Merci à Aimée-Lys pour son aide et son sourire.

Souvent, face à une question de protocole ou à la recherche d'un anticorps, la phrase « demande à Sabine » résonne. Alors, je tiens évidemment à la remercier de partager son expérience avec générosité et patience. Mais surtout, je la remercie pour sa douceur, son altruisme, son immense bienveillance, ses conseils et ses paroles réconfortantes.

Je remercie Freddy pour son aide au laboratoire, d'être un rayon de soleil quand les journées sont difficiles, pour son humour et sa bonne humeur.

Je tiens à remercier mes deux acolytes de toujours, Valérie (Val) et Sandrine (Sandy), pour ces années sur les bancs de l'institut Paul Lambin, à travailler, à faire des présentations sur le phosphore dignes d'un show télévisé, à rire, à pleurer parfois mais surtout à vivre certains de nos plus beaux moments ensemble. Je les remercie de cultiver encore notre amitié et de rester des amies en or.

Le plus grand des mercis, je l'adresse évidemment à mes parents, Yves et Elodia. Je ne les remercie pas seulement de m'avoir soutenue dans mes études et

ma thèse. Je les remercie, aussi et surtout, d'avoir toujours été présents dans les bons et les moins bons moments, de nous avoir donné, à mon frère et moi, une enfance heureuse, des souvenirs inoubliables, des aventures mémorables en Italie, une éducation sensible au monde qui nous entoure et le respect de la nature et des animaux. Je les remercie de nous avoir énormément aidés, de nous avoir fait confiance et de nous avoir encouragés dans tout. Je vous dois tout, merci de tout cœur.

En parlant de mon frère, je n'aurais pas pu rêver d'un meilleur grand-frère que le mien, Quentin. Je le remercie d'avoir pris soin de moi depuis que je sais marcher, de m'avoir protégée, aidée et guidée. Je le remercie pour tous ces souvenirs qu'on a créés tous les deux : des cabanes en couvertures aux descentes du Piave en bateau gonflable, en passant par nos répliques de films préférés. Je te remercie d'être qui tu es et je suis fière de toi.

Et pour finir, je remercie la personne qui m'a probablement le plus soutenue, surtout dans cette dernière année qui a été aussi difficile pour lui que pour moi, mon compagnon, Xavier. Merci d'avoir été si patient, si compréhensif et d'avoir fait tant de sacrifices sans jamais t'en plaindre. Merci aussi de réaliser mes rêves en transformant (souvent seul) notre vieille maison en un paradis où les chevaux et les chats (peut-être un chien bientôt ?) sont en sécurité, auprès de nous. Merci pour ton courage, ton amour et de prendre soin de moi.

Pour terminer, je ne serais pas moi-même sinon, j'ai non pas des remerciements mais une pensée sincère pour les animaux de laboratoire sacrifiés pour faire avancer la recherche et notamment mon propre projet. Sans ces vies sacrifiées, nous, humains, ne serions pas là où nous en sommes dans les connaissances scientifiques et dans les avancées médicales. Je pense que nous leur devons beaucoup et en premier lieu le respect.

TABLE OF CONTENTS

LIST OF ABBREVIATIONS

AA	Amino-Acid
AMN	Amnionless
AP	Adaptor Protein
ARME	Apical Receptor-Mediated Endocytosis
Cap	Adenylyl cyclase-associated protein
ClC-5	Chloride channel-5
CMA	Chaperone-Mediated Autophagy
CR	Complement-type Repeats
CUBAM	Cubilin-Amnionless complex
DAB	Disabled proteins
Dab-2	Disabled-2
DAT	Dense Apical Tubule
EB	Ezrin-Binding
ECL	Extracellular Loop
EE	Early Endosome
EGF	Epidermal Growth Factor
ELS	Endo-Lysosomal System
ERM	Ezrin-Radixin-Moesin
ERT	Enzyme Replacement Therapy
ESRD	End-Stage Renal Disease
FcRn	Neonatal Fc Receptor
GBM	Glomerular Basement Membrane
GLUT2	Glucose Transporter isoform-2
GPI	Glycosylphosphatidylinositol
HGSNAT	Heparan-alpha-glucosaminide N-acetyltransferase
HSC70	Heat Shock Cognate 71 kDa protein
ICL	Intracellular Loop
LAMP	Lysosome-Associated Membrane Protein
LAMP-1	Lysosome-Associated Membrane (glyco)Protein-1

LDL	Low-Density Lipoprotein
LE	Late endosome
LIMP2	Lysosome Integral Membrane Protein-2
LMW	Low-Molecular Weight
LMWPs	Low Molecular Weight Proteins
LRP2	Low-Density Lipoprotein Receptor-Related Protein 2
LSD	Lysosomal Storage Disease
LYNUS	Lysosomal nutrient sensing machinery
MCOLN1	Mucolipin-1
MPR	Mannose 6-Phosphate Receptor
mTORC1	Mammalian Target of Rapamycin Complex-1
NaPi-IIa	Sodium/Phosphate cotransporter-IIa
NEU1	Neuraminidase-1
NHE1	Sodium/Hydrogen Exchanger-1
NHERF-1	Na^+/H^+ Exchange Regulatory Factor-1
OSOM	Outer Stripe of the Outer Medulla
Ostm 1	Osteopetrosis Associated Transmembrane Protein-1
PCSK9	Proprotein Convertase Subtilisin/Kexin type 9
PDZ	Postsynaptic density 95 - Disc large - Zona occludens
PPCA	Protective Protein/Cathepsin A
PQLC2	PQ loop repeat-containing-2
PSAP	Prosaposin
PT	Proximal Tubule
PTC	Proximal Tubular Cell
PTH	Parathyroid Hormone
Rab	Ras-related protein isolated from rat brain
RER	Rough Endoplasmic Reticulum
S1	initial short convoluted cortical segment of proximal tubule
S2	the majority of the cortical segment of the proximal tubule
S3	straight medullary segment of the proximal tubule
SAP	Sphingolipid Activator Protein
SGLT-2	Sodium-Glucose Transporter-2
SNARE	Soluble N-ethylmaleimide-sensitive factor Attachment protein Receptor
TFEB	Transcription Factor EB

TM	Transmembrane
TSH	Thyroid Stimulating Hormone
UPR	Unfolded Protein Response
Vps34	Vacuolar protein sorting-34
β-GAL	beta-Galactosidase

SUMMARY

Nephropathic cystinosis is a multisystemic lysosomal storage disease due to deletion or inactivating mutations of the cystinosin gene (*CTNS*) which encodes the lysosomal cystine transporter. Suppressed lysosomal exodus leads to cystine accumulation then precipitation as crystals. The earliest clinical manifestation of cystinosis is a renal Fanconi syndrome characterized by massive urinary losses of water, solutes and low-molecular weight proteins, typically reflecting global dysfunction of proximal tubular cells (PTCs), associated with inexorable progression to kidney failure. Current treatment with cysteamine slows down lysosomal cystine accumulation and kidney failure but does not correct the Fanconi syndrome. Better understanding of the pathophysiology of the disease in kidneys could identify new therapeutic targets. A fresh look is even more relevant since cystinosin has recently been found to be associated with transport-independent functions, suggesting that cystine accumulation may not be the only cause of cellular defects in cystinosis.

To characterize subcellular mechanisms of cystinosis in PTCs, we analyzed its time-course in *Ctns*$^{-/-}$ mice of the appropriate C57BL/6J background, which largely reproduce the multiple facets of this multisystemic disease, including the renal tubular phenotype. This analysis allowed to delineate a sequence of lysosomal and tissular alterations. Next, since PTCs are extremely active in endocytic recapture of ultrafiltrated disulfide-rich plasma proteins via the megalin pathway, and since cystine is an obligatory end-degradation product of lysosomal proteolysis of disulfide-rich plasma proteins, we hypothesized that endocytosis by megalin is the major source of cystine in PTCs, thus a key cause of injury. To test this hypothesis, we generated *Ctns*$^{-/-}$ mice with kidney-specific megalin

inactivation driven by Wnt-4 Cre ("double KO"). Finally, in a translational perspective, assuming that megalin ablation would protect against cystine accumulation and renal dysfunctions, we explored if a similar benefit could be gained by inhibition of the megalin pathway. To this aim, we focused on oral supplementation with dibasic amino acids, lysine or arginine, which have been previously demonstrated to be megalin inhibitors in cultured epithelial cells and upon in vivo gavage.

As in cystinotic children, we found that *Ctns*$^{-/-}$ PTCs undergo apical dedifferentiation, accumulate cystine crystals and finally become atrophic, with a characteristic longitudinal tubular extension starting from the glomerulo-tubular junction (known as swan-neck lesions). Subcellular defects are characterized by lysosomal enlargement reflecting first impaired proteolysis then distortion by crystals. Increased apoptosis and proliferation reflect accelerated PTC turn-over. In the double KO model, we showed that ablation of megalin-mediated endocytosis in *Ctns*$^{-/-}$ kidneys prevent swan-neck atrophy and normalize PTC turn-over. Preservation of apical markers in double KO PTCs indicated protection against apical dedifferentiation. Besides absence of cystine crystals in these cells, we showed that kidney cystine content was decreased by up to 10-fold as compared with *Ctns*$^{-/-}$ kidneys. Finally, after checking that dietary supplementation with dibasic amino-acids was well tolerated in WT mice and led to inhibition of protein recapture by kidney cortex PTCs, our preliminary results suggest that early implementation of long-term supplementation with dibasic amino-acids tends to decrease cystine accumulation and swan-neck lesions in cystinotic female kidneys by 6 months of age. Further characterization is ongoing with larger cohorts and longer follow-up.

In conclusion, we characterized the renal phenotype of cystinosis by defining the mechanisms responsible for subcellular changes and the longitudinal extension of atrophy along the proximal tube, to form a swan-neck. In addition, we demonstrated that megalin-dependent apical endocytosis is a major pathway for progression of nephropathic cystinosis, thus a potential therapeutic target. Indeed, preliminary data suggest that oral supplementation by dbAAs, currently used in other genetic diseases, is safe and effective as megalin inhibitors in cystinotic mice, thus could represent an inexpensive, titrable adjuvant therapy for cystinotic patients.

1. INTRODUCTION

1.1. Kidney proximal tubular cells, with focus on apical structure and functions

1.1.1. Structural specializations for reabsorption in proximal tubules and their segmental differentiation

The kidneys, paired organs belonging to the urinary system, are located on the posterior part of the abdominal cavity on each side of the spinal column. Blood enters through the two renal arteries and leaves through the two renal veins while the two ureters drive final urine to the bladder. Beside-other functions such as the production or modification of several important hormones or gluconeogenesis, the main function of the kidneys is to ensure the homeostasis of water and electrolytes (osmoregulation) by eliminating their excess but also to eliminate the many toxic wastes of metabolism including nitrogen after incorporation into urea. On a longitudinal kidney section, two distinct layers can be observed: the outer layer (or cortex), and the inner layer (or medulla). Cortex and medulla are composed of different domains of the nephrons, the structural and functional units of the kidney. In human, each of the two kidneys is made up of slightly more than one million nephrons (between 10.000 to 20.000 nephrons in mice).

T***he nephron*** consists of a renal corpuscle (also called glomerulus for simplification) followed by a renal tubule (Fig. 1). Plasma filtration occurs in the ***renal corpuscle*** at the glomerulus proper comprising a convoluted arteriolo-arteriolar capillary network (glomerular tuft), surrounded by the Bowman's

capsule, a single layer of simple squamous epithelium (parietal epithelium) which delimits the urinary space (Bowman's space).

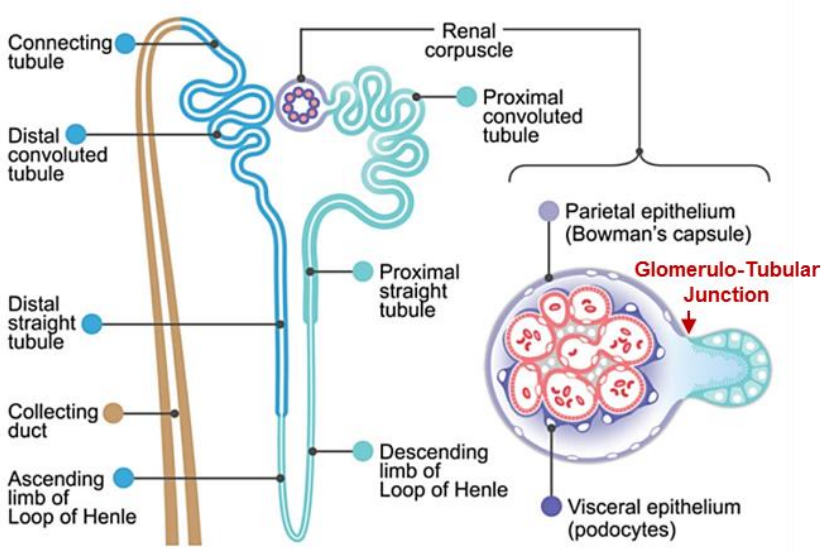

Figure 1. Schematic structure of the nephron, the functional unit of the kidney. Structurally, the nephron consists of the renal corpuscle and the renal tubule. The renal corpuscle, responsible for plasma ultrafiltration, is surrounded by the Bowman's capsule, a single layer of simple squamous epithelium (or parietal epithelium) enclosing the urinary space. The glomerulus, that apparently invaginates from Bowman's capsule, is made of convoluted capillaries surrounded by podocytes (or visceral epithelium), and comprises axial contractile mesangial cells. Collecting the primary ultrafiltrate, the lengthy renal tubule extends from Bowman's capsule (arrow stresses the abrupt boundary of glomerulo-tubular junction) to its junction with the collecting duct and is segmented into different areas exhibiting distinct substructure and functions. The proximal convoluted tubule is followed by the proximal straight tubule making together the proximal tubule, where most reabsorption takes place; the descending and ascending limbs of Loop of Henle, allowing for urine concentration; the distal straight tubule and the distal convoluted tubule, for final urine tuning; and via the connecting tubule, the collecting duct opening to the pelvis. Color codes identify distinct embryologic origins or local transcriptional networks. *From McMahon et al, 2016.*

The blood enters the renal corpuscle by the afferent arteriole, travels across the glomerulus and leaves by the efferent arteriole. The glomerular endothelium is fenestrated, thus permeable to the acellular blood filtrate, and rests on trilaminar basement lamina (or glomerular basement membrane, GBM). The GBM is supported by podocytes (visceral epithelium), constituting together a highly specialized filtration unit. Podocytes extend interdigitated foot processes connected by foot junctions (specialized local equivalent of tight junctions with additional role in ultrafiltration). This thick filtration barrier reduces the entry of high molecular weight solutes into the urinary space, a sieving property named permselectivity, each macromolecule exhibiting intrinsic sieving coefficient, ranging from 1 (free to cross the filtration barrier, e.g. insulin) to 0 (no crossing, e.g. ferritin). Generally considered as very low, the exact sieving coefficient of albumin is hotly debated, and varies between species and even between strains and sex (higher for FVB mice than C57BL/6 mice).(Ishola et al. 2006) However, because of its huge abundance in plasma, albumin is a major protein in the primary ultrafiltrate. Glomerulus also includes mesangial cells, specialized pericytes which maintain integrity and porosity of the endothelium and, by contractile properties, regulate glomerular blood flow thus primary urine output.

Once in the urinary space, the primary glomerular ultrafiltrate thus contains water, salts (such as sodium, chloride or phosphate), glucose and amino-acids (AAs) in exactly the same proportion as in plasma, as well as fractions of plasma proteins according to their respective sieving coefficient. The ultrafiltrate rapidly flows across the renal tubule (within minutes; about 20 sec for the proximal tubule only), leaving little time for its constituents to be reabsorbed. Thus, full reabsorption is an outstanding challenge, met by the extraordinary specialization of this segment. The epithelium of the ***renal tubule*** extends from the Bowman's capsule, reabsorbs various elements essential to body homeostasis and finally

carries urine into the collecting ducts; it functions as a series of specialized segments with distinct substructures and functions. At important segments, the renal tubule shows a highly convoluted shape, a remarkable histological specialization allowing considerable length extension, thus probability (efficiency) of reabsorption, in a limited organ volume, i.e. compaction. The first segment after the glomerulus, also the longest, is the proximal convoluted tubule which constitutes most of the mass of the cortex. The proximal convoluted tubule, itself subdivided in two similar yet functionally distinct subsegments, named S1 and S2, is followed by the proximal straight tubule (also named S3): they make together the proximal tubule. This proximal part of the renal tubule exerts the major reabsorption function for vital molecules such as water, salts, glucose, amino acids and ultrafiltrated plasma proteins. Proximal tubular cells are therefore in high demand of energy. By its position, receptor equipment and endocytic specialization, this part also takes up several toxic factors including nephrotoxic antibiotics (e.g. gentamicin). The proximal tubule is thus most vulnerable, both to energy shortage and to intoxication. The following segment, responsible for urinary concentration[1], is called the loop of Henle. This thin yet long loop plunges into the medulla and comes back into the cortex, to respectively form the descending and ascending limbs of Loop of Henle. The urine then flows through the distal straight tubule and the distal convoluted tubule for final urine tuning. Then, connecting tubule and collecting duct drain urine to the renal pelvis (Fig. 1).(Christensen, Wagner, and Kaissling 2012)

[1] The urinary concentration depends on a mechanism called countercurrent multiplication in kidneys. Briefly, the ascending limb of loop of Henle, impermeable to water, establishes a salt gradient in the medulla by active sodium reabsorption creating a hyperosmolar fluid in the interstitium. In contrast, the descending limb is passively permeable to water (aquaporin-1). Therefore, water moves passively down its concentration gradient out of the tubular fluid in the descending limb into the interstitial space, until it reaches equilibrium.

Nephrons can be further classified according to the positioning of glomerular corpuscle (and consequently of tubular segments) in anatomical layers: the cortex, outer medulla with two stripes (outer and inner) and the inner medulla. The juxta-medullary nephrons, or long-looped nephrons, are first formed during kidney development and have their renal corpuscles situated in the juxta-medullary cortex. The long loop descends deeper in the inner medulla. On the other hand, the more superficial cortical nephrons, or short-looped nephrons, are last to develop during peripheral kidney parenchyma expansion, thus are characterized by renal corpuscles located in peripheral layers of the cortex and a short loop that does not descend beyond the inner stripe of outer medulla (Fig. 2 A). Of note, glomeruli and the proximal convoluted tubules are all confined within the cortex while the proximal straight tubule extends into the outer stripe of the outer medulla (OSOM).

Kidneys are key organs, not only for the regulation of body fluid and salt balance, but also for blood pressure homeostasis. Moreover, since human primary filtrate reaches 170 L/day (creatinine clearance of ~ 120 ml/min x 1440 min/day), which is approximately a hundred times the final volume of urine excreted on a day, it follows that 99% of fluids and electrolytes are recaptured and return to the circulation, which implies a huge reabsorption capacity of the renal tube by several mechanisms which will be detailed below. By so limiting losses of essential substances, kidneys can ensure the survival for a few days, even in extreme conditions of total water deprivation. Conversely, during rapid and excessive ingestion of water or salts, renal excretion will be increased. The primary ultrafiltrate also contains very low-molecular weight proteins in the same concentration as in plasma but larger globular proteins are increasingly excluded depending on size, net charge and shape as well as blood pressure. These proteins

are normally almost completely recaptured by endocytosis and, according to the prevalent view, degraded in lysosomes for amino-acid recycling.

Although full reabsorption of metabolically useful solutes is achieved by the combined action of proximal and distal segments of the renal tubule, ***the proximal convoluted tubule***, highly adapted for this purpose, is by far the main actor. Responsible for the reabsorption of approximately 65% of the filtered water and electrolytes, almost all amino acids, as well as low molecular weight proteins, proximal tubules also maintain the acid-base balance of the body (80% reabsorption of filtered bicarbonate) and plays a key role in glucose homeostasis (full glucose reabsorption amounts to >100 g/day as detailed below; and regulation of gluconeogenesis). Conversely, defective reabsorption of solutes and proteins by proximal tubules causes the renal Fanconi syndrome, reflected by massive urinary loss of water, salts, glucose and proteins.

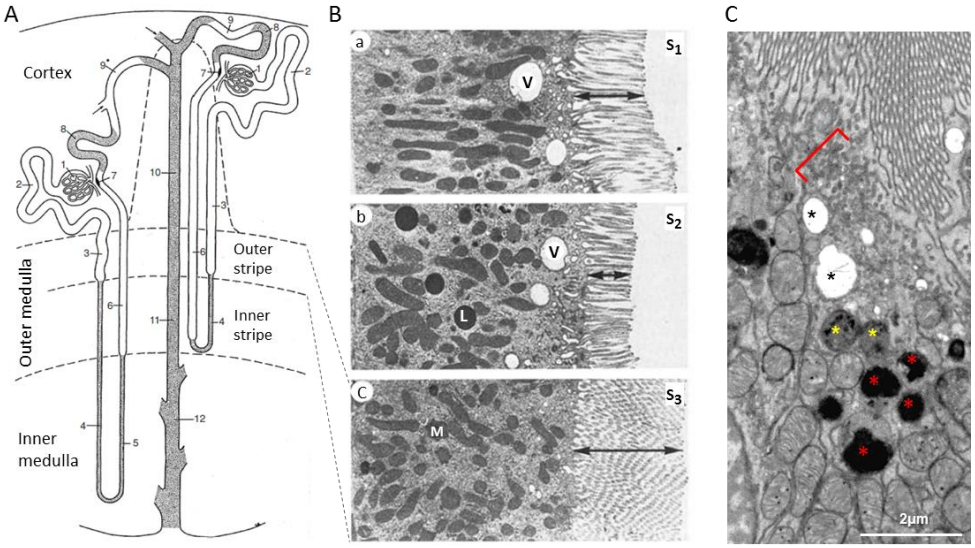

Figure 2.

Figure 2. Nephron positioning in the kidney and axial heterogeneity within proximal tubules. **A.** Schematic representation showing two types of nephrons with unequal segment positioning among anatomical layers: cortex, outer medulla with two stripes (outer and inner) and inner medulla. The cortico-medullary boundary can be recognized in kidney sections by the presence of arcuate vessels, running parallel to the capsule. At left, a long-looped nephron (or juxta-medullary, early nephron generation) and at right, a short-looped nephron (or peripheral, later nephron generation). Each contains: 1- glomerulus; 2- proximal convoluted tubule; 3- proximal straight tubule; 4- descending limb and 5- ascending limb of Loop of Henle; 6- distal straight tubule; 8- distal convoluted tubule; 9- connecting tubule) and a collecting duct (10- cortical; 11- outer medullary; 12- inner medullary). This scheme illustrates that glomeruli and the proximal convoluted tubules are always confined within the cortex while the proximal straight tubule extends into the outer stripe of the outer medulla (OSOM). As will be shown by our results, immunofluorescence for NaPi-IIa or megalin can be used as distinct markers of PTC subsegment boundaries. **B.** Electron micrographs of kidney depict axial ultrastructural heterogeneity within the proximal tubule which is subdivised into three sub-segments: S1 (a) and S2 (b) convoluted parts, and S3 (c), straighter part. The main differences, suggesting specific functions, lie in the thickness of the brush border (double arrows), the abundance of large electron-lucent endocytic vesicles (V), lysosomes (L), mitochondria (M) (mitochondria also differ in size and orientation) and the abundance and depth of basal plasma membrane invaginations (barely seen at this magnification). **C.** Apical stratification of endocytic organelles in WT mouse S1 is illustrated by electron microscopy. Immediately under the brush border is a dense layer of dense apical tubules (red bracket), suggesting that exocytosis is a rate-limiting step. Below are apical vacuoles (sorting endosomes, two black asterisks), then endo-lysosomes (yellow asterisks) and a cluster of secondary lysosomes (red asterisks). For full panel, see supplementary Fig. 5 of Janssens et al, 2019. *Adapted from Christensen et al, 2012 (A), Venkatachalam et al, 1978 (B) and Janssens et al, 2019 (C).*

To fulfill these specific functions, proximal tubular cells (PTCs) are highly polarized with apical and baso-lateral domains acting in sequence. Their apical membrane area is considerably increased thanks to tightly packed, regularly spaced long microvilli, called the brush border, very similar to that of enterocytes.(Crawley, Mooseker, and Tyska 2014)

This brush border harbors a huge collection of channels (e.g. aquaporins) and transporters (such as Na^+/H^+ antiporters - exemplified by NHE1; Na^+/phosphate co-transporters - NaPi-IIa; and Na^+/glucose co-transporters - SGLT-2). The deepest part of the brush border also exposes abundant endocytic receptors that will be sequestered into clathrin-coated pits for rapid endocytosis. The “upper” part of PTCs (apical cytoplasm) is merely a collection of endosomes, including large endocytic vacuoles (for sorting) and dense apical tubules (for recycling). Lysosomes are located below. This stratification is illustrated in Figure 2C. The “lower” part of PTCs (basolateral cytoplasm) contains among the most abundant mitochondria among body cells. These are aligned perpendicular to the tubular basement membrane and are in close proximity to deep invaginations of the basolateral plasma membrane, which harbor the major energy consumer, $3Na^+/2K^+$-ATPase, also named the “sodium pump”. This organization maximizes coupling between mitochondrial energy production with energy consumption by the sodium pump. The basolateral membrane also contains many other transporters, acting in complementarity to apical ones to drive net transepithelial reabsorption. For example, both apical and basolateral membrane are rich in aquaporins. This makes PTCs essentially freely porous to water that may iso-osmotically follow ion reabsorption.

Besides division into the convoluted and straight parts, the proximal tubule is classically divided into three segments on the basis of structural and functional

differences: ***the initial short convoluted cortical segment (S1), the majority of the cortical segment (S2)*** *and* ***the straight medullary segment (S3)****.* The main structural differences, which actually reflect distinct functional differentiation, relate to the brush border thickness, the abundance of large-electron-lucent endocytic vesicles, lysosomes and mitochondria and also the abundance and depth of basal membrane invaginations (Fig. 2B). Regarding the endo-lysosomal system (ELS), electron-lucent endocytic vesicles are more abundant and larger in S1 and S2 segments whereas they are rarer and smaller in S3 segment. Secondary lysosomes are most numerous in S2. The mitochondria are long and oriented perpendicular to the basal cell pole in S1 but become shorter and randomly oriented in S2 and S3 where they are more abundant. Finally, the S1 segment shows deep and numerous basolateral plasma membrane invaginations whereas they are much less developed in S2 and almost absent in S3. It goes without saying that such structural differences suggest specific functions for each segment but also different molecular composition.(Christensen, Wagner, and Kaissling 2012)

Three mechanisms allow PTCs to recapture the many components of the urinary filtrate, either (1) using the paracellular pathway or (2) through the epithelial cells via transport proteins, as well as (3) by receptor-mediated endocytosis. Firstly, *paracellular transport* of water and ions passes through the lateral intercellular space. On the apical side, adjacent PTC membranes are connected by tight junctions while their lateral membranes define a very narrow intercellular space. The direction of solutes and water is determined by physical factors such as peritubular capillary and intrarenal interstitial oncotic pressure and hydrostatic pressure. At the basal pole, the active transport of sodium via the Na^+/K^+-ATPase transporter drives hypertonicity of the intercellular compartment, which, combined with intraluminal hypotonicity, ensures and regulates the

paracellular reabsorption of water and ions. These are then recovered by the peritubular capillaries (or water can be discharged into the lumen of the renal tubule in case of hyponatremia). Secondly, *transepithelial transport* of water, salts and other solutes involves specific multi-transmembrane (TM) proteins at the apical and basolateral poles of the proximal tubular cells. Thirdly, PTCs exhibit an extremely efficient mechanism for recapture of ultrafiltrated plasma proteins, thanks to high expression of polyvalent tandem endocytic receptors and components of the *receptor-mediated endocytic* machinery. These three mechanisms are dependent on membrane proteins.

Before describing in details key membrane actors of solutes transporters and endocytic receptors, it is useful to briefly review some basic aspects of membrane:protein interactions. Biological membranes are composed of a very thin phospholipid bilayer, forming a fine semi-permeable boundary between the cytoplasm and the extracellular medium and recruiting/supporting a huge collection of proteins. With a short polar hydrophilic head group and two long hydrophobic tails, phospholipids are amphipathic molecules organized in a double layer to generate an inner hydrophobic barrier whereas hydrophilic head groups on both surfaces can accommodate contact with aqueous media.

Proposed by Singer and Nicolson in 1972, the fluid mosaic model of plasma membrane structure in which proteins are inserted into the bilayer is generally accepted as the basic model for the organization of cellular membranes. Some proteins, called **integral membrane** proteins, are indeed intrinsically incorporated into the plasma membrane through one (e.g. megalin) or several (transporters, e.g. NaPi-IIa) TM domains. Other proteins are also anchored by covalently attached lipids or glycolipids such as GPI-linked proteins (glycosylphosphatidylinositol anchors) or are acylated proteins (e.g.

palmitoylation of cubilin at the outer leaflet and geranylgeranylation of Rabs at the inner leaflet). **Peripheral membrane proteins** are extrinsic proteins closely associated with the plasma membrane via interactions with membrane components, either integral proteins by protein:protein interactions (e.g. via PDZ domains, see below) or the phosphate heads of phospholipids (e.g. ERM proteins such as ezrin, linking cortical actin microfilaments to the apical plasma membrane including NaPi-IIa; or ankyrin stabilizing Na^+/K^+-ATPase at the basolateral plasma membrane). Thus, the function of peripheral proteins is to anchor the plasma membrane to the intracellular cytoskeleton and to components of the extracellular matrix (e.g. laminin at the basement membrane), as well as to stabilize essential membrane proteins at their expected site of activity.

Integral proteins, also called transmembrane proteins, cross the lipid bilayer so as to expose domains on both sides of the plasma membrane and have therefore an amphipathic nature with hydrophilic domains, cytoplasmic or exoplasmic, *versus* hydrophobic domains buried in the lipid bilayer, usually forming alpha-helices or multiple beta-strands. In addition to integrating intrinsic proteins into the membrane, TM domains may lead to dimerization in case of receptors, thereby participating in signaling, or form transmembrane pores in the case of channels, transporters or pumps. When the protein comprises several TM domains, some cytoplasmic loops which connect them usually comprise key regulatory domains.

Some cellular processes, such as cell signaling, trafficking, cell proliferation or polarity, are regulated by interactions between TM proteins and other cytoplasmic proteins via adaptors. Indeed, the C-terminal segment of many TM proteins contains a PDZ motif (where PDZ for Postsynaptic density 95/Disc large/Zona occludens) that allows protein:protein interactions with

complementary PDZ domains of extrinsic scaffolding proteins that assemble junctional, ion channeling and signal transduction proteins, particularly in polarized epithelial cells. These domains, made of 80 to 90 amino acids, comprise beta strands and alpha-helices forming a globular structure with an elongated surface to which the PDZ motif of the ligand binds.

1.1.2. **Transmembrane transport: key transporters and apical targeting/retention machinery**

At the brush border of PTCs, transporters are responsible for the reuptake of phosphate ions, glucose and amino acids, all of which are co-transported with Na^+ ions, thus are indirectly dependent of the basolateral sodium pump. Having an important place in this study, two key transporters will be addressed in this section: the main phosphate and glucose co-transporters in nephrons, NaPi-IIa and SGLT-2.

1.1.2.1 NaPi-IIa

Phosphate reabsorption by kidneys and intestine is crucial for phosphate homeostasis. In mammalian cells, there are three types of sodium-phosphate (NaPi) co-transporters: type I, II and III. Type II (also named SLC34 gene family) further includes three NaPi co-transporters isoforms: NaPi-IIa, b and c.(Murer et al. 2003) While NaPi-IIa and NaPi-IIc isoforms are both expressed in the brush border of PTCs, type IIa is the most abundant, thus the key transporter in PTCs. NaPi-IIb ensures the transport of phosphate in the other tissues such as in

enterocytes (Murer et al. 2003; Yoshioka et al. 2011), without evidence for renal expression.(Hilfiker et al. 1998)

NaPi-IIa, thus the major sodium-phosphate transporter acting at the brush border of PTCs, reabsorbs approximately 80% of filtered inorganic phosphate by supporting the translocation of one HPO_4^{2-} anion coupled with that of 3 Na^+ cations. This unidirectional electrogenic translocation, from the lumen into PTCs, is driven by the low cytosolic Na^+ concentration generated by the basolateral sodium pump. The apparent Km is 0.1 mM for HPO_4^{2-} *vs* 50 mM for Na^+.(Murer et al. 2003) In the proximal tubule, NaPi-IIa expression is highest in S1 segment of deep nephrons and decreases towards the S3 segment.(Custer et al. 1994) Structurally, NaPi-IIa is an intrinsic protein composed by eight transmembrane segments and two functional regions, an intracellular loop (ICL1) and an extracellular loop (ECL3), involved in the coupled transport of phosphate and sodium (Fig. 3 A).

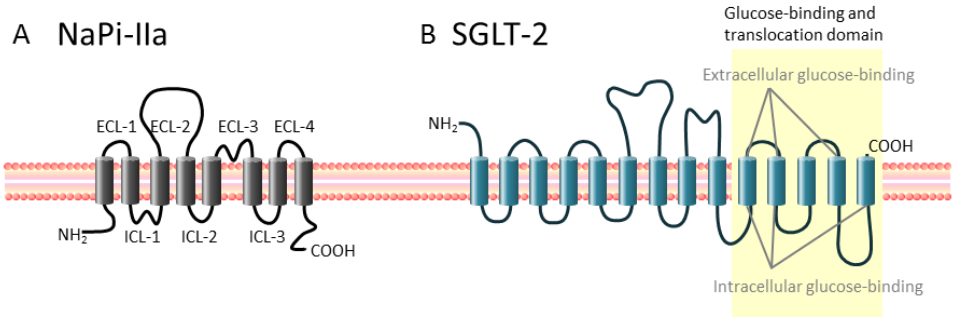

Figure 3. Molecular structure of key sodium co-transporters at the brush border of proximal tubular cells. A. The main phosphate co-transporter, NaPi-IIa (90kDa), contains eight transmembrane segments. Two regions are involved in the coupled transport of one PO_4^{3-} together with three Na^+: intracellular loop-1 (ICL1) and extracellular loop-3 (ECL3). The NaPi-IIa cytoplasmic C-terminal tail is able to interact with an apical regulatory PDZ-based scaffold of several components, shown at Figure 4, that, through signaling pathways, determine either fixed membrane anchoring (low phosphate diet, no PTH) or internalization of NaPi-IIa into degradative lysosomes (high phosphate diet, PTH). **B.** The key glucose transporter, SGLT-2 (75kDa), contains 14 transmembrane helices, five of which (yellow box) being involved in glucose binding, and both extracellular N- and C-termini. SGLT-2 supports the coupled entry of one glucose with one Na^+. *Redrawn from Virkki et al, 2005 (A) and Dardi et al, 2016 (B). Notice that loops are not drawn at the same scale.*

NaPi-IIa C-terminal tail interacts with three PDZ-proteins: Cap1 (orthologue of PDZK1 in human), Cap2 and NHERF-1. Cap1 binds the three amino acids sequence Thr-Arg-Leu at the C-terminus of NaPi-IIa and is implicated in its apical sorting/positioning. Indeed, truncation of these three amino acids abrogates apical sorting of NaPi-IIa in OK cells. NHERF-1 (Na^+/H^+ Exchange Regulatory Factor-1) contains two tandem PDZ-domains and a carboxyl-terminal ezrin-binding (EB) region that provide a strong connection to the apical cortical actin cytoskeleton thanks to ezrin, the founding member of ERM protein family (Fig. 4). Accordingly, in PTCs under basal conditions, NaPi-IIa is indeed localized along, and restricted to, the entire surface of microvilli. While Cap1 and NHERF-1 are found exclusively in microvilli, Cap2 is mainly located in the subapical compartment of PTCs and appears to be associated with vesicular structures still unknown. The vesicular proteins that may interact with Cap2 and the link with NaPi-IIa remain to be determined.(Gisler et al. 2001)

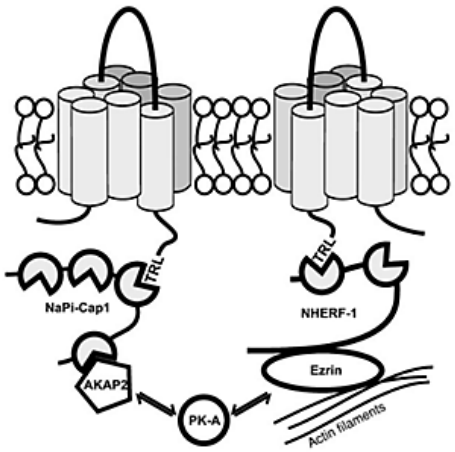

Figure 4. NaPi-IIa topological regulation by interaction with PDZK1 and NHERF-1. NHERF-1 (Na^+/H^+ Exchange Regulatory Factor-1) (50kDa) shown at right contains two tandem PDZ-domains and a carboxyl-terminal ezrin-binding (EB) region. Ezrin is a linker with actin microfilaments and a stabilizer of plasma membrane attachment. PDZK1 (also called NaPi-Cap1; 63kDa) is an adaptor protein comprising four PDZ-domains. PDZ domain-containing proteins such as NHERF-1 and PDZK1 have a multitude of functions based on scaffolding. Besides trafficking that supports apico-basal polarity, they connect intrinsic plasma membrane proteins with extrinsic linkers such as ezrin and thus provide a lasting bridge to the actin cytoskeleton. They also engage in signaling pathways as, for example, the activation of PKA cascade that leads instead to NaPi-IIa down-regulation by endocytosis. *From Murer et al, 2003.*

Regarding the regulation of phosphate reabsorption, NaPi-IIa co-transporter activity depends on extracellular pH because of the competition of Na^+ with protons at the binding site. In addition, NaPi-IIa internalization (and thus its availability / activity at the membrane) is regulated by the dietary phosphate level and by parathyroid hormone (PTH).(Murer et al. 2003) Under high phosphate diet (by a still poorly understood sensing mechanism) or upon high PTH, NaPi-IIa surface abundance is down-regulated, so as to decrease phosphate reabsorption. This is achieved by an elegant mechanism of induced endocytosis without apical recycling of NaPi-IIa, which is instead sorted out from subapical compartment and routed to lysosomes. When occurring at low concentration in proximal tubule lumen, PTH is primarily endocytozed and degraded. In contrast, at high luminal concentration, PTH also binds to and stimulates its apical receptor. This binding leads to the activation of various protein kinases (PK-A, PK-C, PK-G) followed by NaPi-IIa internalization. This mechanism has been proposed as an explanation for phosphaturia in Dent's disease.(Piwon et al. 2000) In Dent's disease, mutation in the CLCN5 gene encoding the vesicular chloride channel, ClC-5, causes an inherited renal Fanconi syndrome with proteinuria, hyperphosphaturia and hypercalciuria. ClC-5 is a H^+/Cl^- exchange transporter expressed in apical endosomes of proximal tubular cells. By using CLCN5 KO model, Jentsch and colleagues have demonstrated that ClC-5 ensures the electrogenic H^+-ATPase activity by an electric shunt. In these mice, endosomes are less acidified than wild-type resulting in drastic impairment of endocytosis. Therefore, luminal PTH concentration increases so as to stimulate apical PTH receptors and down-regulate NaPi-IIa, resulting in phosphaturia.

Friedlander and co-workers have shown that natural mutations of NaPi-IIa (Ala48 and Val147) cause urinary phosphate loss in humans.(Prie et al. 2002) Later

on, the same group showed that three natural mutations of NHERF-1 decreased phosphate uptake.(Karim et al. 2008)

1.1.2.2 SGLT-2

Although fat and, to a lesser extent, amino acids are important energy sources, glucose is the main flexible source of energy, and is essential for the brain. Glucose being unable to cross impermeable membrane bilayers, it passes through a family of dedicated transporters, that have been named GLUT-x or SGLT-x. Glomerular ultrafiltration transfers into primary urine >100 g of glucose in man every day (1 g glucose/L plasma x 0.12 L ultrafiltrate/min x 1440 min/day = 173 g/day), that would be lost without appropriate reabsorption systems. The sodium and glucose co-transporter (SGLT) gene family includes six members, SGLT-1 to SGLT-6. **SGLT-2** is localized almost exclusively in the apical membranes of proximal convoluted tubules where it represents the major transporter for glucose uptake. SGLT-2 is found primarily in the S1 segment where it is responsible for 90% of glucose reabsorption (Vallon et al. 2011) while a tiny part of ultrafiltrated glucose is recaptured by SLGT-1 in the S3 segment.(Hediger and Rhoads 1994; Bakris et al. 2009) SGLT-2 structure includes 14 transmembrane domains, 5 of which are involved in glucose binding. Both C and N termini tails of SGLT-2 face the lumen (Fig. 3B). SGLT-2 ensures the coupled entry of one glucose with one Na^+.(Zhuo and Li 2013; Vallon et al. 2011; Scheepers, Joost, and Schurmann 2004) Coupled transport of glucose and sodium across the plasma membrane to the cytoplasm is driven by the low cytosolic sodium concentration and the membrane potential. Cytosolic sodium, having entered via several apical co-transporters such as NHE1, NaPi-IIa and SGLT-2, is then excreted into the inner

milieu via the sodium pump across the basolateral membrane, readily diffusing back to blood circulation. As for glucose, it leaves the cell at the basal pole via a distinct glucose transporter called GLUT2.

1.1.3. The multiligand apical endocytic receptor complex and its ultrafast recycling

In addition to the uptake of small molecules by transmembrane transporters, eukaryotic cells can also internalize extracellular macromolecules by vesicular uptake, a process known as endocytosis. In 1963, Christian de Duve coined the term “endocytosis” (from the Greek “into – cells”) which refers to cell ingestion of either large particles, called phagocytosis, or absorption of fluids and macromolecules into small vesicles, called pinocytosis. The specialized **phagocytic cells** expose membrane surface receptors creating multiple progressive linkage (or “zip”) with large particles such as bacteria or cell debris. By actin movement, the cell then emits membrane extensions, or pseudopodia, which wrap and eventually encloses the particle to form the phagosome, a large intracellular vesicle. Its fusion with lysosomes forms the phagolysosome where the prey is normally digested by lysosomal acid hydrolases. Preformed urate or cystine crystals are also phagocytozed by macrophages but cannot be dissolved, so as to trigger the inflammasome.(Prencipe et al. 2014) Depending on the type of specialized cell practicing phagocytosis, this mechanism is a source of nutrients (amoebae), a defense against microorganisms (macrophages and neutrophils), or a way to eliminate damaged or fragmented (apoptotic) cells. On the contrary, **pinocytosis** is shared by all eukaryotic cells. Beside elementary pinocytosis (or fluid-phase endocytosis) defined by the volume of engulfed extracellular fluid, which can be magnified by micropinocytosis, receptor-mediated endocytosis is a much more

efficient and selective form of pinocytosis that allows cells to absorb specific macromolecules.

Receptor-mediated endocytosis implies several events in which cargo molecules are first recognized by the specific endocytic receptors and concentrated via the adaptor complex AP-2 into plasma membrane clathrin-coated pits that further bud from the membrane under the action of dynamin and accessory proteins as clathrin-coated vesicles. Clathrin-coated vesicles then uncoat to become primary endocytic vesicles which, by homotypic fusion, become early endosomes (EEs) containing both receptors and their bound ligands. The lumen of early endosomes becomes mildly acidic by the modest activity of less abundant vacuolar proton pump than at lysosomes (Mellman, Fuchs, and Helenius 1986) and its calcium concentration dramatically decreases[2].(Gerasimenko et al. 1998; Ghislat and Knecht 2013) Combination of both events triggers dissociation of megalin and cubilin ligands, a segregation that is essential for transfer of unoccupied receptors to dense apical tubules.(Andersen and Moestrup 2014) Geometry easily explains that these narrow tubular extensions from early endosomes allow for the selective recycling of the receptors via transport vesicles carrying them back to the plasma membrane, while the bulk of fluid remains in the central vesicle that eventually forms late endosomes (discussed by Courtoy 1991).

[2] In the formation of early endosomes, endocytosis vesicles fuse together or with preexisting similar vesicles. This process, named homotypic fusion, is catalyzed by Rab5 protein and depends on phosphoinositides (PIPs) and consists of several step: tethering, docking and blending. After docking through v- and t-SNAREs interaction, a release of luminal Ca^{2+} from endolysosomal compartments is thought to trigger fusion events near Ca^{2+} release sites. Several candidates have emerged to function as lysosomal/endosomal Ca^{2+} release channels such as transient receptor potential cation channel, subfamily M, member 2 (TRPM2) and two-pore channels (TPCs).

The dynamics of early endosomes is regulated by the endocytic catalyst, Rab5a, while that of recycling tubules depends on Rab11. The function of Rab5a depends on phosphatidylinositol 3-phosphate, the product of PI3-kinase type III/Vps34. Work to which I was associated demonstrated that Vps34 inhibition or genetic ablation abrogates apical endocytic recycling (see publications 4 and 5 in the Appendix).(Carpentier et al. 2013; Grieco et al. 2018) The central vacuolar structure then matures of its own into late endosomes (LEs) and finally into degradative secondary lysosomes, responsible for ligand proteolysis and AA recycling via lysosomal membrane transporters such as cystinosin for cystine and PQLC2 for dibasic amino-acids. The late components (LEs and lysosomes) of this endocytic apparatus are now commonly named together endolysosomes because of their dynamic continuity (ongoing fusion and fission) and compositional overlap (high concentration of vacuolar proton pump and presence of Rab7 and LAMP-1 markers) (reviewed by Luzio, Pryor, and Bright 2007). The term “endolysosomes” may however cause confusion with the recently coined “endolysosome system” (ELS) that is meant to encompass the entire (apical?) endocytic apparatus.(Schuh et al. 2018)

The endocytic apparatus of PTCs is highly polarized and particularly expanded (especially in segments S1 and S2). In these cells, a highly organized, packed system of dense apical vesicles, dense apical tubules, early and late endosomes (and lysosomes in mice, but not rats or man) establish a clear apical zone (without mitochondria), easily distinguishable by light microscopy. In PTCs, pioneering studies by Werner Straus more than half a century ago, based on cytochemical demonstration of apical endocytosis of an injected robust tracer, horseradish peroxidase, allowed to delineate this sequence and, in fact, provided the first evidence for the individuality of endosomes as intermediate compartment before lysosomes.(Straus 1964b, 1964a) Incidentally, peroxidase is often erroneously

referred to as a fluid-phase tracer while Straus clearly documented competition by lysozyme.(Straus 1962)

Thanks to the huge expression and extraordinary fast recycling of multiligand tandem endocytic receptors protruding into the urinary lumen, megalin and cubilin, this apical endocytic apparatus plays a central role in complete reabsorption of ultrafiltrated plasma proteins, and of the vitamins some of them carry, **by apical receptor-mediated endocytosis** (ARME, for a review, Christensen and Birn 2002) Megalin and cubilin are often described as tandem receptors because, although each has some preferred ligands, they cooperate by sharing the binding of many common ligands such as albumin or vitamin D-binding protein (Table 1).(Leheste et al. 1999; Amsellem et al. 2010)

Amnionless (AMN) acts as an essential chaperone bringing cubilin to the cell surface, thus joining in a functional triad. AMN and cubilin also form a megalin-independent and functional complex (CUBAM) in which cubilin brings its own specific binding capacities, for example for transferrin, while AMN provides physical support for endocytosis. In this subsequent part of this Section, the structure, functions and particularities of these key actors are detailed.

Megalin	Cubilin
Vitamin carrier proteins	***Vitamin carrier proteins***
Transcobalamin–vitamin B_{12}	Intrinsic factor vitamin B_{12}
Vitamin D–binding protein	Vitamin D–binding protein
Retinol-binding protein	
Folate-binding protein	
Other carrier proteins	***Other carrier proteins***
Albumin	Albumin
Myoglobin	Myoglobin
Hemoglobin	Hemoglobin
Lactoferrin	Transferrin
Selenoprotein P	
Metallothionein	
Neutrophil gelatinase–associated lipocalin	
Odorant-binding protein	
Transthyretin	
Liver-type fatty acid–binding protein	
Sex hormone–binding globulin	
Lipoproteins	***Lipoproteins***
Apolipoprotein B	Apolipoprotein A-I
Apolipoprotein E	High-density lipoprotein
Apolipoprotein J/clusterin	
Apolipoprotein H	
Apolipoprotein M	
Hormones and signaling proteins	***Hormones and signaling proteins***
Parathyroid hormone	Fibroblast growth factor
Insulin	
Epidermal growth factor	
Prolactin	
Thyroglobulin	
Sonic hedgehog protein	
Angiotensin II	
Leptin	
Bone morphogenic protein 4	
Connective tissue growth factor	
Insulin-like growth factor	
Survivin	
Aprotinin	
Trichosanthin	
Colistin	
Receptors	***Receptors***
Cubilin	Megalin
Transcobalamin II–B_{12} receptor	
Others	***Others***
Receptor-associated protein	Receptor-associated protein
Ca^{2+}	
Cytochrome C	
Seminal vesicle secretory protein II	
Coagulation factor VII	Coagulation factor VII
Coagulation factor VIII	
Enzymes and enzyme inhibitors	***Enzymes and enzyme inhibitors***
Plasminogen activator inhibitor type I	
Plasminogen activator inhibitor type I–urokinase	
Plasminogen activator inhibitor type I–tissue plasminogen activator	
Pro-urokinase	
Lipoprotein lipase	
Plasminogen	
α-Amylase	
Lysozyme	
Cathepsin B	
α-Galactosidase A	
Cystatin C	
Recombinant activated factor VIIa	Recombinant activated factor VIIa
Immune- and stress-related proteins	***Immune- and stress-related proteins***
Ig light chains	Ig light chains
Pancreatitis-associated protein 1	Clara cell secretory protein
α_1-Microglobulin	α_1-Microglobulin
β_2-Microglobulin	
Drugs and toxins	***Drugs and toxins***
Aminoglycosides	Aminoglycosides
Polymyxin B	

Table 1. Specific *vs* shared ligands for megalin and cubilin. Although recent, this list is not up-to-date. I contributed to the study demonstrating that the complex of pro-MMP-2:TIMP2 is a ligand for megalin (Johanns et al, 2017; see Appendix 3) *From Nielsen et al. 2016*.

Megalin (also called LRP2, for low-density lipoprotein receptor related protein-2) is a huge transmembrane protein of > 600 kDa belonging to the low-density lipoprotein (LDL) receptor family. Compared to the family prototype, LDL-receptor, bearing a single ligand binding site, a propeller domain regulating association and dissociation and a transmembrane/cytoplasmic domain with a single tyrosine-based rapid endocytosis motive, the megalin gene has expanded its extracellular domain by multiple duplications of the ligand-binding domain with not less than 36 cysteine-rich complement-type repeats (CR), supporting most of ligand binding capacity (see below), 16 growth factor repeats separated by 8 YWTD propeller domains (for tyrosine-tryptophan-threonine-aspartic acid), involved in pH- dependent endosomal dissociation of ligands, and one epidermal growth factor (EGF)-like repeat (Fig. 5). The ability of megalin to specifically bind an extraordinary large number of ligands (Table 1) is probably due to the different combinations that are possible for flexible repeats and to the differences in electrostatic surface potential among the repeats. Linked to the extracellular domain by the usual hydrophobic transmembrane sequence, the much longer intracellular tail of megalin contains domains that distinguish it from other receptors and are involved in transport and signaling. In particular, two endocytic motifs (NPXY) allow, by interactions with the AP-2 and Dab-2 adaptors, the clustering of the receptor within the coated-pits and thus, rapid internalization.(Christensen, Verroust, and Nielsen 2009)

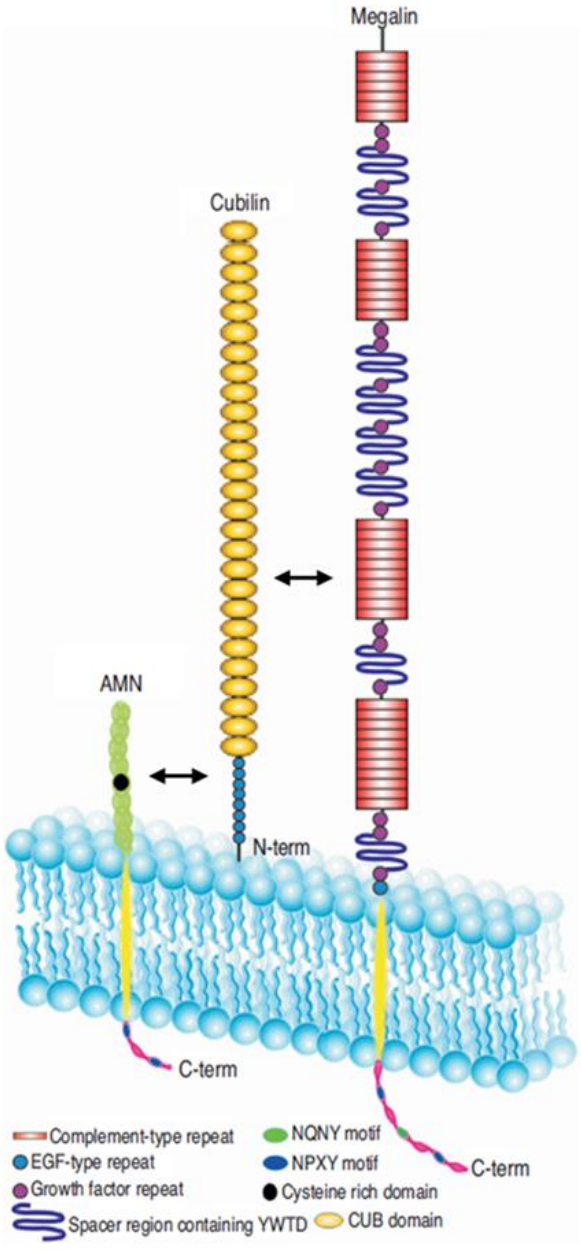
Megalin
Cubilin
AMN
N-term
C-term
C-term
Complement-type repeat
EGF-type repeat
Growth factor repeat
Spacer region containing YWTD
NQNY motif
NPXY motif
Cysteine rich domain
CUB domain

Figure 5.

Megalin is co-expressed with cubilin in several absorptive epithelia such as enterocytes in the small intestine, renal proximal tubules, the visceral yolk sac and the placenta. However, megalin is also highly expressed alone in several other epithelial tissues such as glomerular podocytes, thyrocytes, type II pneumocytes of lung alveoli, choroid plexus ependymal cells in cerebral ventricles, endometrium- and oviduct-lining cells and associated glands, epididymal epithelial cells, ciliary epithelium and cells of the inner ear.(Christensen and Birn 2002) Lastly, megalin is also expressed in the endoderm derived-parathyroid.

Figure 5. Megalin, a pivotal element within the ternary apical endocytic receptor complex of kidney proximal tubular cells. Within the proximal convoluted tubule, endocytic recapture of ultrafiltrated plasma proteins relies on the cooperation of three receptors that co-localize at the apical membrane of proximal tubular cells: megalin, cubilin and amnionless (AMN). Each of them presents different extracellular domains and motifs that are detailed in this scheme with a color-code and assign to each ligand specificity. Horizontal double-headed black arrows indicate lateral interaction. The corresponding structures are depicted as a linear strand, which is probably incorrect as it would exceed the diameter of the lumen of recycling endosomes (dense apical tubules). **Megalin** (also called LRP2), so named because of its huge size (>600 kDa large glycoprotein), belongs to the low-density lipoprotein (LDL) receptor family and binds a wide variety of ligands including most ultrafiltrated "low-molecular-weight" proteins and xenobiotics such as aminoglycoside antibiotics at its cysteine-rich complement type repeats, separated by growth factor repeats and YWTD-containing spacer/propeller regions. The latter domains undergo a conformational change at acidic pH, contributing together with luminal calcium lowering to ligand dissociation. Megalin is membrane-inserted by a single transmembrane domain and is equipped with a large cytoplasmic domain bearing two "rapid endocytosis" NPXY motives (drawn in blue) and NPXY-like motives (or NQNY), specifically involved in apical sorting (drawn in green). Like megalin, **AMN** (38-50 kDa) is also a transmembrane domain and contains two rapid endocytosis NPXY motives. **Cubilin** (460 kDa) includes 27 highly homologous CUB domains involved in ligand binding and eight epidermal growth factor-like repeats but is only loosely linked to the outer membrane leaflet via a palmitoyl anchor and lacks a cytoplasmic domain, thus is intrinsically defective of apical targeting and endocytosis motives, for which it relies on association with AMN and/or megalin. *From Christensen et al, 2012.*

Disabled (DAB) proteins play an important role in endocytic trafficking of cell surface receptors such as megalin. Indeed, Dab-2 (disabled-2), a scaffold protein connecting megalin to clathrin, is required for its endocytosis by clathrin-coated pits, which is essential as early as during embryonal brain development. In the absence of clearance by megalin of signaling proteins, severe brain malformations such as holoprosencephaly ("cyclopean brain") develop, explaining the term "disabled" (reviewed by Willnow and Christ 2017). In foetal and adult kidney PTCs, Dab-2 operates as an adaptor protein for megalin-mediated endocytosis of ultrafiltrated proteins. Immaturity of endocytosis in premature babies explains the loss of vitamins such as vitamins A and D, normally endocytozed together with their specific carrier (vitamin A-binding protein or ABP; vitamin D-binding protein, or DBP, respectively), with potentially severe consequences.(Charlton et al. 2019)

In the low-density lipoprotein (LDL) receptor gene family, the predicted overall structure of megalin is at first glance quite similar to that of LRP-1, also known as scavenger receptor. Indeed, similarly to megalin/LRP2, LRP-1 harbors four ligand binding domains separated by clusters of EGF-precursor repeats and YWXD spacer repeats. However, whereas megalin/LRP2 also includes four ligand-binding domains, its first one, with seven ligand binding repeats, is typical of megalin and largely differs from the corresponding domain in LRP-1. In addition, a unique furin endopeptidase processing site in the LRP-1 ectodomain is normally cleaved to form the mature receptor, which is a disulfide-linked heterodimer of 515 kDa and 85 kDa subunits. Moreover, although overall structurally similar, these "false-twin receptors" differ in cytoplasmic motives that dictate their opposite membrane polarity. In polarized epithelial cells such as PTCs, transmembrane proteins can be addressed to apical, basolateral or both poles of cells. A polarized distribution depends on sorting sequences in the cytoplasmic tail of proteins. The nature of the sorting signal and the mechanism that allows it to

be decoded determine the trafficking route and thus, the ultimate protein localization. Among addressing motifs already known, tyrosine-based (NPxY or Yxxϕ) or dileucine (LL) motifs are involved in the basolateral sorting of several transmembrane proteins including LDL-receptors. The cytoplasmic tail of LRP1 includes especially two NPxY motifs, one Yxxϕ motif (recently shown as the dominant endocytosis motif) and two LL motifs for direct basolateral targeting. Of note, phosphorylation of the LRP1 tail by PK-A plays a role in the internalization of the receptor. Thus, NPxY motifs can have distinct sorting functions. Moreover, comparing the two NPxY motifs of LRP1, the first (Y29) and the second (Y63) tyrosine contribute to the basolateral sorting but with different efficiencies. Tyrosine at position 29, also close to crucial acidic residues, is the most efficient.(Marzolo et al. 2003) Although containing similar basolateral adressing motifs, megalin/LRP2 includes other (dominant) motifs for its apical routing. Indeed, in addition to NPxY and LL motifs, the cytoplasmic tail of megalin contains a PDZ-terminal motif and two proline-rich motifs, one of which includes a PPPSP sequence responsible for the phosphorylation of megalin by the glycogen synthase kinase-3 (GSK3β). Apical localization of megalin depends on the combination of these signals.(Yuseff et al. 2007; Marzolo and Farfan 2011)

Megalin is homogenously expressed throughout the proximal tubule, from S1 segment to S3. However, the prominent development of the apical endocytic apparatus (i.e. the complete endocytic machinery drived by receptors, ranging from internalization at the apical pole to the lysosomes) in S1 segment, together with most abundant endosomes (early, late and recycling) and lysosomes, are structural hallmarks that uptake of low molecular weight proteins (LMWPs) by receptor-mediated endocytosis is concentrated in this segment. Conversely, the apical endocytic apparatus is less extensive in S2 and poorly present in S3 (pars recta), explaining the lower up to marginal endocytic activity in these segments

(Fig. 6). Thus, S1 segment is by far the major site for reabsorbing LMWPs and toxic xenobiotics under normal condition.(Schuh et al. 2018) However, under certain pathological conditions as in the case of nephropathic cystinosis, S1 segment becomes defective leading to the suppression of endocytic function in this area. Then, the more distal segments of the proximal tube (S2 and then S3) face the loads of proteins and other substrates. The responsibility for endocytosis is thus transferred longitudinally as lesions progress.(Gaide Chevronnay et al. 2014)

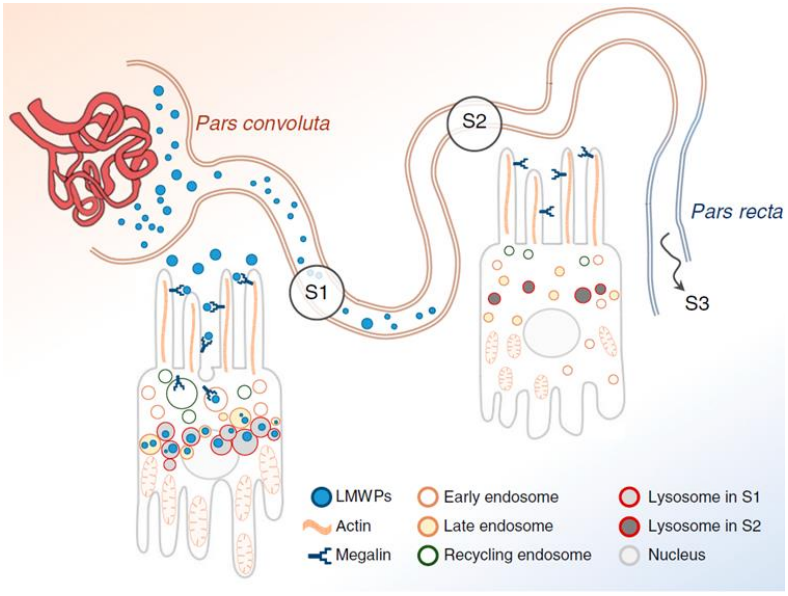

Figure 6. Axial differences in endo-lysosomal system (ELS) structure and function between S1, S2 and S3 segments of the proximal tubule. This representation of proximal tubule emphasizes the characteristic expansion of the endo-lysosomal system in S1. Despite megalin being expressed throughout the proximal tubule, uptake of low-molecular weight proteins (LMWPs) by receptor-mediated endocytosis (RME) is concentrated on S1 where cells contain numerous large endosomes (early and late or recycling) and lysosomes. ELS is much less developed in S2 and almost absent in S3 (pars recta). In view of these differences, the S1 segment is considered to have the highest capacity to reabsorb LMWPs and toxic xenobiotics under normal conditions. *From Schuh et al, 2018.*

Cubilin, a very large peripheral protein of 460 kDa, lacks transmembrane and intracellular domains, thus necessarily depends on the endocytic capacity of megalin or AMN for its internalization. The three regions that make up cubilin are a N-terminal stretch, 8 EGF-like repeats, and 27 highly homologous CUB domains which have the potential to bind a variety of ligands although, compared to megalin, fewer candidates have been identified so far, the main one being the complex of vitaminB12:intrinsic protein in enterocytes (Table 1). In PTCs, transferrin is considered a *bona fide* cubilin ligand. The loose membrane attachment of cubilin is ensured by an amphipathic and a palmitoylation site at its N-terminal segment. The N terminus and CUB domain 1 and 2 are the predicted sites for interaction with megalin (Fig. 5).(Christensen, Verroust, and Nielsen 2009)

The remarkable overlap of ligands between megalin and cubilin, in particular for albumin, despite totally different primary AA sequence has attracted much attention. Molecular modelling based the effects of site-directed mutagenesis combined with co-crystallization with a respective paradigmatic ligand revealed a fascinating example of convergent evolution, ending up in superimposable electrostatic interaction maps (Fig. 7).(Andersen and Moestrup 2014) As stated above, CR domains and CUB repeats are the major domains conferring the binding specificity of megalin and cubilin, respectively. However, CR (megalin) repeats and CUB (cubilin) domains show overwhelming similarities in the calcium-dependent ligand binding mechanism. In both cases, calcium ions indeed interact with acidic residues at the ligand-binding domain for the interaction with positively charged crucial lysine (or arginine) residues in their cargo/partner. Of note, cubilin and the LDLR family also include EGF-like domains. Similarity exists between the principal domains for ligand recognition in megalin, CR repeats, and EGF-like domains. In EGF-like domains, a calcium ion coordinates an aspartate residue then able of

interacting with an arginine residue of PCSK9 (proprotein convertase subtilisin/kexin type 9), a negative regulator of LDL-receptors.(Andersen and Moestrup 2014)

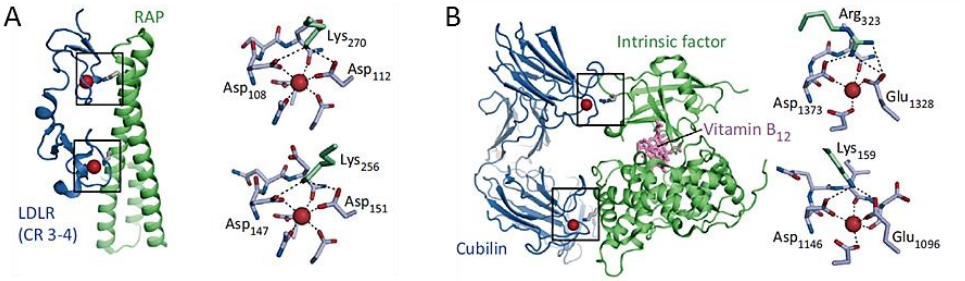

Figure 7. Structure of megalin and cubilin. These evidence-based molecular models emphasize the similarity of calcium-dependent reciprocal electrostatic interactions of CR domain of the prototypic LDL-receptor complexed by its chaperone RAP (at A), as compared with those between a CUB domain in cubilin and the vitaminB12:intrinsic factor complex (at B), both considered in the exoplasmic space. Calcium is represented by red balls. In the upper parts of the enlargements of receptors shown at right of each panel, calcium coordination brings in close vicinity a dibasic amino-acid (lysine or arginine) with an acidic amino-acid, aspartate in the receptor sequence. This tripartitite pocket can then interact with high affinity with a crucial acidic amino-acid (aspartate or glutamate) in a sterically accessible region of the ligand (represented below). Calcium release in the endosomes disrupts the receptor pocket, thus cause ligand dissociation. *Adapted from Andersen and Moestrup, 2014.*

Finally, **AMN** is a family of five transmembrane proteins from 50 to 38 kDa, resulting from alternative transcription of a single amnionless gene, with decreasing extensions at the N-terminus. This part of the gene is essential for vitamin B12 uptake, but not for embryonic development.(Tanner et al. 2003) Structurally, AMN consists of an N-terminal extracellular domain containing a cysteine-rich region, a transmembrane segment and a cytoplasmic tail with two

rapid endocytosis NPXY motifs (Fig. 5). As stated previously, AMN and cubilin interact through EGF-like repeats of cubilin to form the CUBAM complex. This association guarantees the translocation of both proteins from rough endoplasmic reticulum (RER) to the plasma membrane, which is not possible if each is expressed alone ("reciprocal chaperones").(Christensen, Verroust, and Nielsen 2009)

Figure 8 shows the abundance and localization of megalin, as corner stone in ARME in PTCs.(Christensen, Wagner, and Kaissling 2012; Verroust and Christensen 2002)

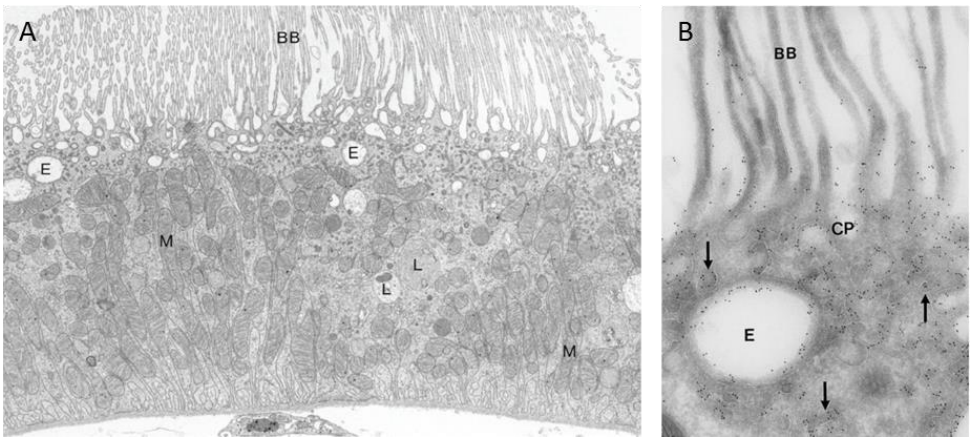

Figure 8. Localization of megalin into the segment S1 of the proximal tubule epithelium. A. Electron micrography of rat segment S1 shows a well-developed brush border (BB) at the apical surface. The subapical area contains endocytic vacuoles (E) and, deeper, lysosomes (L). In mice S1, lysosomes lie instead much closer to the apical membrane. Numerous long mitochondria are stacked perpendicular to the basal membrane. **B.** Immunogold labelling for megalin localizes the receptor on microvilli of the brush border (mostly in their deepest third) and more intensely in apical coated pits (CP), endosomes (E) and recycling dense apical tubules (arrows) illustrating the endocytic pathway followed by the receptor. *From Christensen et al, 2012 (A) and Verroust and Christensen, 2002 (B).*

Figure 9 depicts the endocytic route followed by megalin, cubilin, and AMN, and illustrates the fact that these three elements acting together can be considered as a multiligand complementary apical endocytic receptor complex rapidly internalized and recycled back to the membrane.(Nielsen, Christensen, and Birn 2016)

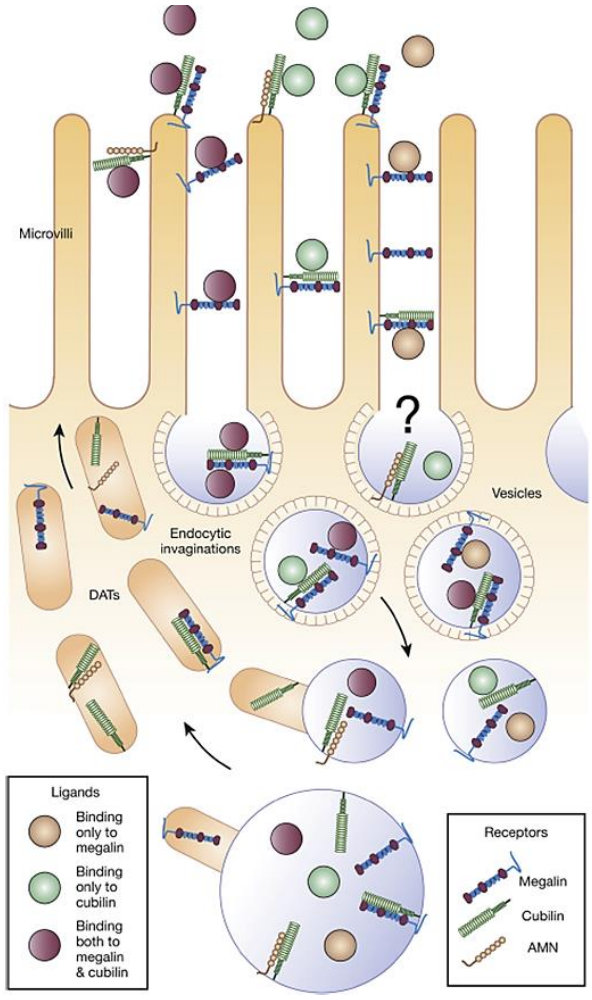

Figure 9. Proximal tubule endocytic pathway with cargo delivery to lysosomes and fast receptor recycling. At the brush border, megalin and cubilin are able to capture rapidly passing ligands, either private or shared (albumin, LMWP, vitamin-binding proteins, lipoproteins, iron-binding proteins…, see Table I). They also interact with one another, thereby supporting internalization of cubilin, which otherwise lacks a transmembrane domain and a NPXY rapid-internalization motif to cluster into clathrin-coated pits. Alternatively, cubilin can rely on its specific interaction with the dedicated transmembrane chaperone amnionless (AMN). Preference is no longer a concern if the three form a ternary complex. After clustering into clathrin-coated pits which pinch off as primary endocytic vesicles and fuse with acidified apical endosomes, ligands are released from their receptors. Unoccupied receptors are then quickly recycled to the apical membrane through dense apical tubules (DATs). *From Nielsen et al, 2016.*

For convenience, receptors are represented as long straight molecules. However, this conformation would cause steric hindrance since linear cubilin is >30 nm long as shown by electron microscopy (and presumably megalin even longer), while dense apical tubules (DATs) are only 30 nm in diameter. In reality, cubilin contains a hinge region allowing it to bend. In contrast to receptors, various cargoes are delivered to lysosomes where proteolysis generally follows quite rapidly.

In turn, this releases some essential components which are transferred into the internal milieu, either directly (vitamin A, iron) or indirectly (after conversion of 25OH-provitaminD into 1-25diOH-vitaminD, also named calcitriol, D3, by mitochondrial 1-alpha-hydroxylase). Potentially nephrotoxic drugs such as gentamicin are presumably retained on lysosomal phospholipids and cause phospholipidosis (reviewed in Nielsen, Christensen, and Birn 2016). An alternative, controversial model of massive albumin transcytosis across PTCs has been proposed by B. Molitoris and colleagues (Wagner et al. 2016) and is described in Figure 10. In this model, massive amounts of albumin ultrafiltrated from the plasma are retrieved intact through a two-step process. The first step, by which megalin mediates endocytic recapture of albumin from the proximal tubule (PT) lumen, followed by dissociation in endosomes, is generally accepted. However, the model differs from the conventional route of the cargo to lysosomes by invoking a second step in which secondary binding of albumin at the endosomal acidic pH to the FcRn receptor that cycles with the basolateral membrane (like LRP-1) drives transcytosis across the PTC and ligand dissociation at the neutral pH of the internal milieu (thus recycling into plasma). This model implies an unusually high albumin glomerular sieving coefficient, which was estimated from critical (thus criticized) measurements of albumin concentration in the urinary space by vital multiphoton microscopy.(Wagner et al. 2016)

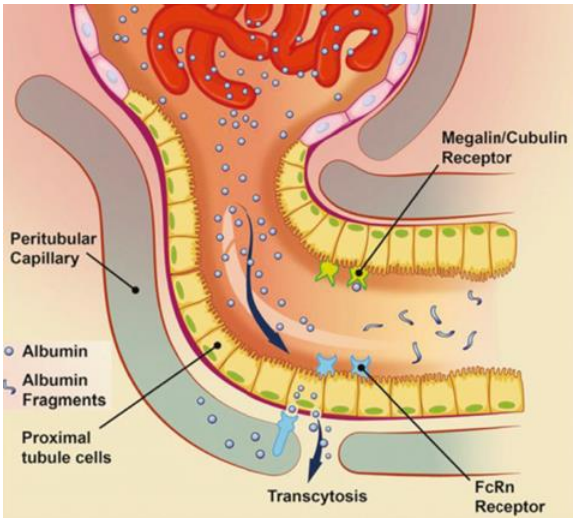

Figure 10. Alternative, controversial model of massive albumin transcytosis across PTCs. This hypothetical model, put forward by Molitoris and co-workers, proposes that massive amounts of albumin are ultrafiltrated across naturally leaky glomeruli but retrieved intact thanks to two-step process. This would involve endocytic recapture from the PT lumen via megalin at the apical pole and dissociation into endosomes as in the generally accepted model described at Figure9, but followed by secondary binding to FcRn receptor which drives transcytosis, back into the internal milieu (thus recycling). For Discusion, see text. From Wagner et al, 2016.

This pathway is qualitatively supported by appearance in blood of intact tagged albumin only expressed by podocyte. This indeed implies transcytosis through PTC to the plasma of the tagged albumin secreted into the urinary space. This process was abolished upon FcRnKO.(Tenten et al. 2013) However, absence of quantitation of this secretion in data by Tenten et al do not allow to conclude on the magnitude of the process and the overall model proposed by Molitoris and colleagues is contradicted by comparison of albumin synthesis and blood concentration in single podocin KO (to induce glomerular leak thus nephrotic

syndrome) with triple podocin+megalin+cubilin KO experiments (to suppress thefirst step of the proposed transcytotic route) : no further difference in plasma albumin concentration nor increased liver synthetic rate was observed when endocytic receptors were abolished.(Weyer et al. 2018) Anyhow, to the extent that the hypothetical transcytosis of *intact* albumin would not lead to the generation of cystine in PTCs, this controversial pathway can be neglected for the purpose of our thesis.

1.2. Structure and function of lysosomes, with emphasis on cystinosin

After a brief presentation of key features of cystinosin, the protein defective in cystinosis, I shall here summarize crucial information on lysosome structure and composition, biogenesis and functions, with emphasis on cystinosin whenever possible.

Cystinosin, the only known lysosomal membrane cystine transporter, acts as a H^+:cystine co-transporter, and exhibits a remarkably high affinity for cystine (Km for cystine of 75 microM when protonated as in acidified lysosomes *vs* 250 microM when facing a neutral environment (Ruivo et al. 2012), contrasting with the mM range for other AA transporters, such as PQLC2 for lysine and arginine.(Jezegou et al. 2012) This high affinity might be evolutionary related to the relatively low abundance of disulfide bonds in most proteins (albumin and thyroglobulin being exceptions), thus lower concentration of cystine released by proteolysis than for other AAs. Quantitative analysis by mass spectrometry of cultured human fibroblasts estimates cystinosin abundance at 5,000 copies per cell, or about 10 copies per lysosome on the average.(Thoene et al. 2013) In normal cells, this low abundance is normally compensated by the ongoing

fusion/fission of lysosomes, that randomizes digestive workload, proteolytic enzymes and membrane transporters. However, this low number indicates that cystinosin abundance is overall rate-limiting, so that heterozygotic cells for null mutations or deletion have a two-fold lower rate of cystine efflux than WT cells (discussed in Cherqui and Courtoy 2017).

The predicted cystinosin structure is a 7-TM integral membrane protein with a long flexible luminal domain bearing several N-glycosylation sites, one large cytoplasmic loop involved in trafficking of the short isoform and a C-terminal cytoplasmic differing between the two isoforms (Fig. 11). The canonical short isoform of cystinosin (367 AA in human) bears two lysosomal targeting sequences recognized by the AP-3 adaptor complex operating at the trans-Golgi network (TGN), one in the long cytoplasmic loop, the other at its C-terminus, thus is directly targeted to lysosomes (generally located in the perinuclear region, thus close to the TGN). In contrast, its longer isoform (400 AA), generated by alternative splicing, bears only one C-terminal trafficking motive recognized only by the AP-2 adaptor complex operating at the plasma membrane. Thus, the LKG long isoform first trafficks “by default” to the plasma membrane where a significant fraction may remain, thus complementing the dedicated cystine transporter, rBAT–b(0,+)AT. It is recaptured therefrom by cell surface clathrin-coated pits to reach lysosomes via endosomes. This pathway is thus shared with lysosomal acid phosphatase (see below, page 69).

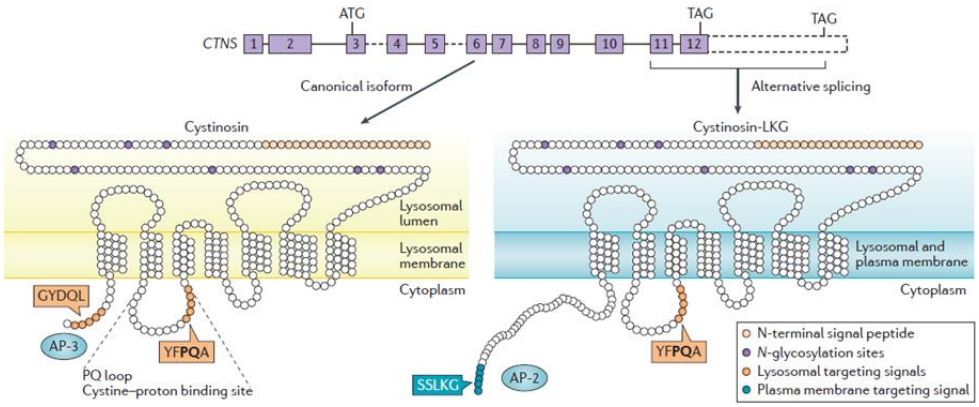

Figure 11. Structure of two cystinosin isoforms. The CTNS gene contains 12 exons (purple boxes) including exon 3 which carries the start codon (ATG) and exon 12 which has two possible stop codons (TAG). Therefore, by alternative splicing, CTNS encodes two isoforms of cystinosin. Both share the N-terminal signal peptide and present seven transmembrane domains but differ in their cytoplasmic C-terminal composition and subcellular localization. At left, the ubiquitous and most abundant, canonical isoform, exhibits two lysosome-targeting signals resulting into exclusive lysosomal localization: the usual tyrosine-based C-terminal motif GYDQL (recognized by the adaptor protein complex 3, AP-3, responsible for clustering of most lysosomal constituents into trans-Golgi clathrin-coated pits and leading to direct lysosomal targeting) and an unique additional YFPQA lysosomal targeting motif in the PQ loop, that also contains a cystine-proton binding site. At right, the C-terminal region of the cystinosin-LKG isoform, rarer, contains the SSLKG motif wich interacts instead with the AP-2 complex. Absence of GYDQL motif allows constitutive secretion of cystinosin-LKG from the trans-Golgi network to the plasma membrane where interaction of the SSLKG motif with the AP-2 complex, shared with megalin (a.o.), triggers endocytic trafficking and, presumably by default, retention into lysosomes. *From Cherqui and Courtoy, 2017.*

1.2.1. **Molecular anatomy of lysosomes**

Discovered in 1955 by Christian de Duve and his co-workers at Louvain University, the lysosome is a central acidic organelle involved in the luminal degradation of virtually every biological substrate by the activity of a comprehensive set of about sixty different *soluble* acid hydrolases highly concentrated in its acidic lumen. This enzymatic equipment thus includes endopeptidases, nucleases, glycosidases, lipases, phosphatases and sulphatases. Lysosomes are therefore able to fully hydrolyse a huge variety of biological substrates, including virtually all proteins, nucleic acids, glycosaminoglycans, sphingolipids and glycogen (when sequestered from the cytosol by autophagy). Of note, the lysosomal *membrane* also contributes pro-catabolic enzymes such as HGSNAT (for heparan-alpha-glucosaminide N-acetyltransferase) which catalyzes transmembrane acetylation of the non-reducing terminal glucosamine residues of intralysosomal heparan sulfate before its luminal hydrolysis by alpha-N-acetyl glucosaminidase. Likewise, acid hydrolases acting on membrane lipids need assistance by dedicated *activators*. For example, prosaposin (PSAP) is cleaved into four, non-redundant sphingolipid activator proteins (SAPs) which facilitate the catabolism of glycosphingolipids with short oligosaccharide groups in specialized intra-lysosomal vesicles. The prevailing model implies that saposins extract their substrate from the hydrophobic membrane environment for presentation to the hydrophilic catabolic site of the dedicated hydrolase to release sugar and ceramide.(Hill et al. 2018) However, this Section will dwell on novel aspects of lysosomes besides “digestive bags” and attempt to address the much broader scope of lysosomal functions that depend on the lysosomal membrane and extend beyond the simple degradation of macromolecules to include central metabolic signaling, regulated exocytosis and membrane repair.

The lysosomal compartment is confined by a 9 nm-thick biomembrane showing similarities with the plasma membrane with which it is connected by vesicular trafficking. The lysosomal membrane is composed of a single-lipid bilayer and harbors a variety of extrinsic or transmembrane proteins (Fig. 12A). ***Structurally abundant, heavily glycosylated proteins*** include LAMP-1 (lysosome-associated membrane glycoprotein 1), a major sialic acid-rich component of luminal glycocalyx, thus originally thought to merely protect the structural integrity of lysosomal membrane as an electrostatic shield against acid hydrolases. However, LAMP-1 has since been shown to mainly participate in lysosomal trafficking by mediating the attachment of lysosomes to the long-distance microtubule-based transport machinery, despite its very short (11AA) cytoplasmic tail (unfortunately the representation of LAMP-1 orientation is incorrectly inversed at Figure 12).(Huynh et al. 2007) Of note, final fusion events depend on actin polymerization. Other lysosomal membrane proteins play a role in trafficking and fusion, be it for vesicle recognition (SNAREs) or fusion catalysis (Rabs).

Lysosomal ion channels comprise (i) the stem of v-ATPase complex which support the luminal very acidic pH by allowing ATP-driven import of protons from the cytosol into the lysosome; (ii) ClC-7, and its obligatory partner, osteopetrosis-associated transmembrane protein 1 (Ostm 1), for coupled chloride import necessary for electroneutrality (for a review, Jentsch and Pusch 2018); and (iii) mucolipin-1 (MCOLN1) for calcium uptake, a recently recognized lysosomal function yet presumably an ancestral acquisition. Indeed, the bloodstream parasite responsible for sleeping sickness, *Trypanosoma brucei* which diverged from mammalian cells since > 200 million years, comprises acidified vesicles endowed with huge calcium storage, named “acidocalcisomes”. (Coppens et al. 1993) Calcium storage is essential for lysosomal signaling, for

lysosomal biogenesis and autophagy as well as for lysosome exocytosis.(Medina et al. 2015; Medina and Ballabio 2015; Sbano et al. 2017)

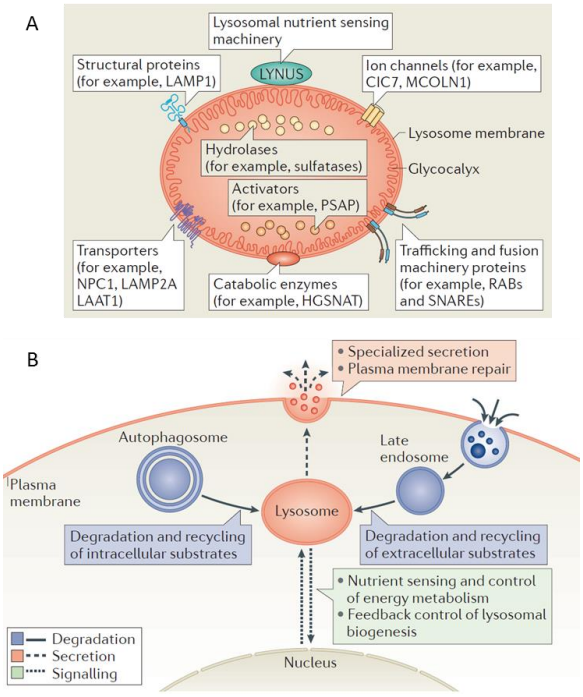

Figure 12. Structure and functions of the lysosome. A. *Schematic structure of the lysosome.* For details, see Text. ***B. Lysosomal functions***. First represented in blue, *intracellular degradation and monomer recycling* of intracellular (autophagy) or extracellular (endocytosis) substrates follow lysosomal fusion with autophagosomes or late endosomes, respectively. Depending on the cellular needs, the monomeric products can either be reused for assembly of new cellular components, or fully degraded to provide energy. A second specialized function to specific cells or situations, depends on *exocytosis* of content or membrane and is represented in red. Through lysosomal Ca^{2+} regulated exocytosis, lysosomes are able to secrete their content in the extracellular medium. This function mediates specialized physiological processes (release of lytic vesicles by liganded cytotoxic T lymphocytes, bone resorption by osteoclasts, spreading of pigmentation by melanocytes,…). By the same pathway and after the rapid centrifugal (peripheral) migration, lysosomes can insert their own membrane to repair a damage to the plasma membrane. As a major recent shift of paradigm applicable to all cell types including yeast, lysosomes are now recognized as a central metabolic regulator via *nutrient sensing and complex signaling* pathways (represented in green). Especially, the lysosomal localization of mTORC1, a central protein complex controlling cell growth or autophagy, suggests a crucial role in the balance between anabolism and catabolism. This notably involves LYNUS and the regulation of TFEB, a master transcription factor controlling lysosomal biogenesis. *From Settembre et al, 2013.*

The extracellular space is an oxidative compartment. In contrast, a ***reducing lysosomal environment*** seems essential, not only to support the activity of cathepsins B, C and E (named cysteine proteases as they depend on reduced cysteine in their catalytic site), but also to reduce internal disulfide bonds in proteinaceous target. For exemple, disulfide bonds of albumin internalized into PTC lysosomes are reduced in lysosomal lumen. This allows protein unfolding, which is required for accessibility of endoproteases, including cysteine proteases and the aspartyl protease, cathepsin D. Of note, reduction of internal disulfide bonds depends ***on inflow of cysteine from the cytosol by a still elusive transporter***, and cystine released by the reaction does not arise from the protein disulfides *per se*, but from the concomitant oxidation of incoming cysteine.(Lloyd 1986) However, once in lysosomes, free cysteine cannot become directly oxidized into free cystine.(Thoene et al. 1977) Under special conditions, lysosomal proteases are also involved in antigen processing (interrupted degradation generates an epitope), initiation of apoptosis (cathepsin release into the cytosol to activate caspases) and degradation of the extracellular matrix (upon exocytosis e.g. by osteoclasts into bone-resorbing lacunae).

Complex substrates (polymers or complex molecules) carried out by vesicular trafficking along endocytosis or by autophagy reach lysosomes. Since lysosomes are the intracellular organelles dedicated to the full degradation of these substrates, it follows that specific outward transporters for all end-products (“monomers”) released by macromolecule hydrolysis are necessary. Of note, there is also an inward transporter for unfolded proteins to be degraded by chaperone-mediated autophagy, named LAMP-2A. ***Transporters for monomers*** can be exemplified in the context of my thesis by cystinosin for cystine and PQLC2 for basic amino-acids. ***Signaling components*** of the mTOR-complex including lysosomal nutrient sensing machinery (LYNUS) make the lysosome a central

metabolic regulator. LYNUS is composed of several proteins including the mammalian target of rapamycin complex 1 (mTORC1) and the v-ATPase complex which allow LYNUS to sense lysosomal nutrient levels. If the cellular environment is rich enough in nutrients such as amino acids, LYNUS interacts with the transcription factor EB (TFEB), a master transcription factor controlling lysosomal biogenesis, which is then phosphorylated by mTORC1 on the lysosomal surface and thus inactivated. During starvation, LYNUS releases mTORC1 into its inactive form, thus unable to phosphorylate and sequester TFEB at the lysosome membrane. Once dephosphorylated by calcineurin, TFEB translocates into the nucleus, where it induces its own transcription and up-regulates the expression of several genes involved in the lysosomal-autophagy pathway. This sequence of events supports a key homeostatic mechanism: when food is abundant, autophagy is repressed; when food is scarce, cells survive on autophagy. Lysosome biogenesis is thus triggered by TFEB, and a simple way to do so is to load lysosomes by endocytic supply of undigestible material such as sucrose. Conversely, when endocytosis is interrupted (e.g. by megalin KO in PTCs), the lysosomal compartment shrinks (“no endocytosis, no lysosomes”). TFEB promotes cellular clearance by several way (e.g. lysosomal biogenesis, exocytosis, and autophagy), and its signaling can be triggered by the drug genistein. This drug thus offers an interesting perspective for cystinosis in which lack of cystinosin reduces TFEB expression and induced TFEB nuclear translocation.(Rega et al. 2016)

In terms of trafficking events, lysosome biogenesis requires assembly of its constituents in the secretory apparatus, then derouting to the lysosomal pool. ***Lysosomal targeting of most acid hydrolases*** depends on a unique mannose 6-phosphate motif, which is built up by the sequential action of a phosphotransferase and a phosphodiesterase in the secretory apparatus and which is further recognized by two different mannose 6-phosphate receptors

(MPRs), respectively cation-independent or -dependent, able to drive the protein into the late endosome via AP-3:clathrin complexes at the trans-Golgi network. Of note, another possible mechanism for lysosomal localization was recently identified for β-glucocerebrosidase and is mediated in part by the lysosomal receptor LIMP2 (lysosome integral membrane protein 2; also known as SCARB2), via the same direct intracellular route.(Honing, Sandoval, and von Figura 1998) An alternative route is illustrated by the soluble ***lysosomal acid phosphatase*** (LAP). This paradigmatic enzyme, at the origin of the discovery of lysosomes, is responsible for final excision of phosphate at the sixth carbon of mannose of the other lysosomal enzymes, thus requires a distinct delivery to avoid premature loss of this recognition system. LAP is first encoded as a transmembrane protein and its journey involves first transfer to the plasma membrane and secondary routing to lysosomes by AP2-mediated endocytosis still as a transmembrane protein, with final release from the membrane once in lysosomes by cathepsin D.(Braun, Waheed, and von Figura 1989; Gottschalk et al. 1989; Peters et al. 1990)

Newly synthesized lysosomal membrane proteins are mostly directly targeted via AP-3:clathrin recognition as most lysosomal hydrolases. The canonical (short) cystinosin isoform bearing *two lysosomal targeting signals* (YFPQA in the cytoplasmic loop between the 5^{th} and the 6^{th} transmembrane domain; and GYDQL near the C-terminus, recognized by AP-3) makes no exception.(Andrzejewska et al. 2015) However, alternative splicing of its 12th exon generates a longer isoform without the GYDQL signal (thus not recognizable by AP-3) but with a C-terminal SSLKG motif allowing recognition by AP-2). This long, SSLKG isoform thus reaches the plasma membrane before secondary endocytosis, exactly as LAP, underlining the weak targeting potential of the first, YFPQA motif.(Bellomo et al. 2016)

1.2.2. **Functions of lysosomes**

As stated above, three main types of lysosomal functions can be described (Fig. 12B).

Lysosome-mediated degradation

Three pathways transport extracellular and intracellular substrates to the lysosome. Firstly, ***endocytosis*** (this term includes several processes such as clathrin-mediated endocytosis, caveolin-mediated endocytosis phagocytosis, macropinocytosis,) leads extracellular macromolecules and integral membrane proteins to lysosomes, as detailed previously by the example of apical receptor-mediated endocytosis. Of note, only clathrin-mediated endocytosis applies to PTCs, which do not express caveolin and do not show phagocytosis nor macropinocytosis Gradually, the internal pH of endocytic organelles decreases to values down to about 5 in late endosomes/mature lysosomes (due to the activity of the highly expressed proton-pumping v-ATPase). This low pH allows the release of acid hydrolases from MPRs in the late endosome lumen and recycling of unoccupied MPRs back to the trans-Golgi network.

Secondly, ***autophagy***, triggered under conditions of cellular stress such as nutrient deprivation, growth factor depletion, infection or hypoxia, is a regulated catabolic pathway used by cells to allow the degradation and monomer recycling from non-vital or dysfunctional components such as protein aggregates or misfolded proteins, oxidized lipids, damaged organelles and intracellular pathogens; or to provide energy to survive. Autophagy is an important process ensuring cellular homeostasis through its implication in development, differentiation, cell repair, immunologic defense as well as protein quality control.(Dikic and Elazar 2018; Yang et al. 2013) In microautophagy, invagination

of the lysosomal or endosomal membrane directly leads to internalization of cytosolic proteins while macroautophagy requires the formation of independent autophagosomes, double-membrane vesicles, that sequester cytoplasmic cargo and then fuse with lysosomes. Currently, macroautophagy and microautophagy can be in bulk or exceptionally selective depending on the material sequestered. In macroautophagy, cytosolic receptor proteins, including sequestosome 1 (p62), assisted by LC3, assemble cargo and ensure the formation of a limiting membrane around the cargo, the autophagosome. Selective degradation by microautophagy is possible through interaction between target proteins and surface proteins of lysosomes or late endosomes. In this process, a cytosolic chaperone, the heat shock cognate 70 kDa protein (HSC70), is involved in selective protein degradation by microautophagy.(Kaushik and Cuervo 2018)

Thirdly, and always selective, ***chaperone-mediated autophagy (CMA)*** is a very distinct mechanism implying recognition of individual proteins to be disposed of by a broad targeting motif, KFERQ-*like*, for selective degradation (for review, Kaushik and Cuervo 2012). This KFERQ-like motif-bearing protein is recognized by a cytosolic chaperone, the HSC70-*containing* complex. Upon recognition, the protein is unfolded and driven to the lysosomal membrane for translocation into the lysosomal lumen through a unique receptor, named lysosome-associated membrane protein type 2A (LAMP2A). What makes CMA unique compared to other types of autophagy is that proteins cross the lysosomal membrane one by one with high selectivity. Once in the lysosome, CMA substrates are degraded by the well-known panoply of acid proteases.

Lysosomal exocytosis

Besides the classical secretion mediated by the ER-Golgi-secretory vesicle pathway, lysosomes can secrete their content by lysosomal exocytosis in specific

cells or conditions. Indeed, upon appropriate stimulation, lysosome can migrate along microtubules from their usual perinuclear region (when the end-minus motor, dynein is dominant) towards the plasma membrane (thus switching to end-plus motor, kinesin) and, through lysosomal Ca^{2+}-regulated exocytosis (involving the important mediator MCOLN1), the lysosomal membrane fuse with the plasma membrane leading to the release of the content in extracellular medium. Lysosomal exocytosis involves a complex molecular machinery including, on lysosome, the vesicle SNARE (v-SNARE) VAMP7, the Ca^{2+} sensor synaptotagmin VII (SYTVII) and several Rab proteins and, on plasma membrane, the target SNAREs (t-SNAREs) SNAP23 and syntaxin 4.

Lysosomal exocytosis was long known to mediate specialized physiological processes such as release of lytic vesicles by liganded cytotoxic T lymphocytes (degranulation), bone resorption by osteoclasts or pigmentation spreading by melanocytes. Thus, lysosomal exocytosis was considered a unique attribute to specialized cell types such as hematopoietic cells but it is now known to be shared by all cell types, as a fast and effective way for urgent plasma membrane repair.(Andrews and Corrotte 2018) Indeed, after the rapid centrifugal (from usual perinuclear location to plasma membrane) migration, lysosomes can insert their own membrane by fusion to repair the injured plasma membrane. Of note, TFEB is also implied in lysosomal exocytosis regulation by increasing expression of genes governing lysosomal dynamics and local increase of subcellular Ca^{2+} concentration that triggers fusion upon regulated release from the lysosomal store (e.g. MCOLN1).

Signalling from lysosomes

Over the last decade, the lysosome has further emerged as a central metabolic regulator involved in cell homeostasis and growth through nutrient

sensing and complex signaling pathways (for review by Sabatini's lab, see Efeyan, Comb, and Sabatini 2015). This unanticipated, revolutionary concept has become evident since the demonstration, in yeast then in mammalian cells, that the kinase complex first known as mammalian target of rapamycin complex 1 (mTORC1), a master cell and organism growth regulator which is part of the LYNUS machinery, exerts its activity on the lysosomal surface where it is activated in response to nutrient availability. A posteriori, the beauty of the system is that lysosomal localization of mTORC1 is strategically placed to integrate the balance between anabolism and catabolism. mTORC1 activation is finely tuned according to the cellular needs and thus depends on the energy level, the cellular stress, other signals such as growth factors and hormones, as well as availability of amino acids, glucose and oxygen.(Settembre et al. 2013; Settembre et al. 2012; Laplante and Sabatini 2012; Russell, Yuan, and Guan 2014)

In presence of nutrients, mTORC1 is recruited and retained at the lysosomal membrane by several small GTPases, called Rag GTPases, and the Ragulator complex. The recruitment of mTORC1 to the lysosomal surface brings it closer to its activator, the small GTPase Rheb that belongs to the superfamily of Ras GTPases. Once activated, mTORC1 stimulates the biosynthesis of proteins, mRNAs and lipids as well as ATP production, while repressing autophagy. Indeed, downstream signaling involves phosphorylation of key effector or regulatory proteins such as ribosomal protein S6 kinase (S6K1) and eukaryotic translation initiation factor 4E-binding protein (phosphorylation of 4E-BP1 causes its release from the eukaryotic translation initiation factor 4E (eIF4E) which is therefore free to initiate protein synthesis). Moreover, it leads to autophagy inhibition by repressing lysosomal biogenesis and catabolic programs mainly via phosphorylation of the general transcription factor of the CLEAR pathway, TFEB. When phosphorylated, TFEB is sequestered in the cytoplasm, thus silenced. Only

upon dephosphorylation by calcineurin, TFEB can reach the nucleus to stimulate transcription of its target genes (the same process applies to MITF and TFE3, also involved in lysosomal biogenesis and autophagy). While generous amino acids and glucose availability promote the accumulation of active conformation, starvation transforms Rag GTPases into an inactive conformation, thereby releasing inactive mTORC1 from lysosomes, unleashing autophagy so that cells adapt to exogenous AA shortage by feeding upon itself. These observations underline that mTORC1 activity depends on lysosome AA release. Of note, long-term mTOR inhibition leads to megalin downregulation and proteinuria in kidneys.(Gleixner et al. 2014) The complex LYNUS machinery allows the lysosome to play a central role in nutrient sensing and metabolic signal transduction. Among the large number of its important interactions, the fifth loop of cystinosin plays an important role in the interaction with the mTORC1 complex, raising the fascinating hypothesis of coupled export and sensing.(Andrzejewska et al. 2016)

1.2.3. **The various causes and manifestations of lysosomal diseases**

Although each one is rare, lysosomal storage diseases (LSDs) are many, thus represent together a significant medical burden. LSDs considerably differ both in frequency and manifestations. Some appear discreetly in adulthood (such as Fabry disease, due to accumulation of globotriaosylceramide, abbreviated GL-3 or GB-3, upon defect of alpha-galactosidase), other are lethal from the first years of life (such as Morquio disease, due to accumulation of glycosaminoglycans). The symptoms are very variable, ranging from neurological problems to organ dysfunctions, stunted growth or bone abnormalities. As diverse as they may be, LSDs have one thing in common: the homogenous intra-lysosomal accumulation of either one specific unmetabolized substrate, when one hydrolytic activity falls below a very low level (this is the case for most of them, the first discovered and

probably best example being selective glycogen accumulation in Pompe disease due to defective acid maltase); or a particular catabolic end-product, when its transporter is defective (this is the case for cystine in cystinosis and sialic acid in de Salla disease).

Although the genetic and molecular bases of accumulation have been identified for the various LSDs, there are still many unclear aspects concerning the biochemical and cellular consequences that lead to dysfunctions characteristic of each of them, apparently in correlation with the type of accumulated substrate. Better understanding of the processes involved in these diseases could allow the development of specific drug treatments or replacement therapies, currently limited to a few LSDs, and might provide an improved knowledge of the robust physiology of healthy cells. Given the multitude of non-redundant, irreplacable lysosomal constituents, the absence or deficit of any of these can lead to an autosomal recessive disease with accumulation of one specific unprocessed macromolecule or non-exportable catabolic product. Usually, the characteristic compound gives its name to the disease, for example cystinosis when cystine accumulates. Rarely multiple compounds accumulate causing inclusions (I-cell-disease). One of these diseases, called nephropathic cystinosis, is the main subject of this thesis. Before describing it in detail, this section defines the possible causes of LSDs with some examples (Fig. 13).

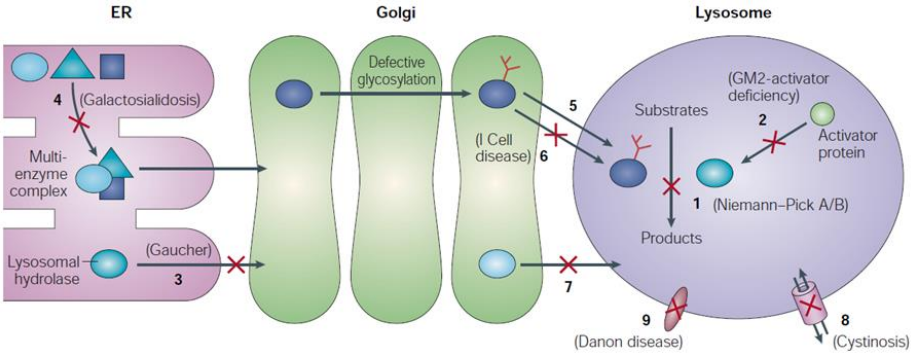

Figure 13. Various causes of lysosomal storage diseases (LSDs). Mutations can directly lead to non-functional acid hydrolases (1) or affect activators that are unable to provide optimal hydrolase activity (2). A mutation can also cause misfolding of the enzyme that cannot leave the endosplasmic reticulum (RE) to join the lysosome (3). Deficit of any component of multi-enzyme complexes that ensure the delivery of acidic hydrolases from the ER to the lysosome are typical of I-cell disease. (4). Defective glycosylation of lysosomal enzymes in Golgi can lead to a decrease in the intrinsic catalytic activity or stability of the enzyme (5) or prevent transport to the lysosome if it affects build-up or recognition of mannose 6-phosphate (key recognition marker for targeting many hydrolases to lysosomes) (6). The transport of the enzyme from the Golgi to the lysosome can also be disrupted independently of the glycosylation (7). In addition to soluble hydrolytic enzymes, membrane proteins of the lysosome can also be at the basis of lysosomal diseases. *Most important for this thesis, mutations can abolish the transport of molecules (the export of metabolites) across the lysosomal membrane (8)* or impact lysosomal proteins involved in the stability and integrity of the lysosome as well as in the process of chaperone-mediated autophagy (9). Finally, LSDs could be due to defects in other components (adaptor proteins, coat proteins or lysosome-specific receptors) of transport pathways to and from lysosomes that would mis-target lysosomal hydrolases or membrane proteins. *From Futerman and van Meer, 2004.*

Most LSDs are caused by mutations that ***directly affect the catalytic function*** of lysosomal acid hydrolases. Mutations can directly lead to absent or non-functional acid hydrolases, or affect activators required for optimal hydrolase activity. For example, Niemann-Pick disease types A and B, which are inherited and severe metabolic disorders due to sphingomyelin accumulation in lysosomes, are due to mutations in the SMPD1 gene leading to impaired activity of lysosomal sphingomyelinase. Symptoms include hepatosplenomegaly, thrombocytopenia, neurological dysfunctions, dementia and seizures. Alternatively, ***no protein reaches the lysosome*** due to a variety of causes. This can result from ***large deletions*** or more subtle mutations causing ***misfolding*** in the endoplasmic reticulum (RE) preventing to reach the lysosome. This is the case in Gaucher disease, due to a deficient glucocerebrosidase or to a deficient saposin-C activator, causing accumulation of glucocerebroside in cells of the macrophage-monocyte system, and resulting especially in hepatosplenomegaly, anemia and bone pain or overt fractures***. A variant on this theme*** originates from deficit of any component of multi-enzyme complexes that ensure the ***delivery*** of acidic hydrolases from the ER to the lysosome which is typical of I-cell disease. ***Multiple defects can result from impaired glycosylation of lysosomal enzymes*** in the secretory pathway, as they can lead to a decrease in the intrinsic catalytic activity or stability of the enzyme, or prevent transport to the lysosome when preventing build-up or recognition of mannose 6-phosphate (key recognition marker for targeting many hydrolases to lysosomes). Of note, transport of the enzyme from the Golgi to the lysosome can also be disrupted independently of the glycosylation. An interesting case is ***stability in lysosomes***, which indeed poses the problem as to how lysosomal enzymes resist proteolysis. For example, galactosialidosis, a glycoprotein storage disease, is due to mutations in the CTSA gene encoding lysosomal protective protein/cathepsin A (PPCA) and leads to

combined deficiency of beta-galactosidase (β-GAL) and neuraminidase 1 (NEU1). A defective PPCA is not able to form a complex with β-GAL and NEU1, a configuration that ensures activity and stability of both enzymes in lysosomes. It is characterized by coarse facial features, macular cherry-red spots, angiokeratoma (dark red spots on the skin), vertebral deformities, epilepsy and ataxia.

In addition to soluble hydrolytic enzymes, ***membrane proteins of the lysosome*** can also be at the basis of lysosomal diseases. Most important for this thesis, mutations can abolish the ***transport of molecules*** (the export of metabolites) across the lysosomal membrane or impact lysosomal proteins involved in the ***stability and integrity of the lysosome*** as well as in the process of chaperone-mediated autophagy. Finally, LSDs could be due to ***defects in other components*** (adaptor proteins, coat proteins or lysosome-specific receptors) of transport pathways to and from lysosomes. For example, Danon disease is an X-linked lysosomal and glycogen storage disorder associated with a mutation of the LAMP2 gene. Symptoms include hypertrophic cardiomyopathy, skeletal muscle weakness, and intellectual disability.(Futerman and van Meer 2004)

1.2.4. Natural course and therapeutical options for lysosomal storage diseases

The primary cause of the LSDs, intra-lysosomal accumulation of unmetabolized substrates or retained degradation products, gives rise to a variety of symptoms which depend of the overload nature but also suggest that several secondary biochemical and cellular pathways are affected leading to the pathology. Indeed, not every lysosomal accumulation is pathogenic: a remarkable example is malondialdehyde, also known as “lipofuchsin”, which accumulates

with age and can contribute up to 1/5th of neuronal cytoplasm after 80 years of age. So far, little is known about how lysosomal accumulation of undigested metabolites might impact downstream pathways and cause disease. However, several pathways are suspected to contribute to disease progression.

Substrate overload could possibly impact on ***lysosomal stability, integrity or permeability*** leading to the release of acidic hydrolases and accumulating metabolites into the cytosol with disastrous consequences for the cell. This can be exemplified by storage of crystals or ROS-favoring compounds such as hemoglobin or hemosiderin. Undegraded metabolites overload in lysosomes could also block ***intracellular trafficking*** to, from and between lysosomes because of the limiting lysosomal storage capacity. As stated above, lysosome is involved in cell homeostasis and growth through nutrient sensing and complex signaling pathways. Several ***defective signaling pathways*** resulting from a deficient or absent actor can carry on multiple outcomes such as ***altered gene expression***. Other possible secondary processes could be mentioned such as the ***activation of cell-death signaling***, ***alteration of plasma membrane lipid content*** (affecting receptor responses and subsequent signaling events), ***inflammatory cascade***, ***the unfolded protein response*** (UPR, leading to ER stress and apoptosis) and ***dysregulation of autophagy***.(Futerman and van Meer 2004; Boustany 2013)

Unfortunately, we know very little about all these aspects for most LSDs which have thus few therapeutical options at the moment: supportive medical options are merely restricted to alleviate symptoms and to manage disease consequences (e.g. loss replacement in case of life-threatening acute electrolyte loss due to the Fanconi syndrome of cystinosis) rather than etiological therapy. Similarly, splenectomy is a common option to reduce thrombocytopenia or anemia in Gaucher disease and other LSDs. In late-stage nephropathic cystinosis,

kidney transplantation is often inevitable. It is thus crucial to better understand the cellular basis of each LSD to find new specific or complementary treatments (Fig. 14).

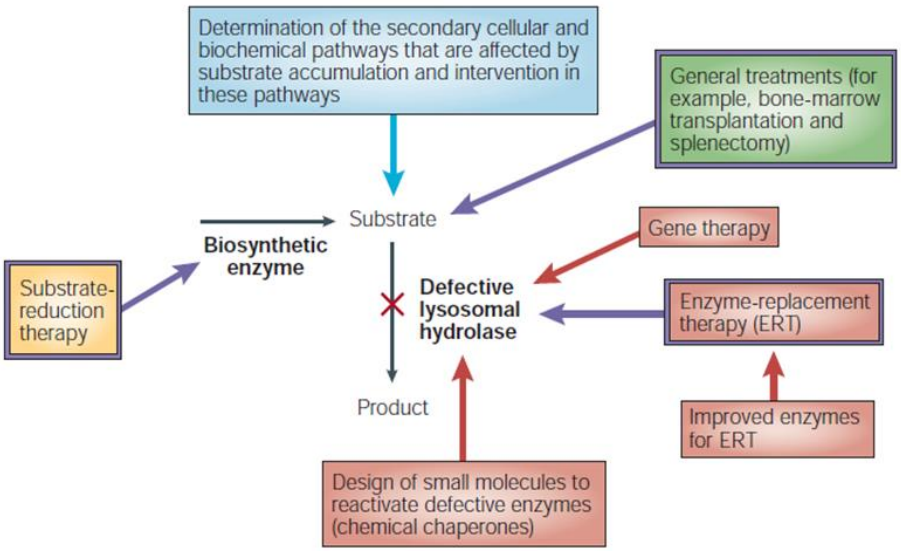

Figure 14. Therapeutic strategies in lysosomal storage diseases (LSDs). Depending on their target, LSDs treatments can ideally be divided into four conceptual groups. The therapy can (1) directly target an enzymatic defect (red, e.g. enzyme replacement therapy such as regular infusion of recombinant glucocerebrosidase in Gaucher disease; or more generally bone marrow transplantation which provides healthy cells secreting functional lysosomal enzymes); (2) the source of the accumulating substrate or substrate rerouting to a preserved pathway (yellow, e.g. substrate-depletion therapy such as cysteamine in cystinosis, see below); (3) the symptoms of the disease (green, e.g. kidney transplantation in late-stage nephropathic cystinosis) or biochemical signaling pathways that are disrupted in LSDs (blue; more hypothetical). Unfortunately, most LSDs are not yet well understood, characterized and diagnosed and therefore cannot benefit from specific and definitive treatments. *From Futerman and van Meer, 2004.*

Directly targeting an enzymatic defect is a rational, but often theoretical solution. Indeed, enzyme replacement therapy (ERT) such as regular infusion of recombinant glucocerebrosidase in Gaucher disease or bone marrow transplantation that provide healthy cells secreting functional lysosomal enzymes, is the most successful available treatment for LSDs. The main challenge in this treatment is to target the enzyme to the defective cells. A possibility, already used in several LSDs, is to produce a recombinant enzyme bearing a recognizing signal for a specific receptor which could allow endocytosis and thus delivery to lysosomes. Many works are trying to improve the efficacy of ERT by better targeting the affected cells and/or by increasing the stability or catalytic efficiency of recombinant enzymes.

Although knowledge is still limited regarding the affected metabolic pathways in LSDs, ***specific substrate-depletion therapy*** could aim to prevent the metabolic and cellular defects resulting from accumulation of undegraded substrates. To prevent this accumulation, drugs can target the source of the accumulating substrate (partial synthesis inhibition) or redirect the substrate to a preserved pathway. The scope of this option appears broader and is already applicable in certain diseases, as exemplified by cystine depletion with diligent early cysteamine therapy in nephropathic cystinosis, which proves remarkably helpful when patients comply.

Logically, specific ***gene therapy*** should represent the most effective treatment for LSDs but remains a still very controversial option for the moment. However, several *ex vivo* and *in vivo* gene transfer methods have been tested to transfer the relevant genetic material into defective cultured cells leading to enzyme activity reconstitution. Unfortunately, these methods are not yet generally applicable to humans for the moment. Two particular cases however

are already quite appealing. The first one is pharmaceutical correction of point mutations interrupting transcription, based on drug-induced jump-over the mutation. Proof-of-principle was offered by gentamicin against the W138X frequent mutation of the cystinosin gene in the Province of Québec, Canada. Paul Goodyer and colleagues discovered that gentamicin, then a more specific compound, proved effective to restore cystinosin expression in cultured cells bearing this mutation (Goodyer, personal communication to PJC and manuscript in revision). The second case is lentivirus-based *ex vivo* correction of patient's hematopoietic stem cells before autologous transplantation. This approach is actively pursued by Stephanie Cherqui for the first clinical trial to be launched in the near future, as recently announced on the website of the Cystinosis Research Foundation.

Stem cell therapy is indeed receiving considerable attention, in particular in cystinosis. Conceivably, stem cells would be attracted into diseased tissue and (i) replace dead cells, or (ii) fuse with suffering cells to form polyploid nuclei including normal gene, or (iii) secrete microvesicles or exosomes bearing correcting normal mRNAs or normal proteins. The latter mechanism has been recently evidenced *in vitro* and *in vivo*.(Iglesias et al. 2012; Thoene et al. 2013; Naphade et al. 2015; Gaide Chevronnay et al. 2016) Of great interest, the two last papers have demonstrated that hematopoietic stem cells engrafted into cystinotic mice can send their own proteins across basement membrane surrounding diseased proximal tubules or even penetrate into diseased thyroid follicles. This correlated with almost normalization of thyroid histology and function (see Appendix 2).

1.3. The case of nephropathic cystinosis: a lysosomal transport disease

1.3.1. **Etiology, cause and diagnostic**

Belonging to lysosomal storage diseases, ***nephropathic cystinosis*** is a rare autosomal recessive disease due to inactivating point mutations up to full deletion of the *CTNS* gene, located on chromosome 17p13, which encodes cystinosin, the lysosomal cystine transporter described above.(Gahl, Thoene, and Schneider 2002) Defective cystinosin leads to an accumulation of cystine in all organs. In developed countries, the general incidence of cystinosis is about 1:100 000 - 1:200 000 live births but much higher incidence can be observed in isolated communities. For example, Brittany stands out with 1 case every 26 000 births while the rest of France reports only one case per 326 000 births. On the contrary, long isolated communities could have been spared, such as Finland.(Manz and Gretz 1985; Bois et al. 1976) Underestimation due to lack of diagnosis of cystinosis is likely in large countries such as Russia, India and China.(Kir'ianov, Bazhenov, and Stetsenko 1992; Tang et al. 2009; Yang, Hu, et al. 2015)

Among the three types of cystinosis (infantile, juvenile and non-nephropathic or ocular), infantile cystinosis is the most frequent and most severe form and is referred to as “cystinosis” in this manuscript.(Cherqui and Courtoy 2017) Its earlier signs result from early involvement of kidney PTCs (hence renal Fanconi syndrome and evolution to end-stage renal failure) and corneal cystine deposits (hence photophobia). Milder and rarer than the multi-systemic infantile cystinosis, juvenile and ocular cystinosis manifest around 12 years of age and in adulthood respectively. Juvenile type of the disease leads to photophobia and a combination of glomerular and tubular alterations responsible for proteinuria,

eventually leading to end-stage renal disease (ESRD) while ocular cystinosis is characterized by photophobia without renal dysfunctions.

The disease was first described in 1903 when pathological cystine crystals were observed in the liver and spleen of a young infant who died after dehydration and growth failure.(Baumner and Weber 2018) In the infantile (nephropathic) form, cystinotic children are normal at birth but develop growth retardation, rickets and signs of kidney dysfunction, such as polyuria and polydipsia, in the first year of life. Without treatment, renal failure may lead to renal insufficiency before 10 years of age and to death in the second decade of life. If started early (before 5 years of age and preferably earlier), cysteamine treatment, described in detail below, can delay the onset of renal failure to about 20 years of age.(Cherqui and Courtoy 2017) Early diagnosis therefore represents a major point regarding the clinical future of the cystinotic patient. At this stage, three methods are available to establish the diagnosis of cystinosis. ***Detection of elevated cystine levels in leucocytes*** by high-performance liquid chromatography or liquid chromatography-tandem mass spectrometry (LC-MS/MS) is very sensitive and accurate, thus currently the standard method. ***Genetic diagnosis*** by gene sequencing of the relatively small CTNS gene (12 exons but only 10 are coding) is also a common confirmatory tool although more time-consuming and ineffective for 5% of patients in whom the mutation is profoundly intronic, in the promoter region or an infrequent deletion or duplication. Also used to confirm the diagnosis, ***detection of corneal cystine crystals*** is a reliable and affordable method, the main one in developing countries, but nevertheless requires some experience of the ophthalmologist to identify crystals. Of note, the late appearance of corneal crystals (during the second year of life) may unfortunately delay the diagnosis, thus treatment.(Elmonem et al. 2016) Of note, the avascular cornea does not respond to oral cysteamine therapy and crystal intensity

therefore cannot be used to evaluate the systemic response to the drug.(Veys et al. 2017)

1.3.2. **Cystinosis as multisystemic disease**

As stated above, cystinosis is due to accumulation of cystine in every tissue of the body. At acidic pH and high concentration, cystine precipitates and forms crystals which are typical of the disease. Kidneys, having an important reabsorption function, are particularly sensitive to the cystine accumulation and are thus firstly impacted with the most serious and early consequences. However, this multi-systemic disease leads to alteration of many other organs such as thyroid that we studied in detail (see Appendix 1 and 2). This section will attempt to give an overview of cystinotic symptoms (Fig. 15).(Baumner and Weber 2018)

1.3.2.1 Kidneys and renal Fanconi syndrome

In cystinosis, the renal phenotype is the earliest, worst and most frequent. Renal impairment is characterized by a Fanconi syndrome whose clinical signs become evident from 6 months of age and a progressive loss of glomerular function leading to end-stage renal disease.

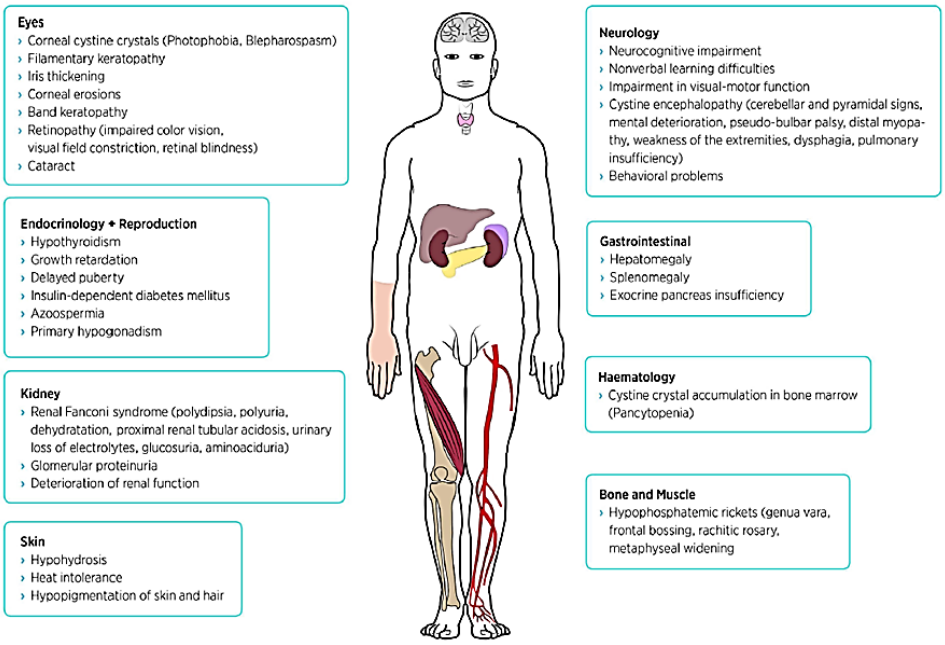

Figure 15. Cystinosis, a multisystemic disease. Cystinosis is due to defective cystinosin, the only known cystine transporter at the lysosomal membrane. Since all cells in the body contain lysosomes, cystinosis affects all organs including kidneys and eyes from the first year as evidenced by Fanconi syndrome and corneal crystals, thyroid and other endocrine organs in the first decade, then bones and muscles and eventually brain. This figure presents a comprehensive list of natural disease complications. *From Baumner and Weber, 2018.*

Renal Fanconi syndrome consists of a generalized dysfunction of the proximal tubule, characterized by urinary loss of water, sodium, potassium, bicarbonate, magnesium, carnitine, calcium, phosphate, amino acids, glucose and low molecular weight proteins (LMWPs such as beta-2-microglobulin, alpha-1-microglobulin, retinol-binding protein) to intermediate molecular weight proteins (IMW such as albumin, transferrin, vitamin D binding protein).(Elmonem et al. 2016; Cherqui and Courtoy 2017) In the Results of this work in a mouse model of

cystinosis, we will show that the early loss of expression of key apical proximal tubular endocytic receptors and transporters is the main cause of proteinuria, glucosuria and phosphaturia and precedes proximal tubular atrophy. This observation actually provided the first molecular explanation of the renal Fanconi syndrome prior to swan-neck lesions. As glomerular lesions later develop, glomerular proteinuria is reflected by excessive urinary losses of albumin and high molecular weight proteins. As a result, cystinotic children suffer from growth retardation, polyuria with daily excretion of 2 to 6 liters of dilute urine (Fig. 16A), polydipsia, dehydration and electrolyte imbalance, vomiting, constipation and rickets due to impaired vitamin D metabolism (with decreased uptake of vitamin D-binding protein and conversion by alpha-1 hydroxylase in renal proximal tubules). As stated above, early diagnosis is crucial because ESRD develops by the end of the first decade of life if treatment is too late.(Elmonem et al. 2016; Baum 1998) At this stage of the disease, kidney transplantation is inevitable.

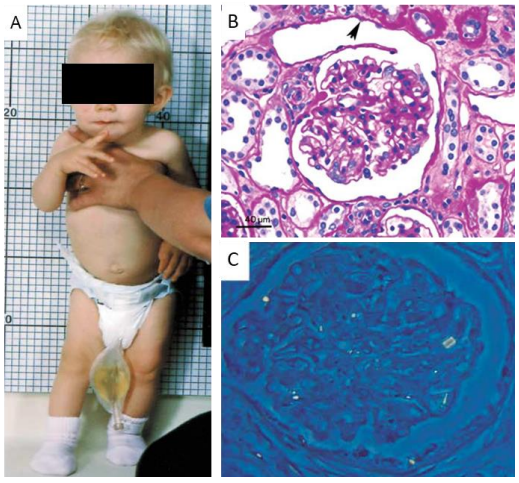

Figure 16. Kidney damage in cystinosis. Presumably because of their huge reabsorptive function, kidneys are usually the first organs affected by cystinosis, before the age of 12 months. **A.** 11-month-old cystinotic girl with polyuria. The blondness of hair is characteristic of Caucasian patients. **B. Histology of a cystinotic kidney** with PAS staining: arrowhead points to typical atrophy of S1 at the glomerulo-tubular junction, referred to as swan-neck lesion. **C.** Post mortem kidney cortex section from an 8-year-old boy viewed under polarized light showing a renal glomerulus with many non-dissolved cystine crystals sometimes having a rectangular shape. *Compiled from Gahl et al, 2002, Larsen, 2010 and Chevalier, 2016.*

Histologically, proximal tubular atrophy is typical in cystinotic kidney sections (Fig. 16B) and these deformities are usually called “swan-neck” lesions because of their shape (see below). Cystine accumulating in acidic lysosomes precipitates above 5 mg/ml. Microscopy under polarizing prisms allows to visualize hexagonal or polymorphous cystine crystals if they have not been dissolved in water at neutral pH during kidney fixation or staining (aqueous solvents should be avoided; in this work, we used alcoholic Bouin fixative).(Gahl, Thoene, and Schneider 2002) In Figure 16C, cystine crystals, sometimes having a rectangular shape, are visible in a glomerulus from a post-mortem cystinotic kidney section.

Figure 17 demonstrates the 3-dimensional appearance of swan-neck deformities, as evidenced by kidney microdissection, and schematizes their origin and consequences, as delineated by time-course analysis in the mouse model. In cystinosis, the glomerulo-tubular junction is the site of the first lesions. At this point, there is a sharp transition between the flat epithelium of the Bowman's capsule and the thick cylindrical epithelium formed by the proximal tubular cells with a characteristic brush border at their apical pole.

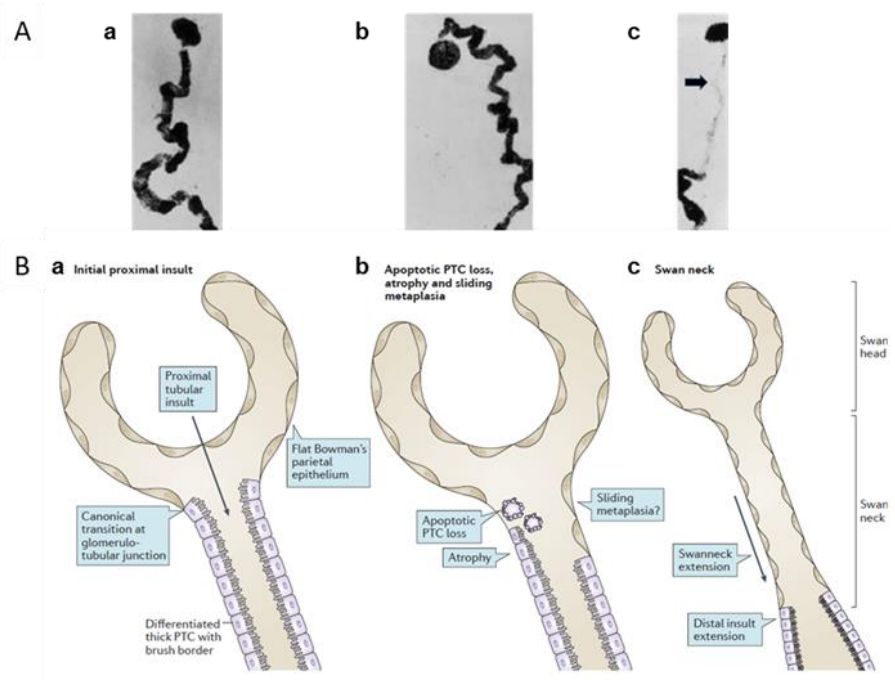

Figure 17. Swan-neck deformities. A. Lesions. Micro dissection showing nephrons from a normal child (a) and from a cystinotic patient at 5 months (b) and 14 months of age (c), arrow showing a typical swan-neck lesion. This name derives from the appearance of microdissected cystinotic nephrons, where the protected glomerulus represents the swan head, the atrophic proximal segment is the swan-neck, and the more distal, preserved convoluted segment would be the swan body. **B. Tentative histopathological explanation.** *(a) Lysosomal swelling in S1.* In cystinosis, PTCs immediately after the glomerulo-tubular junction are the site of the first lesions. Ultrafiltrated plasma proteins, including disulfide-rich proteins such as albumin, are reabsorbed in large amounts by the most proximal cells whose lysosomes are rapidly overloaded by cystine in the absence of cystinosin. As proteolysis is impaired, lysosomes swell. ***(****b) Dedifferentiation followed by crystals and atrophy*. In this second phase, starting from the glomerulo-tubular junction, the tubular epithelium appears dedifferentiated/atrophied. The most proximal S1 epithelium appears completely flat, resulting into typical lesions of cystinosis, called swan-neck deformities. It is possible that an extension of Bowman's epithelium compensates for the loss of cells in the proximal tube (sliding metaplasia hypothesis). (c). *Longitudinal extension*. As disease progresses, alterations extend longitudinally as if burden of ultra-filtered toxic substances having escaped recapture by atrophic upstream tissue is transferred to the next area, which in turn undergoes the same pathological process. *Compiled from Mahoney and Striker, 2000 (A); Cherqui and Courtoy, 2017 (B).*

Ultrafiltrated plasma proteins, including disulfide-rich proteins such as albumin, are reabsorbed in large amounts by the most proximal tubular cells (S1) whose lysosomes are rapidly overloaded by cystine in the absence of cystinosin. Cystine accumulation leads to lysosomal lumen oxidation and thus impairs proteolysis by several possible mechanisms. Indeed, lysosomal reducing environment is crucial for unfolding of disulfide-bonded substrates and thus unmasking peptide bonds for endoproteolysis, for activation of mature lysosomal cathepsins that belong to cysteine proteinases (depend on preservation of the reduced thiol in their catalytic site) and finally for autoactivation and hetero-activation of pro-cathepsins by proteolytic excision of the masking pro-peptide.(Cherqui and Courtoy 2017) Oxidative conditions thus impact all these processes. Resulting impaired proteolysis causes lysosomal enlargement, before any crystal can be detected. In a second phase, starting from the glomerulo-tubular junction, the tubular epithelium becomes dedifferentiated and atrophied. Crystals are seen in PTCs at this stage. Cell death, including by apoptosis, causes luminal shedding thus crystal disappearance. Eventually, the most proximal S1 epithelium appears completely flat, without crystals, resulting into typical swan-neck deformities. We attribute the absence of tubular crystals in biopsies from cystinotic patient, contrasting with interstitial crystals in macrophages, by their late stage. It is possible that an extension of Bowman's epithelium compensates for the loss of cells in the proximal tube (sliding metaplasia hypothesis). As disease progresses, the alterations of the proximal tubule extend distally along the proximal tubule. This suggests that when upstream tissue becomes dysfunctional, the burden of ultra-filtered toxic substances is transferred to downstream PTCs, which in turn undergo the same pathological process.(Mahoney and Striker 2000; Cherqui and Courtoy 2017)

1.3.2.2 Thyroid and hypothyroidism

Hypothyroidism is the most common endocrine perturbation in cystinotic patients followed by type I diabetes or pubertal delay.(Emma et al. 2014) Male hypogonadism with infertility is also frequent, due to azoospermia despite intact spermatogenesis at testicular level.

Like PTCs, thyroid follicular epithelium gradually accumulates cystine, including in the form of crystals which can be seen also in the colloid, indicative of cell shedding in a closed cavity, as opposed to washing out by urine (Fig. 18B). That leads to fibrosis and atrophy (Fig. 18C and D to compare normal and cystinotic histology) and causes primary hypothyroidism, with elevated serum TSH (thyroid stimulating hormone) level, which is the most frequent and earliest endocrine perturbation. These thyroid abnormalities may also partially explain short stature and delayed bone age observed in cystinotic patients. A typical hypothyroidism facies was often noted in untreated patients (Fig.18A).(Lucky et al. 1977)

Clinically, serum level of T3 and T4 are normal in the majority of patients but elevated serum concentration of TSH reflects the response of the pituitary gland to abnormal thyroid hormone production. In our thyroid study of the cystinotic mouse model, we demonstrated that thyroid changes affect thyroglobulin synthesis (linked to ER stress/UPR response) and iodo-thyroglobulin processing (due again to alteration of endolysosomal trafficking) with impaired hormone production, leading to TSH elevation despite normal T3 and T4 plasma concentrations.(Gaide Chevronnay et al. 2015) Eventually, this would lead to colloid exhaustion thus loss of pro-hormone reserve. To protect this pool and

prevent subclinical hypothyroidism, cystinotic patients are treated with thyroid hormones up to TSH normalization.

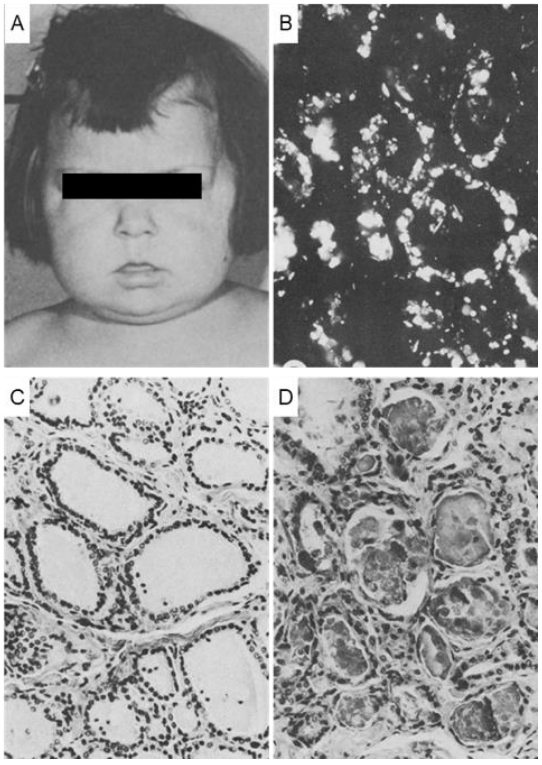

Figure 18. Thyroid damages in cystinosis. A. Photograph of an 8-year-old cystinotic patient who developed a characteristic hypothyroid facies. **B.** Cystinotic thyroid section in polarized illumination showing cystine crystals in thyrocytes and in colloid. **C and D.** HE stained thyroid sections from autopsied children showing a normal histology (C) and a cystinotic profile with increased fibrosis, atrophic flattened thyrocytes and colloid abnormalities (D). *Compiled from Chan et al, 1970 (A) and Lucky et al, 1977 (B-D).*

1.3.2.3 Other organs

I emphasized above kidneys and thyroid as two types of organs where primary affected cells (PTCs, thyrocytes) are specialized in apical endocytosis. However, since all cells bear lysosomes, cystinosis is by necessity a multisystemic disease. For example, cystine also rapidly accumulates to high levels in liver and spleen because of the abundance of macrophages therein (Küppfer cells, splenic macrophages), which become filled with crystals that these cells apparently better tolerate. Presence of birefringent crystal in macrophages of bone marrow aspirates previously helped diagnosing cystinosis as the cause of unexplained Fanconi syndrome. I hereafter dwell on particular organs.

Early in the development of the disease, photophobia result from ***deposition of cystine crystals in the cornea*** (Fig. 19A-B) which leads to blepharospams, corneal erosions, superficial punctuate and band keratopathy (corneal damage). Later, the retina can be affected and cause vision loss. Since the cornea is not vascularized, oral cysteamine therapy does not reduce eye symptoms. However, ophthalmic drops with cysteamine are commonly used but are also very demanding since they must be instilled 6-12 times a day causing eye pain, redness, and ocular inflammation. An ingenious alternative recently tested could avoid these disadvantages. Indeed, Cys nanowafer (Cys-NW) is being developed to be directly applied to the eye and to slowly and continuously release cysteamine.(Marcano et al. 2016)

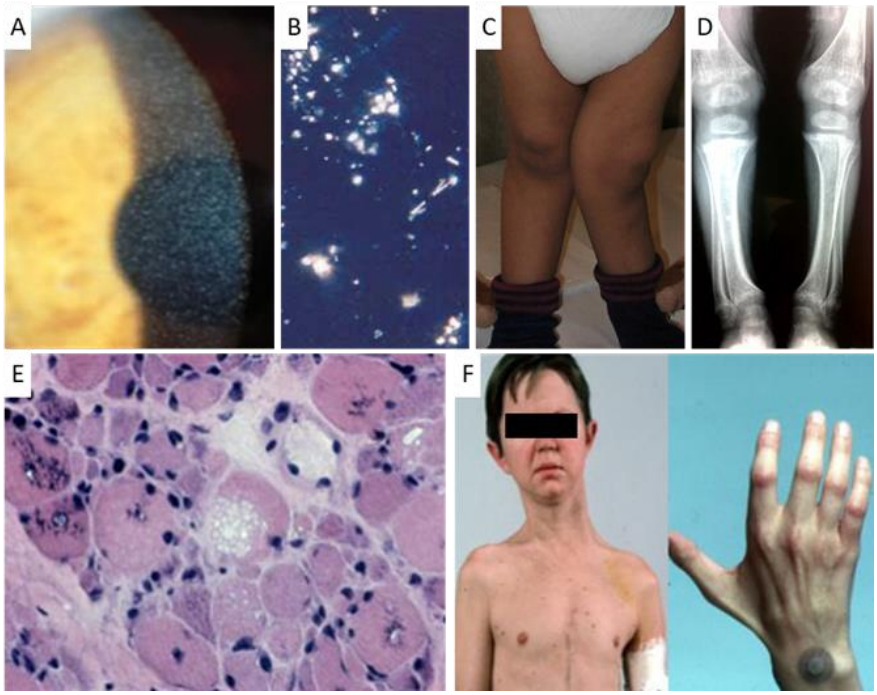

Figure 19. Others organ damages in cystinosis. A. Corneal crystals on slit lamp examination, often accompanied by photophobia. **B.** Birefringent cystine crystals in liver section under cross-polarizing light (Küppfer cells). **C.** Bone deformities. **D.** Rickets by X-rays. **E.** Vacuoles and cystine crystals under polarized light in muscle cells. **F.** Trunk muscle wasting and hand muscle atrophy in adult patient. *Compiled from Nesterova and Gahl, 2012, Elmonem et al, 2016 and Gahl et al, 2002.*

Bones and muscles (Fig. 19C-F) are also affected with clinical signs of growth retardation (usually treated with growth hormone), bone deformities and fragility, genua vara (legs bowed outward at the knee), frontal bossing, rachitic rosary and metaphyseal widening on skeletal X-rays. As stated above, hypophosphatemic rickets result from increased urinary loss of phosphate, calcium, and disruption of vitamin D metabolism (defective conversion of 25-hydroxyvitamin D into active calcitriol in the kidney). Distal myopathy (muscle atrophy) is a major concern.

Combination of weakness in respiratory muscles with altered motion at deglutition leads to false-route and aspiration pneumonia, which has become a significant cause of death.

Neurocognitive impairment due to crystal accumulation in brain causes nonverbal learning difficulties (for example, manual tasks) without verbal or intellectual problems. ***Neurological symptoms*** are visual-motor function impairment and, at long term, complications such as encephalopathy, mental deterioration, pseudo-bulbar palsy (inability to control facial movements) and a contribution to distal myopathy (see above).

Furthermore, cystinotic patients develop ***skin*** problems such as hypopigmentation of skin and hair (Fig.16), which recalls that melanosomes are special lysosome-related organelles***.*** ***Gastrointestinal*** anomalies (hepato-splenomegaly) are due to macrophage loading by cystine crystals (see above) and reduction in the number of red and white blood cells, as well as platelets, are also attributed to cystine crystal accumulation in ***bone marrow***.(Baumner and Weber 2018; Cherqui and Courtoy 2017)

1.3.3. **General pathophysiology**

It is now well established that the alteration of the cystine export out of the lysosome, due to the absence of functional cystinosin, results in an impressive intralysosomal accumulation of cystine, the primary cause of cystinosis signs. The main source of cystine overload is the degradation of disulfide-rich proteins.(Thoene et al. 1977; Thoene and Lemons 1982) Receptor-mediated endocytosis of ultrafiltrated plasma proteins is thus a crucial factor of

nephropathic cystinosis. The many processes involved when PTCs lysosomes are affected by cystine accumulation can be better summarized in a cartoon, reproduced in Figure 20 that compares healthy and cystinotic PTCs and fully detailed in its legend.(Cherqui and Courtoy 2017)

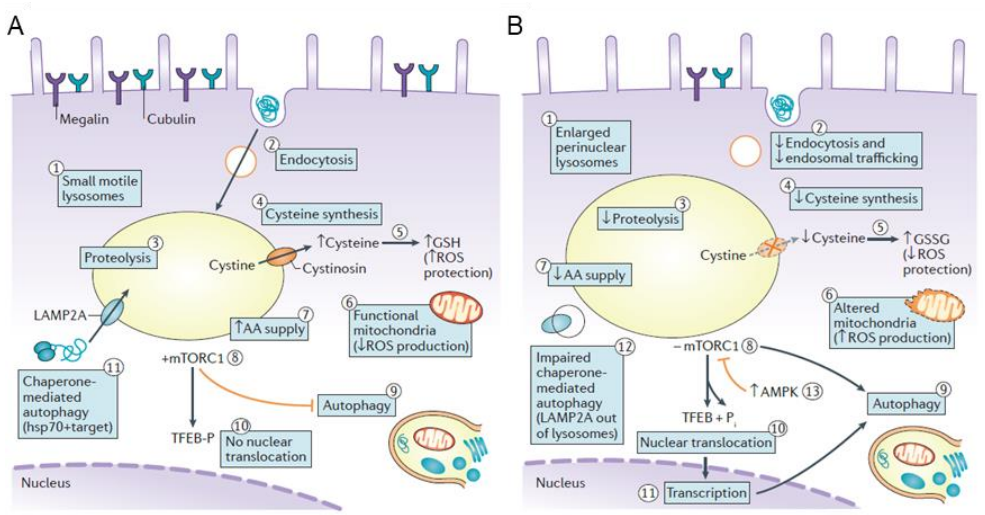

Figure 20. General pathophysiology in cystinotic proximal tubular cells. A. In healthy proximal tubular cells (PTCs), lysosomes are small and motile thus easily reached by endosomes (1). The multi-ligand tandem receptors, megalin and cubilin, are abundantly expressed at the apical pole, and undergo very fast endocytosis and apical recycling (2). The endocytic cargo, mostly including ultrafiltrated, disulfide-rich plasma proteins, is instead transferred to late-endosomes-lysosomes resulting into degradation. Proteolysis (3) provides a large amount of amino acid momomers and free cystine. At the lysosomal membrane, cystinosin allows the export of cystine to the cytosol where it is reduced into cysteine by glutathione (GSH). Cysteine is also a building block for glutathione synthesis (4) that protects the cell against reactive oxygen species (ROS) (5). Furthermore, in the healthy cell, mitochondria release very little ROS (6). Thanks to high amino acids supply (7), the mTORC1 complex is recruited at the lysosomal membrane and maintained in its active kinase form (8). The active complex inhibits macro-autophagy (9) while promoting cell anabolism. It also prevents unnecessary lysosome synthesis by phosphorylating the

transcription factor, TFEB, which blocks its nuclear importation, thus transcriptional activity (10). The very special chaperone-mediated autophagy is dedicated to the disposal of altered cytosolic proteins relies on translocation into lysosomes by the transporter LAMP2-A (11). **B.** The absence or loss-of-function of cystinosin abolishes cystine export to the cytosol. Cystine accumulation impairs the lysosomal reducing environment necessary for proteolysis (3), thus undigested proteins accumulate in the lysosomes which become enormous and concentrate around the nuclei, thus far from endocytosis and exocytosis pathways (1). The consequences for the cell are numerous. Megalin and cubilin expression is reduced leading to decreased endocytosis (2). The endocytic source of cysteine is lost (4) leading to a reversal of the GSH/oxidized glutathione (GSSG) ratio and thus loss of protection against ROS (5) increasing produced ROS due to damaged mitochondria, resulting in oxidative stress. The shortage of free amino-acids (7) combined with AMPK activation due to energy depletion (13) inhibit the mTORC1 complex (8), which activates autophagy while TFEB is dephosphorylated and undergoes a nuclear translocation (10) allowing for transcriptional activation of lysosome (11) and autophagosome biosynthesis (9). Excess autophagy is deleterious to cells. By unexplained mechanism, LAMP2A can no longer transit to the lysosomal membrane and is unable to provide chaperone-mediated autophagy, thus causing defective clearance of misfolded cytosolic proteins (12). Following these multiple imbalances, cell enters atrophy and possibly apoptosis. *From Cherqui and Courtoy, 2017.*

1.3.4. **Treatment and involvement of the non-transport functions of cystinosin.**

Already mentioned several times, the specific cysteamine treatment is up to now the most effective global therapeutic option, supplemented by symptomatic treatments.(Nesterova and Gahl 2013) Once in the lysosome, cysteamine can reshuffle disulfide bridges, resulting in the cleavage of cystine. Thus, one cysteine is released and the other forms a mixed disulfide with cysteamine. The latter leaves the lysosome via the cationic amino acid transporter, PQLC2 (Fig. 21). This therapeutic mechanism allows to drain the lysosome and to delay the symptoms of cystinosis (including ESRD).(Brodin-Sartorius et al. 2012) However, the simple act of purging the lysosome of cystine is not enough to stop Fanconi syndrome or to correct alterations in signaling pathways or autophagy in deficient cells.(Cherqui 2012) This suggests that the accumulation of cystine cannot be the only cause of these pathological manifestations (Wilmer, Emma, and Levtchenko 2010) and that cystinosin itself, beyond its role as transporter, is a central player in biological mechanisms (still partially unknown) such as, for example, recruitment of mTORC1 at the lysosomal membrane.(Andrzejewska et al. 2016)

Moreover, treatment with cysteamine is tedious (conventional cysteamine bitartrate pills must be taken every 6 hours) and has significant side-effects such as a very unpleasant body odor and serious gastrointestinal problems. Cutaneous toxicity of still elusive pathophysiology is also experienced by some patients. (Besouw et al. 2011; Besouw, Schneider, et al. 2013; Besouw, van den Heuvel, et al. 2013) Significant recent improvement of cysteamine therapy is based on delayed release technology allowing ingestion only twice-a-day (Dohil et al. 2010), which greatly improves the quality of life of patients, but is sold at prohibitive price, or eye application of the Cys nanowafers to replace eyedrops.

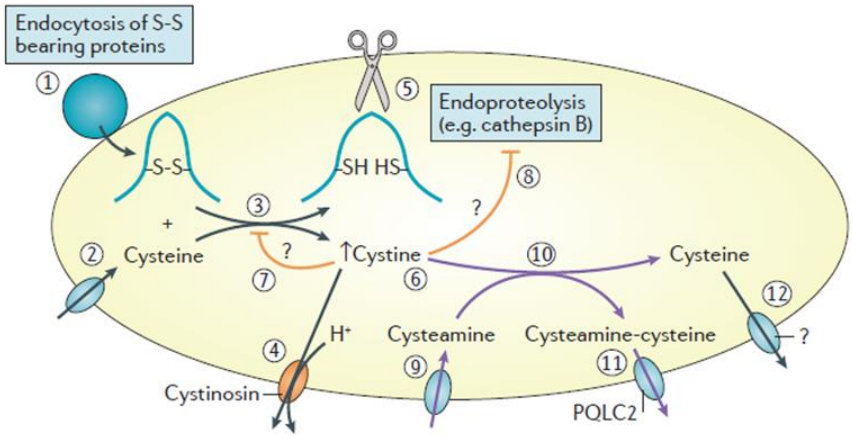

Figure 21. Cysteamine therapy targets cystine overload. Endocytosed disulfide-rich proteins are transferred to lysosomes (1). In parallel, cysteine can penetrate into lysosomes via an unknown mechanism (2). In the acidic lysosomal lumen, two cysteine reduce one disulfide bridge and are themselves oxidized into free cystine. (3). Normally, cystine rapidly leaves the lysosome via the functional cystinosin (4). Due to loss of internal disulfide bonding, proteins unfold which makes peptide bonds more accessible to the endoproteolytic action of lysosomal cathepsins such as the cysteine protease, cathepsin B (5). In the case of cystinosis, the export of cystine to the cytosol is abolished and leads to intralysosomal cystine overload (6) which inhibits the disulfide reduction (7) and the cysteine proteases (8). These processes would help slow the release of cystine. Cysteamine therapy targets the cystine overload. After entering the lysosome via its transporter (9), cysteamine reacts with free cystine to produce a mixed disulfide of cysteamine-cysteine and a free cysteine molecule (10). The mixed disulfide can then leave the lysosome by an alternative exporter, the intact lysine transporter PQLC2 (11). Cysteine is exported on its own into the cytosol by a still unknown transporter (12). *From Cherqui and Courtoy, 2017.*

These new approaches combined with symptomatic treatments nevertheless remain a heavy burden for patients and any new therapeutic advance would be most welcome.(Cherqui and Courtoy 2017)

Besides energy depletion, oxidative stress and lysosomal enlargement, altered autophagy, lysosomal signalling and trafficking, and apoptosis are probably all involved in Fanconi syndrome (Fig.20B) and thus constitute new potential therapeutic targets. For example, rescuing CMA or reducing lysosomal overload by enhancing cystine excretion could reinforce the effects of cysteamine.(Zhang et al. 2017) Stimulating autophagy, lysosomal biogenesis and exocytosis by inducing TFEB expression and nuclear translocation may be another way for the cell to reduce lysosomal cystine storage. Indeed, in the conditionally immortalized PTCs derived from the urine of a cystinotic patient, the activation of TFEB by genistein leads to reduction of intracellular cystine level and improvement of endocytosis.(Rega et al. 2016) However, since genistein has several effects such as inhibiting the mTOR signaling (Lee, Kim, and Choi 2016) already impacted in the cystinotic PTCs, this approach still requires caution.

1.4. A mouse model of nephropathic cystinosis

Throughout this introduction, I have tried to emphasize the importance of better understanding the subcellular mechanisms involved in the complex pathophysiology of cystinosis. On the road to new therapies, two major issues are (i) the scope of transport-independent cystinosin functions and implications and (ii) the biological pathways that, upstream or downstream of cystine accumulation, contribute to the development of the disease. Thanks to the efforts

of Corinne Antignac and her team, researchers have a valuable animal model to reach these goals, namely mice with a full absence of cystinosin in a congenic C57BL/6J background, also named C57BL / 6 *Ctns*$^{-/-}$ mice. These mice reproduce quite well the main symptoms of the disease, especially the renal phenotype, except for a very mild Fanconi syndrome. The genetic invalidation of cystinosin in mice is based on the replacement of the last four exons of the *Ctns* gene, which encode the last five transmembrane domains of cystinosin, with an IRES-βgal-neo cassette. Considering *in vitro* data, the resulting truncated protein, if stable, should be mislocalized to the plasma membrane and unable to carry cystine transport.(Cherqui et al. 2002) *In vivo*, the first *Ctns*-knockout mouse was obtained from a C57BL6/129sv mixed background, which exhibited cystine accumulation and crystal build-up in all tissues but no signs of renal dysfunction. Since the genetic background is generally recognized as influencing the phenotype, successive crosses yielded knockout mice in pure genetic background, C57BL/6J and FVB/N.(Nevo et al. 2010)

By comparing these two lineages, the genetic context indeed proved crucial. Besides huge cystine accumulation increasing with age and in all organs except brain (Fig. 22B), the C57BL/6J *Ctns* knockout line develops renal dysfunctions with impaired proximal tube function (Fig. 22C-D), which will be described in detail in the first part of the Results Section, making this model a most valuable tool for studying cystinosis. In contrast, although a slight accumulation of cystine was observed in FVB knockout mouse kidneys, no renal abnormalities were observed (Fig. 22A).(Nevo et al. 2010)

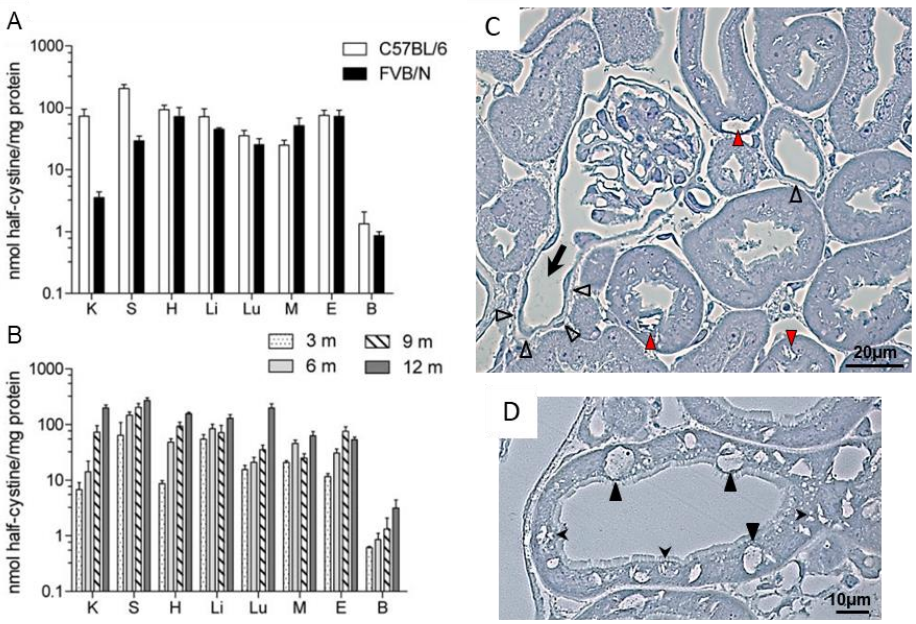

Figure 22. Genetic background-dependent mouse model of cystinosis. Ctns KO C57BL/6J mice reproduce key lesions found in young cystinotic patients. A. Semi-log representation of cystine levels for comparison between 9-month-old congenic C57BL/6 and FVB/N *Ctns*$^{-/-}$ mice in different tissues. C57BL/6 model shows a more marked cystine increase in kidneys and in spleen. **B.** Time-course of cystine overload in C57BL/6 *Ctns*$^{-/-}$ mice shows exponential increase in kidneys (semi-log representation). Congenic C57BL/6 *Ctns*$^{-/-}$ mice are therefore considered the best mouse model to reproduce and study cystinosis. K = kidney, S = spleen, H= heart, Li = liver, Lu = lung, M = muscle, E = eye and B = brain. **C-D.** C57BL/6 *Ctns*$^{-/-}$ mice develop typical histological lesions in kidneys. **C-D :** Semithin plastic kidney sections from knockout mice showing **C.** Typical swan-neck lesion (characterized by atrophic PTCs without crystals starting from the glomerulo-tubular junction (thick arrow) and surrounded by a thick basement membrane (open arrowheads). Crystals are found in non-atrophic distal PTCs (red arrowheads). **D.** Crystals in non-atrophic PTCs are either small and dispersed (small arrowheads) or assembled in a large vacuole (large arrowheads). *Compiled from Nevo et al, 2010 (A-B) and Gaide Chevronnay et al, 2014 (C-D).*

As in cystinotic children, Swan-neck lesions characterize C57BL/6J Ctns$^{-/-}$ kidneys and could result from adaptation mechanisms in proximal tubular cells in response to hypoxic and oxidative stress.(Galarreta et al. 2015) Preserved PTCs contain crystals reflecting cystine accumulation in kidneys that is, in mice, significantly higher in females than in males.(Harrison et al. 2013) The importance of the genetic background as well as the gender difference in cystine accumulation highlight the possibility of a complex genetic context in which the renal phenotype of cystinosis is influenced by modifier genes.(Cherqui and Courtoy 2017) Histologically, Ctns$^{-/-}$ kidneys develop also fibrosis with inflammatory infiltration.(Nevo et al. 2010) More recently, cell biological analysis of primary PTC cultures from Ctns$^{-/-}$ mice revealed a link between defective autophagy and impact on ZONAB signaling as attractive explanation of PTC dedifferentiation.(Festa et al. 2018) However, evidence presented showed surprising cellular homogeneity whereas in vivo, cystinotic PTC alterations are quite heterogeneous between adjacent cells, thus questioning a simple effect of uniform junctional alterations.(Emma et al. 2014) Interestingly, it has been demonstrated that upregulation of CMA rescued Rab11 trafficking, CMA receptor LAMP2A localization and finally megalin expression. CMA could therefore constitute a new potential therapeutic target for attenuation of Fanconi syndrome.(Zhang et al. 2019)

This efficient mouse model allowed us to characterize the thyroid phenotype of cystinosis. Indeed, we reported primary hypothyroidism in cystinotic mice in which we have shown that, as in patients, the serum levels of thyroid hormones T3 and T4 are normal contrary to the level of TSH which is increased. TSH thus continuously stimulates thyroid for hormonal production and ensures normal levels of thyroid hormones. This is histologically reflected by hyperplasia, thyrocytes hypertrophy and colloid exhaustion. We suggest that cystine

accumulation causes alteration of lysosomal redox status impacting cathepsin activity. Lysosomal iodo-thyroglobulin is therefore impaired decreasing T3 and T4 production (primary hypothyroidism) and leading to the compensatory TSH response and histological alterations. Cellular turnover is also observed with increased apoptosis and proliferation in thyrocytes of $Ctns^{-/-}$ mice. We showed that, in cystinosis, ER stress and UPR activation prevent synthesis and secretion of the thyroglobulin. Furthermore, we highlighted accelerate endocytosis and impaired endolysosomal trafficking. Altogether, these results define the cellular alterations leading to "compensated" hypothyroidism and validate C57BL/6J *Ctns*$^{-/-}$ mice as optimal model to study thyroid impairments in cystinosis (see Appendix 1).(Gaide Chevronnay et al. 2015)

C57BL/6J *Ctns*$^{-/-}$ mice also faithfully reproduce the ocular phenotype encountered in patients. Corneal alteration, cystine crystals and inflammatory infiltration in eyes have been shown.(Kalatzis et al. 2007; Simpson et al. 2011) Quite recently, study of bone structure biology in *Ctns* KO mice at 1 month of age, i.e. before any sign of kidney dysfunction, clarified that besides the historical explanations of hypophosphatemic rickets, impaired maturation of vitamin D3, the cell biology of cystinotic bone cells is autonomously and early affected. (Battafarano et al. 2019)

2. AIMS OF THE STUDY

Cystinosis was the first discovered lysosomal storage disease (LSD) due to a defective lysosomal membrane transporter, the proton/cystine exporter called cystinosin. Cystinosis thus leads to lysosomal cystine accumulation. This identification also led to the discovery of the first rational efflux treatment, cysteamine, which achieves cystine swapping to a distinct, preserved transporter, PQLC2. Like other LSDs, cystinosis is a multisystemic disease, yet kidneys (Fanconi syndrome) and eyes (corneal crystals) are the first affected organs, which is unique among LSDs. Cysteamine delays all manifestations of cystinosis, such as kidney failure and hypothyroidism but does not provide a cure, nor protects against the Fanconi syndrome. Thus, at the tissular and organ level, the pathophysiology of cystinosis remains enigmatic and new therapeutical avenues must be explored.

The two initial objectives of this study are to delineate the early events in the pathophysiology of cystinosis in kidneys and to test our hypothesis that megalin-mediated endocytosis is the major source of cystine in proximal tubular cells (PTCs). If this is the case, we would open a new therapeutic pathway by interfering with endocytosis to decrease cystine build-up. Indeed, dibasic amino acids are used in other genetic diseases and are known to inhibit megalin although the mechanism is not yet known.

Specific aims

- **Delineation of the early steps of cystinosis pathophysiology in kidney and highlighting subcellular and tissular changes leading to typical swan-neck lesions.**

About a decade ago, a mouse model based on full cystinosin KO was developed by Corinne Antignac and her colleagues and reasonably well mimicks human cystinosis under a strict C57BL/6J background. We will use this model to define the time-course of tissular lesions and adaptations of nephropathic cystinosis in kidney proximal tubular cells (PTCs). We will focus on lysosomal changes and expression of key apical endocytic receptors (megalin and cubilin) and solute carriers (NaPi-IIa and SGLT-2) likely involved in the Fanconi syndrome, thus in relation with clinical manifestations. We will also examine the rate of apoptosis and proliferation as parameters of tissular remodeling.

- **The role of the megalin pathway in cystinosis progression**

In the second part of the study, we will test the hypothesis that apical endocytosis in PTCs could be the main source of cystine by genetic ablation of megalin, considered as cornerstone of apical endocytosis in these cells. Since full megalin KO causes embryonic lethality related to major brain defects, we will resort to kidney-specific excision of the floxed megalin gene using *Wnt4*-driven Cre expression in cystinotic PTCs (triple transgenic, “double KO” mice). We will compare control, single cystinosin KO, single megalin KO and double KO mice, all derived from the same founders. In this new model, we will analyze if megalin ablation protects kidneys from cystine overload and from resulting lesions, taking into account recent studies that have evidenced transport-independent functions

of cystinosin (thus cysteamine-insensitive). For example, cystinosin physically interacts with the vacuolar proton pump ATPase and with components of the mTOR complex.

- **PTC endocytosis as a novel targetable pathway**

If we demonstrate that transport-dependent properties of cystinosin are crucial for disease progression and that the megalin pathway could be a new therapeutic target to avoid cystine overload, we will focus on drugs able to interfere with megalin. Since the interaction between megalin or cubilin and their various protein cargos depends on the same electrostatic interactions involving crucial lysine or arginine residues, these dibasic amino-acids appear as attractive candidates for competition. Indeed, previous studies had demonstrated their potential for short-term inhibition of megalin-mediated endocytosis. Moreover, long-term oral supplementation with lysine or arginine is used since decades to treat some genetic diseases (not to mention their use by body builders) thus are known as safe. Therefore, in a pilot study, we will treat cystinotic mice by dietary supplementation with lysine or arginine for up to 9 months. We will investigate whether this treatment blocks endocytosis, tends to slow cystine overload and protects cystinotic kidneys.

3. RESULTS

3.1. Time Course of Pathogenic and Adaptation Mechanisms in Cystinotic Mouse Kidneys

Héloïse P. Gaide Chevronnay, **Virginie Janssens**, Patrick Van Der Smissen, Francisca N'Kuli, Nathalie Nevo, Yves Guiot, Elena Levtchenko, Etienne Marbaix, Christophe E. Pierreux, Stéphanie Cherqui, Corinne Antignac, and Pierre J. Courtoy

February 2014, Journal of the American Society of Nephrology 25(6): 1256-69

In this paper, I contributed to all experiments on a daily basis except for clinical characterization reported at Figure 1, electron microscopy reported at Figure 2 and radioiodinated tracer uptake and tissue localization reported at Figure 6 A, B. I performed alone the quantification of tissue turn-over as reported at Figure 9.

BASIC RESEARCH www.jasn.org

Time Course of Pathogenic and Adaptation Mechanisms in Cystinotic Mouse Kidneys

Héloïse P. Gaide Chevronnay,* Virginie Janssens,* Patrick Van Der Smissen,* Francisca N'Kuli,* Nathalie Nevo,† Yves Guiot,‡ Elena Levtchenko,§ Etienne Marbaix,*‡ Christophe E. Pierreux,* Stéphanie Cherqui,‖ Corinne Antignac,† and Pierre J. Courtoy*

*Cell Biology Unit, de Duve Institute and Université Catholique de Louvain, Brussels, Belgium; †Inserm, U574, Hôpital Necker-Enfants Malades and Université Paris Descartes, Sorbonne Paris Cité, Institut Imagine, Paris, France; ‡Pathology Department, Saint-Luc University Clinics, Brussels, Belgium; §Department of Pediatric Nephrology, University Hospitals Leuven, Leuven, Belgium; and ‖Department of Pediatrics, Division of Genetics, University of California, San Diego, California

ABSTRACT

Cystinosis, a main cause of Fanconi syndrome, is reproduced in congenic C57BL/6 cystinosin knockout (KO) mice. To identify the sequence of pathogenic and adaptation mechanisms of nephropathic cystinosis, we defined the onset of Fanconi syndrome in KO mice between 3 and 6 months of age and analyzed the correlation with structural and functional changes in proximal tubular cells (PTCs), with focus on endocytosis of ultrafiltrated disulfide-rich proteins as a key source of cystine. Despite considerable variation between mice at the same age, typical event sequences were delineated. At the cellular level, amorphous lysosomal inclusions preceded cystine crystals and eventual atrophy without crystals. At the nephron level, lesions started at the glomerulotubular junction and then extended distally. *In situ* hybridization and immunofluorescence revealed progressive loss of expression of megalin, cubilin, sodium-glucose cotransporter 2, and type IIa sodium-dependent phosphate cotransporter, suggesting apical dedifferentiation accounting for Fanconi syndrome before atrophy. Injection of labeled proteins revealed that defective endocytosis in S1 PTCs led to partial compensatory uptake by S3 PTCs, suggesting displacement of endocytic load and injury by disulfide-rich cargo. Increased PTC apoptosis allowed luminal shedding of cystine crystals and was partially compensated for by tubular proliferation. We conclude that lysosomal storage triggered by soluble cystine accumulation induces apical PTC dedifferentiation, which causes transfer of the harmful load of disulfide-rich proteins to more distal cells, possibly explaining longitudinal progression of swan-neck lesions. Furthermore, our results suggest that subsequent adaptation mechanisms include lysosomal clearance of free and crystalline cystine into urine and ongoing tissue repair.

J Am Soc Nephrol 25: ●●●–●●●, 2014. doi: 10.1681/ASN.2013060598

Infantile cystinosis, a multisystemic lysosomal thesaurismosis, causes renal Fanconi syndrome in the first year of life and kidney failure after a decade, even under compliant cysteamine therapy.[1,2] Lysosomal cystine accumulation and precipitation into crystals result from defective export caused by lack of the H^+: cystine membrane symporter, cystinosin (*CTNS*).[3,4] Nephropathic cystinosis is reproduced in congenic $Ctns^{-/-}$ C57BL/6 mice,[5] but strong dependence of genetic background suggests complex disease mechanisms and important modifier genes.

In cystinotic neutrophils, cystine accumulates in lysosomes without changing their equilibrium density, despite high gravity of cystine crystals,

Received June 10, 2013. Accepted November 15, 2013.

Published online ahead of print. Publication date available at www.jasn.org.

Correspondence: Dr. Héloïse P. Gaide Chevronnay, de Duve Institute and Université Catholique de Louvain, 75, Avenue Hippocrate, PO Box B1.75.05, 1200 Brussels, Belgium. Email: heloise.gaidechevronnay@uclouvain.be

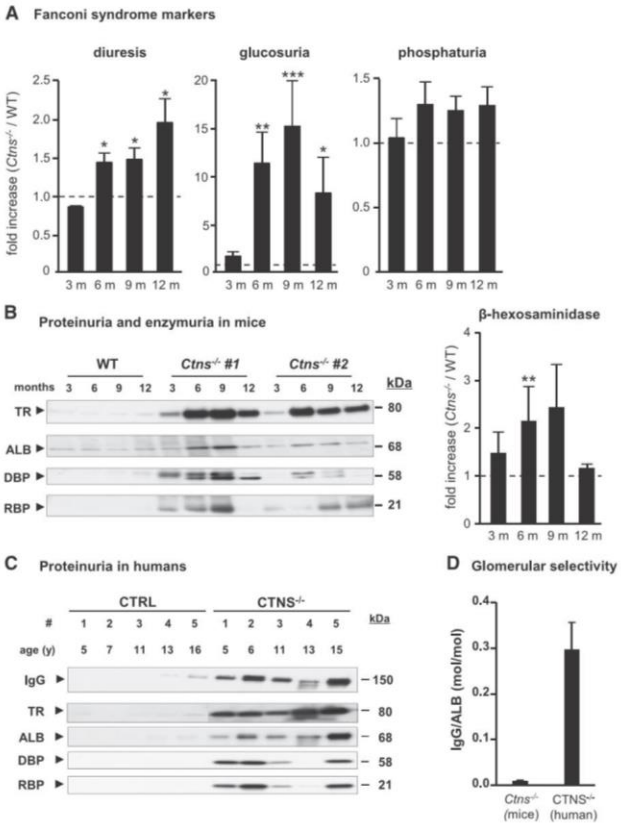

Figure 1. *Ctns*$^{-/-}$ mice develop a partial Fanconi syndrome between 3 and 6 months. Twenty-four–hour urine collections were obtained on ice with protease inhibitors from 3-, 6-, 9-, and 12-month-old C57BL/6 WT and *Ctns*$^{-/-}$ mice (n=8 for each interval). (A) Time course of the loss of solutes in *Ctns*$^{-/-}$ mice. Volume, glucose, and phosphate excretion were normalized to control values in age-matched WT mice. (B) Time course of proteinuria and enzymuria in *Ctns*$^{-/-}$ mice. Representative Western blots for transferrin (TR), albumin (ALB), vitamin D binding protein (DBP), and RBP in one WT and two *Ctns*$^{-/-}$ mice (#1 and #2) in serial collections at the indicated ages (loads normalized to 2 μg creatinine). Blots were processed strictly in parallel. *N*-Acetyl-β-hexosaminidase activity (a representative lysosomal hydrolase[49] insensitive to protease inhibitors) was normalized to control values in age-matched WT mice (there was no detectable change in its mRNA; not shown). Notice the consistent increase of solutes and most tested proteins between 3 and 6 months. *P<0.05; **P<0.01; ***P<0.001. Supplemental Figure 1 shows quantitation of individual proteinuria in all time course collections. (C) Urinalysis by Western blotting in five cystinotic children versus five age-matched controls. Loads were normalized to 2 μg creatinine like in B, and blots were processed strictly in parallel. Note the strong detection of IgG, TR, and ALB in all patients as well as DBP and RBP, except in outlier patient 4 without Fanconi syndrome. CTRL, control. (D) Glomerular selectivity in cystinotic mice but not patients. Normalized urinary loads of five cystinotic children and 3- to 9-month-old mice were analyzed by Western blotting for IgG and ALB by reference to increasing standards of fresh plasma in the same blots. Data are presented as mean±SEM of IgG/ALB molar ratios in cystinotic mice (*Ctns*$^{-/-}$) compared with cystinotic children (CTNS$^{-/-}$).

indicating predominant accumulation in noncrystalline form.[6] Furthermore, by electron microscopy, enlarged acid–phosphatase-labeled structures enclose an amorphous matrix without systematic association with crystals.[7] Cystinotic fibroblasts show enlarged lysosomes without acidification defect[8] and accumulate cystine on degradation of endocytosed disulfide-rich proteins, such as albumin, in proportion to extracellular concentration.[9–12] However, retention is surprisingly low (approximately 1%), possibly because of vesicular exodus.[10,11] Exodus is linked to endocytic recycling,[10–12] which involves tiny tubular endosomes (thus size-limited) and is particularly active in kidney proximal tubular cells (PTCs).[13,14] These observations indicate potent lysosomal discharge, now a recognized common feature of lysosomal storage diseases.[15]

Although the genetic and cellular bases of cystinosis are clear, little is known on (*1*) the early structural and molecular changes in the complex kidney architecture leading to the Fanconi syndrome, (*2*) their significance for cystinosis progression along uriniferous nephron (reviewed in ref.[16]), (*3*) the pathogenic role of cystine crystals, and (*4*) natural adaptation mechanisms. In cystinotic kidneys, Fanconi syndrome is generally attributed to PTC atrophy, starting at the glomerulotubular junction as swan-neck deformities, but earlier functional defects caused by impaired gene expression were not considered.[17] However, as shown in polarized PTCs cultures, expression of apical endocytic receptors strongly depends on differentiation state.[18]

To address these issues, we exploited congenic *Ctns*$^{-/-}$ C57BL/6 mice,[5] which allowed us to study early kidney events that are inaccessible in patients. This established model shows (*1*) high cystine levels,

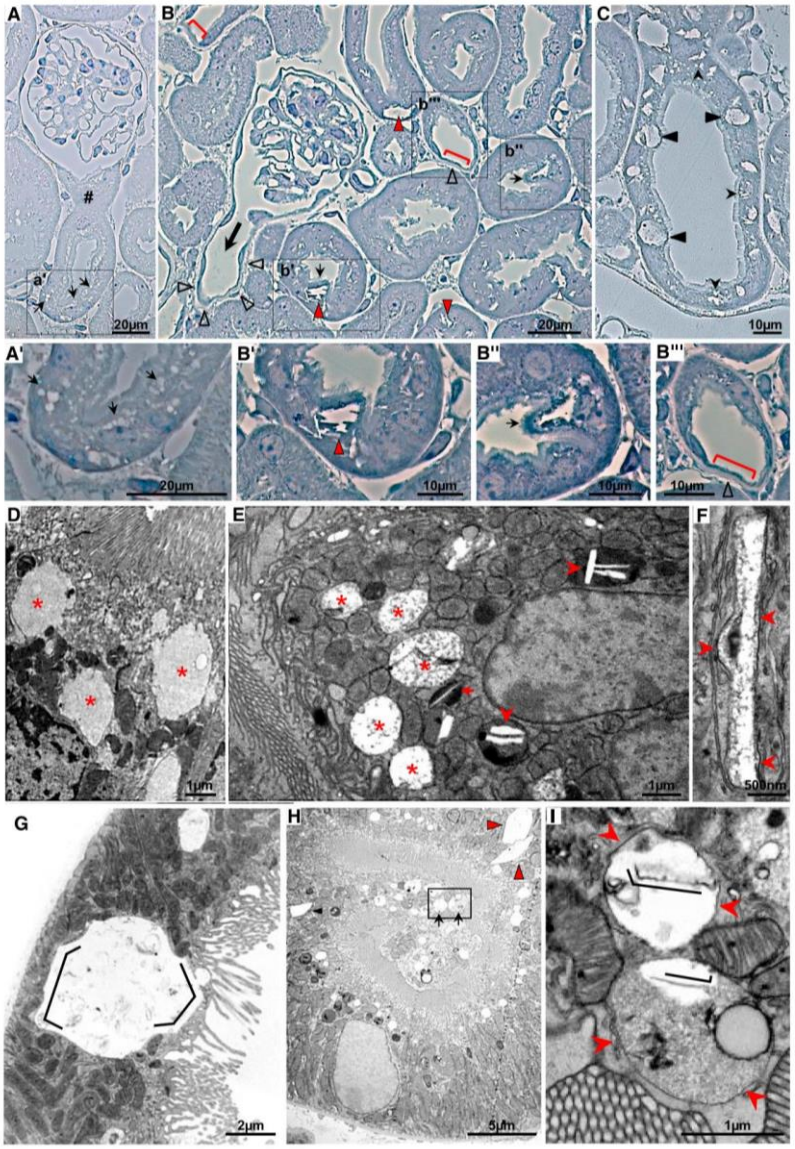

Figure 2. Kidney lesions in cystinotic mice start in S1 proximal tubular cells by apical vacuolation due to amorphous inclusions, which slowly convert into membrane-bound crystals of increasing size. Overview of (A–C) histologic (semithin plastic sections) and (D–I) ultrastructural alterations of *Ctns*$^{-/-}$ mice kidneys. (A) In this representative 6-month sample, notice the early apical vacuolation (small arrows; box is enlarged in A') limited to proximal PTCs at the glomerulotubular junction (#), contrasting with the apparent integrity of all other kidney tissues. (B) In this

including kidney crystals, (*2*) renal lesions with Fanconi syndrome, and (*3*) progression to kidney failure. The aim of our study was to bridge the gaps between cell biologic studies addressing short-term events in cultures of short-lived or rapidly dividing cells and a chronic disease affecting highly differentiated quiescent cells in a complex tubular organ.

To investigate the physiopathology of nephropathic cystinosis progression, we took the perspective of endocytic uptake of ultrafiltrated plasma proteins as an essential cystine source. Disulfide bonds are abundant in plasma proteins (17/albumin) but virtually absent in cytosolic and mitochondrial proteins.[19] In normal human PTCs, daily endocytic reuptake of approximately 7 g albumin[20] is, thus, a major source of lysosomal cystine, far above autophagy.[21] PTCs are specialized to capture ultrafiltrated proteins by apical receptor-mediated endocytosis (ARME) through abundantly expressed, rapidly recycling multiligand tandem receptors, megalin, and cubilin.[22] Megalin- and cubilin-knockout mice show defective PTC endocytosis and urinary loss of ultrafitrated plasma proteins[23–26] and lysosomal enzymes.[27,28] Although defective ARME caused by loss of megalin/cubilin was a possible explanation for proteinuria of cystinotic patients, normal immunolabeling of megalin/cubilin was reported in an end stage cystinotic kidney despite massive proteinuria, calling attention to glomerular leakage.[29]

Ctns$^{-/-}$ mice allowed us to (*1*) identify sequential changes in the form of lysosomal storage, (*2*) distinguish dedifferentiation (including megalin and cubilin loss) from atrophy, and (*3*) identify adaptation mechanisms by cystine discharge (including apoptosis shedding) and proliferative epithelial repair.

RESULTS

A Latent Phase Precedes Renal Fanconi Syndrome in *Ctns*$^{-/-}$ Mice

Ctns$^{-/-}$ mice aged 2–9 months show clinical Fanconi syndrome.[5] To better define the disease time course, we first monitored 24-hour urine collections sampled every 3 months for loss of water, glucose, phosphate, and proteins as renal Fanconi syndrome markers (Figure 1A, Supplemental Figure 1). All rose between 3 and 6 months and further increased at 9–12 months, with major individual variation at given ages despite high congenicity. Proteinuria included albumin, transferrin, vitamin D binding protein, retinol binding protein (RBP), and the very sensitive marker CC16 (250-fold at 12 months). These kinetics resembled early Fanconi syndrome of human nephropathic cystinosis. Negligible IgG loss (IgG/albumin molar ratio=1:100) indicated pure PTC dysfunction (without glomerular leakage). Careful blot inspection in serial collections disclosed asynchronous protein loss (*e.g.*, earlier increase of the cubilin ligand, transferrin, and later megalin ligand, RBP) (Figure 1B). Increased urinary β-hexosaminidase (despite comparable gene expression; not shown) was compatible with defective reuptake of ultrafiltrated lysosomal enzymes. Four cystinotic children aged 5–15 years old with renal Fanconi syndrome also exhibited strong urinary excretion of transferrin, albumin, vitamin D binding protein, and RBP, which was not detected in control samples (Figure 1C), but high IgG/albumin loss (0.3), indicating concomitant glomerular leakage.

Integrated Sequence of Histologic and Lysosomal Changes

Histologic lesions started at approximately 6 months in superficial cortex (Supplemental Figure 2), thus possibly first affecting superficial nephrons,[30] in PTCs next to the glomerulotubular junction (S1) (Figure 2A) and then extended deeper with considerable heterogeneity: typical patterns will, thus, be described. At the cellular level, we first noted apical swelling (Figure 2, A and A′), which corresponded to amorphous inclusions of increasing electron density (Figure 2, D and E) (like in human cystinotic leukocytes) distinct from electron lucent endosomes and more basally located dense bodies. Lysosomal nature of inclusions was confirmed by LAMP-1 immunofluorescence (as the lysosomal membrane marker) and filling with injected horseradish peroxidase (HRP) as a classic endocytic tracer[31] (Figure 3).

representative 9-month sample, PTCs at the glomerulotubular junction have been replaced by a flat epithelium, indistinguishable from Bowman's capsule (thick arrow) and likewise resting on a thick basement membrane (open arrowheads). Crystals are obvious in several other PTCs (red arrowheads), which are better seen in the boxes enlarged in B′ and B″. Arrows points to apical bulging. Brackets delineate individual cell flattening (enlarged at B″′). (C) In this representative 12-month sample, numerous PTCs with preserved height and visible brush border contain collections of small crystals (small arrowheads) or enclose a large vacuole (large arrowheads). (D) This ultrastructural view of the apical region of a *Ctns*$^{-/-}$ PTC at 6 months shows well differentiated brush border and three large inclusions with amorphous content (asterisks). (E) In this 12-month sample, notice the apparent progression of the changes from vacuolation and amorphous inclusion (asterisks) up to dense bodies of normal size harboring small crystals (thin needle at small arrow; thicker crystals at arrowheads). In two other 12-month samples, notice (F) a single membrane-bound (arrowheads) crystal (3-μm long and 200-nm thick) with a fine electron-dense fibrillar matrix and (G) a large vacuole with straight membrane border segments connected at rigid angles (polygonal lines) indicating deformation by packed cystine crystals. This vacuolar expansion almost spans the entire cell height, except for its most basal cytoplasm resting on a nondistorted basement membrane, and causes luminal bulging of the apical surface, which still bears numerous microvilli. (H) In this other 12-month sample (box enlarged in I), largely preserved PTCs (except for a few crystals; arrowheads) surround a lumen enclosing cell debris, including a membrane-bound lysosome (delineated by arrowheads) containing two crystals (polygonal lines).

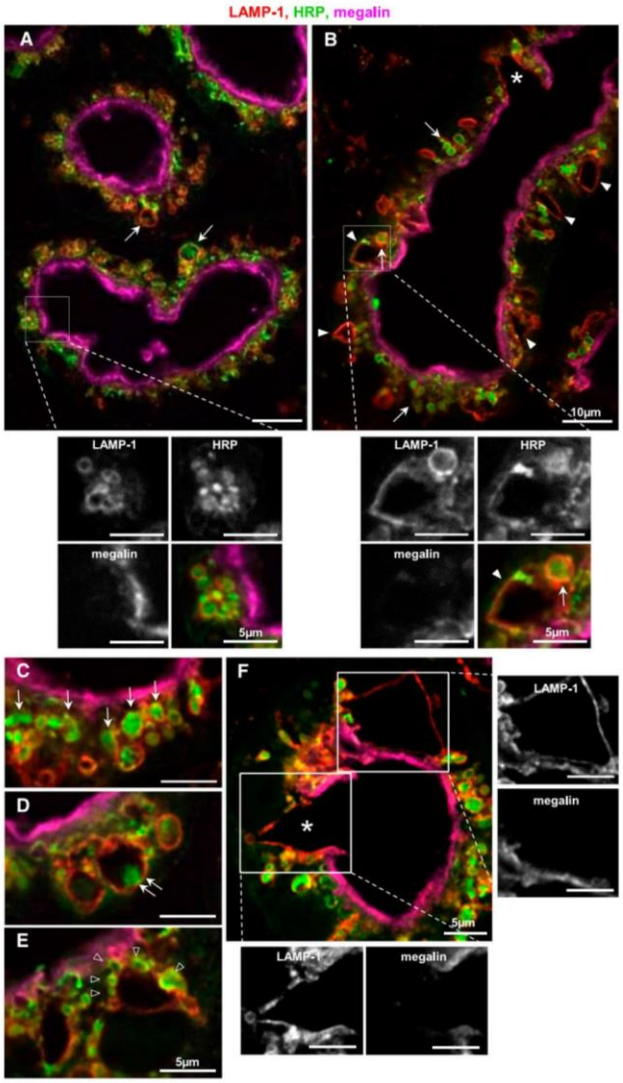

Figure 3. Triple immunofluorescence identifies enlarged vacuoles and crystal-bearing structures as lysosomes, which progressively disconnect from active endocytic trafficking (residual bodies) and can discharge their content into the tubular lumen (lysosomal defecation). Comparison of (A) WT and (B–F) *Ctns*$^{-/-}$ mice for labeling of megalin (magenta) to identify PTCs, LAMP-1 (red) to label the lysosomal membrane, and HRP injected 2 hours before euthanization (green) to test for lysosomal accessibility and matrix filling. In enlarged boxed fields, individual antigens are presented in black and white for optimal resolution and easier pattern comparison as well as merged triple colors. (A) Control. In this 6-month WT mouse kidney, PTCs show homogenous-intense (sub)apical labeling for megalin at the expected position for the base of brush border and endosomes; most lysosomes are clustered and exhibit uniformly round shape, similar size, and extensive filling by HRP. The two short arrows point to very rare enlarged lysosomes. (B–F) *Ctns*$^{-/-}$. In this 6.5-month sample with unusually advanced lesions, notice that most PTCs show (*1*) alterations of LAMP-1–labeled lysosomes, including round expansion with preserved HRP filling (arrows in B and C) or only partial HRP filling (double arrows in D); (*2*) spindle-shaped deformation with progressive loss of accessibility to the endocytic tracer (filled arrowheads in B); (*3*) extensive spindle-shaped or ovoid deformations, almost spanning the cell size, with docked but not fused lysosomes[50] (open arrowheads in E); and (*4*) apparent continuity of LAMP-1 (red) with strong apical megalin labeling (magenta) at adjacent cells (asterisks at B and F; enlarged below). The other field enlarged at right shows a huge lysosome (>10 μm) with straight borders at a rigid angle (upper enlargement) that is resolved from a dense apical megalin signal. It is not possible to distinguish whether these two objects belong to the same or overlapping cells.

Because cystine crystals dissolve on section rehydratation, they were identified as characteristic light and electron lucent needles and then, micrometers-long polyhedric objects enclosed by a limiting membrane. As lesions progressed, we noted crystal buildup in cells with preserved height and microvilli (Figure 2B) and then, coalescence into huge and distorted single vacuoles up to luminal bulging (Figure 2, B′, B″, and C). Vacuoles were still labeled for LAMP-1 but progressively lost accessibility to HRP (Figure 3). Coalescent cystine crystals imposed characteristic polygonal membrane deformation that were visible by electron (Figure 2G) and even light microscopy (Figure 3, B–F). LAMP-1 immunofluorescence revealed occasional cavities within proximal epithelium that were open to lumen, showing apparent continuity between lateral LAMP-1 and apical megalin (of adjacent cells?) and

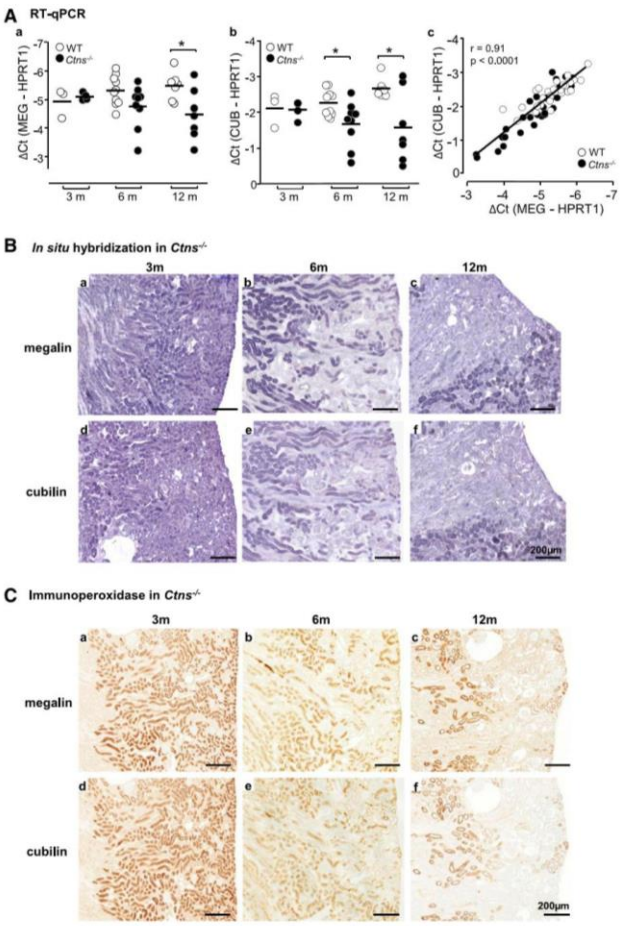

Figure 4. Proximal tubular cells show progressive loss of megalin and cubilin mRNA and protein expression. (A) Quantification by quantitative RT-PCR (RT-qPCR) of (a) megalin (MEG) and (b) cubilin (CUB) mRNAs in WT and $Ctns^{-/-}$ kidneys collected at 3, 6, and 12 months normalized to hypoxanthine phosphoribosyltransferase-1 (HPRT1) and presented as ΔCt values. *$P<0.05$. (c) Robust correlation over a 10-fold range between MEG and CUB mRNA expression levels suggests common transcriptional regulation[18] modulated by variations of local cellular insult (cystine load). Supplemental Figure 2 shows preservation of global mRNA expression of glomerular (podocin) and distal nephron markers (sodium–glucose cotransporter-1 [SGLT-1] and aquaporin-2 [AQP-2]) in $Ctns^{-/-}$ kidneys. (B and C) Localization by (B) *in situ* hybridization and (C) immunoperoxidase of (a–c) megalin and (d–f) cubilin in $Ctns^{-/-}$ mice kidney paraffin sections at (a and d) 3, (b and e) 6, and (c and f) 12 months. Scale bars, 200 μm. Notice progressive extinction of the expression of both receptors from the superficial cortex into deeper zones. Supplemental Figure 4 shows half-kidney sagittal images. Supplemental Figure 5 shows quantification of loss of megalin and cubilin proteins in kidney homogenates by Western blotting.

suggesting fusion of crystal-loaded residual bodies with apical membrane (*i.e.*, luminal exocytosis by living cells) (Figure 3F). Alternatively, apoptotic fragments were shed in lumen, some bearing recognizable crystals (Figure 2, H and I). Shedding caused piecemeal flattening (Figure 2B), sharply alternating with preserved cells. At 9–12 months, all tubular cells close to glomerulotubular junction in affected nephrons became extremely flat, indistinguishable from Bowman's epithelium, and likewise, rested on very thick basement membrane (Figure 2B). All other kidney cells remained unaltered, arguing against uniform cystine production from endogenous proteins. Up to 9 months, glomeruli appeared essentially intact (not shown), but at 12 months, dilated renal corpuscles with enlarged Bowman's space and collapsed capillary tufts, compatible with glomerulotubular disconnection, became obvious.

Altogether, these data showed selective distally extending PTC lesions, with a sequence of lysosomal lesions involving (*1*) amorphous inclusions, (*2*) crystallization into small needles within typical dense bodies, (*3*) larger membrane-bound crystals in residual bodies progressively excluded from endocytic trafficking, (*4*) huge crystal collections in single distorted lysosomal vacuoles, (*5*) luminal discharge by apical fusion or shedding as apoptotic bodies, and (*6*) absence of crystal in established swan-neck lesions.

Defective Megalin and Cubilin Expression in $Ctns^{-/-}$ Mice Kidneys

Because urinary loss of ultrafiltrated plasma proteins suggested defective ARME, we next analyzed endocytic receptors expression at mRNA and protein levels. By quantitative RT-PCR (Figure 4A) and Western blotting (Supplemental Figure 5) on total extracts, megalin and cubilin decreased from 6 to 12 months in $Ctns^{-/-}$ mice, with high variation between individuals at given ages but strong correlation of megalin versus cubilin mRNAs or proteins within individuals (over 1 log). In contrast, neither podocin (glomeruli) nor sodium–glucose transporter-1 (SGLT-1) (straight segment) and aquaporin-2 (collecting duct) expression was significantly altered, confirming lesion selectivity to PTCs

(Supplemental Figure 3B). By *in situ* hybridization and immunoperoxidase, megalin and cubilin mRNA and protein were homogenously distributed in PTCs of wild-type (WT; not shown) and *Ctns*$^{-/-}$ mice at 3 months (Figure 4, B and C). We noticed complete loss of megalin and cubilin expression in superficial foci of *Ctns*$^{-/-}$ cortex at 6 months, extending at 12 months into the outer medulla (Figure 4, B and C) and matching extension of histologic lesions (large fields at Supplemental Figure 4).

Cystinotic Patients Also Show Defective Megalin and Cubilin Expression Associated with Proteinuria

Preservation of megalin/cubilin had, however, been reported in a cystinostic child kidney biopsy.[29] We, thus, reinvestigated megalin/cubilin expression in kidney paraffin blocks archived from a 3-year-old cystinotic child, an age-matched control with preserved renal function, and four older cystinotic children with kidney dysfunction (Supplemental Table 3). In the 3-year-old cystinotic kidney, most PTCs exhibited strong megalin/cubilin immunostaining, which lacked in adjacent atrophic PTCs (Figure 5, B and E, arrowheads). In contrast, all samples from older patients, including the case previously reported,[29] showed only rare foci of PTCs retaining strong megalin/cubilin signal among profoundly disorganized tissue lacking endocytic receptors (Figure 5, C and F). Thus, cystinotic mouse and human kidneys exhibited similar tissue heterogeneity with progressive loss of megalin/cubilin.

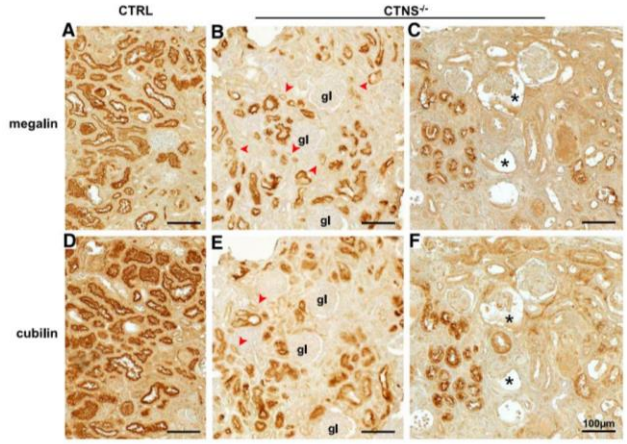

Figure 5. Cystinotic children also show progressive loss of megalin and cubilin in kidney proximal tubules. Immunoperoxidase of (A–C) megalin and (D–F) cubilin on adjacent kidney paraffin sections from (A and D) a control child biopsy (3-year-old child with primary oxaluria), (B and E) a 3-year-old cystinotic girl with Fanconi syndrome but normal plasma creatinine value (early case), and (C and F) an 8-year-old cystinotic girl with end stage kidney disease (terminal case; representative of four cases). In the absence of cystinosis, megalin and cubilin label all PTCs uniformly. (B and E) In the early case of infantile cystinosis, sparse foci with partial or complete loss of megalin and cubilin (arrowheads) are detected among tissue with overall preserved structure and megalin/cubilin expression. gl, glomerulus. (C and F) In the representative terminal case of infantile cystinosis, tissue atrophy is extensive, but some nephrons still express megalin and cubilin. Notice also the two glomerular profiles with expanded Bowman's space and collapsed capillary tuft (asterisks), suggestive of glomerulotubular disconnection. Scale bars, 100 μm.

Apical Receptor-Mediated Endocytosis Is Defective in *Ctns*$^{-/-}$ Kidneys and Causes Transfer of Protein Load in the Nephron

To further test whether proteinuria resulted from defective ARME in PTCs, mice were injected with ^{125}I-β_2-microglobulin or TexasRed-ovalbumin as ultrafiltrated tracers. Average total ^{125}I-β_2-microglobulin uptake only marginally decreased in 12-month-old *Ctns*$^{-/-}$ mice (Figure 6A), contrasting with the severity of histologic lesions. This apparent paradox was addressed by ^{125}I-β_2-microglobulin tissue distribution (Figure 6B). Autoradiography grains were restricted to kidney cortex in WT mice from 3 to 12 months[32] and 3-month-old *Ctns*$^{-/-}$ mice but extended into the outer stripe of outer medulla at 12 months, consistent with transfer of ^{125}I-β_2-microglobulin endocytic load to S3 PTCs on defective S1 uptake.

To establish whether defective uptake correlated with loss of endocytic receptors at the cellular level, we next compared uptake of injected TexasRed-ovalbumin with megalin immunofluorescence (Figure 6C). In WT mice, TexasRed-ovalbumin was restricted to megalin-expressing PTCs, with high cortical load and lesser uptake in a minor fraction of S3 PTCs in the outer stripe of outer medulla. As predicted, cortical *Ctns*$^{-/-}$ PTCs without detectable megalin showed no detectable TexasRed-ovalbumin, which now labeled most S3 *Ctns*$^{-/-}$ PTCs. Thus, decreased megalin/cubilin expression in S1 PTCs resulted in transfer of their normal load of ultrafiltrated disulfide-rich proteins to S3 PTCs, suggesting a molecular and tissular mechanistic explanation for disease extension.

Evaluation of Swan-Neck Lesions by Multiphoton Microscopy

To relate the endocytic defect with extension of swan-neck lesions, kidneys of TexasRed-ovalbumin–injected *Ctns*$^{-/-}$ mice were labeled with Lotus tetragonolobus (LT)-lectin as a PTC marker and analyzed by multiphoton microscopy and three-dimensional reconstruction (Figure 7). PTC dedifferentiation (loss of lectin labeling)

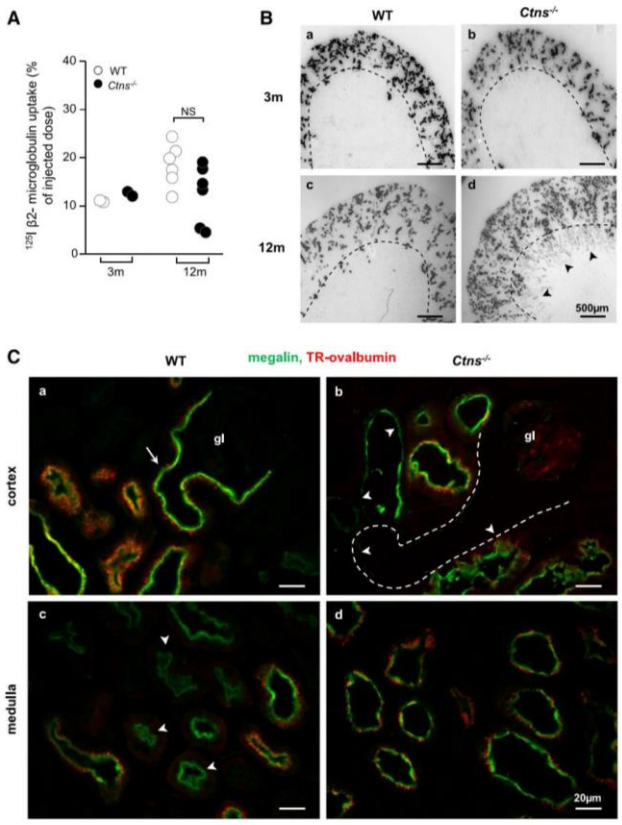

Figure 6. Functional assays by injection of radioiodinated or fluorescent tracers confirm defective apical receptor–mediated endocytosis in affected S1 proximal tubular cells of *Ctns*$^{-/-}$ mice and reveal partial compensatory uptake by S3. (A and B) WT and *Ctns*$^{-/-}$ mice were injected intravenously at 3 or 12 months with ^{125}I-β_2-microglobulin and euthanized after 7 minutes. (A) Quantitation of total uptake in kidney homogenates. Despite strong urinary loss of ultrafiltrated plasma proteins in all *Ctns*$^{-/-}$ mice at 12 months, total renal uptake of ^{125}I-β_2-microglobulin is preserved in most of them. The appoximately 35% average decrease in this cohort is not statistically significant (NS). (B) ^{125}I-β_2-microglobulin localization by autoradiography in representative paraffin kidney sections from (a and b) 3- and (c and d) 12-month-old (a and c) WT and (b and d) *Ctns*$^{-/-}$ mice. Broken lines indicate the corticomedulla boundary. Notice exclusive recapture by cortical PTC segments of control kidneys (a and c) at both intervals and (b) by *Ctns*$^{-/-}$ kidneys at 3 months. (d) In 12-month-old *Ctns*$^{-/-}$ mice, extensive additional distal uptake in PTC of the outer stripe of the outer medulla is indicated by arrowheads. (C) Combination of megalin immunofluorescence with functional study of endocytosis after fluorescent ovalbumin injection. (a and c) WT and (b and d) *Ctns*$^{-/-}$ mice were injected at 9 months with 300 μg TexasRed-ovalbumin (TR-ovalbumin) and euthanized after 20 minutes. Frozen fixed sections were analyzed by double fluorescence microscopy for receptor expression (megalin immunofluorescence is shown by the continuous green apical band) and ligand uptake (ovalbumin is shown by red dots under the megalin layer) in the (a and b) cortex and (c and d) medulla. (a) In WT cortex, notice the strong homogenous double labeling, indicating competence and engagement into ARME by all PTCs in convoluted proximal (cortical) segments, including PTCs at the glomerulotubular junction (arrow). (c) In the WT medulla, tracer uptake is detected in only a fraction of PTCs in the straight segment in the outer stripe of outer medulla, but most S3 profiles are not labeled (arrowheads). (B) In *Ctns*$^{-/-}$ cortex, uptake of TR-ovalbumin is defective in foci of cortical PTCs that have lost megalin (arrowheads), which is best seen at the glomerulotubular junction (contour is indicated by the broken line). (d) In *Ctns*$^{-/-}$ medulla, essentially all S3 PTCs in the outer stripe of outer medulla show preserved megalin expression and are engaged in TR-ovalbumin uptake. This finding suggests partial compensation by S3 uptake in nephrons where ARME is defective in S1 PTCs. Scale bars, 20 μm.

and functional endocytic defect (loss of TexasRed-ovalbumin recapture) could be followed from glomerular junction down to hundreds of micrometers. After abrupt transition, PTCs showed preserved structure (thickness), differentiation (LT labeling), and function (TexasRed-ovalbumin uptake). These data implied that such cells had now become the first line for ARME, thus maximally exposed to uptake of disulfide-rich proteins, and were predicted to be the next to suffer.

Apical Structural and Functional PTC Dedifferentiation in *Ctns*$^{-/-}$ Mice Is Asynchronous

Because megalin immunofluorescence appeared unequal among adjacent *Ctns*$^{-/-}$ PTCs along with crystal deposits (Figure 2C) and lysosomal changes (Figure 3, B–D), we compared megalin/cubilin expression in individual PTCs at 6 months to focus on early dedifferentiation. A significant fraction of megalin-expressing cells had lost detectable cubilin, but the converse was never found (Figure 8A). This finding prompted a systematic immunofluorescence analysis of apical differentiation using markers for brush border (ezrin), apical endocytic apparatus (LT-lectin), and

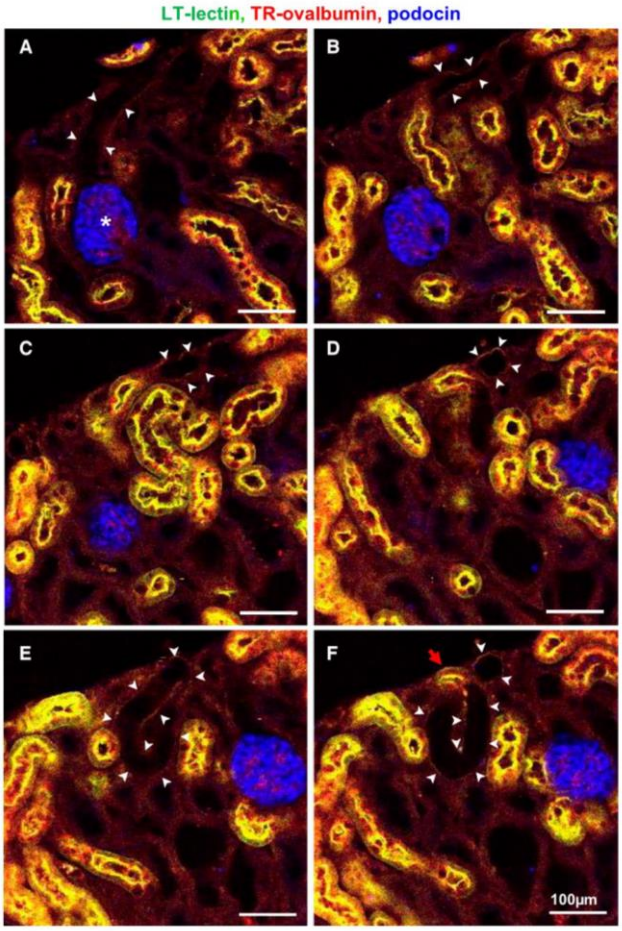

Figure 7. Longitudinal extension of swan-neck lesions in individual nephrons starting from the glomerulotubular junction can be visualized by multiphoton microscopy after multiplex fluorescence labeling. *Ctns*$^{-/-}$ mice were injected at 9 months with 600 μg TR-ovalbumin (red) like shown in Fig 6. Thick kidney slices were labeled for podocin (glomeruli; blue) and LT-lectin (PTCs; green) and resolved by serial optical sectioning over 120-μm thickness by multiphoton microscopy using 0.37-μm increments. Yellow signal indicates combined lectin labeling and ovalbumin uptake. Representative optical sections: (A) 0 μm (start level in the series), (B) 11 μm, (C) 28 μm, (D) 39 μm, (E) 53 μm, and (F) then back to 47 μm to accommodate convolution (follow proximal tubule defect for a length of >300 μm from the glomerulus). In A, PTCs (arrowheads) emerging from the glomerulus (asterisk) have completely lost lectin labeling and TR-ovalbumin uptake. In B–E, extension of swan-neck defect can be appreciated in the serial optical sections. In F, abrupt reappearance of lectin labeling coincides with TR-ovalbumin uptake (red arrow). We suggest that these cells, now first-line competent for ARME, have, thus, become most exposed to uptake of ultrafiltrated plasma proteins.

transporters relevant for Fanconi syndrome: SGLT-2 type IIa sodium-dependant phosphate cotransporter (NaPi-IIa) (Supplemental Figure 3A shows global expression level). All markers labeled WT PTC apices (Figure 8B). In *Ctns*$^{-/-}$ mice, ezrin and LT-lectin labeling selectively vanished where megalin was lost, suggesting global dedifferentiation. However, earlier loss of NaPi-IIa and cubilin over megalin (Figure 8B, d) indicated asynchronous progression into dedifferentiation.

PTC Injury Triggers Apoptosis and Epithelial Proliferation

We finally addressed whether, as reported in cultured cells,[33] cystinosis triggered PTC apoptosis, a possible mechanism for crystal clearance, and if apoptotic loss could be corrected by epithelial proliferation. Apoptosis, monitored by activated caspase-3 immunofluorescence, was hardly detected in control kidneys but easy to find in *Ctns*$^{-/-}$ PTCs after 6 months (Figure 9A, a and b). Apoptosis led to lumen shedding (Figure 9A, c and d) and was linked to PTC proliferation assessed by Ki67 immunolabeling both spatially (Figure 9A, b–d and f) and proportionally (Figure 9B, c). The highly significant correlation between apoptosis and proliferation in individual affected mice (6–12 months) also supported functional coupling (*i.e.*, epithelial regeneration and tissue repair).

DISCUSSION

Ctns$^{-/-}$ Mice Provide a Pure Model of Tubulopathy

C56BL/6 *Ctns*$^{-/-}$ mice reproduce multiple features of cystinotic nephropathy and allow us to dissect its time course. Similar urinary and PTC alterations between cystinotic mice and children indicate that defective ARME is also relevant for human cystinotic nephropathy, but preserved glomerular ultrastructure and IgG urinary absence in *Ctns*$^{-/-}$ mice up to 9 months old suggest a pure model of early tubulopathy, unlike end stage human cystinotic kidneys, which show glomerular lesions[34] and frequent glomerulotubular disconnection.[35,36] This study yielded three main findings that are likely interconnected and relevant to

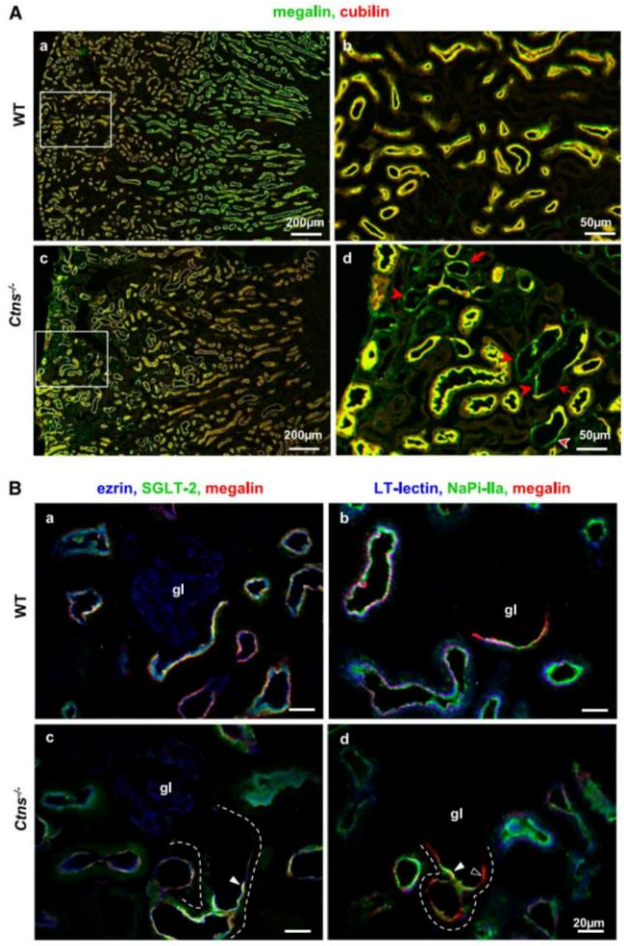

Figure 8. Multiplex immunofluorescence reveals cell-autonomous asynchronous loss of apical endocytic receptors and transporters in *Ctns*$^{-/-}$ mice cortical lesions. (A) Asynchronous loss of endocytic receptors. Paired immunofluorescence for megalin (green) and cubilin (red) in 9-month (a and b) WT and (c and d) *Ctns*$^{-/-}$ mouse kidneys. Boxed areas in a and c are enlarged in b and d. In WT mice, combined uniform expression of megalin and cubilin in the cortex generates a homogenous yellow-to-orange signal. In *Ctns*$^{-/-}$ mice, expression of both receptors is altered in cortical foci. In the enlargement shown at d, notice a triple lesional pattern/stage: (*1*) cells have a thinner apical yellow layer, indicating overall preservation of both receptors in a less-developed brush border and apical cytoplasm (thick arrow); (*2*) cells have an even thinner and only green signal, indicating additionally decreased megalin abundance and loss of detectable cubilin (arrowheads); and (*3*) PTCs do not have detectable fluorescent signal, indicating more advanced combined dedifferentiation (thin arrow). (B) Global apical PTC dedifferentiation in *Ctns*$^{-/-}$ mice cortex. Triple (immuno)fluorescence in 6-month (a and b) WT and (c and d) *Ctns*$^{-/-}$ mouse kidneys. (a and c) Combined immunolabeling for the brush border marker ezrin (blue), the sodium/glucose symporter SGLT-2 (green), and megalin (red). (b and d) Combined labeling by LT-lectin (blue) and immunolabeling for the sodium/phosphate symporter NaPi-IIa (green) and megalin (red). Note asynchronous, cell-autonomous decreased signal for LT-lectin, NaPi-IIa, SGLT-2, ezrin, and megalin in altered proximal tubules with, for example, preferential loss of NaPi-IIa over megalin (open arrowhead) adjacent to cells with combined decreased immunolabeling of megalin and NaPi-IIa or SGLT-2 (filled arrowheads). Scale bars, 20 μm.

early disease progression mechanisms: (*1*) lysosomal inclusions are concomitant with apical PTC dedifferentiation and precede crystals, (*2*) dedifferentiation likely explains the Fanconi syndrome and precedes swan-neck atrophy, and (*3*) adaptation mechanisms include cystine luminal discharge (*e.g.*, by apoptotic shedding) and proliferative epithelial repair.

Progression of the Lysosomal Cystine Form and Implications for Storage

Ctns$^{-/-}$ PTCs first show amorphous lysosomal inclusions like in human cystinotic neutrophils, where cystine is essentially soluble.[6,7] Like cystinotic fibroblasts, which actively generate but poorly retain (approximately 1%) free soluble cysteine continuously discharged by exocytosis,[10–12] PTCs in *Ctns*$^{-/-}$ kidneys incompletely retain cystine generated in lysosomes from recaptured albumin (calculations not shown). In various noncrystalline lysosome storage diseases, lysosomal expansion impacts gene expression by the transcription factor, transcription factor EB,[37] which triggers lysosomal discharge.[15] Among candidate genes promoting lysosomal discharge are Rab27a and related machineries.[38]

Amorphous inclusions are then converted into membrane-bound micrometric crystals that coalesce into huge aggregates, deforming the membrane of lysosomes and becoming progressively excluded from endocytic trafficking (*i.e.*, residual bodies). Distorted lysosomes can discharge their

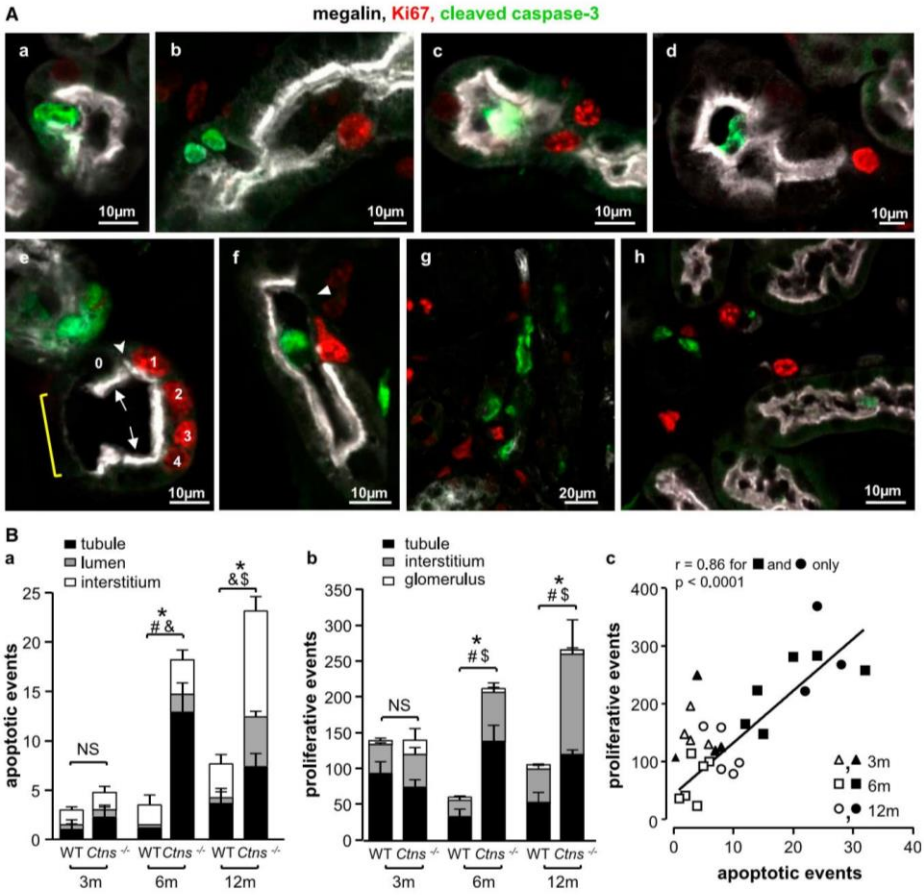

Figure 9. Apoptosis and proliferation are coordinately induced in *Ctns*$^{-/-}$ mice. (A) Triple immunofluorescence for megalin (used here as a PTC marker; white), cleaved caspase-3 (apoptotic marker; green) and Ki67 (proliferation marker; red) in (a, c, f, and g) 6- and (b, d, e, and h) 12-month *Ctns*$^{-/-}$ kidneys. This gallery compiles the following events. (*1*) Protrusion of apoptotic PTCs into the lumen (b) coupled or (a) not with proliferation within the same tubule in the same section plane. (*2*) Shedding of (c and d) apoptotic bodies into a proximal tubule lumen associated with PTC proliferation in the same tubular section. (*3*) Coexistence of (e and f) apoptosis, epithelial flattening, and proliferation. In e, a cluster of four proliferative cells (red nuclei; numbered 1–4) is separated by cells with normal height and megalin labeling (small arrows) from flattened cells with barely detectable megalin (yellow bracket); notice the discontinuity between thinner megalin labeling in proliferating cell 1 and the thicker megalin layer in the adjacent preserved cell 0 (arrowhead). In f, the uniform thick megalin layer is interrupted in the upper right (arrowhead), where a proliferative cell with red nucleus faces an apoptotic body in the lumen (green). (*4*) Extensive apoptosis and proliferation in a strongly remodeled tissue (in g, notice minimal megalin labeling above and below). (*5*) Interstitial apoptosis and proliferation between preserved PTCs (all with megalin labeling). This finding might suggest intense dynamics of the interstitial infiltrate. (B) Quantification of (a) proliferation and (b) apoptosis in 3-, 6-, and 12-month WT and *Ctns*$^{-/-}$ mouse kidneys. Cells immunolabeled for the apoptotic marker (activated/cleaved caspase-3) and the proliferation marker (Ki67) were counted in kidney sections at 3 (n=4 WT, n=4 *Ctns*$^{-/-}$), 6 (n=6 WT, n=6 *Ctns*$^{-/-}$), and 12 months (n=5 WT, n=3 *Ctns*$^{-/-}$). For each mouse, labeled cells were counted over a 2.98-mm^2 section area, corresponding to five random cortical fields. Notice significant increases of apoptosis and proliferation in 6- and 12-month-old mouse kidneys. *P<0.05 for comparison with

content by apical membrane fusion (*i.e.*, lysosomal defecation[39]) (ref.[40], figure 15). Cystine crystals are also discharged by apoptotic shedding. Although urinalysis revealed a 3- to 4-fold increase of total daily urinary cystine in *Ctns*$^{-/-}$ mice,[5] we cannot reliably quantitate the contribution of discharge as crystals, because they can dissolve in neutral urine, after which free cystine is normally recaptured by the nephron. Of note, cystinotic macrophages and corneal cells have no opportunity for luminal discharge, likely explaining the faster liver and spleen storage and early corneal crystals in patients and knockout mice.[1,41] Switching from soluble to crystalline cystine storage in cystinotic PTCs and their unique access to luminal discharge have important implications for the clock of disease progression as well as the explanation of the Fanconi syndrome, which is discussed below.

Explanation of Fanconi Syndrome and Swan-Neck Lesions

In human cystinosis, Fanconi syndrome has been attributed to PTC atrophy and is manifested as swan-neck deformities.[17] However, *Ctns*$^{-/-}$ mice reveal a clear discrepancy in timing: urinalysis narrows down the onset of the Fanconi syndrome at 3–6 months (*i.e.*, before PTC atrophy). Instead, we show an earlier loss of expression of megalin/cubilin, SGLT-2, and NaPi-IIa, which together provide a straightforward molecular explanation of proteinuria, glucosuria, and phosphaturia. Dedifferentiation before atrophy implies reversal of the apical differentiation program and might account for asynchrony between individual apical components as reported in cultured PTCs.[18] Long considered as degradative organelles, lysosomes emerge as signaling compartments that are able to impact on gene expression.[37] The signaling and transcriptional linkages between lysosomal expansion before crystals and repressed apical differentiation before atrophy deserve additional studies.

PTC atrophy, thus, develops later in *Ctns*$^{-/-}$ mice, starting at the glomerulotubular junction and extending longitudinally into typical swan-neck lesions, such as seen in cystinotic children (Figures 2B and 7).[5] What links dedifferentiation with atrophy? What accounts for longitudinal extension of swan-neck deformities? Atrophy may be considered as an ultimate stage of dedifferentiation and likely also involves autophagy, which is not addressed in this study. What we document, however, is defective apical endocytosis in S1 cells that not only leads to proteinuria but also, displaces endocytic load of disulfide-rich proteins into farther PTCs (S3). Whether distal transfer of harmful cystine load is sufficient to cause longitudinal disease progression is currently under investigation.

Another nonmutually exclusive explanation for swan-neck lesions is metaplasia by extension from Bowman's squamous epithelium into S1. This mechanism would also account for (*1*) the disappearance of PTCs normally enclosed within the Bowman's capsule of the mouse (compare Figure 2A with Figure 2B), (*2*) the much thicker basement membrane in flattened cells at swan-neck compared with normal PTCs that is similar to Bowman's capsule, and (*3*) their apparent lack of cystine crystals.

Adaptation by Cystine Disposal and Repair of Apoptosis by Epithelial Proliferation

Three potential mechanisms could account for cystine disposal: (*1*) continuous exocytosis of soluble cysteine that is able to traverse tiny tubular endosomes,[13] (*2*) later crystal exocytosis by active lysosomal defecation,[39] and (*3*) apoptotic crystal shedding. Apoptotic luminal shedding, a known mechanism of lysosomal clearance in gentamicin-induced phospholipidosis,[42] is, of course, a one-shot discharge, but it is also a trigger for epithelial proliferation. Our quantitative time course study shows increased apoptosis in 6- to 12-month-old *Ctns*$^{-/-}$ kidneys, which was reported *in vitro* based on acute cystine loading of normal cells or depletion by cysteamine of human cystinotic fibroblasts.[33] Moreover, correlation between apoptosis and PTC proliferation indicates functional coupling. Epithelial proliferation not only helps protect PTC mass and repair epithelial continuity but also, replenishes dividing cells with fresh lysosomes during the G1 phase, which may also slow down disease progression.

CONCISE METHODS

Reagents

Primers, markers, and tracers are shown in Supplemental Tables 1 and 2.

Tissues

Mouse kidneys were perfusion-fixed with 4% formaldehyde, paraffin-embedded or sucrose-infused, and frozen. Archived biopsies of four

age-matched WT for all events; $^{\#}P<0.05$ for tubular events; $^{\&}P<0.05$ for luminal events; $^{\$}P<0.05$ for interstitial events. An approximately 10-fold higher frequency for Ki67 immunolabeling compared with cleaved caspase-3 is expected, because Ki67 is expressed throughout the cell division cycle (approximately 20–24 hours), whereas apoptosis is a short event, thus with much lower probability to capture. In c, notice limited apoptosis in WT (open symbols) and 3-month *Ctns*$^{-/-}$ mice (filled triangles). In contrast, notice the strong, highly significant correlation between apoptosis and proliferation in *Ctns*$^{-/-}$ mice at 6 and 12 months (filled squares and circles), which suggests that these two events are coupled. Adaptation repair is also suggested by full preservation of relative kidney weight up to 9 months (8.46±0.27 versus 8.53±0.35 mg wet kidney/g body weight in WT versus knockout, mean±SEM, n=20 in each group, P=NS by t test; at 12 months, 8.68±0.37 versus 7.73±0.36 mg wet kidney/g body weight in WT versus knockout, mean±SEM, n=7 in each group, P=0.11, P=NS by t test).

cystinotic children and one described case[29] were compared with control human kidney.

Urinalysis

Daily (mice) or morning urine samples (from five other cystinotic children and age-matched healthy controls) (Supplemental Table 3) were analyzed for volume, glucose (glucose oxidase), inorganic phosphate,[43] proteins (Western blotting), and β-hexosaminidase.[28]

Morphology

Electron microscopy,[44] immunoperoxidase,[45] uptake of ultrafiltrated HRP (immunofluorescence), TexasRed-ovalbumin,[46] and ^{125}I-β_2-microglobulin,[27,32] multiplex (immuno)fluorescence on 5-μm frozen sections, and whole-mount (immuno)fluorescence on 200-μm vibratome slices[47] were as described or slightly modified.

RT-PCR and *In Situ* Hybridization

Quantitative RT-PCR and *in situ* hybridization on 8-μm paraffin sections were completed as described.[45,48]

Statistical Analyses

Values are means±SEMs (bar histograms) or means of individual symbols (significance of differences tested by t or Mann–Whitney test, respectively).

ACKNOWLEDGMENTS

We thank the biolibrary of the Université Catholique de Louvain for providing renal tissue of cystinotic and control patients, Dr. M.C. Gubler (Necker) for collecting old cystinotic kidney blocs and generously providing advice, Dr. A. Bernard and Mr. X. Dumont for performing CC16 immunoassays, Dr. E. Van Schaftingen and Mrs G. Noel for assays of glucosuria and phosphaturia, Dr. N. Van Baren for generous help in high-content imaging and reporting, L. Thanh for electron microscopy and autoradiography, and Y. Abid and S. Godecharles for assistance in morphometry.

This work was mainly supported by the Cystinosis Research Foundation, European Union Seventh Programme (EuNefron; E.L., S.C., C.A., and P.J.C.) and Belgian Science Policy Office—Interuniversity Attraction Poles Programme IAP P7/43-BeMGI. It was also supported by the Belgian Fonds de la Recherche Scientifique (FRS-FNRS) and Actions de Recherche Concertées (C.E.P. and P.J.C.) and National Institutes of Health Grants R01-DK090058 (to S.C.) and R21-DK090548 (to S.C.). The Platform for Imaging Cells and Tissues was financed by National Lottery, Région bruxelloise, Région wallonne, Université Catholique de Louvain and de Duve Institute (P.J.C.). H.P.G.C. is a Postdoctoral Researcher and C.E.P. is a Senior Research Associate at FRS-FNRS.

DISCLOSURES

None.

REFERENCES

1. Gahl WA, Thoene JG, Schneider JA: Cystinosis. *N Engl J Med* 347: 111–121, 2002
2. Nesterova G, Gahl WA: Cystinosis: The evolution of a treatable disease. *Pediatr Nephrol* 28: 51–59, 2013
3. Kalatzis V, Cherqui S, Antignac C, Gasnier B: Cystinosin, the protein defective in cystinosis, is a H(+)-driven lysosomal cystine transporter. *EMBO J* 20: 5940–5949, 2001
4. Kalatzis V, Nevo N, Cherqui S, Gasnier B, Antignac C: Molecular pathogenesis of cystinosis: Effect of CTNS mutations on the transport activity and subcellular localization of cystinosin. *Hum Mol Genet* 13: 1361–1371, 2004
5. Nevo N, Chol M, Bailleux A, Kalatzis V, Morisset L, Devuyst O, Gubler MC, Antignac C: Renal phenotype of the cystinosis mouse model is dependent upon genetic background. *Nephrol Dial Transplant* 25: 1059–1066, 2010
6. Schulman JD, Bradley KH, Seegmiller JE: Cystine: Compartmentalization within lysosomes in cystinotic leukocytes. *Science* 166: 1152–1154, 1969
7. Hummeler K, Zajac BA, Genel M, Holtzapple PG, Segal S: Human cystinosis: Intracellular deposition of cystine. *Science* 168: 859–860, 1970
8. Oude Elferink RP, Harms E, Strijland A, Tager JM: The intralysosomal pH in cultured human skin fibroblasts in relation to cystine accumulation in patients with cystinosis. *Biochem Biophys Res Commun* 116: 154–161, 1983
9. Thoene JG, Oshima RG, Ritchie DG, Schneider JA: Cystinotic fibroblasts accumulate cystine from intracellular protein degradation. *Proc Natl Acad Sci U S A* 74: 4505–4507, 1977
10. Thoene JG, Lemons R: Modulation of the intracellular cystine content of cystinotic fibroblasts by extracellular albumin. *Pediatr Res* 14: 785–787, 1980
11. Thoene JG, Lemons RM: Cystine accumulation in cystinotic fibroblasts from free and protein-linked cystine but not cysteine. *Biochem J* 208: 823–830, 1982
12. Pisoni RL, Acker TL, Lisowski KM, Lemons RM, Thoene JG: A cysteine-specific lysosomal transport system provides a major route for the delivery of thiol to human fibroblast lysosomes: Possible role in supporting lysosomal proteolysis. *J Cell Biol* 110: 327–335, 1990
13. Christensen EI: Rapid membrane recycling in renal proximal tubule cells. *Eur J Cell Biol* 29: 43–49, 1982
14. Carpentier S, N'Kuli F, Grieco G, Van Der Smissen P, Janssens V, Emonard H, Bilanges B, Vanhaesebroeck B, Gaide Chevronnay HP, Pierreux CE, Tyteca D, Courtoy PJ: Class III phosphoinositide 3-kinase/VPS34 and dynamin are critical for apical endocytic recycling. *Traffic* 14: 933–948, 2013
15. Medina DL, Fraldi A, Bouche V, Annunziata F, Mansueto G, Spampanato C, Puri C, Pignata A, Martina JA, Sardiello M, Palmieri M, Polishchuk R, Puertollano R, Ballabio A: Transcriptional activation of lysosomal exocytosis promotes cellular clearance. *Dev Cell* 21: 421–430, 2011
16. Christensen EI, Wagner CA, Kaissling B: Uriniferous tubule: Structural and functional organization. *Compr Physiol* 2: 805–861, 2012
17. Mahoney CP, Striker GE: Early development of the renal lesions in infantile cystinosis. *Pediatr Nephrol* 15: 50–56, 2000
18. Lima WR, Parreira KS, Devuyst O, Caplanusi A, N'kuli F, Marien B, Van Der Smissen P, Alves PM, Verroust P, Christensen EI, Terzi F, Matter K, Balda MS, Pierreux CE, Courtoy PJ: ZONAB promotes proliferation and represses differentiation of proximal tubule epithelial cells. *J Am Soc Nephrol* 21: 478–488, 2010
19. Toledano MB, Delaunay-Moisan A, Outten CE, Igbaria A: Functions and cellular compartmentation of the thioredoxin and glutathione pathways in yeast. *Antioxid Redox Signal* 18: 1699–1711, 2013

20. Christensen EI, Verroust PJ: Megalin and cubilin, role in proximal tubule function and during development. *Pediatr Nephrol* 17: 993–999, 2002
21. Pfeifer U, Scheller H: A morphometric study of cellular autophagy including diurnal variations in kidney tubules of normal rats. *J Cell Biol* 64: 608–621, 1975
22. Christensen EI, Birn H: Megalin and cubilin: Multifunctional endocytic receptors. *Nat Rev Mol Cell Biol* 3: 256–266, 2002
23. Leheste JR, Rolinski B, Vorum H, Hilpert J, Nykjaer A, Jacobsen C, Aucouturier P, Moskaug JO, Otto A, Christensen EI, Willnow TE: Megalin knockout mice as an animal model of low molecular weight proteinuria. *Am J Pathol* 155: 1361–1370, 1999
24. Weyer K, Storm T, Shan J, Vainio S, Kozyraki R, Verroust PJ, Christensen EI, Nielsen R: Mouse model of proximal tubule endocytic dysfunction. *Nephrol Dial Transplant* 26: 3446–3451, 2011
25. Weyer K, Nielsen R, Christensen EI, Birn H: Generation of urinary albumin fragments does not require proximal tubular uptake. *J Am Soc Nephrol* 23: 591–596, 2012
26. Amsellem S, Gburek J, Hamard G, Nielsen R, Willnow TE, Devuyst O, Nexo E, Verroust PJ, Christensen EI, Kozyraki R: Cubilin is essential for albumin reabsorption in the renal proximal tubule. *J Am Soc Nephrol* 21: 1859–1867, 2010
27. Christensen EI, Devuyst O, Dom G, Nielsen R, Van der Smissen P, Verroust P, Leruth M, Guggino WB, Courtoy PJ: Loss of chloride channel ClC-5 impairs endocytosis by defective trafficking of megalin and cubilin in kidney proximal tubules. *Proc Natl Acad Sci U S A* 100: 8472–8477, 2003
28. Nielsen R, Courtoy PJ, Jacobsen C, Dom G, Lima WR, Jadot M, Willnow TE, Devuyst O, Christensen EI: Endocytosis provides a major alternative pathway for lysosomal biogenesis in kidney proximal tubular cells. *Proc Natl Acad Sci U S A* 104: 5407–5412, 2007
29. Wilmer MJ, Christensen EI, van den Heuvel LP, Monnens LA, Levtchenko EN: Urinary protein excretion pattern and renal expression of megalin and cubilin in nephropathic cystinosis. *Am J Kidney Dis* 51: 893–903, 2008
30. Zhai XY, Birn H, Jensen KB, Thomsen JS, Andreasen A, Christensen EI: Digital three-dimensional reconstruction and ultrastructure of the mouse proximal tubule. *J Am Soc Nephrol* 14: 611–619, 2003
31. Straus W: Cytochemical observations on the relationship between lysosomes and phagosomes in kidney and liver by combined staining for acid phosphatase and intravenously injected horseradish peroxidase. *J Cell Biol* 20: 497–507, 1964
32. Jouret F, Walrand S, Parreira KS, Courtoy PJ, Pauwels S, Devuyst O, Jamar F: Single photon emission-computed tomography (SPECT) for functional investigation of the proximal tubule in conscious mice. *Am J Physiol Renal Physiol* 298: F454–F460, 2010
33. Park M, Helip-Wooley A, Thoene J: Lysosomal cystine storage augments apoptosis in cultured human fibroblasts and renal tubular epithelial cells. *J Am Soc Nephrol* 13: 2878–2887, 2002
34. Wilmer MJ, Emma F, Levtchenko EN: The pathogenesis of cystinosis: Mechanisms beyond cystine accumulation. *Am J Physiol Renal Physiol* 299: F905–F916, 2010
35. Larsen CP, Walker PD, Thoene JG: The incidence of atubular glomeruli in nephropathic cystinosis renal biopsies. *Mol Genet Metab* 101: 417–420, 2010
36. Chevalier RL, Forbes MS: Generation and evolution of atubular glomeruli in the progression of renal disorders. *J Am Soc Nephrol* 19: 197–206, 2008
37. Sardiello M, Palmieri M, di Ronza A, Medina DL, Valenza M, Gennarino VA, Di Malta C, Donaudy F, Embrione V, Polishchuk RS, Banfi S, Parenti G, Cattaneo E, Ballabio A: A gene network regulating lysosomal biogenesis and function. *Science* 325: 473–477, 2009
38. Johnson JL, Napolitano G, Monfregola J, Rocca CJ, Cherqui S, Catz SD: Upregulation of the Rab27a-dependent trafficking and secretory mechanisms improves lysosomal transport, alleviates endoplasmic reticulum stress, and reduces lysosome overload in cystinosis. *Mol Cell Biol* 33: 2950–2962, 2013
39. De Duve C, Wattiaux R: Functions of lysosomes. *Annu Rev Physiol* 28: 435–492, 1966
40. Maunsbach AB: Observations on the ultrastructure and acid phosphatase activity of the cytoplasmic bodies in rat kidney proximal tubule cells. With a comment on their classification. *J Ultrastruct Res* 16: 197–238, 1966
41. Simpson J, Nien CJ, Flynn K, Jester B, Cherqui S, Jester J: Quantitative in vivo and ex vivo confocal microscopy analysis of corneal cystine crystals in the Ctns knockout mouse. *Mol Vis* 17: 2212–2220, 2011
42. Tulkens PM: Experimental studies on nephrotoxicity of aminoglycosides at low doses. Mechanisms and perspectives. *Am J Med* 80[Suppl 6B]: 105–114, 1986
43. Fiske CH, Subbarow Y: The colorimetric determination of phosphorus. *J Biol Chem* 66: 375–400, 1925
44. Maunsbach AB: The influence of different fixatives and fixation methods on the ultrastructure of rat kidney proximal tubule cells. I. Comparison of different perfusion fixation methods and of glutaraldehyde, formaldehyde and osmium tetroxide fixatives. *J Ultrastruct Res* 15: 242–282, 1966
45. Gaide Chevronnay HP, Cornet PB, Delvaux D, Lemoine P, Courtoy PJ, Henriet P, Marbaix E: Opposite regulation of transforming growth factors-beta2 and -beta3 expression in the human endometrium. *Endocrinology* 149: 1015–1025, 2008
46. Caplanusi A, Parreira KS, Lima WR, Marien B, Van Der Smissen P, de Diesbach P, Devuyst O, Courtoy PJ: Intravital multi-photon microscopy reveals several levels of heterogeneity in endocytic uptake by mouse renal proximal tubules. *J Cell Mol Med* 12: 351–354, 2008
47. Pierreux CE, Cordi S, Hick AC, Achouri Y, Ruiz de Almodovar C, Prévot PP, Courtoy PJ, Carmeliet P, Lemaigre FP: Epithelial: Endothelial cross-talk regulates exocrine differentiation in developing pancreas. *Dev Biol* 347: 216–227, 2010
48. Hick AC, van Eyll JM, Cordi S, Forez C, Passante L, Kohara H, Nagasawa T, Vanderhaeghen P, Courtoy PJ, Rousseau GG, Lemaigre FP, Pierreux CE: Mechanism of primitive duct formation in the pancreas and submandibular glands: A role for SDF-1. *BMC Dev Biol* 9: 66, 2009
49. Norden AG, Gardner SC, Van't Hoff W, Unwin RJ: Lysosomal enzymuria is a feature of hereditary Fanconi syndrome and is related to elevated CI-mannose-6-P-receptor excretion. *Nephrol Dial Transplant* 23: 2795–2803, 2008
50. Luzio JP, Pryor PR, Bright NA: Lysosomes: Fusion and function. *Nat Rev Mol Cell Biol* 8: 622–632, 2007

This article contains supplemental material online at http://jasn.asnjournals.org/lookup/suppl/doi:10.1681/ASN.20130600598/-/DCSupplemental.

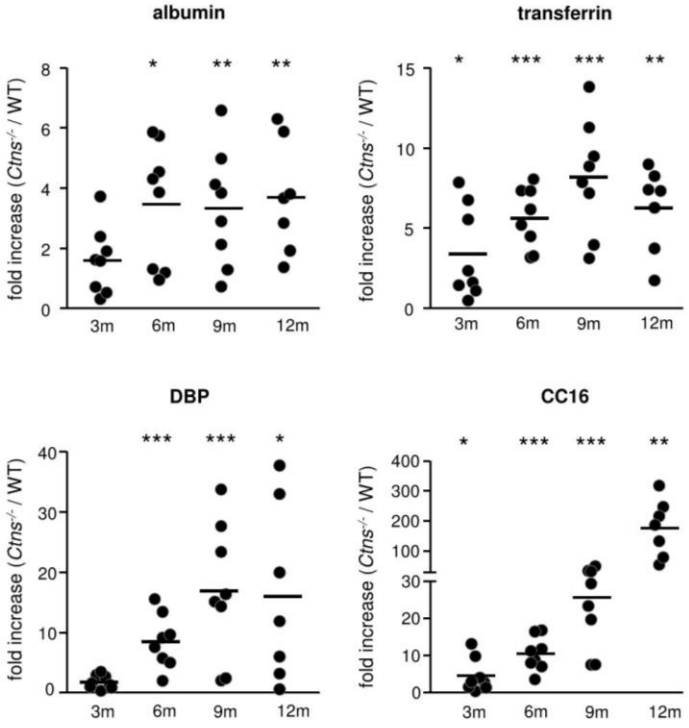

Supplemental Fig 1. Quantitation of time-course of proteinuria. Daily urine collections of 3 months (n=8), 6 months (n=8), 9 months (n=8) and 12 months (n=7) WT and *Ctns*$^{-/-}$ mice were probed by quantitative western blotting for the plasma proteins albumin, transferrin and vitamin D-binding protein as at Fig1B. The very low-molecular weight toxicological marker, CC16 (~10 kDa; released from bronchiolar Clara cells) was assayed by a sensitive latex immunoassay, as described[51]. Data are presented as fold-increase in *Ctns*$^{-/-}$ mice urine as compared to mean values in corresponding WT urine.

Supplemental Figure 1

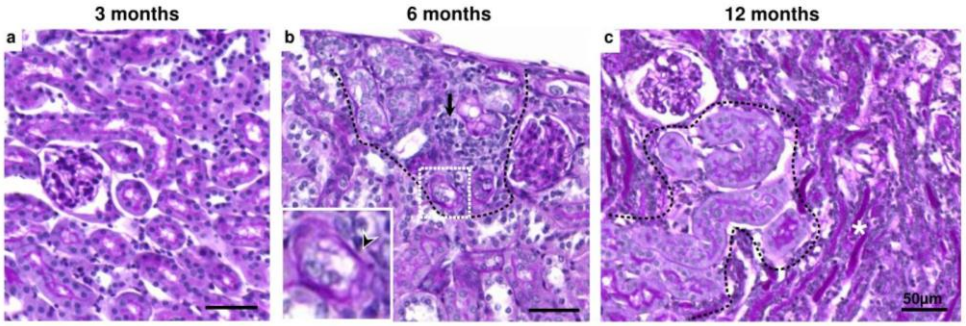

Supplemental Figure 2. Progression of histological lesions in *Ctns*$^{-/-}$ mice kidneys (paraffin sections, PAS staining). (a, 3 months) Notice preserved PTC thickness including brush border, without detectable interstitial infiltrate. **(b, 6 months)** Discrete foci of atrophic PTC (delineated by broken line) are first detected under the kidney capsule, as evidenced by vanished brush border, flattened epithelial cells with irregular nuclear stratification, and basement membrane thickening (see enlargement of boxed area; arrowhead). The arrow points to a discrete inflammatory infiltrate. **(c, 12 months)** Radial bundles of atrophic proximal tubules indicate longitudinal disease progression towards the medulla. Deep atrophic tubules frequently enclose protein casts (asterisk), which strongly label for megalin, indicating shedding (not shown). Notice sharp demarcation from apparently intact tissue (broken line), with intact glomerulus at upper left. Bars, 50µm.

Supplemental Figure 2

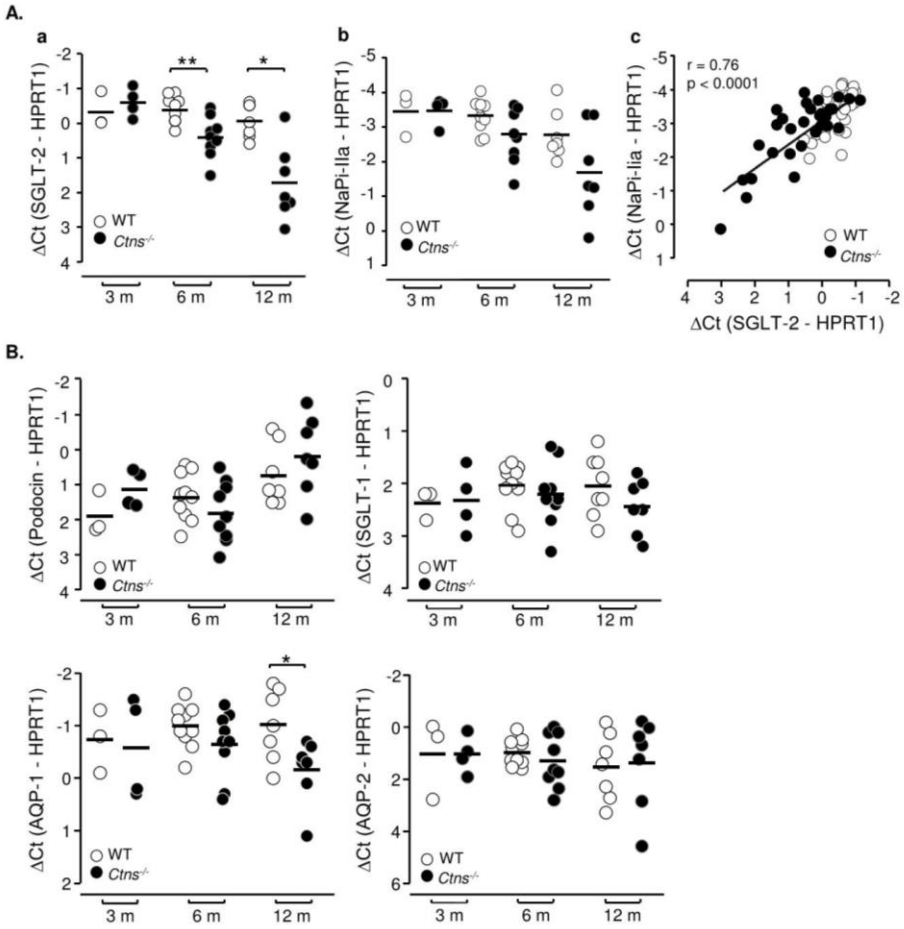

Supplemental Figure 3

Supplemental Figure 3. Time-course of sodium/glucose transporter-2 (SGLT-2), sodium/phosphate cotransporter type II-a (NaPi-IIa), podocin, sodium/glucose transporter-1 (SGLT-1) and aquaporins-1 (AQP-1) and -2 (AQP-2) mRNA expression in WT *vs* *Ctns*$^{-/-}$ mice kidneys. **(A)** Quantification by RT-qPCR of SGLT-2 (a) and NaPi-IIa (b) mRNAs in WT and *Ctns*$^{-/-}$ kidneys collected at 3, 6 and 12 months as used for Fig4A. (c) Correlation between global NaPi-IIa and SGLT-2 mRNA expression. Notice comparable decrease of SGLT-2 and NaPi-IIa mRNAs as for megalin and cubilin at Fig4A, but with somewhat weaker correlation. **(B)** Comparison with abundance of podocin, sodium/glucose transporter-1 (SGLT-1) and aquaporin-1 (AQP-1) and -2 (AQP-2) mRNAs in WT and *Ctns*$^{-/-}$ kidneys sampled, analyzed and presented as at Fig4A. Notice lack of significant variation of expression of podocin (glomerulus), SGLT-1 (straight PTC) and AQP-2 (convoluted tubule) but late decline of AQP-1 (proximal marker). These data confirm that lesions studied were restricted to proximal tubular cells.

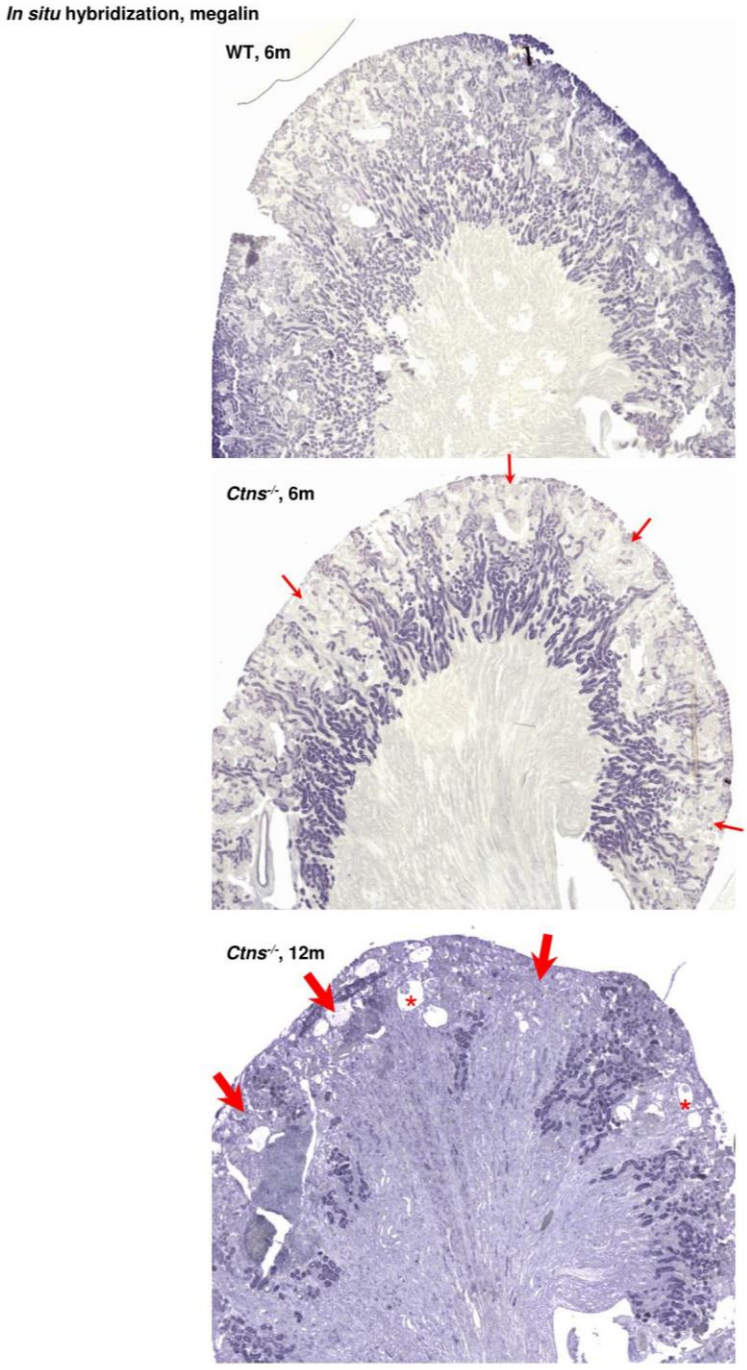

Supplemental Figure 4A

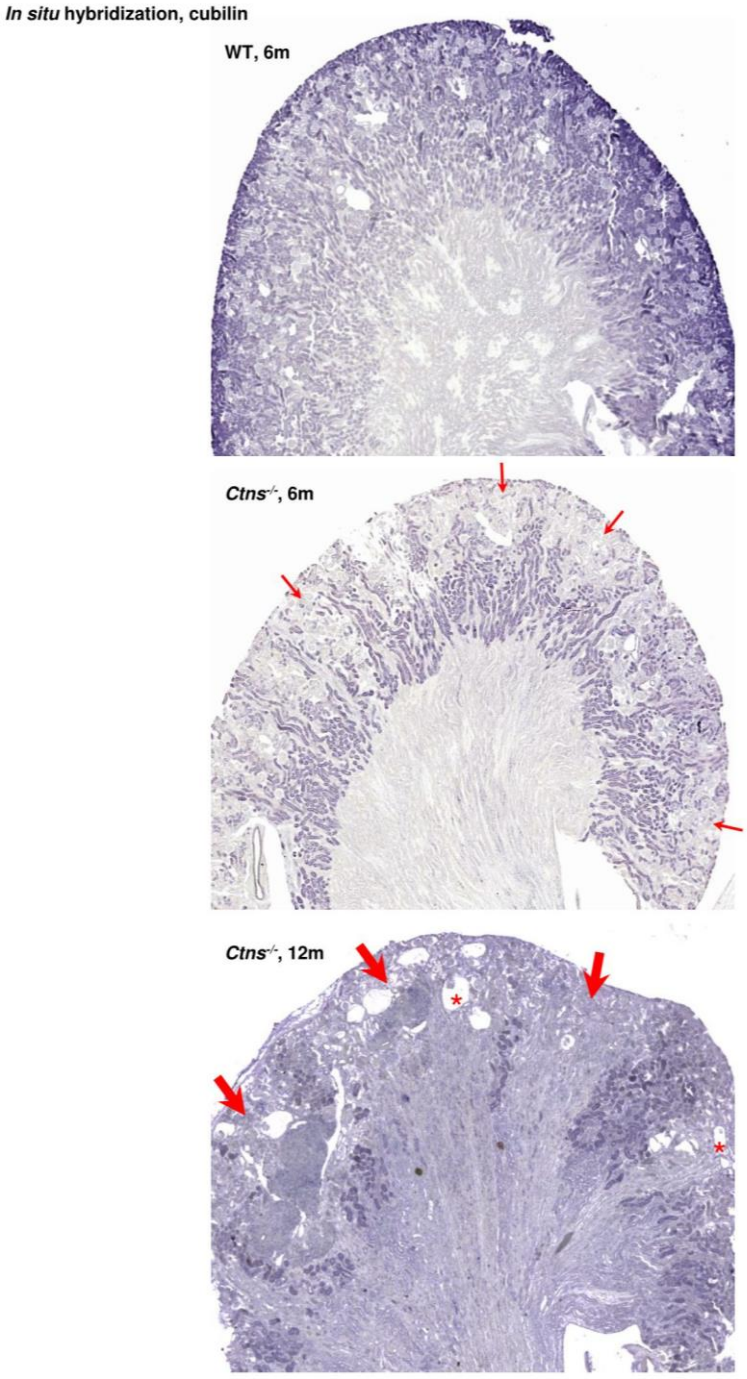

Supplemental Figure 4B

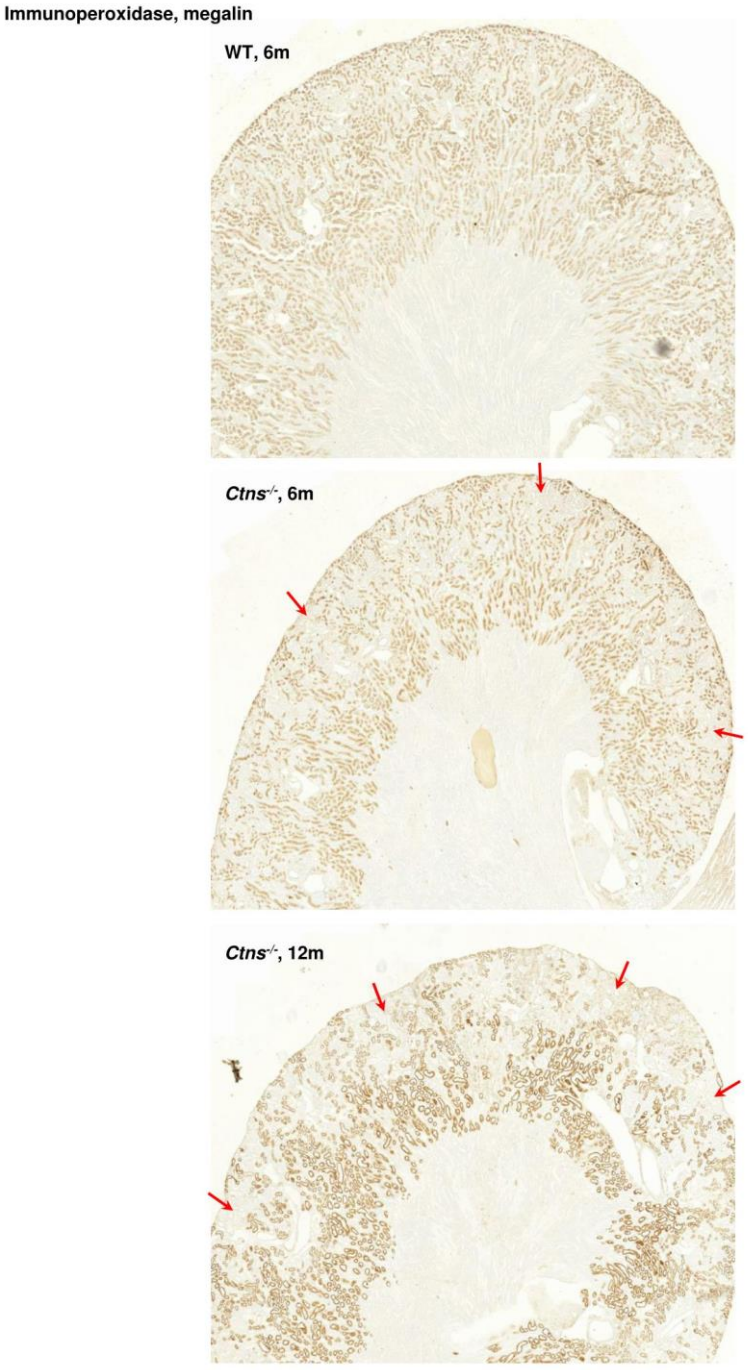

Supplemental Figure 4C

Supplemental Figure 4D

Supplemental Figure 4. Large fields showing temporal and spatial loss of megalin and cubilin in *Ctns*$^{-/-}$ mice kidneys. Localization by *in situ* hybridization **(A, B)** and immunoperoxidase **(C, D)** of megalin **(A, C)** and cubilin **(B, D)** in WT (6 months) and *Ctns*$^{-/-}$ (6 and 12 months) mice kidneys. In WT and *Ctns*$^{-/-}$ kidneys at 6 months, both methods could successfully be applied for the two endocytic receptors in adjacent sections from the same blocs. In WT kidney, notice essentially uniform labeling of PTCs in cortex and OSOM of WT mice. This contrasts with extending foci characterized by loss of megalin and cubilin expression in *Ctns*$^{-/-}$ kidneys at 6 months (thin arrows), up to large areas with total loss of expression at 12 months (thick arrows). Asterisks show dilated renal corpuscles with enlarged Bowman's space and collapsed capillary tufts, compatible with glomerulo-tubular disconnection. Of note, the unequal background between *in situ* hybridization images reflects limited reproducibility of the method. Likewise, immunoperoxidase reliably identifies expressing cells, but labeling intensity varies between samples processed separately. Thus, variation of intensity in presented images (e.g. in OSOM between *Ctns*$^{-/-}$ at 6 months and 12 months) cannot be taken as evidence of increased expression at later times.

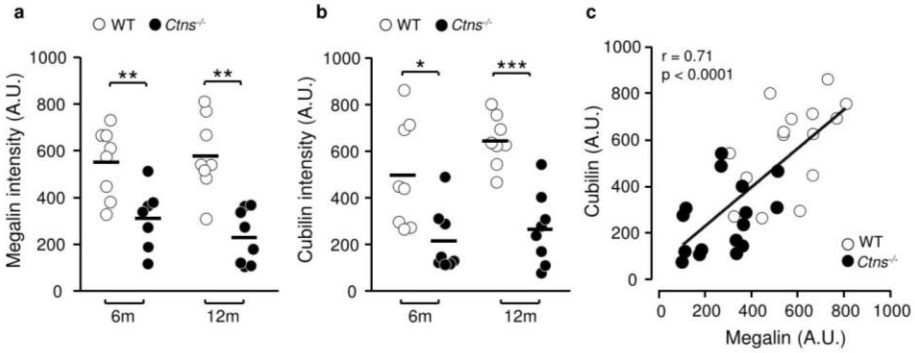

Supplemental Figure 5. Quantitation of loss of endocytic receptors by western blotting of kidney lysates. Two µg protein of lysates from 8 WT and 8 *Ctns*$^{-/-}$ kidneys at 6 and at 12 months were analysed in blots processed strictly in parallel for each time. Data are presented as intensity in arbitrary units (A.U.).* $p<0.05$, ** $p<0.01$, *** $p<0.001$. At right, note strong correlation between megalin and cubilin proteins, as shown at their mRNA levels (Fig4Ac).

Supplemental Figure 5

Supplemental Table I:

gene	forward primer (5' → 3')	reverse primer (5' →3')	Use
cubilin	TACCTGACTGAGGACAGCAAGAG	CCTCTCATTTGAATACTTATGTC	ISH
megalin	CAGTTCAATGGAGGATGCAGCC	CATCGCCCATTGGCACAAGT	ISH
AQP-1	GCTGTCATGTACATCATCGCCCAG	AGGTCATTGCGGCCAAGTGAAT	RT-qPCR
AQP-2	TGAGCCTCAAGAAGGGTCTC	TCTCCAGAGCTCTCCGTCTC	RT-qPCR
cubilin	TCATTGGCCTCAGACATTCC	CCCAGACCTTCACAAAGCTG	RT-qPCR
HPRT-1	ACATTGTGGCCCTCTGTGTG	TTATGTCCCCCGTTGACTGA	RT-qPCR
megalin	CAGTGGATTGGGTAGCAGGA	GCTTGGGGTCAACAACGATA	RT-qPCR
NaPi-IIa	AGGTGAGCTCCGCCATTCCGA	CCCTGCAAAAGCCCGCCTGA	RT-qPCR
podocin	AAGGACAGATATGGGCACTGTCA	CCAGGAGCACCTAAGCTATGGAA	RT-qPCR
SGLT-1	TGCCTTCCTGATGCAGCACACT	TCGGTGGGTGACCCCCTGTG	RT-qPCR
SGLT-2	GCTGGTCATTGGTGTTGGCTTGTG	GAACAGAGAGGCTCCAACCGGC	RT-qPCR

Supplemental Table I. List of primer sequences. ISH, *in situ* hybridization; RT-qPCR, real-time quantitative PCR.

Supplemental Table II:

antibodies, lectins and tracers	source	reference	use	dilution
goat anti-mouse albumin	Santa Cruz	P-20, sc-46293	WB	1/1000
rabbit anti-human transferrin	Dako	A0061	WB	1/1000
rabbit anti-human RBP	Dako	A0040	WB	1/1000
rabbit anti-human DBP	Dako	A0021	WB	1/1000
sheep anti-rat megalin	R. Kozyraki	Verroust et al., 2002 [52]	IP, IF	1/1000, 1/800
rabbit anti-rat cubilin	R. Kozyraki	Verroust et al., 2002 [52]	IP, IF	1/1200, 1/1000
rabbit anti-mouse NaPi-IIa	J. Biber	Custer et al. 1994 [53]	IF	1/1000
rabbit anti-human SGLT-2	Santa Cruz	Sc-98975	IF	1/100
rabbit anti-podocin	C. Antignac	Roselli et al., 2002 [54]	IF	1/500
mouse anti-ezrin	ThermoScientific	MS-661-P1	IF	1/100
mouse anti-Ki67	BD Pharmingen	556003	IF	1/250
rabbit anti-cleaved caspase-3	Cell Signaling	9661S	IF	1/200
rat anti-LAMP-1	Hybridoma Bank	1D4B	IF	1/100
Alexa488 goat anti-HRP	Jackson	123-545-021	IF	1/500
biotinylated LT-lectin	Vector labs	B-1325	IF	1/100
fluorescein LT-lectin	Vector labs	FL-1321	IF	1/100
TexasRed-ovalbumin	Invitrogen	O23021	IF, MP	300µg, 600µg
Horseradish peroxidase	Sigma	P8375	IF	120ng/g bw
β2-microglobulin	Sigma	M4890	AR	200ng/g bw

Supplemental Table II. List of antibodies, lectins and tracers. WB, western blotting; IP, immunoperoxidase; IF, immunofluorescence; MP, multiphoton; AR, autoradiography.

Supplemental Table III:

A. kidney histology					
#	**sex**	**age (years)**	**Fanconi**	**plasma creatinine (µmol/l)**	**Other**
LC	F	3	Yes	51	corneal cystine crystals 18.8 nmoles half cystine/mg fibroblast protein
IM	F	8	Yes	352	
BC	M	10	Yes	1061	corneal cystine crystals
GM	F	12	Yes	283	
EL	M	8	Yes	?	genotype c.922_923insG ; [29]

B. urine					
#	**sex**	**age (years)**	**genotype**	**Fanconi**	**plasma creatinine (µmol/l)**
1	F	5	57kbdel+c.927_928insG	Yes	56
2	F	6	57kbdel+c.927_928insG	Yes	51
3	M	11	hom57kbdel	Yes	40
4	M	13	57kbdel+c.198_218del21	**No**	82
5	M	15	hom 57kbdel	Yes	122

Supplemental Table III. Clinical data for patients with cystinosis.

Plasma creatinine concentration was at time of renal biopsy for patient #LC (shown at Fig4b,e). For #IM (nephrectomy specimen shown at Fig4c,f) value was at 2 months before nephrectomy without hemodialysis. For kidney histology of patient EL, see [29].

Complete Material and Methods

Mice

Congenic C57BL/6 *Ctns*$^{-/-}$ mice have been described[5]. Mice were treated according to the NIH Guide for Care and Use of Laboratory Animals.

Patients

Four cystinotic renal tissues, traced from the virtual biolibrary of the Université catholique de Louvain, were retrieved as Bouin-fixed, paraffin-embedded samples from the archives of the Pathology Department at Saint-Luc Academic Hospital, after approval of the Ethical Committee. One was a kidney biopsy from a 3-year old girl for diagnosis of growth failure with a kidney Fanconi syndrome. The others were nephrectomy specimens taken during renal transplantation. A kidney biopsy from a 3-year old primary oxaluric boy served as control. Urinary samples were collected from 5 other cystinotic children (2 girls, 3 boys; 5–to-15-year old) and age-matched healthy controls (4 girls, 1 boy; 5-to-15-year old) after informed consent. Diagnosis of cystinosis was confirmed by molecular analysis of the CTNS gene in all patients. All patients but #4 had overt Fanconi syndrome. For comparison, we reanalyzed the previously studied cystinotic kidney paraffin bloc provided by the Leuven University Hospitals, Nephrology Department[29].

Urine analysis

Mice urine was collected in metabolic cages for 24 h on ice with protease inhibitors cocktail, (Complete™ Protease Inhibitor Cocktail Tablets, Roche, Mannhein, Germany). Children urine samples were collected at morning raise on protease inhibitors and immediately frozen. This procedure optimizes preservation of excreted proteins from urinary proteases, which is particularly important to prevent biases due to increased urinary excretion of ultrafiltrated lysosomal cathepsins normally recaptured by PTCs as megalin ligands[28]. Diuresis (weight) glucosuria (enzymatic assay) and inorganic phosphaturia (Fiske) were measured by standard methods. Beta-hexosaminidase activity assays and Western blots (equivalent of 2µg urinary creatinine/lane) were performed as described[27]. Proteins were resolved into precasted gels (Mini protean TGX 4-15%, 456-1083, Bio-Rad). The following primary antibodies were

used: goat anti-mouse albumin (ALB; P-20, sc-46293, Santa Cruz Biotechnology, Heidelberg, Germany), rabbit anti-human transferrin (TR; A0061, DakoCytomation, Glostrup, Denmark), rabbit anti-human retinol-binding-protein (RBP; A0040, DakoCytomation), and rabbit anti-human vitamin D-binding protein (DBP; A0021, DakoCytomation). Peroxidase-labelled secondary antibodies were revealed by enhanced chemiluminescence. Clara cell 10-16kDa protein, released from the non-ciliated Clara cells in terminal and respiratory bronchioles, was assayed by a latex immunoassay exactly as described[51].

Histological studies and immunoperoxidase

Mice kidneys were fixed *in situ* by whole-body perfusion-fixation through the left ventricle under a height of 120 cm, after right atrium excision for outlet. Blood was flushed with phosphate-buffered saline (PBS) for ~2 min, then perfusate was switched to 4% neutral-buffered formaldehyde (4%F) for 5 min. Kidneys were excised, capsule was pulled away, then slices were post-fixed overnight with 4%F and processed for paraffin embedding. Seven µm-thick sections were stained with periodic acid Schiff. Immunoperoxidase was performed as described[45] without antigen retrieval. Sections were incubated overnight at 4°C with sheep anti-rat megalin (1/1000) or rabbit anti-rat cubilin (1/1200; both kind gift of Dr. R. Kozyraki[55]). For megalin, rabbit anti-sheep IgG (1/1000; 31240, ThermoScientific, Rockford, IL) were used as secondary antibodies. All other antigens were revealed with peroxidase-conjugated dextran molecules carrying anti-rabbit antibodies (Envision; DakoCytomation) followed by incubation with H_2O_2 and diaminobenzidine. Full-section images were acquired using a Zeiss Mirax Midi microscope.

Electron microscopy

Kidneys were perfusion-fixed *in situ* as above using 2% (v/v) glutaraldehyde at room temperature, then post-fixed overnight at 4°C. Very small blocks were post-fixed with 1% (w/v) OsO_4 in 0.1M cacodylate buffer for 1h, rinsed in veronal buffer (4 x 5min) and stained overnight "en bloc" in 1% neutral uranyl acetate, all at 4°C. After extensive washing in veronal buffer, blocks were dehydrated in graded ethanol and embedded in Spurr. Ultrathin (70nm nominal) sections were obtained with a Reichert ultramicrotome (Reichert, Wien, Austria), collected on rhodanium 400 mesh grids and contrasted with 3% uranyl acetate

followed by lead citrate, 10 min each. Grids were washed with water, dried, and examined in a FEI CM12 electron microscope operating at 80 kV.

Tracer injection and autoradiography

All tracers were injected i.v. in the orbital plexus. To monitor endocytic upake, human β2-microglobulin (Sigma-Aldrich, Bornem, Belgium) was radiolabelled with iodobeads (mean value 4.6 10^7 cpm/µg β2-microglobulin; >95% trichloroacetic acid-precipitable) and 200ng/g of body weight was injected. At 7min after injection, kidneys were exsanguinated and total radioactivity was measured in one kidney homogenate. The other kidney was fixed overnight with 4%F for paraffin embedding and autoradiography on 7µm-thick sections using Ilford L4 emulsion (Ilford Scientific Product, Marly, Switzerland) was revealed after 2 weeks exposure. To monitor transfer to S3 PTCs, mice were injected with 300µg TexasRed-ovalbumin (Invitrogen) at 20 min before sacrifice. To monitor access to lysosomes, mice were injected with 120µg/ g body weight horseradish peroxidase (Sigma-Aldrich) at 2 h before sacrifice[31].

Multiplex (immuno)fluorescence

(Immuno)fluorescence was performed on 5µm-thick frozen sections. Briefly, after whole-body perfusion with 4%F, slices were equilibrated overnight in 20% sucrose and embedded in Tissue-Tek Optimal Cutting Medium (Sakura Finetek, Torrance, CA). Antigen retrieval was promoted in citrate buffer, pH 6.0, at 95°C for 20min using a Lab Vision Pretreatment Module™ (Thermo Scientific). Tissue was permeabilized with PBS/0.3% Triton-X100 for 5min, then incubated for a further 1h with 10% bovine serum albumin (BSA) and 3% milk to block non-specific sites. Sections were incubated overnight at 4°C with primary antibodies (see Supplemental Table 2) in blocking buffer. Ezrin, the founding member of the ERM family (ezrin/radixin/moesin) linking plasma membrane to cortical actin microfilaments was used as a convenient marker to probe the development of the brush border and to delineate the basolateral membrane contour. Proliferating cells were identified by monoclonal antibody Ki67 (Kiel, clone 67), a highly sensitive marker to label cells that entered the cell division cycle. Apoptotic cells were identified by immunolabelling of the cleaved (activated) form of caspase-3. After washing, sections were incubated with the indicated AlexaFluor-secondary antibodies and/or streptavidin (Invitrogen) for 1h at room temperature in 10% BSA/0.3% Triton-X100, mounted with Dako Faramount Aqueous Mounting Medium and imaged on a

spinning disk confocal microscope using a EC Plan-NeoFluar 40X/1.3 Oil DIC objective (Cell Observer Spinning Disk; Zeiss, Oberkochen, Germany). Alternatively, full-section images were acquired using a Zeiss Mirax Midi fluorescence microscope.

Multiphoton microscopy

For three-dimensional reconstruction, kidneys were flushed at 20 min after iv injection of 600µg Texas-Red ovalbumin (Invitrogen), perfusion-fixed with 4%F for 5min, excised and post-fixed for 2h in the same fixative. Two hundred µm-thick slices were obtained with a Vibratome and washed in 50mM Tris/HCl pH7.5, 150mM NaCl, 0.1% Triton-X100 (TBST). Non-specific sites were blocked with 10% normal goat serum in TBST at room temperature for 1h then slices were incubated at 4°C for 63h with rabbit anti-podocin antiserum (1/500) [54]. After extensive washing with TBST, slices were incubated for 63h at 4°C with fluorescein-Lotus Tetragonolobus lectin (1/100) combined with AlexaFluor-secondary antibodies. After extensive washing with TBST and post-fixation overnight at 4°C with 4%F, slices were cleared by increasing concentrations of methylsalicylate (Sigma) and mounted therein between two coverslips. Z-stacks were recorded by multiphoton microscopy (LSM510-NLO, Zeiss, Germany) using a Chameleon laser (Coherent, Santa Clara, CA, USA) and a 63x objective with 1.4 numerical aperture.

In situ Hybridization

Antisense RNA probes were produced by RT-PCR followed by *in vitro* transcription with T7 RNA polymerase in the presence of digoxigenin-labelled uridine 5-triphosphate (Roche). Probes spanning nucleotides 8145 to 8435 of the mouse coding sequence for megalin (fw primer CAGTTCAATGGAGGATGCAGCC, rv primer CATCGCCCATTGGCACAAGT) and nucleotides 9541 to 9860 of the mouse coding sequence for cubilin (fw primer TACCTGACTGAGGACAGCAAGAG; rv primer CCTCTCATTTGAATACTTATGTC) were used. For *in situ* hybridization, 8 µm-thick sections were hybridized overnight at 60°C with specific probes in hybridization solution containing 50% (v/v) formamide, 10% (w/v) dextran sulfate, 2% (v/v) Denhardt's solution, and 10% (v/v) saline solution (2M NaCl, 89mM Tris HCl pH 7.5, 11mM Tris base, 50mM sodium phosphate, 50mM disodium phosphate, 50mM EDTA) and 50µg/ml tRNA. Sections were washed at 65°C with 50% (v/v) formamide in 150mM NaCl, 15mM sodium citrate and 0.1% (v/v) Tween20 then washed at

room temperature with PBS/0.1%Triton-X100 (PBST). After non-specific sites were blocked with 10% fetal calf serum in PBST at room temperature for 1h, sections were incubated with anti-digoxigenin-Fab fragments coupled with alkaline phosphatase (#11093274910, Roche) diluted 1:500 in blocking buffer. After washing in PBST, PBS then NTMT (0.1M NaCl, 0.1M Tris/HCl, pH 9.5, 0.05M $MgCl_2$, 0.1% Tween), labelling was detected with 4-nitroblue tetrazolium chloride/5-bromo-4-chloro-3-indolyl-phosphate (Roche).

RT-qPCR

Total RNA was extracted (SV total RNA isolation system; Promega, Madison, WI). Aliquots of 300ng RNA were reverse-transcribed by M-MLV reverse transcriptase (Invitrogen, Carlsbad, CA) with the random hexamers protocol. Primer sequences for hypoxanthine phosphoribosyltransferase 1 (HPRT-1), megalin, cubilin, NaPi-IIa, SGLT-1, SGLT-2, AQP-1, AQP-2 and podocin are described in Supplemental Table 1. Real-time qPCR was performed as described[45] in presence of 250nM of specific primers with Kappa SYBR Fast qPCR Master Mix (Kapa Biosystems, Woburn, MA) on a CFX384 touch real-time PCR Detection System (Bio-Rad). Results are presented as Delta Ct values, normalized to HPRT-1, used as internal standard.

3.2. Protection of cystinotic mice by kidney-specific megalin ablation supports an endocytosis-based mechanism for nephropathic cystinosis progression.

Virginie Janssens, Héloïse P. Gaide Chevronnay, Sandrine Marie, Marie-Françoise Vincent, Patrick Van Der Smissen, Nathalie Nevo, Seppo Vainio, Rikke Nielsen, Erik I. Christensen, François Jouret, Corinne Antignac, Christophe E. Pierreux*, Pierre J. Courtoy*.

2019, Journal of the American Society of Nephrology, Sep 23. doi: 10.1681/ASN.2019040371 *(*, equal senior authors)*.

BASIC RESEARCH www.jasn.org

Protection of Cystinotic Mice by Kidney-Specific Megalin Ablation Supports an Endocytosis-Based Mechanism for Nephropathic Cystinosis Progression

Virginie Janssens,[1] Héloïse P. Gaide Chevronnay,[1] Sandrine Marie,[2] Marie-Françoise Vincent,[2] Patrick Van Der Smissen,[1] Nathalie Nevo,[3] Seppo Vainio,[4] Rikke Nielsen,[5] Erik I. Christensen,[5] François Jouret,[6] Corinne Antignac,[3] Christophe E. Pierreux,[1] and Pierre J. Courtoy[1]

Due to the number of contributing authors, the affiliations are listed at the end of this article.

ABSTRACT

Background Deletions or inactivating mutations of the cystinosin gene *CTNS* lead to cystine accumulation and crystals at acidic pH in patients with nephropathic cystinosis, a rare lysosomal storage disease and the main cause of hereditary renal Fanconi syndrome. Early use of oral cysteamine to prevent cystine accumulation slows progression of nephropathic cystinosis but it is a demanding treatment and not a cure. The source of cystine accumulating in kidney proximal tubular cells and cystine's role in disease progression are unknown.

Methods To investigate whether receptor-mediated endocytosis by the megalin/LRP2 pathway of ultrafiltrated, disulfide-rich plasma proteins could be a source of cystine in proximal tubular cells, we used a mouse model of cystinosis in which conditional excision of floxed *megalin/LRP2* alleles in proximal tubular cells of cystinotic mice was achieved by a Cre-LoxP strategy using Wnt4-CRE. We evaluated mice aged 6–9 months for kidney cystine levels and crystals; histopathology, with emphasis on swan-neck lesions and proximal-tubular-cell apoptosis and proliferation (turnover); and proximal-tubular-cell expression of the major apical transporters sodium-phosphate cotransporter 2A (NaPi-IIa) and sodium-glucose cotransporter-2 (SGLT-2).

Results Wnt4-CRE–driven *megalin/LRP2* ablation in cystinotic mice efficiently blocked kidney cystine accumulation, thereby preventing lysosomal deformations and crystal deposition in proximal tubular cells. Swan-neck lesions were largely prevented and proximal-tubular-cell turnover was normalized. Apical expression of the two cotransporters was also preserved.

Conclusions These observations support a key role of the megalin/LRP2 pathway in the progression of nephropathic cystinosis and provide a proof of concept for the pathway as a therapeutic target.

JASN 30: ●●●–●●●, 2019. doi: https://doi.org/10.1681/ASN.2019040371

In kidney proximal tubular cells (PTCs), recapture of ultrafiltrated albumin and low molecular weight (LMW) proteins is a major pathway leading to lysosomes.[1,2] Endocytosis efficiency in PTCs relies on the tandem multiligand receptors, megalin/LRP2 (hereafter simply megalin) and cubilin, which are abundantly expressed and undergo extremely fast endocytosis and recycling.[3–5] In turn, fast vesicular trafficking relies on high expression in segment 1 (S1) of rate-limiting components of the endocytic machinery depending on mammalian target of

Received April 12, 2019. Accepted July 31, 2019.

C.E.P. and P.J.C. contributed equally to this work.

Published online ahead of print. Publication date available at www.jasn.org.

Correspondence: Prof. Christophe E. Pierreux, de Duve Institute and Université Catholique de Louvain, 75 Avenue Hippocrate, PO Box B1.75.05, 1200-Brussels, Brabant, Belgium. Email: christophe.pierreux@uclouvain.be

rapamycin 1 (mTOR1).[6,7] Albumin, an abundant ligand in PTC lumen shared by both endocytic receptors, is a globular protein stabilized by 17 disulfide bridges and thus a precursor of 17 cystine molecules. Similarly abundant LMW proteins are additional precursors of cystine. Receptor-mediated endocytosis in PTCs is abrogated upon megalin and cubilin knockout (KO).[8,9] Perinatal death of most full megalin KO mice[10] can be circumvented by kidney-specific *megalin/LRP2* gene excision (Meg^{ksKO} mice); one copy of Wnt-4–driven Cre recombinase is sufficient to specifically excise the floxed *megalin/LRP2* gene in virtually all PTCs during nephrogenesis.[9] Reports indicate megalin ablation does not affect overall PTC histology until approximately 9 months, but causes atrophy of the apical endocytic apparatus (much fewer endosomal vacuoles and dense apical tubules) with secondary effects on fluid-phase endocytosis and sodium-phosphate cotransporter 2A (NaPi-IIa) trafficking.[11,12] Megalin is also the port of entry of nephrotoxic drugs, such as aminoglycosides,[13] and this megalin pathway can be targeted by inhibitory drugs.[14] Alternatively, apical PTC endocytosis can be acutely blocked by bolus intravenous injection of dibasic amino acids (especially lysine) in human volunteers[15] and by 1-day oral lysine gavage to rats,[16] but long-term inhibition has not yet been reported.

Nephropathic cystinosis, in brief "cystinosis," is a rare lysosomal storage disease and the main cause of hereditary renal Fanconi syndrome (reviewed in [16]; for perspective, see [17]). Deletion or inactivating mutations of the cystinosin gene (*CTNS*), encoding the only known lysosomal cystine/hydrogen ion symporter, leads to cystine accumulation and characteristic crystals at acidic pH.[17] Cystine is an obligatory end-degradation product of disulfide-rich proteins,[18] and its accumulation in cystinotic fibroblasts is proportional to the absolute endocytic velocity and relative disulfide abundance in endocytic cargo.[19,20] Cultured cells also internalize amino acids, and thus cystine, by fluid-phase endocytosis.[21] The source of lysosomal cystine *in vivo* is unknown.[22]

Although lysosomal cystine accumulation occurs in all tissues of patients with nephropathic cystinotic, the kidneys and eyes are first affected. The earliest clinical manifestation is usually a renal Fanconi syndrome combining urinary losses of solutes and LMW proteins. In kidneys, cystinosis leads to PTC apical dedifferentiation and flattening/atrophy, starting at the glomerulo-tubular junction (GTJ) and extending longitudinally downstream (swan-neck deformities);[23] interstitial fibrosis; glomerular lesions; and kidney failure.[24] Swan-neck lesions are considered an early adaptation to PTC insult and precede glomerulo-tubular disconnection resulting into atubular glomeruli.[25–27] Very early, diligent implementation of compliant cysteamine (a cystine-depleting agent and currently the only drug approved by the Food and Drug Administration) treatment was reported to preserve kidney, growth, and thyroid function for over a decade;[28] but long-term surveys of large cohorts show delayed progression to kidney insufficiency and other failures, and little control of the Fanconi syndrome, thus calling for novel therapeutic approaches.[29,30]

Significance Statement

Nephropathic cystinosis is the result of deletion or inactivating mutations of the gene encoding the lysosomal cystine transporter cystinosin, but the extent to which disease progression depends on cystine accumulation or transport-independent effects of cystinosin is unknown. Cysteamine, the current treatment to prevent cystine accumulation, delays progression to renal failure but does not correct the Fanconi syndrome nor does it provide a cure. The authors demonstrate that suppression of endocytosis in kidney proximal tubular cells of cystinosin-deficient mice by genetic excision of *megalin/Lrp2* largely prevents cystine accumulation and can help preserve kidney structure and proximal tubular cell differentiation. These observations stress the importance of cystine accumulation in disease progression and provide proof of concept for exploring novel strategies aiming at blocking the megalin pathway.

$Ctns^{-/-}$ mice on congenic C57BL/6 background closely reproduce the kidney disease,[26,31,32] except for a mild/incomplete Fanconi syndrome that has been further vanishing in several colonies including ours, probably due to inbreeding. This mouse model nevertheless was instrumental for deciphering pathogenic and adaptation mechanisms. Pathogenic mechanisms are either transport-related or -independent defects[24]; their respective contribution to nephropathic cystinosis is unknown. Transport-independent defects include alterations of endolysosomal trafficking,[33] of macroautophagic[34,35] and chaperone-mediated autophagic fluxes,[36] of mTOR complex 1 activation,[37] as well as propensity to kidney inflammation.[38] Several adaptation mechanisms have been evidenced: (*1*) early apical PTC dedifferentiation offering reduced workload, as shown by repressed expression of endocytic receptors (megalin and cubilin) and apical solute transporters (main symporters for phosphate, NaPi-IIa, and glucose, sodium-glucose cotransporter-2 [SGLT-2]); (*2*) active luminal crystal exocytic discharge; and (*3*) increased PTC turnover with crystal disposal by luminal apoptotic shedding and PTC regeneration by proliferation, which provides fresh lysosomes.[26]

Calculations predict that uptake of disulfide-rich proteins such as albumin could be the major source of lysosomal cystine accumulation in cystinotic PTCs and thus represent a potential therapeutic pathway.[24,26] We tested this hypothesis by generating a triple transgenic model: $Ctns^{-/-}$; Wnt4-CRE; $Meg^{Fl/Fl}$, referred to hereafter as $Ctns^{-/-}/Meg^{ksKO}$ or simply "double KO" mice. Data show that megalin ablation (*1*) blocks cystine accumulation, thereby preventing crystal deposition in cystinotic kidneys; (*2*) protects PTCs from structural lesions; and (*3*) normalizes PTC turnover. The apical expression of NaPi-IIa and SGLT-2 is largely preserved in $Ctns^{-/-}/Meg^{ksKO}$ mice. These observations support a key role of endocytosis in the progression of nephropathic cystinosis and pave the way to medical intervention targeting the megalin pathway.

Results

METHODS

Mice and Genotyping

Congenic C57BL/6J *Ctns*$^{-/-}$ mice and Wnt4-Cre mice (C57BL/6) have previously been described.[31,39] Mice bearing the megalin loxP/loxP gene[40] were initially generated by Dr. T. Willnow. For genotyping, PCR on DNA extracted from tail samples was used to identify mice bearing wild-type (WT), cystinotic, and floxed megalin alleles. The cystinosin allele was analyzed with pairs of primers centered on exon 10 (Ex10 forward, 5′-CTCCAGATGTTCCTCCAGTC-3′; and Ex10 reverse, 5′-AGTCCGAACTTGGTTGGGT-3′) and on the cassette (K7 forward, 5′-GCAGGAATTCGATATCAAGC-3′; and K7 reverse, 5′-AAAGTGGAGGTAGGAAAGAGG-3′). The size of the amplicons revealing the WT and the transgenic Ctns allele were 260 and 215 bp, respectively. For megalin genotyping, a common forward primer (5′-AGGCTCC-GACTTCGTAACTG-3′) was used with two reverse primers to amplify the WT (5′-TGAAAACCACACTGCTCGATCCG-GAAC-3′) and/or the floxed allele (5′-ACCTTGCGT-GAATTCTGGG-3′). The size of the amplicons was approximately 300 bp for the WT allele and approximately 400 bp for the floxed allele. Presence of the Wnt4-Cre transgene was assessed using forward and reverse primers (Cre forward, 5′-GCACGTT-CACCGCATCAAC-3′; and Cre reverse, 5′-CGATGCAAC-GAGTGATGAGGTTC-3′; product size 332 bp). Experiments were approved by the Ethical Committee of the Medical School of the Université Catholique de Louvain (2016/UCL/MD/006 and 2018/UCL/MD/026). Mice were treated according to the National Institutes of Health Guide for Care and Use of Laboratory Animals, and used with parsimony.

Tissues

After blood collection, mice were exsanguinated with PBS by perfusion *via* the left ventricle under irreversible anesthesia by 2% xylazine and 50 mg/ml ketamine (250 μl per mouse, intramuscularly). Fresh tissues (left kidney, spleen, and one liver lobe) were immediately collected using vascular clamps to maintain a closed blood circulatory system, and right kidneys were then fixed *in situ* by switching to whole-body perfusion fixation with cold (4°C, nominal) 4% formaldehyde (from heat-depolymerized paraformaldehyde) in 0.1 M phosphate buffer, pH 7.4, for approximately 3 minutes. They were then excised, decapsulated, and weighed. Hemi-sagittal sections were postfixed by immersion in 4% formaldehyde at 4°C under gentle stirring overnight. Samples were paraffin embedded and 7-μm-thick sections were collected for histology and confocal fluorescence imaging.

Cystine Assays

A quarter of the unfixed left kidney was homogenized into 600 μl of 5.2 mM *N*-ethylmaleimide (Sigma-Aldrich) in 10× diluted PBS and briefly sonicated, then 200 μl of 12% 5-sulfosalicylic acid (dehydrated; Merck-Millipore) was added. Samples were vortexed and frozen at −80°C. Cystine assays were carried out by liquid chromatography–tandem mass spectrometry (liquid chromatography–MS/MS) as previously described[41] with modified MS/MS detection[42] and normalized to kidney protein. Briefly, the extract was microfuged at 13,000 rpm for 10 minutes at 4°C. The residual pellet was resuspended in 1 ml of 0.1 N sodium hydroxide for protein assay by the Lowry method using BSA as standard. Cystine assays were performed on 50 μl of supernatant, diluted in water if necessary (according to the 0.2–10 μM cystine calibration). After butylation, final samples were resuspended in 100 μl water and 15 μl was injected into liquid chromatography–MS/MS (Quattro micro; Waters).

Visualization of Cystine Crystals

To highlight cystine crystals by polarized light microscopy, a quarter of the perfused-fixed kidneys were instead postfixed by immersion in alcoholic Bouin solution at 4°C overnight, and then paraffin embedded without any passage in aqueous medium. Sections were deparaffinized and mounted with Q Path Coverquick 3000 mounting medium (Labonord). Slides were analyzed by polarized microscopy at high then low light intensity (highlighting crystals) and recorded images were pseudo-colored in green.

Histology, Multiplex (Immuno)Fluorescence, and Morphometry

Sections were stained with hematoxylin and eosin. For (immuno) fluorescence, antigen retrieval was promoted in citrate buffer, pH 6, at 95°C for 20 minutes using a Lab Vision Pretreatment Module (Thermo Scientific). Tissue was permeabilized with PBS/0.3% Triton X-100 for 5 minutes, and then for a further 1 hour with 10% BSA/3% milk to block nonspecific sites. Sections were incubated overnight at 4°C with the following primary reagents in blocking buffer: sheep anti-megalin (1:800; kindly provided by Dr. P. Verroust and Dr. R. Kozyraki, INSERM U968, Paris, France), rat anti–lysosome-associated membrane protein-1 (anti–LAMP-1; 1:100, 1D4B; Hybridoma Bank), rabbit anti–mouse NaPi-IIa (NaPi-IIa carboxy-terminal peptide, 1:1000; a kind gift from Dr. J. Biber and Dr. C. Wagner, Zurich, Switzerland), rabbit anti–human SGLT-2 (1:100, sc-98975; Santa Cruz Biotechnology), mouse anti-Ki67 (1:250, 556003; BD-Pharmingen), rabbit anti–active caspase-3 (1:200, 9661; Cell Signaling), or biotinylated *Lotus tetragonolobus* lectin (1:100; Vector Laboratories). After washing, sections were further incubated with the appropriate Alexa Fluor secondary antibodies and/or streptavidin (Invitrogen) or Hoechst bisbenzimide H 33258 (Sigma-Aldrich) for 1 hour at room temperature in 10% BSA/0.3% Triton X-100, mounted with Faramount Aqueous Mounting Medium (Dako), and imaged on a spinning disk confocal microscope using an EC Plan-NeoFluar 40×/1.3 or 100×/1.4 oil differential interference contrast objective (Cell Observer Spinning Disk; Zeiss). Differential interference contrast (Nomarski microscopy) images were obtained using

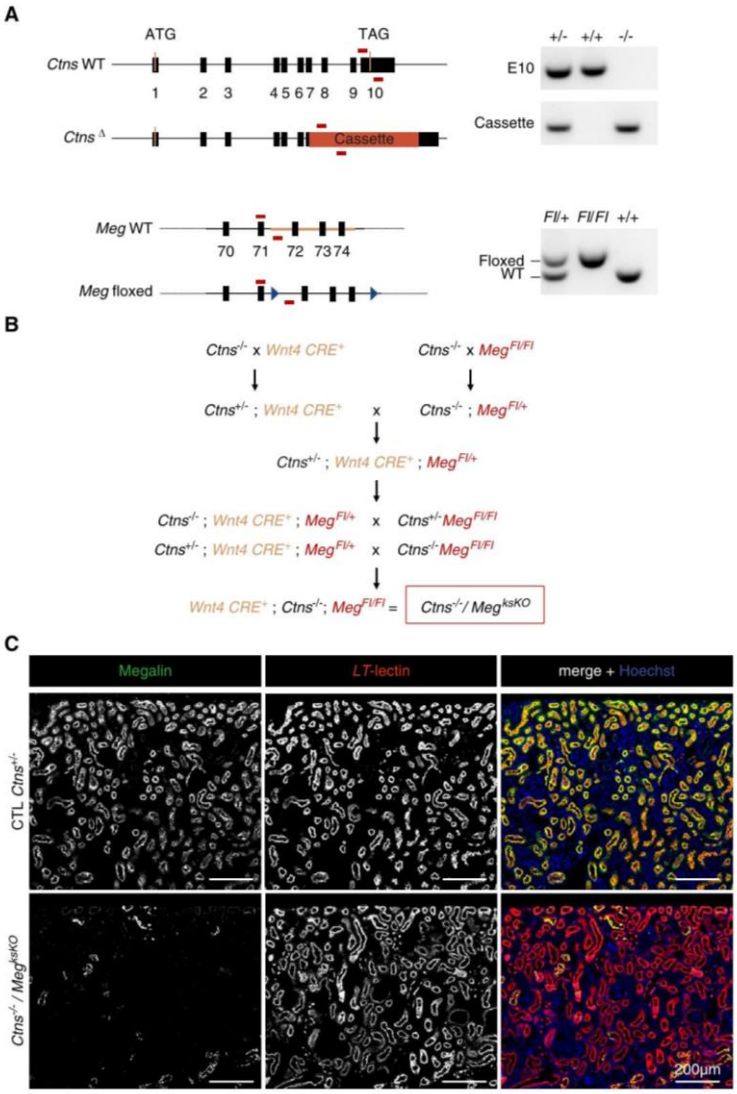

Figure 1. Generation and validation of Ctns/Meg double KO in kidneys. (A) Genotyping: Cystinosin and megalin floxed alleles were identified by PCR on tail DNAs. For cystinosin, WT exon 10 (E10) or cassette (IRES-βgal-neo) replacing the last four exons (vertical black bars) of *Ctns* were amplified with two different oligonucleotides pairs (horizontal red bars), allowing for identification of WT, heterozygous, and $Ctns^{-/-}$ mice. For megalin, a common forward oligonucleotide was used with two different reverse oligonucleotides specific to the WT or floxed allele, containing LoxP recombination sites (blue triangles). Amplification of the Wnt4-CRE locus is not depicted. (B) Crossings: This crossing program aimed at comparing mice with various genotypes strictly derived from the same

bright-field microscopy, with a polarizing filter added between the light source and the condenser, and a Wollaston prism to increase the contrast. Alternatively, whole kidney images (histology and fluorescence) were acquired using a Pannoramic 250 Flash III microscope (3DHistech).

At least four mice were analyzed for each condition. Swan-neck morphometry was performed by survey of an entire sagittal section across the hilum. In 32 such sections (including all controls, single KOs, and double KOs except the case mentioned hereafter), on average 21±8 GTJs per section were identified (mean±SD, range 8–36). One double KO mouse at 9 months with less than five GTJs identified was rejected. Comparison of the three groups by Mann–Whitney test showed no significant difference in GTJ abundance, but significant difference in frequency of swan necks (Supplemental Methods).

Statistical Analysis

All statistical analyses were conducted by Prism software (GraphPad Software) using the nonparametric Mann–Whitney test. Differences were considered statistically significant when $P<0.05$.

RESULTS

Wnt4-CRE–Driven, Kidney-Specific Megalin Ablation in Cystinosin KO Mice and Validation of the Model

The breeding program used to achieve triple transgenic mice ($Ctns^{-/-}/Meg^{ksKO}$ or double KO), genotyped as shown at Figure 1A, is outlined at Figure 1B. Because the cystinotic renal phenotype in *Ctns* KO mice strongly depends on genetic background,[31] breeding was designed to compare kidneys of "control" ($Ctns^{+/-}$), full single *Ctns* KO ($Ctns^{-/-}$), single *ksMeg* KO (Wnt4-CRE; $Meg^{Fl/Fl}$), and double KO ($Ctns^{-/-}$; Wnt4-CRE; $Meg^{Fl/Fl}$) mice derived from the same C57BL/6J founders. Genotypes of all offspring followed expected Mendelian proportions. There was no significant difference in body growth or kidney weight between all genotypes up to 9 months (longest endpoint; Supplemental Figure 1), indicating phenotype attenuation since the original report.[31] At the time of euthanasia, urinary signs of partial Fanconi syndrome, previously reported to discriminate $Ctns^{-/-}$ mice from control littermates,[26,31] were no longer found, which was also noticed in $Ctns^{-/-}$ colonies at other laboratories. There was also no significant alteration in urea and creatinine plasma values, except for increased mean urea in double KO mice at 9 months (74.5±26.0 mg/dl, $P<0.05$ versus 54.6±8.1 in control and $P<0.05$ versus 51.2±11.6 in $Ctns^{-/-}$; means±SD). This paradoxic increase will be explained hereafter. Confocal immunofluorescence, using proximal tubule-specific labeling by *L. tetragonolobus* lectin as a reference, showed almost complete disappearance of megalin expression in double KO PTCs (Figures 1C and 2C). Thus, $Ctns^{-/-}/Meg^{ksKO}$ mice appeared adequate to test the role of endocytosis in the progression of kidney lesions in cystinotic mice. However, histology revealed in the cortex of about half, but not all, single *ksMeg* KO and double KO mice massive periarterial lymphocyte collections and extending inflammation, causing large zones with gross tissue remodeling after 6 months (see further in Figure 3 and Supplemental Figure 6, A and B). These mice were not excluded from the assays but conclusions reported hereafter for double KO were validated for mice without such extensive remodeling zones.

Megalin Ablation in $Ctns^{-/-}$ Kidneys Blocks Cystine Accumulation in Lysosomes and Prevents Crystal Deposition

To assess whether suppressing endocytosis into PTCs by genetic megalin ablation would prevent cystine accumulation, we first performed cystine assays in kidneys at 6, 7.5, and 9 months of age in each genotype. At all time points, renal cystine levels in $Ctns^{-/-}$ mice were significantly different from control ($Ctns^{+/+}$, $Ctns^{+/-}$) and single *ksMeg* KO mice (Supplemental Figure 2). We thus focused on the comparison of renal cystine levels between $Ctns^{-/-}$ and double KO mice. As positive controls of cystinosis and negative controls of megalin ablation, we also assayed cystine in liver and spleen, in which the *Wnt4* gene is not expressed (Figure 2A, Supplemental Figure 2). In $Ctns^{-/-}$ kidneys, cystine accumulation increased exponentially with age, reaching on average 103 nmol hemi-cystine/mg tissue protein at 9 months, in good agreement with Nevo *et al.*,[31] but this leveled off at 13 nmol hemi-cystine/mg tissue protein in double KO kidneys. Thus, kidney-specific megalin gene ablation in $Ctns^{-/-}$ almost entirely suppressed kidney cystine overload. In contrast, there was no consistent change in cystine levels in spleen or liver. Suppression of cystine accumulation could not be explained by modifier genes associated with Meg^{Fl} or Wnt4-CRE loci, because two double transgenic $Ctns^{-/-}$; $Meg^{Fl/Fl}$ mice and at least one $Ctns^{-/-}$; Wnt4-CRE mouse—all expected to express megalin normally—still showed high kidney cystine levels (red or green color code in Figure 2A). In $Ctns^{-/-}$

founders. Offspring were observed at the expected Mendelian proportions. (C) Validation of Wnt4-CRE–driven excision of megalin in double KO mice by double confocal fluorescence (6 months): Low-power view for megalin immunofluorescence in green, and apical labeling of PTCs by *L. tetragonolobus* lectin (LT-lectin) in red. Single channels at left and center, merged emission at right combined with nuclear labeling by Hoechst (blue). As compared with control (CTL; all labeled tubular sections appear yellow), note the almost complete disappearance of megalin in double KO (very few yellow tubular sections).

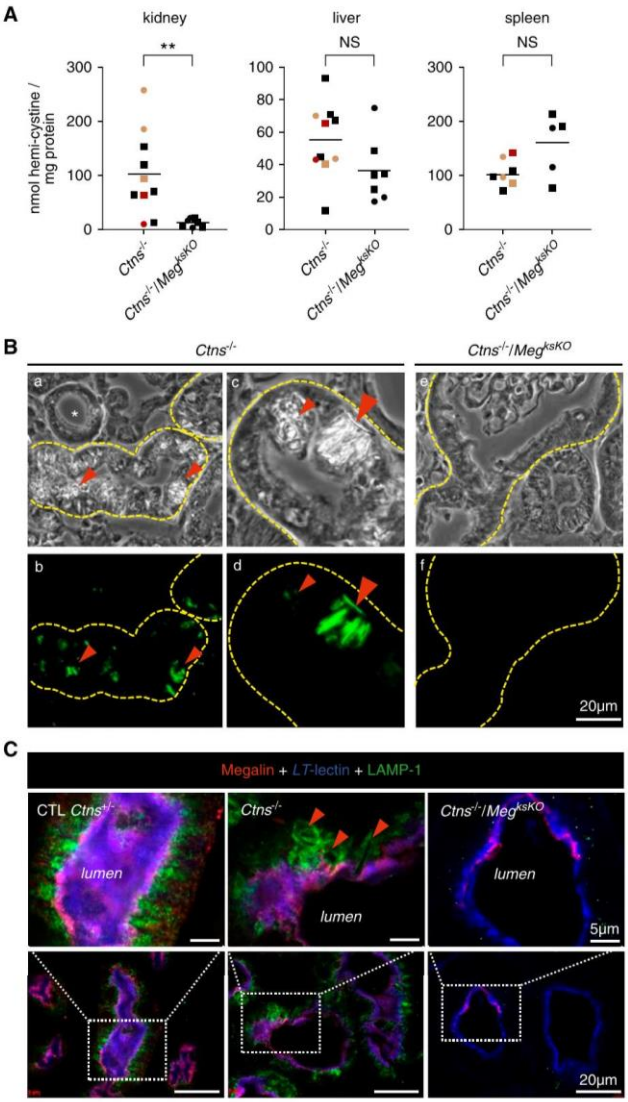

Figure 2. Megalin ablation in Ctns$^{-/-}$ kidneys prevents cystine accumulation and crystal deposition. (A) Comparison of cystine content in kidneys, liver, and spleen between Ctns$^{-/-}$ and double KO mice at 9 months of age for males (filled squares) or females (filled circles) (**P<0.01). Green, Orange and red symbols refer to Ctns$^{-/-}$ mice with either two floxed megalin alleles but no Wnt4-Cre, or one Wnt4-Cre but no floxed megalin allele, respectively. For time course of cystine accumulation between 6 and 9 months, see Supplemental Figure 2. (B) Histologic evidence of cystine crystals (red arrowheads) by polarized light (top panel) and green pseudo-color (bottom panel) in Ctns$^{-/-}$ kidneys (a, b, c, d) versus their absence in double KO kidneys at 7.5 months (e, f). For large fields, see

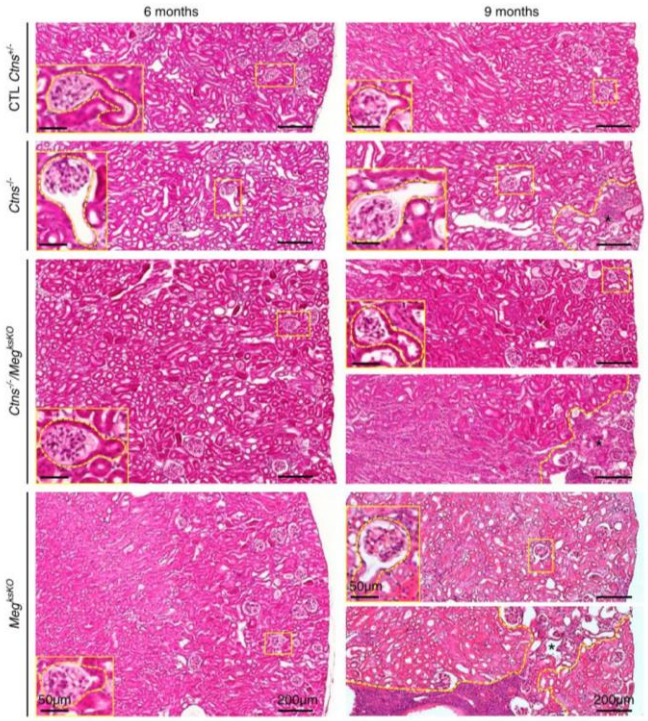

Figure 3. Histology of cystinotic kidneys is preserved upon megalin ablation (whole-cortical views after staining with hematoxylin and eosin at 6 and 9 months). Broken yellow lines delineate inflammatory areas with parenchymal atrophy at 9 months (*). Representative GTJs are enlarged. In single *Cystinosin* KO mice at 9 months, small foci of atrophy are always present but limited to the superficial cortex. For double KO and single *Megalin* KO kidneys at 9 months, two examples are shown to illustrate either absence or presence of grossly remodeled areas that can span the entire cortex (see also Supplemental Figure 6B). CTL, control.

PTCs, lysosomal cystine accumulation results in lysosomal swelling and then deformities due to cystine crystallization at the acidic lysosomal pH.[26,31] Cystine crystals, readily evidenced in $Ctns^{-/-}$ PTCs by polarized microscopy, were no longer detected upon megalin ablation (Figure 2B, Supplemental Figure 3). Of note, no crystals were detected in atrophic $Ctns^{-/-}$ PTCs at swan-neck deformities.

Moreover, lysosome labeling by LAMP-1 immunofluorescence revealed frequent lysosomal dilation and characteristic deformation by crystals in $Ctns^{-/-}$ PTCs but never in $Ctns^{-/-}/Meg^{ksKO}$, indicating protection against lysosomal abnormalities (Figure 2C). Altogether, these data demonstrated that genetic abrogation of apical endocytosis into $Ctns^{-/-}$ PCTs was very efficient in preventing cystine accumulation,

Supplemental Figure 3. (C) Triple confocal fluorescence imaging of *N*-fucosyl glycosides (LT-lectin, blue), megalin (red), and late-endosome/lysosome membrane (LAMP-1, green) at 6 months. In control PTCs, brush border is uniformly purple (combined blue and red emissions); lysosomes are all round and of similar size. In $Ctns^{-/-}$ PTCs, notice several enlarged and deformed lysosomes due to cystine crystal buildup (red arrowheads); brush border is preserved here. In double KO PTCs, brush border is only labeled in blue in most cells, reflecting megalin absence, and LAMP-1 signal is much reduced by comparison with controls as a consequence of abrogation of endocytic uptake. LT-lectin, *L. tetragonolobus* lectin.

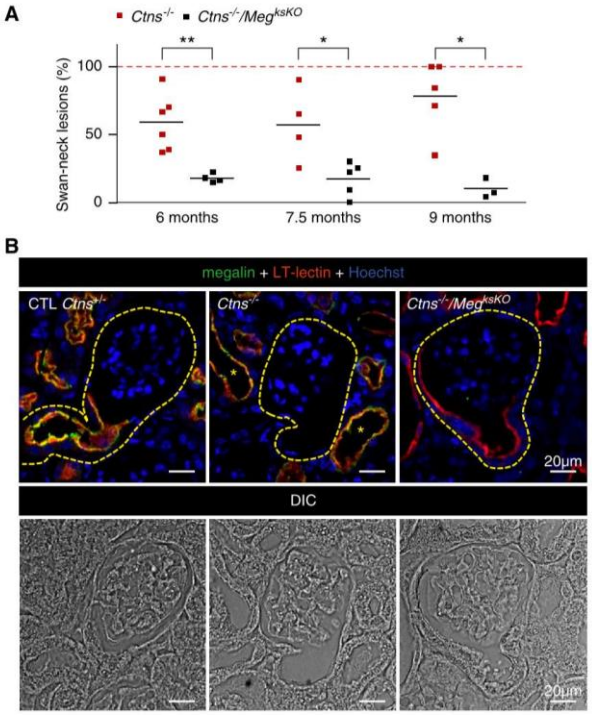

Figure 4. Megalin ablation in Ctns$^{-/-}$ kidneys prevents swan-neck lesions at GTJs. (A) Quantification of swan-neck lesions in Ctns$^{-/-}$ versus double KO mice from 6 to 9 months of age as percentage of all well defined GTJs over the entire sagittal kidney section, except at large inflammatory zones, as illustrated at Figure 3. *P<0.05, **P<0.01, nonparametric Mann–Whitney test). (B) Triple fluorescence confocal imaging with reference to differential interference contrast (DIC) imaging in Ctns$^{-/-}$ versus double KO mice at 6 months of age for *L. tetragonolobus* lectin (LT-lectin) labeling (red) and megalin (green) combined with nuclear Hoechst labeling (blue). Contours of GTJs are delineated by yellow broken lines. Notice in the central image that megalin is not detected at this representative Ctns$^{-/-}$ GTJ due to dedifferentiation/atrophy, but is preserved in more distal PTCs, together with LT-lectin labeling (yellow *). In contrast, the right image shows that megalin inactivation in Ctns$^{-/-}$ kidneys (no green signal) generally preserves PTC thickness and LT-lectin labeling at the GTJ. CTL, control.

indicating the endocytic pathway is indeed the key source of cystine storage in nephropathic cystinosis.

Megalin Ablation in *Ctns*$^{-/-}$ Kidneys Preserves Proximal Tubular Structure

As in cystinotic children,[23] mouse *Ctns*$^{-/-}$ kidneys show typical swan-neck lesions after 6 months.[26,27] To determine whether megalin ablation would further protect the proximal tubule structure, we compared double KO with *Ctns*$^{-/-}$ full-kidney sagittal sections by histology after staining with hematoxylin and eosin (Figure 3, quantified in Figure 4A) and by plastic sections of smaller blocks after toluidine-blue staining (Supplemental Figure 4). The majority of GTJs in *Ctns*$^{-/-}$ kidneys from 6–9 months of age showed typical swan-neck lesions, with apparently increasing prevalence with age, in good agreement with morphometry by Galarreta *et al.*[27] In contrast, only approximately 20% of GTJs in double KO showed swan-neck pattern without increase in age. This conclusion was confirmed by confocal microscopy based on *L. tetragonolobus* lectin labeling, as a general apical proximal tubule marker for brush border and apical endocytic apparatus, combined with megalin immunofluorescence. In control mice, double labeling produced a yellow signal. In *Ctns*$^{-/-}$ kidneys, both signals were suppressed at most GTJs and downstream. In double KO PTCs, lectin labeling was largely preserved (Figure 4B). Thus, megalin ablation in *Ctns*$^{-/-}$ kidney protected against overall PTC dedifferentiation and atrophy. Electron microscopy confirmed the preservation of double KO PTCs, except for atrophy of the apical endocytic apparatus and paucity of lysosomes, which was also the case in single *Megalin* KOs (Supplemental Figure 5).

Megalin Ablation in *Ctns*$^{-/-}$ Kidneys Preserves the Apical Expression of NaPi-IIa in PTCs and Prevents Increased PTC Turnover

Dedifferentiation of cystinotic PTCs, starting at the GTJ, includes loss of expression of megalin and cubilin, as well as of the main sodium-phosphate symporter, NaPi-IIa, and the main sodium-glucose symporter, SGLT-2, which are all relevant to Fanconi syndrome. Because swan-neck lesions are considered an early adaptation to PCT insult,[26,27] we next addressed whether double KO PTCs would escape this defensive mechanism. As shown by immunolabeling for NaPi-IIa (Figure 5A) and SGLT-2 (Figure 5B), all *Ctns*$^{-/-}$ cortices showed diffuse loss of expression of both transporters, yielding a mottled appearance at low magnification, but double KO preserved expression, except at large inflammatory areas where histology was grossly altered (for whole-cortical views, see Supplemental Figure 6, A and B). Because urinanalysis of Fanconi syndrome

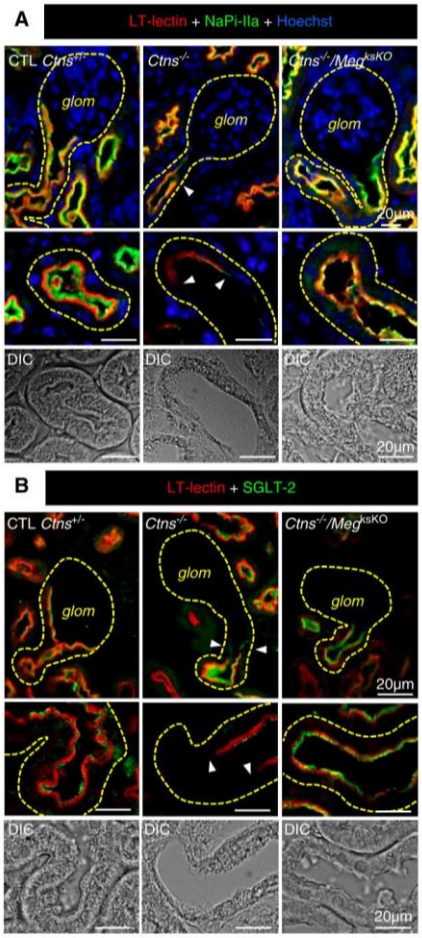

Figure 5. Protection against apical dedifferentiation in double KO kidneys. Double (or triple, Hoechst in blue) confocal fluorescence at 6 months for *L. tetragonolobus* lectin (LT-lectin) labeling (red), and either (A) NaPi-IIa or (B) SGLT-2 in green. Top panels, GTJs; bottom panels, enlargement of representative proximal tubule sections. On the left, notice in control (CTL) PTCs restriction of NaPi-IIa and SGLT-2 to the brush border but extension of LT-labeling subapically, resulting in apical label stratification. In $Ctns^{-/-}$ PTCs (central panels), LT-lectin and NaPi-IIa or SGLT-2 signals are greatly decreased or absent (arrowheads indicate sharp boundary with preserved cells). On the right, megalin ablation in *Ctns−/−* kidneys preserves apical signal of LT-lectin and NaPi-IIa or SGLT-2; stratification is lost due to atrophy of subapical endocytic apparatus. For whole-cortex views, see Supplemental Figure 6, A and B. For RT-PCR, see Supplemental Figure 7. DIC, differential interference contrast; glom, glomerulus.

was no longer relevant due to loss of this phenotype in our $Ctns^{-/-}$ colony, we performed quantitative RT-PCR measurements of cubilin, NaPi-IIa, and SGLT-2 mRNAs at 9 months (Supplemental Figure 7). There was a consistent decreasing trend in $Ctns^{-/-}$ kidneys as compared with control littermates, in agreement with previous reports,[26,32] contrasting with apparent protection in double KO, although differences did not reach statistical significance. Altogether, immunofluorescence and quantitative RT-PCR data were compatible with the hypothesis that the Fanconi syndrome of nephropathic cystinosis could be attenuated by targeting the megalin pathway.

Another adaptation mechanism to cystine overload in *Ctns−/−* PTCs is cell death, including by apoptotic shedding leading to luminal crystal discharge, coupled with compensatory proliferation, *i.e.*, replenishment by dividing cells to yield fresh lysosomes.[26] In contrast to $Ctns^{-/-}$ cortices, apoptosis and proliferation (monitored by cleaved caspase-3 and Ki67 immunofluorescence, respectively) were not detectably increased in double KO cortices, indicating no change in PTC turnover (Figure 6). Thus, megalin ablation in cystinotic kidneys, which suppressed exogenous cystine supply, also normalized apoptosis and proliferation rates.

DISCUSSION

This report demonstrates genetic ablation of the megalin/LRP2 pathway in cystinotic kidneys (*1*) suppresses cystine accumulation and crystal deposition, (*2*) protects tissue structure (except for grossly remodeled areas), and (*3*) preserves PTC differentiation and presumably function. This benefit was observed throughout the kidney cortex outside of those grossly remodeled areas, as expected from early Wnt4-CRE–driven excision, and is consistent with megalin being the cornerstone for PTC endocytosis in S1 (and S2) segments.[6,7,43] Using Wnt4-Cre, double megalin/cubilin KO causes higher albuminuria than single megalin KO (1.5-fold) and single cubilin KO (threefold).[9] However, full inhibition of endocytosis is not needed for a major benefit on cystine level in cystinotic PTCs, because a significant fraction of cystine released in lysosomes can be further disposed of by apical vesicular efflux (discussed in [24]). Conversely, side effects like suppressed endocytic supply of potential nephroprotective proteins, such as iron siderophore neutrophil gelatinase-associated lipocalin[44] or survivin,[45] must be taken into account and could explain the 20% of swan-neck lesions in double KO kidneys. Alternatively, these residual lesions could be due to a defective nontransport function of cystinosin. Perinatal ablation of the megalin pathway, used here as an experimental artifact, should not be confused with the natural course of nephropathic cystinosis where receptor-mediated endocytosis in S1/S2 spontaneously declines after 3–6 months as part of adaptive dedifferentiation to decrease workload.[26,27,32] Conceivably, secondary attenuation of apical endocytosis might be mediated by impaired mTOR signaling

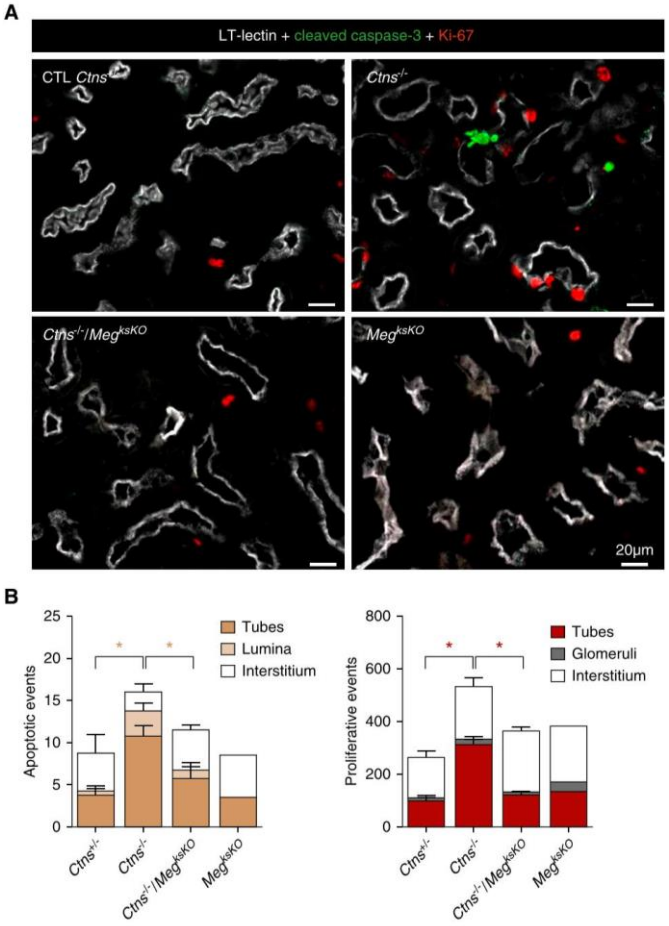

Figure 6. Megalin ablation in Ctns$^{-/-}$ kidneys protects against apoptosis and prevents increased PTC turnover. (A) Triple fluorescence confocal imaging for *L. tetragonolobus* lectin (LT-lectin) signal as proximal tubule marker (represented in white), caspase-3a (cleaved, active caspase-3) as apoptotic marker (tan), and KI-67 as proliferation marker (red) in representative low-power views. Notice increased labeling for both markers in Ctns$^{-/-}$ but not double KO kidneys. (B) PTC turnover quantification. Cells labeled for caspase-3a or Ki67 were counted in kidney sections at 6 months (four mice in Ctns$^{+/-}$, Ctns$^{-/-}$, and Ctns$^{-/-}$/Meg^{ksKO}; two mice for Meg^{ksKO}; ten random cortical fields totaling 2.98 mm^2 per section). Statistical analysis of the significance of differences of frequencies in tubes (combined with lumina for apoptosis) by Mann–Whitney test, *P<0.05. Increased apoptotic and proliferation indices in Ctns$^{-/-}$ kidneys indicate accelerated PTC turnover, not observed in double KO. CTL, control.

due to absence of cystinosin,[37] which negatively affects the apical endocytic machinery.[6] Conversely, nonrecaptured disulfide-rich proteins are reclaimed by more distal cells, which in turn get affected.[26] This would readily explain distal/longitudinal disease extension (see Visual Abstract).

Megalin/LRP2 ablation in mice and in-depth study of patients with Donnai–Barrow syndrome[46] (who have genetic megalin/LRP2 deficiency) were instrumental in establishing its multiple roles in kidney physiology (reviewed in [47]). Endocytic receptor KO models have also been essential to revise

or refine concepts involving the role of proteinuria as a risk factor to kidney insufficiency[48] or the still-debated albumin transcytotic recycling route.[49] Here, megalin KO revealed that endocytosis is the major pathway for the accumulation of cystine in nephropathic cystinosis, and provided proof of concept for the megalin pathway as therapeutical target. Because the kidney phenotype in *Ctns*$^{-/-}$ mice critically depends on the genetic background, we ensured that we compared mice derived from the same founders and excluded a role of floxed *megalin* and Wnt4-CRE loci. This concern was particularly important for the Wnt4-CRE locus because CdC42, key regulator of apical differentiation, lies immediately behind the Wnt4 gene on *Mus musculus* chromosome 4, locus D3. A limitation of our study is the inflammatory/immune reaction causing gross tissue remodeling in approximately half of mice at 9 months. This unexplained side effect of Wnt4-CRE–driven megalin excision (not reported in other, less complete, megalin KO models) likely explains the paradoxic increase (and large variation) of average plasma urea concentration in double KO mice at 9 months. However, the resulting gross remodeling is very different from the diffuse mottled appearance in *Ctns*$^{-/-}$ kidneys. Moreover, cortex between extensively remodeled areas in affected double KO mice as well as the entire cortex in double KO mice without remodeling showed remarkable structural protection. Thus, we feel it is safe to conclude that structural protection in double KO mice could be attributed to genetic ablation of the megalin pathway, and that suppression of this pathway by other means, not inducing gross inflammatory remodeling, could represent a desirable objective.

Our starting hypothesis was that receptor-mediated endocytosis of ultrafiltrated, disulfide-rich plasma proteins—exemplified by, but not limited to, albumin—was the main cystine source of PTCs. However, calculations indicate the much higher concentrations of free as compared with protein-bound cystine in the primary ultrafiltrate (approximately two orders of magnitude higher) may balance the much lower efficiency of fluid-phase versus receptor-mediated endocytosis (approximately two orders of magnitude lower)[50,51] so that contribution of fluid-phase endocytosis to cystine supply[21] into normal PTCs cannot be *a priori* neglected. Moreover, because megalin ablation not only arrests receptor-mediated endocytosis but also causes a marked atrophy of the apical endocytic apparatus and impairs fluid-phase endocytosis,[12] data in this report do not allow us to discriminate the two modes of endocytosis. The term "megalin pathway" used here intends to cover both mechanisms. Further studies, *e.g.*, by direct megalin competition for protein binding, are necessary to clarify this issue.

Acute suppression of the megalin pathway can be achieved by inhibition with dibasic amino acids, as shown with cultured cells[16,52] and by bolus injection into human volunteers,[15] perfusion in patients with cancer to prevent nephrotoxicity of radiochemicals,[53] or oral gavage in rats.[16] Long-term supplementation with arginine in man is considered safe,[54] is part of the treatment of genetic diseases of the urea cycle,[55] and is commonly used by body builders. Long-term supplementation with lysine is used for prevention of gyrate atrophy in hereditary ornithinemia.[56] Preliminary data from our laboratory have shown that dietary supplementation of *Ctns*$^{-/-}$ mice by L-lysine or L-arginine can significantly decrease kidney cystine accumulation and swan-neck lesions. However, dibasic amino acids can affect several metabolic pathways[57] and have several potential cellular targets, such as direct competition for receptor binding, inhibition of endocytic trafficking, and/or stimulation of the mTOR pathway[58] which is defective in cystinotic cells.[37] Thus, besides the need for confirmation in large cohorts, further mechanistic studies are required to clarify the mechanism of protection upon long-term supplementation.

The respective roles in the pathogeny and manifestations of nephropathic cystinosis of cystine transport-dependent (defined as cysteamine-responsive) versus transport-independent (cysteamine-insensitive, reviewed in [24]) functions of cystinosin, is also unknown. Cysteamine insensitivity of Fanconi syndrome contrasts with improved kidney outcome upon early compliant drug implementation.[30,59] Delayed progression to kidney insufficiency stresses the importance of effective cystine kidney clearance, although actual level of depletion, inferred from leukocyte assays, may not be complete in kidneys, as suggested in cysteamine-treated *Ctns*$^{-/-}$ mice.[60] Our article sheds more light on this debate by evidencing a causal link between cystine accumulation and structural dedifferentiation of PCTs in the mouse model, because prevention of cystine overload correlated with structural preservation; thus these results somewhat swing the pendulum back toward the pathogenic role of cystine overload.

ACKNOWLEDGMENTS

We thank Dr. R. Kozyraki and Dr. P. Verroust for anti-megalin and anti-cubilin antibodies, as well as Dr. J. Biber and Dr. C. Wagner for anti–Na-Pi-IIa antibodies; they are outstanding reagents. We express our gratitude to Dr. P. Henriet for supervision of statistical tests and *in silico* analysis of genomic DNA around cystinosin, megalin, and Wnt4 loci. We are particularly grateful to the wise reviewer who suggested considering fluid-phase endocytosis of free cystine as an additional mechanism to receptor-mediated endocytosis.

Janssens, Pierreux, and Courtoy designed the study; Nevo, Vainio, Nielsen, Christensen, and Antignac provided mice; Janssens, Gaide Chevronnay, Marie, Vincent, and Jouret carried out experiments; Van Der Smissen performed electron microscopy. Janssens, Gaide Chevronnay, Nielsen, Christensen, Jouret, Antignac, Pierreux, and Courtoy analyzed the data; Janssens and Courtoy created the figures; Janssens, Pierreux, and Courtoy drafted and revised the paper; all authors approved the final version of the manuscript.

Gaide Chevronnay was a postdoctoral researcher and Pierreux is a senior research associate at Fonds de la Recherche Scientifique, Fonds National de la Recherche Scientifique (F.R.S.–FNRS). Jouret is a PhD postdoctoral fellow of the F.R.S.–FNRS, Belgium.

DISCLOSURES

Work performed by Courtoy, Gaide Chevronnay, Janssens, Marie, Pierreux, Van Der Smissen, and Vincent was supported by grants from the Cystinosis Research Foundation (CRF).

FUNDING

This study was supported by the CRF (running costs, Janssens salary). The Imaging Cells and Tissues core facility was financed by National Lottery, Région bruxelloise, Région wallonne, Université Catholique de Louvain and de Duve Institute.

SUPPLEMENTAL MATERIAL

This article contains the following supplemental material online at http://jasn.asnjournals.org/lookup/suppl/doi:10.1681/ASN.2019040371/-/DCSupplemental.

Supplemental Methods. Semi-thin sections and electron microscopy RT-PCR.

Supplemental Figure 1. Time-course of body and kidney weight.

Supplemental Figure 2. Megalin ablation in $Ctns^{-/-}$ kidneys selectively prevents cystine accumulation (complementary to Figure 2A).

Supplemental Figure 3. Megalin ablation in $Ctns^{-/-}$ kidneys prevents cystine crystal deposition: gallery of images (complementary to Figure 2B).

Supplemental Figure 4. Toluidine-stained plastic sections of $Ctns^{-/-}$ vs double KO kidneys.

Supplemental Figure 5. Electron microscopy.

Supplemental Figure 6. Diffuse mottled appearance resulting from loss of transporter expression in $Ctns^{-/-}$ PCTs contrasts with large areas of inflammatory remodelling in double KO. (A) Low power cortical views. (B) Extended views of whole kidney sections (complementary to Figure 5).

Supplemental Figure 7. RT-PCR of megalin, cubilin, NaPi-IIa and SGLT-2.

Supplemental References.

REFERENCES

1. Christensen EI, Wagner CA, Kaissling B: Uriniferous tubule: Structural and functional organization. *Compr Physiol* 2: 805–861, 2012
2. Eshbach ML, Weisz OA: Receptor-mediated endocytosis in the proximal tubule. *Annu Rev Physiol* 79: 425–448, 2017
3. Christensen EI, Birn H: Megalin and cubilin: Multifunctional endocytic receptors. *Nat Rev Mol Cell Biol* 3: 256–266, 2002
4. Birn H, Christensen EI, Nielsen S: Kinetics of endocytosis in renal proximal tubule studied with ruthenium red as membrane marker. *Am J Physiol* 264: F239–F250, 1993
5. Perez Bay AE, Schreiner R, Benedicto I, Paz Marzolo M, Banfelder J, Weinstein AM, et al.: The fast-recycling receptor Megalin defines the apical recycling pathway of epithelial cells. *Nat Commun* 7: 11550, 2016
6. Grahammer F, Ramakrishnan SK, Rinschen MM, Larionov AA, Syed M, Khatib H, et al.: mTOR regulates endocytosis and nutrient transport in proximal tubular cells. *J Am Soc Nephrol* 28: 230–241, 2017
7. Schuh CD, Polesel M, Platonova E, Haenni D, Gassama A, Tokonami N, et al.: Combined structural and functional imaging of the kidney reveals major axial differences in proximal tubule endocytosis. *J Am Soc Nephrol* 29: 2696–2712, 2018
8. Amsellem S, Gburek J, Hamard G, Nielsen R, Willnow TE, Devuyst O, et al.: Cubilin is essential for albumin reabsorption in the renal proximal tubule. *J Am Soc Nephrol* 21: 1859–1867, 2010
9. Weyer K, Storm T, Shan J, Vainio S, Kozyraki R, Verroust PJ, et al.: Mouse model of proximal tubule endocytic dysfunction. *Nephrol Dial Transplant* 26: 3446_3451, 2011
10. Willnow TE, Hilpert J, Armstrong SA, Rohlmann A, Hammer RE, Burns DK, et al.: Defective forebrain development in mice lacking gp330/megalin. *Proc Natl Acad Sci U S A* 93: 8460–8464, 1996
11. Leheste JR, Rolinski B, Vorum H, Hilpert J, Nykjaer A, Jacobsen C, et al.: Megalin knockout mice as an animal model of low molecular weight proteinuria. *Am J Pathol* 155: 1361–1370, 1999
12. Bachmann S, Schlichting U, Geist B, Mutig K, Petsch T, Bacic D, et al.: Kidney-specific inactivation of the megalin gene impairs trafficking of renal inorganic sodium phosphate cotransporter (NaPi-IIa). *J Am Soc Nephrol* 15: 892–900, 2004
13. Schmitz C, Hilpert J, Jacobsen C, Boensch C, Christensen EI, Luft FC, et al.: Megalin deficiency offers protection from renal aminoglycoside accumulation. *J Biol Chem* 277: 618–622, 2002
14. Hori Y, Aoki N, Kuwahara S, Hosojima M, Kaseda R, Goto S, et al.: Megalin blockade with cilastatin suppresses drug-induced nephrotoxicity. *J Am Soc Nephrol* 28: 1783_1791, 2017
15. Mogensen CE, Sølling: Studies on renal tubular protein reabsorption: Partial and near complete inhibition by certain amino acids. *Scand J Clin Lab Invest* 37: 477–486, 1977
16. Thelle K, Christensen EI, Vorum H, Ørskov H, Birn H: Characterization of proteinuria and tubular protein uptake in a new model of oral L-lysine administration in rats. *Kidney Int* 69: 1333_1340, 2006
17. Gahl WA, Thoene J, Schneider JA: Cystinosis: a disorder of lysosomal membrane transport. In: *The metabolic and molecular bases of inherited disease*, Vol. 3, edited by Scriver CR, Beaudet AL, Sly WS, Valle D, New York, NY, McGraw Hill, 2001, pp 5085–5108
18. Lloyd JB: Disulphide reduction in lysosomes. The role of cysteine. *Biochem J* 237: 271–272, 1986
19. Thoene JG, Lemons RM: Cystine accumulation in cystinotic fibroblasts from free and protein-linked cystine but not cysteine. *Biochem J* 208: 823–830, 1982
20. Thoene JG, Lemons R: Modulation of the intracellular cystine content of cystinotic fibroblasts by extracellular albumin. *Pediatr Res* 14: 785–787, 1980
21. Thoene JG, Forster S, Lloyd JB: The role of pinocytosis in the cellular uptake of an amino acid. *Biochem Biophys Res Commun* 127: 733–738, 1985
22. Wilmer MJ, Emma F, Levtchenko EN: The pathogenesis of cystinosis: Mechanisms beyond cystine accumulation. *Am J Physiol Renal Physiol* 299: F905–F916, 2010
23. Mahoney CP, Striker GE: Early development of the renal lesions in infantile cystinosis. *Pediatr Nephrol* 15: 50–56, 2000
24. Cherqui S, Courtoy PJ: The renal Fanconi syndrome in cystinosis: Pathogenic insights and therapeutic perspectives. *Nat Rev Nephrol* 13: 115–131, 2017
25. Larsen CP, Walker PD, Thoene JG: The incidence of atubular glomeruli in nephropathic cystinosis renal biopsies. *Mol Genet Metab* 101: 417–420, 2010
26. Gaide Chevronnay HP, Janssens V, Van Der Smissen P, N'Kuli F, Nevo N, Guiot Y, et al.: Time course of pathogenic and adaptation

mechanisms in cystinotic mouse kidneys. *J Am Soc Nephrol* 25: 1256–1269, 2014
27. Galarreta CI, Forbes MS, Thornhill BA, Antignac C, Gubler MC, Nevo N, et al.: The swan-neck lesion: Proximal tubular adaptation to oxidative stress in nephropathic cystinosis. *Am J Physiol Renal Physiol* 308: F1155–F1166, 2015
28. Kleta R, Bernardini I, Ueda M, Varade WS, Phornphutkul C, Krasnewich D, et al.: Long-term follow-up of well-treated nephropathic cystinosis patients. *J Pediatr* 145: 555–560, 2004
29. Cherqui S: Cysteamine therapy: A treatment for cystinosis, not a cure. *Kidney Int* 81: 127–129, 2012
30. Emma F, Nesterova G, Langman C, Labbé A, Cherqui S, Goodyer P, et al.: Nephropathic cystinosis: An international consensus document. *Nephrol Dial Transplant* 29[Suppl 4]: iv87–iv94, 2014
31. Nevo N, Chol M, Bailleux A, Kalatzis V, Morisset L, Devuyst O, et al.: Renal phenotype of the cystinosis mouse model is dependent upon genetic background. *Nephrol Dial Transplant* 25: 1059–1066, 2010
32. Raggi C, Luciani A, Nevo N, Antignac C, Terryn S, Devuyst O: Dedifferentiation and aberrations of the endolysosomal compartment characterize the early stage of nephropathic cystinosis. *Hum Mol Genet* 23: 2266–2278, 2014
33. Ivanova EA, De Leo MG, Van Den Heuvel L, Pastore A, Dijkman H, De Matteis MA, et al.: Endo-lysosomal dysfunction in human proximal tubular epithelial cells deficient for lysosomal cystine transporter cystinosin. *PLoS One* 10: e0120998, 2015
34. Festa BP, Chen Z, Berquez M, Debaix H, Tokonami N, Prange JA, et al.: Impaired autophagy bridges lysosomal storage disease and epithelial dysfunction in the kidney. *Nat Commun* 9: 161, 2018
35. Sansanwal P, Yen B, Gahl WA, Ma Y, Ying L, Wong LJ, et al.: Mitochondrial autophagy promotes cellular injury in nephropathic cystinosis. *J Am Soc Nephrol* 21: 272–283, 2010
36. Napolitano G, Johnson JL, He J, Rocca CJ, Monfregola J, Pestonjamasp K, et al.: Impairment of chaperone-mediated autophagy leads to selective lysosomal degradation defects in the lysosomal storage disease cystinosis. *EMBO Mol Med* 7: 158–174, 2015
37. Andrzejewska Z, Nevo N, Thomas L, Chhuon C, Bailleux A, Chauvet V, et al.: Cystinosin is a component of the vacuolar H+-ATPase-ragulator-rag complex controlling mammalian target of rapamycin complex 1 signaling. *J Am Soc Nephrol* 27: 1678–1688, 2016
38. Lobry T, Miller R, Nevo N, Rocca CJ, Zhang J, Catz SD, et al.: Interaction between galectin-3 and cystinosin uncovers a pathogenic role of inflammation in kidney involvement of cystinosis. *Kidney Int* 96: 350–362, 2019
39. Shan J, Jokela T, Peltoketo H, Vainio S: Generation of an allele to inactivate Wnt4 gene function conditionally in the mouse. *Genesis* 47: 782–788, 2009
40. Leheste JR, Melsen F, Wellner M, Jansen P, Schlichting U, Renner-Müller I, et al.: Hypocalcemia and osteopathy in mice with kidney-specific megalin gene defect. *FASEB J* 17: 247–249, 2003
41. Chabli A, Aupetit J, Raehm M, Ricquier D, Chadefaux-Vekemans B: Measurement of cystine in granulocytes using liquid chromatography-tandem mass spectrometry. *Clin Biochem* 40: 692–698, 2007
42. García-Villoria J, Hernández-Pérez JM, Arias A, Ribes A: Improvement of the cystine measurement in granulocytes by liquid chromatograhy-tandem mass spectrometry. *Clin Biochem* 46: 271–274, 2013
43. Jouret F, Bernard A, Hermans C, Dom G, Terryn S, Leal T, et al.: Cystic fibrosis is associated with a defect in apical receptor-mediated endocytosis in mouse and human kidney. *J Am Soc Nephrol* 18: 707–718, 2007
44. Mori K, Lee HT, Rapoport D, Drexler IR, Foster K, Yang J, et al.: Endocytic delivery of lipocalin-siderophore-iron complex rescues the kidney from ischemia-reperfusion injury. *J Clin Invest* 115: 610–621, 2005
45. Jobst-Schwan T, Knaup KX, Nielsen R, Hackenbeck T, Buettner-Herold M, Lechler P, et al.: Renal uptake of the antiapoptotic protein survivin is mediated by megalin at the apical membrane of the proximal tubule. *Am J Physiol Renal Physiol* 305: F734–F744, 2013
46. Dachy A, Paquot F, Debray G, Bovy C, Christensen EI, Collard L, et al.: In-depth phenotyping of a Donnai-Barrow patient helps clarify proximal tubule dysfunction. *Pediatr Nephrol* 30: 1027–1031, 2015
47. Nielsen R, Christensen EI, Birn H: Megalin and cubilin in proximal tubule protein reabsorption: From experimental models to human disease. *Kidney Int* 89: 58–67, 2016
48. Theilig F, Kriz W, Jerichow T, Schrade P, Hähnel B, Willnow T, et al.: Abrogation of protein uptake through megalin-deficient proximal tubules does not safeguard against tubulointerstitial injury. *J Am Soc Nephrol* 18: 1824–1834, 2007
49. Weyer K, Andersen PK, Schmidt K, Mollet G, Antignac C, Birn H, et al.: Abolishment of proximal tubule albumin endocytosis does not affect plasma albumin during nephrotic syndrome in mice. *Kidney Int* 93: 335–342, 2018
50. Christensen EI, Maunsbach AB: Effects of dextran on lysosomal ultrastructure and protein digestion in renal proximal tubule. *Kidney Int* 16: 301–311, 1979
51. Schiller A, Taugner R: The renal handling of low molecular weight polyvinylpyrrolidone and inulin in rats. In: *Functional Ultrastructure of the Kidney*, edited by Maunsbach AB, Steen Olsen T, Christensen EI, London, Academic Press, 1980, pp 315–326
52. Barone R, Van Der Smissen P, Devuyst O, Beaujean V, Pauwels S, Courtoy PJ, et al.: Endocytosis of the somatostatin analogue, octreotide, by the proximal tubule-derived opossum kidney (OK) cell line. *Kidney Int* 67: 969–976, 2005
53. Behr TM, Sharkey RM, Sgouros G, Blumenthal RD, Dunn RM, Kolbert K, et al.: Overcoming the nephrotoxicity of radiometal-labeled immunoconjugates: Improved cancer therapy administered to a nude mouse model in relation to the internal radiation dosimetry. *Cancer* 80 [Suppl]: 2591–2610, 1997
54. McNeal CJ, Meininger CJ, Reddy D, Wilborn CD, Wu G: Safety and effectiveness of arginine in adults. *J Nutr* 146: 2587S–2593S, 2016
55. Molema F, Gleich F, Burgard P, van der Ploeg AT, Summar ML, Chapman KA, et al.: Additional individual contributors from E-IMD: Evaluation of dietary treatment and amino acid supplementation in organic acidurias and urea-cycle disorders: On the basis of information from a European multicenter registry [published online ahead of print February 8, 2019]. *J Inherit Metab Dis* doi: 10.1002/jimd.12066
56. Elpeleg N, Korman SH: Sustained oral lysine supplementation in ornithine delta-aminotransferase deficiency. *J Inherit Metab Dis* 24: 423–424, 2001
57. Morris SM Jr.: Arginine metabolism revisited. *J Nutr* 146: 2579S_2586S, 2016
58. Wolfson RL, Sabatini DM: The dawn of the age of amino acid sensors for the mTORC1 pathway. *Cell Metab* 26: 301–309, 2017
59. Gahl WA, Balog JZ, Kleta R: Nephropathic cystinosis in adults: Natural history and effects of oral cysteamine therapy. *Ann Intern Med* 147: 242–250, 2007
60. Cherqui S, Sevin C, Hamard G, Kalatzis V, Sich M, Pequignot MO, et al.: Intralysosomal cystine accumulation in mice lacking cystinosin, the protein defective in cystinosis. *Mol Cell Biol* 22: 7622–7632, 2002

AFFILIATIONS

[1]Cell Biology Unit, de Duve Institute and Université Catholique de Louvain, Brussels, Belgium; [2]Biochemical Genetics, Academic Hospital Saint-Luc, Brussels, Belgium; [3]Laboratory of Hereditary Kidney Diseases, Institut National de la Santé et de la Recherche Médicale (INSERM) U1163, Imagine Institute, Paris Descartes University, Paris, France; [4]Faculty of Biochemistry and Molecular Medicine, Laboratory of Developmental Biology, Oulu Center for Cell-Matrix Research, Biocenter Oulu, University of Oulu, Oulu, Finland; [5]Department of Biomedicine, Aarhus University, Aarhus, Denmark; and [6]Groupe Interdisciplinaire de Génoprotéomique Appliquée (GIGA), Cardiovascular Sciences, University of Liège, Liège, Belgium

Supplemental Material

Supplemental Section for

Protection of cystinotic mice by kidney-specific megalin ablation supports an endocytosis-based mechanism for nephropathic cystinosis progression.

Virginie Janssens[1], Héloïse P. Gaide Chevronnay[1], Sandrine Marie[2], Marie-Françoise Vincent[2], Patrick Van Der Smissen[1], Nathalie Nevo[3], Seppo Vainio[4], Rikke Nielsen[5], Erik I. Christensen[5], François Jouret[6], Corinne Antignac[3], Christophe E. Pierreux[1]*, Pierre J. Courtoy[1]*.

Table of Contents

Supplementary Methods

Semi-thin sections and electron microscopy

Kidneys were perfusion-fixed *in situ* with 4% formaldehyde in 0.1 M phosphate buffer, pH 7.4 as above, then excised and small blocks of cortices were immediately post-fixed in 4% formaldehyde supplemented by 0.5% (v/v) glutaraldehyde in 0.1 M cacodylate buffer, pH 7.4 at 4°C, overnight in rotating vessels. Samples were further processed exactly as described in [1]. Briefly, blocks were further osmicated, stained "en bloc" with uranyl acetate, dehydrated and embedded in Spurr. Semi-thin sections (1-microm, nominal) were collected on glass slides and stained with toluiduine blue. Ultrathin sectioning (70-nm nominal) was guided by toluidine-stained semi-thin sections. Ultrathin sections were collected on 400-mesh rhodanium grids, sequentially contrasted with uranyl and lead, and examined in a FEI CM12 electron microscope operating at 80 kV.

RT-PCR

Total RNA was extracted (SV total RNA isolation system; Promega). Aliquots of 500 ng RNA were reverse-transcribed by M-MLV reverse transcriptase (Invitrogen) with the random hexamers protocol (primer random $p(dN)_6$, Roche). Primer sequences for hypoxanthine phosphoribosyltransferase 1 (HPRT-1; used as house-keeping gene), glyceraldehyde 3-phosphate dehydrogenase (GAPDH; used to test primer efficiency), cubilin, SGLT-2 and NaPi-IIa are described in Gaide Chevronnay et al. 2014. [1] Real-time qPCR was performed as described [2] in presence of 250 mM of specific primers with Kappa SYBR Fast qPCR Master Mix (Kapa Biosystems) on a CFX96 touch real-time PCR Detection System (Bio-Rad). Data were analyzed using the ΔΔCT method, using HPRT-1 as internal standard, and presented as fold-change.

Supplementary Figures

Supplementary figure 1

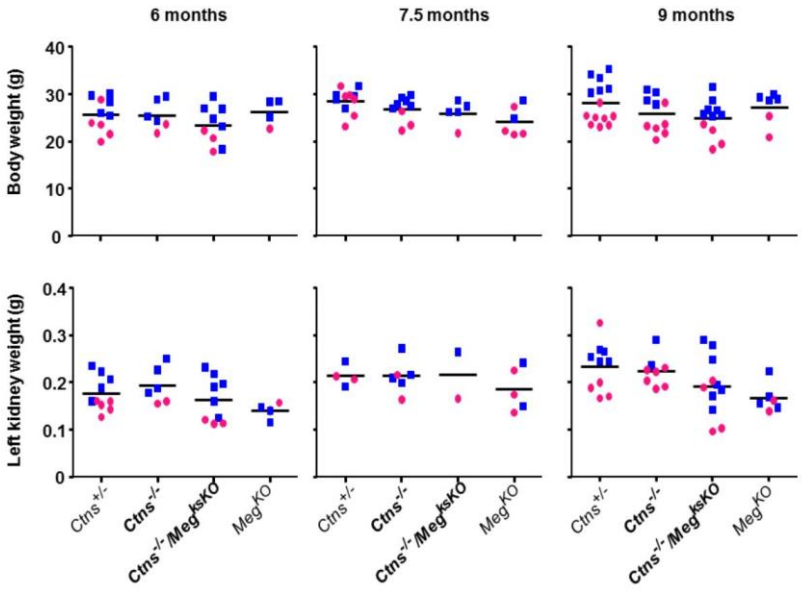

Body and kidney weights. Mice and left kidneys (not fixed by perfusion; when saved) were weighed at the time of sacrifice (males, blue squares; females, red disks). There was no significant difference between any genotype in our colony.

Supplementary figure 2 (complementary to Figure 2A)

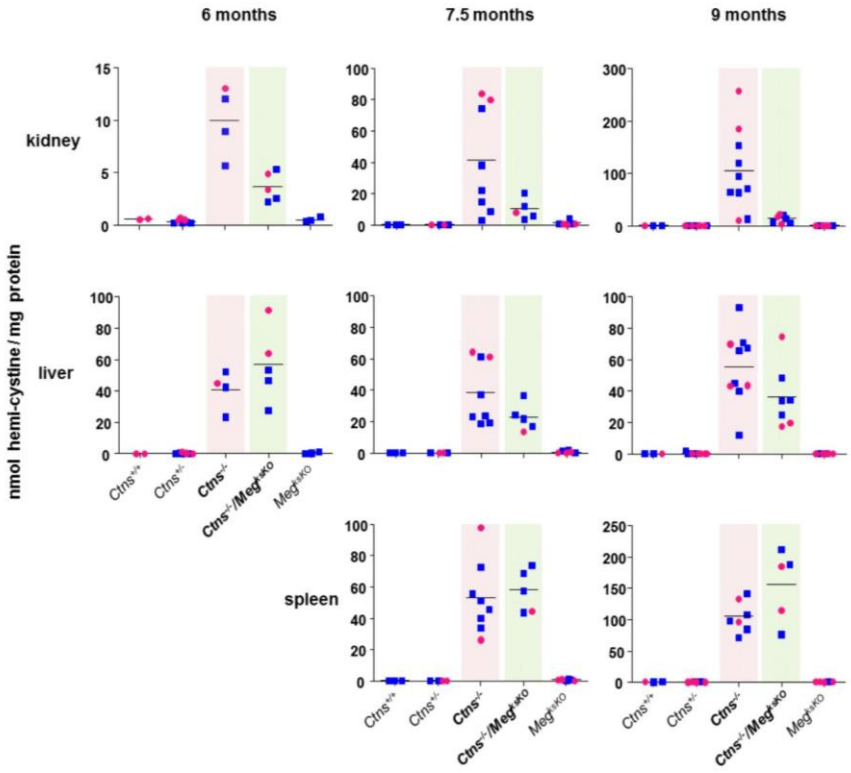

Megalin ablation in Ctns$^{-/-}$ kidneys selectively prevents cystine accumulation: time-course in comparison with liver and spleen. Time-course of cystine content in kidneys, liver and spleen of 6, 7.5 and 9 months-old mice of the indicated genotypes (males, blue squares; females, red disks). In *Ctns$^{-/-}$* kidneys, median cystine content increases exponentially between 6 and 9 months (note difference of ordinate scale). In double KO kidneys, content is moderately increased yet remains rather low at all time-points. In contrast, liver and spleen content in *Ctns$^{-/-}$* and double KO mice, serving as positive controls for cystinosin deletion, show high cystine levels irrespective of megalin ablation. Data on spleen at 6 months are not available.

Supplementary figure 3 (complementary to Figure 2B)

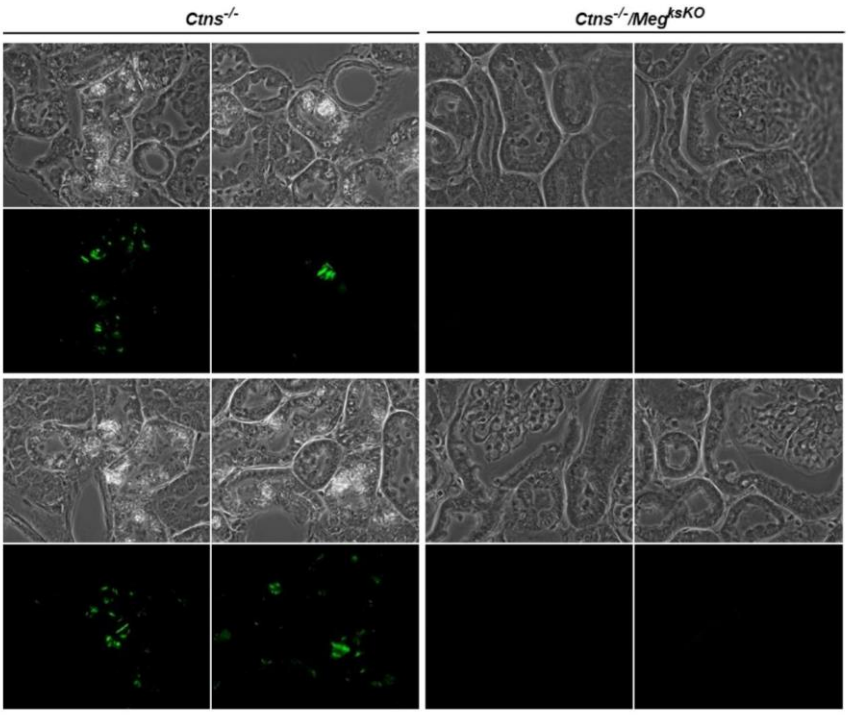

Megalin ablation in Ctns$^{-/-}$ kidneys prevents cystine crystal deposition: gallery of images as in Figure 3B.

6

Supplementary figure 4

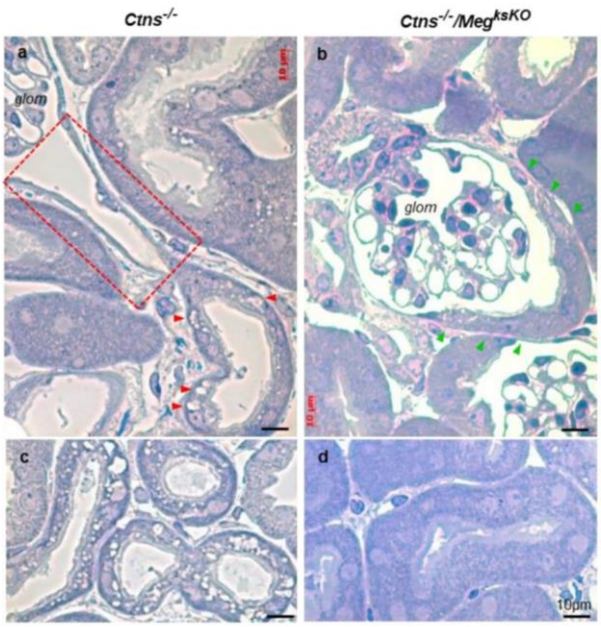

Toluidine-stained plastic sections of Ctns$^{-/-}$ vs double KO kidneys *(9 months).* Upper panels (a-b), GTJs; lower panels (c-d), clusters of proximal tubules; all at identical magnification. In the upper panel, notice at left swan-neck lesion (in red box) and structural abnormalities in continuing S1 PCTs (red arrowheads) of *Ctns$^{-/-}$* kidney, contrasting with preservation in double KO (green arrowheads). In lower panel, notice extensively vacuolated and much thinner *Ctns$^{-/-}$* PCTs as compared with double KO.

Supplementary figure 5

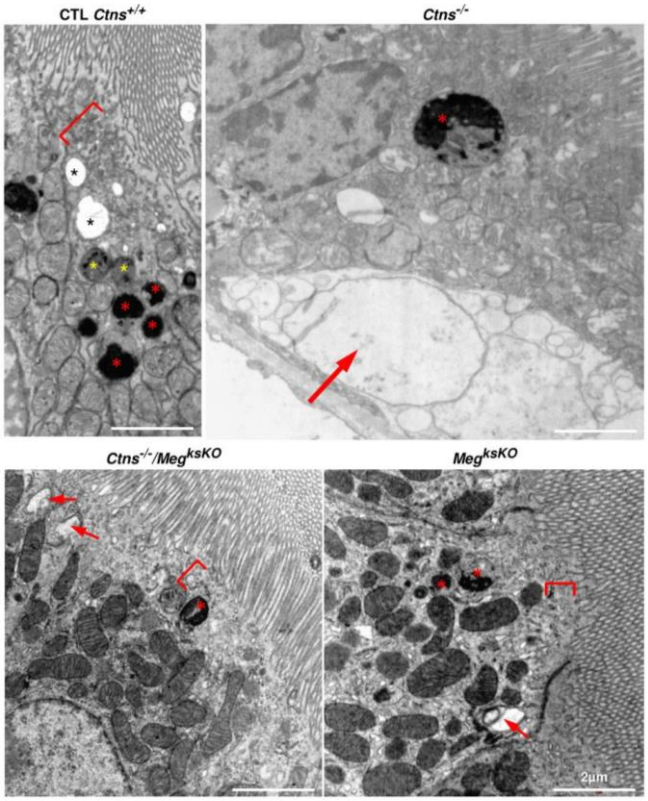

Electron microscopy *(6 months).* In this favorable view of a control PCT, notice the remarkable stratification of the apical endocytic apparatus. Immediately under the brush border is a dense layer exclusively made of packed dense apical tubules (recycling endosomes; bracket). Below are apical vacuoles (sorting endosomes, two black asterisks), then intermediate organelles resulting from fusion between late endosomes and lysosomes (endo-lysosomes, two yellow asterisks), then a cluster of dense bodies (secondary lysosomes, four red asterisks). In this *Ctns*$^{-/-}$ kidney, a partially preserved PCT with a huge lysosome (red asterisk) lies over a dead PCT still in contact with the tubular basement membrane (large arrow). In double KO as in single megalin KO kidneys, PTCs are overall well preserved, except for the absence of dense apical (recycling) tubules (indicated by brackets) and fewer small lysosomes (red asterisks). Arrows point to autophagic structures. All equal scale bars at 2 microm.

Supplementary figure 6A (complementary to Figure 5)

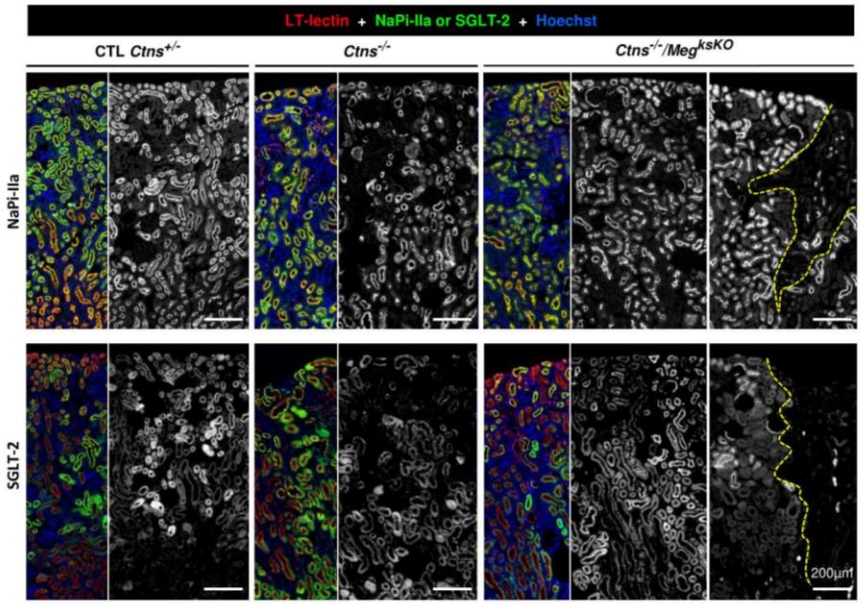

Supplementary figure 6B (complementary to Figure 5)

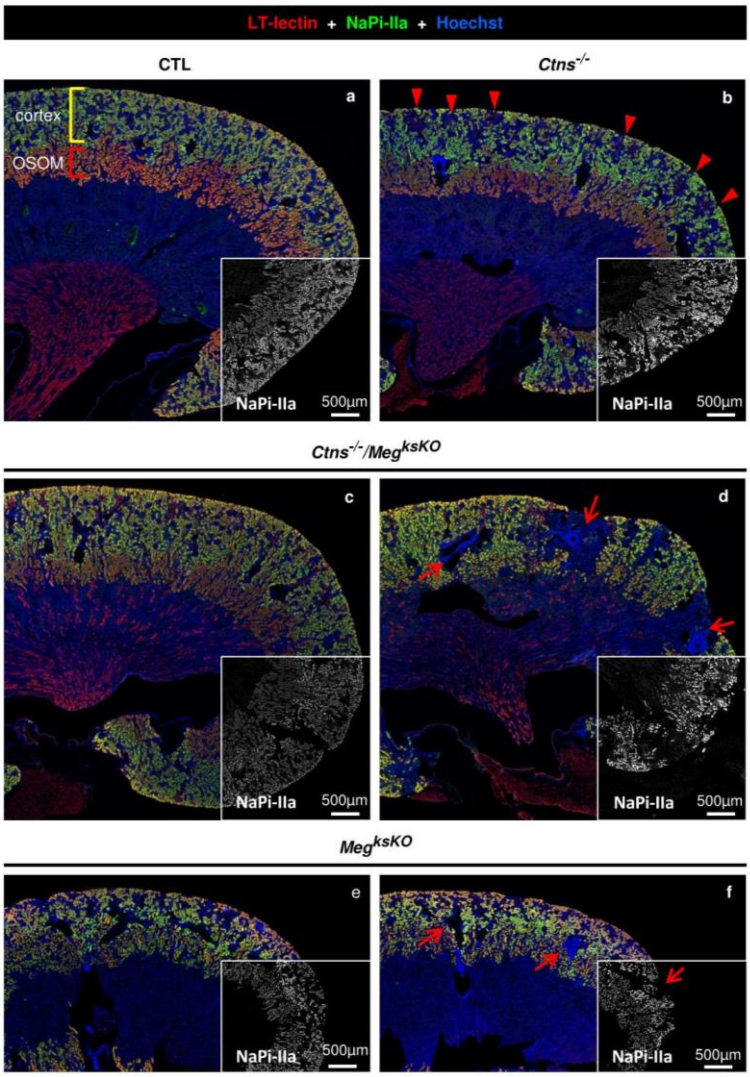

10

Diffuse mottled appearance resulting from loss of transporter expression in Ctns$^{-/-}$ PCTs contrasts with large areas of inflammatory remodelling in double KO. A. Low power views across the cortex at 9 months of age. Whole kidney sections were processed for triple fluorescence labelling to compare NaPi-IIa or SGLT-2 (both in green) to LT-lectin (red) and nuclei (Hoechst, blue) and presented at left of each pair in triple color, or limited at right to NaPi-IIa (upper panel) or SGLT-2 (lower panel) presented in black and white. ***B.*** Extended views of whole kidney sections showing triple labelling with NaPi-IIa (triple color) or only NaPi-IIa (black/white; continuing field). In WT (a), LT-lectin labeling encompasses the entire OSOM (thus including S3; red only) whereas NaPi-IIa is sharply limited to cortex (together with LT-lectin, thus yellow). In *Ctns*$^{-/-}$ (b), arrowheads point to mottled appearance. Two examples illustrate the variable pattern of double KO (c,d) and single *Meg* KO (e,f). At right (d,f), arrows point to grossly remodeled cortical zones centered on radial artery (blue rings). At left, overall appearance of this double KO (c) is comparable to a WT; for this single megalin KO (e), fewer areas with gross remodeling are seen. All identical scale bars at 500 microm.

Supplementary figure 7

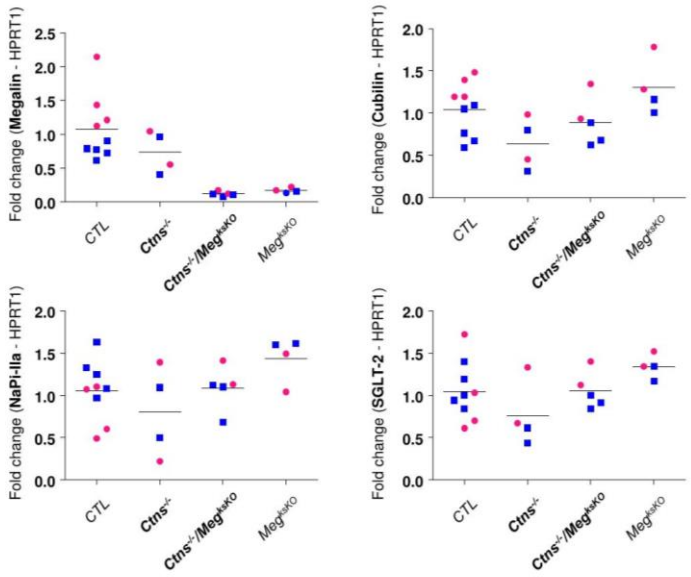

RT-PCR. Megalin ablation in Ctns KO kidneys appears to prevent loss of cubilin, NaPi-IIa and SGLT-2 mRNAs (males, blue squares; females, red disks).[1, 2]

Supplementary References

1. Gaide Chevronnay, H.P., et al., *Time course of pathogenic and adaptation mechanisms in cystinotic mouse kidneys.* J Am Soc Nephrol, 2014. **25**(6): p. 1256-69.
2. Dupasquier, S., et al., *Validation of house-keeping gene and impact on normalized gene expression in clear cell renal cell carcinoma: critical reassessment of YBX3/ZONAB/CSDA expression.* BMC Mol Biol, 2014. **15**: p. 9.

3.3. Preliminary Results - Long-term dietary supplementaion of cystinotic mice with dibasic amino-acids protects against swan-neck lesions

Janssens V et al*

**Preliminary draft based on Results collected so far at CELL; to be revised when complemented by, among other, results from Drs Cheung W. and Mak R., UCSD (in-depth analysis of structural and functional effects of long-term dbAA supplementation in Ctns$^{-/-}$ kidneys) and mechanistic insights by Biacore from Drs Moestrup S. K. and Graversen J. K., University of Aarhus and Odense, DK.*

ABSTRACT

Nephropathic cystinosis is a multisystemic lysosomal storage disease due to deletion or inactivating mutations of the lysosomal cystine transporter, cystinosin, and leading to cystine accumulation in lysosomes. Since extensive Wnt-4Cre-driven perinatal genetic *excision* of the floxed megalin gene in kidney proximal tubular cells (PTCs) of *Ctns*$^{-/-}$ mice dramatically decreased cystine accumulation therein and conferred remarkable protection against the characteristic swan-neck lesions (previous Chapter), we here explored whether a similar benefit could be gained by *inhibition* of the megalin pathway in young *Ctns*$^{-/-}$ mice. This pathway can indeed be blocked by dibasic amino-acids (dbAAs) in cultured epithelial cells and upon acute dbAA loading *in vivo*. To this aim, we first showed that dietary supplementation of WT mice at 2 months of age with L-arginine or L-lysine in drinking water for two weeks was well-tolerated

(e.g. no effect on weight), non-toxic and led to inhibition of protein recapture by PTCs in the kidney cortex, as shown by induced LMW proteinuria and suppressed acute PTC uptake of injected TexasRed-ovalbumin. We next found that chronic supplementation of both dbAAs from two months of age tended to decrease cystine accumulation and swan-neck lesions in cystinotic female kidneys by 6 months of age. These preliminary observations are currently extended to large mice numbers and longer treatment. They also pave the way to a pilot clinical test in cystinotic children.

INTRODUCTION

Nephropathic cystinosis (NC) is a devastating lysosomal storage disease due to deletion or inactivating mutations of the lysosomal cystine transporter, cystinosin.(Gahl, Thoene, and Schneider 2002) Major affected organs in NC are kidneys and eyes in infancy, endocrine glands in childhood, or muscle in adulthood (a.o.). Renal Fanconi syndrome may cause acute life-threatening dehydration and kidney evolves to insufficiency. Muscle wasting is a major concern in early adulthood and may lead to fatal aspiration pneumonia. The only approved drug, cysteamine, delays disease progression, but does not provide a cure.(Emma et al. 2014; Brodin-Sartorius et al. 2012; Cherqui 2012) Thus, new effective therapeutic approaches are urgently needed. The natural course of this disease and effects of therapies can be studied in a cystinosin knockout mouse model (*Ctns*$^{-/-}$, Nevo et al. 2010). Focus has been given

on kidneys (Harrison et al. 2013; Gaide Chevronnay et al. 2014), thyroid (Gaide Chevronnay et al. 2015; Gaide Chevronnay et al. 2016), muscles (Cheung et al. 2016) and eyes.(Bishop 2017)

In the previous Chapter, I have presented our observations supporting the view that apical endocytosis of disulfide-rich plasma proteins is the principal source of cystine to PTC lysosomes. Endocytosis therefore contributes importantly to lysosomal cystine accumulation in these cells when transmembrane efflux is abolished by functional cystinosin absence. This view is supported by the spectacular protection against cystine storage and tissue damage in cystinotic kidneys upon organ-specific genetic *excision* of megalin, as cornerstone for apical endocytosis in these cells. Here we will explore whether the megalin pathway can be efficiently *inhibited* by simple oral interventions using dietary supplementation with dibasic amino-acids as most promising candidates. Beside the fact that dbAAs are considered safe and beneficial for muscle in rat, pig and human studies (Yang, Wu, et al. 2015; Hu et al. 2015; McNeal et al. 2016; Benevenga and Blemings 2007; Racusen, Whelton, and Solez 1985; Lo et al. 1996; Peltola et al. 2000; Elpeleg and Korman 2001), L-lysine and L-arginine have already shown their ability to inhibit endocytosis *in vitro.*(Barone et al. 2005; Thelle et al. 2006) However, dietary intervention by dbAAs supplementation has not been considered in NC.

In human, safe oral supplementation has been reported with L-arginine for healthy adults (up to 20g/day, i.e. at 5-fold normal supply; McNeal et al. 2016) and this amino-acid is used since decades at 10-

15g/day for life-long treatment of genetic deficits of urea cycle enzymes.(Batshaw, MacArthur, and Tuchman 2001) Likewise, a similar dose of L-lysine is used in ornithinemia to prevent gyrate atrophy.(Peltola et al. 2000; Elpeleg and Korman 2001) Acute inhibition of kidney protein reabsorption by dbAAs in human volunteers was first reported in a landmark paper by Mogensen & Solling.(Mogensen and Solling 1977) The authors observed immediate increase of urinary excretion of albumin, immunoglobulin light chains and beta2-microglobulin in response to acute infusion of titrated amounts of L-lysine (up to 120 g), L-arginine and related compounds. They concluded to almost full block of tubular reabsorption, in linear correlation with L-lysine plasma concentration. Inhibition of protein binding to isolated brush border was later observed by Ottosen et al, 1985.(Ottosen et al. 1985) *Competition* by L-lysine supplementation was then attempted to prevent nephrotoxicity from the antibiotic aminoglycosides such as gentamicin, later identified as a megalin ligand.(Moestrup et al. 1995) Preliminary studies were initiated in male rats but abandoned because L-lysine dosage used (1.5 g/kg bw/day) proved itself nephrotoxic after 3 days and exacerbated toxicity of gentamicin when given together.(Gilbert et al. 1982) However, there is such a high number of gentamicin binding sites on megalin (estimated at 80 gentamicin sites/megalin molecule; reviewed in Nagai and Takano 2004) that effective competition would probably require huge lysine concentrations. In contrast, only few proteinaceous ligands bind per megalin (in the order of two; Nagai and Takano 2004), offering better prospect for competition. Infusion of a mixture of dibasic amino-acids indeed proved effective to

alleviate acute nephrotoxicity resulting from injection of the radio-octreotide (a peptide) used to treat diffuse endocrine tumors by local irradiation.(Behr et al. 1997)

The underlying mechanism of nephroprotection was later unraveled in the OK (opossum-derived kidney proximal tubular) cell line. This *in vitro* study evidenced inhibition by the dbAA mixture of RAP-competable receptor-mediated endocytosis (RME) of albumin.(Barone et al. 2005) *In vivo*, oral gavage of adult female rats for one day by L-lysine at 80 mmol (i.e.11.6 g) / kg body weight /day was well-tolerated despite 8-fold higher dose than in the study of Gilbert et al (1982).(Gilbert et al. 1982) Moreover, it proved effective to cause low molecular weight (LMW) proteinuria as well as to suppress detection of endogenous albumin uptake inside PTCs.(Thelle et al. 2006) Intriguingly, this paper reported a redistribution of megalin and cubilin, from a normally restricted immunofluorescence signal at both the base of the brush border (where lateral membrane interaction with the brush border cytoskeleton is minimal, thus allowing vesicular fusion and fission, as well as lateral diffusion) and the underlying subapical endosomal layer, towards a single compartment corresponding to the entire thickness of the brush border. This new pattern would suggest that dbAA had blocked receptor endocytosis while recycling would be somehow preserved, so that the entire receptor pool would eventually be trapped at the apical PTC membrane, then slowly randomized along the entire brush border thickness. This redistribution anyhow suggests a more complex mechanism for dbAA than a simple competition for cell surface binding to a

continuously recycling receptor pool. The underlying molecular mechanism of the endocytosis block, besides competition for binding, is still elusive. A hypothesis would be that positively-charged dbAA cross-link with negatively-charged membrane constituents such as phospholipids and/or proteoglycans. This lattice could thus "freeze" the membrane so as to impede lateral diffusion and endocytosis, as has been reported for the cationic drug, azithromycin.(Tyteca et al. 2002; Tyteca et al. 2003)

Besides competition and inhibition of endocytosis, L-arginine has such complex metabolism and hits so many complex pathways that keeping an open mind is essential.(Morris 2016) One such pathway is mTORC1, operating at the lysosomal membrane to orient metabolism towards anabolism while repressing autophagy in normal conditions.(Efeyan, Comb, and Sabatini 2015) Remarkably, lysosomal recruitment and activation of mTORC1 is regulated by amino-acids such as leucine and arginine (not much is known about lysine). Two arginine sensors have been recently identified: (i) SLC38A9 acting in the lysosomal lumen, close to the V-ATPase to which cystinosin is normally associated; and (ii) CASTOR-1, acting in the cytosol.(Wolfson and Sabatini 2017) Since dominant-positive, truncated SLC38A9 constitutively activates mTORC1, one can likewise imagine that constant arginine supply keeps mTORC1 permanently active. Whether this would result in inhibition of endocytosis of (disulfide-rich) cystine precursors, promotion of vesicular efflux to prevent lysosomal sequestration, and/or autophagic flux (both regulated via mTORC1) is open to speculation.

RESULTS AND DISCUSSION

High doses of dibasic amino acid supplementation are not toxic for kidneys and inhibit receptor-mediated endocytosis in wild-type mice.

As a prerequisite to long-term oral dbAA supplementation in cystinotic (*Ctns*$^{-/-}$) C57BL/6 mice with specifically enriched pellets, we first added dbAAs in drinking water (renewed every 2 days) for wild-type (WT) mice during two weeks. L-lysine, L-arginine or L-citrulline (as arginine precursor) were added to reach a two-fold (low dosage) or five-fold (high dosage) higher intake, as compared to untreated (CTL diet) or L-glycine-treated (control) WT mice (i.e. for high doses 7 mg L-lysine, L-arginine or L-citrulline and 6 mg L-glycine / g body weight / day). Thus, the normalized level for chronic L-lysine supplementation in our mice was about 60% that used for acute gavage in rats by Thelle et al.

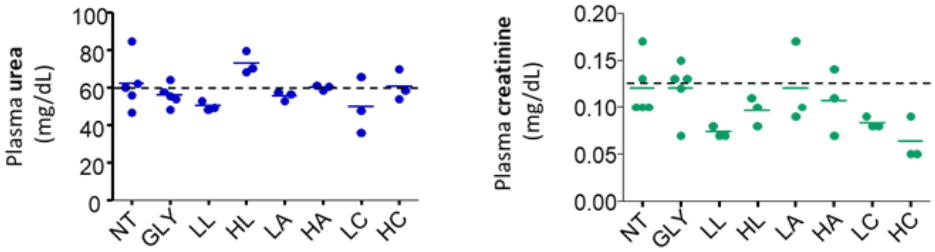

Figure 1. Plasma urea and creatinine assays indicate good tolerance of wild-type mice kidneys to supplementation with dibasic amino-acids (low and high concentrations) in water for 2 weeks. NT, not treated (CTL diet); GLY, L-glycine (for isonitrogenic control); LL, low L-lysine; HL, high L-lysine; LA, low L-arginine; HA, high L-arginine; LC, low L-citrulline (as arginine precursor); HC, high L-citrulline.

The stability of the AAs in water was verified by mass-spectrometry (kindly performed by Dr. V. Stroobant, DDUV mass-spec platform). As shown by Figure 1, there was no increase in blood levels of urea and creatinine after two weeks, indicating lack of toxicity on kidney function.

As shown by Figure 2, 24-hours urinary collections revealed a dose-dependent transferrinuria (sensitive marker of tubular proteinuria) upon high dose for L-arginine and (to a lesser extent) L-citrulline, compatible with defective tubular recapture. Lysine was not included because of failure of urinary collections with this dbAA. This test should be repeated before manuscript submission.

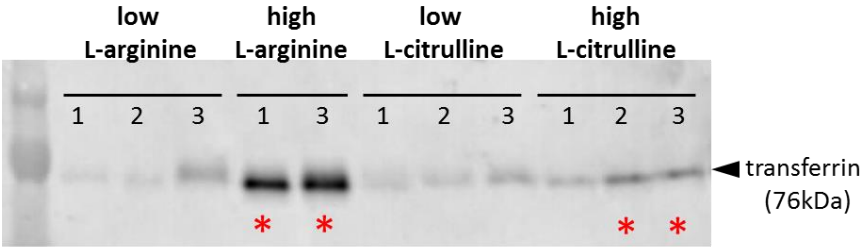

Figure 2. Oral supplementation of WT C57BL/6 mice with L-arginine or its precursor, L-citrulline, for 2 weeks (low, 2-fold; high, 5-fold) induces dose-dependent tubular proteinuria (red asterisks). Loads were normalized to creatinine content.

To directly look for a defect of LMW protein recapture, WT C57BL/6 mice were adapted to inverted light cycle so as to be under feeding with dbAA-supplemented pellets during day hours (when challenged by acute fluoresecent tracer injection). Control or dbAA-treated WT mice were injected with 300 micrograms TexasRed-ovalbumin (TR-OVA; 45 kDa) in the orbital plexus at 20 minutes before sacrifice. Then, kidneys were perfusion-fixed and processed for confocal imaging using multiplex fluorescence labelling. As shown by low magnification sagittal view of untreated mice illustrated at Figure 3A left, TR-OVA labelled the entire cortex with a clear boundary at the cortico-medullary junction, consistent with megalin-dependent uptake in the S1 segment of kidney proximal tubular cells. (Schuh et al, JASN, 2018) At higher magnification (Figure 3B left), cortical PTCs were labeled by megalin (blue) and TR-OVA (red) assumed a dotty apical appearance with significant but not full co-localization with LAMP-1 (lysosomal marker, green), indicating ongoing transfer to late endosomes and lysosomes.

Upon L-lysine supplementation (Figure 3A right), cortical TR-OVA signal was greatly reduced and the tracer instead extended deeper into the outer stripe of outer medulla. These results are consistent with an impaired recapture by S1 segment (most proximal segment of the proximal tubule) and suggest that tracer reabsorption is reported to S3 segment (most distal segment of the proximal tubule) also expressing megalin. At higher magnification (Figure 3B right), TR-OVA dots were much fewer and/or much less brilliant. However, in contrast with previous data obtained by the group of Thelle in L-lysine treated rats (Thelle et al. 2006), megalin

signal did not show a clear redistribution to the entire thickness of brush border, although double labelling of megalin with villin deserves to be examined.

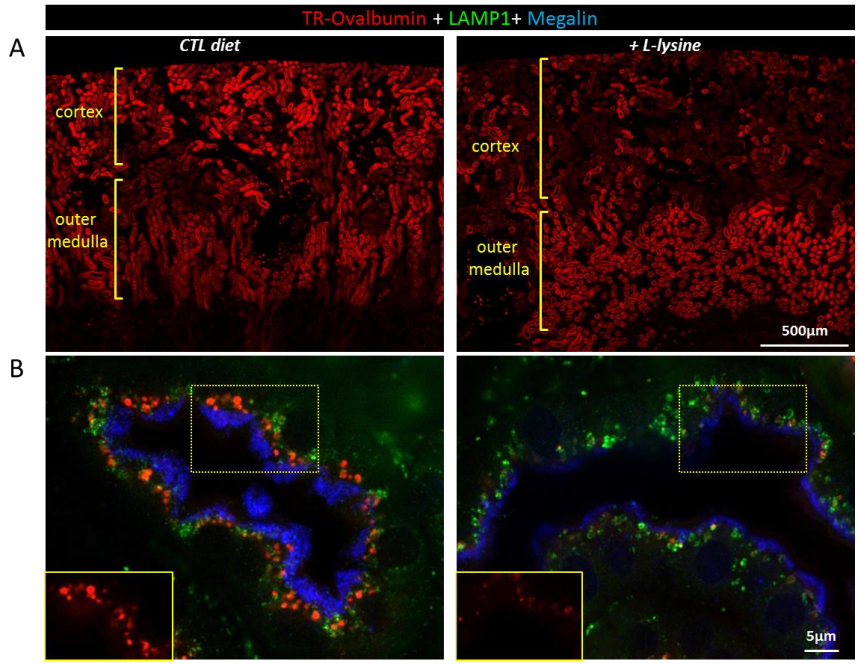

Figure 3. Efficacy of L-lysine supplementation in solid pellets to inhibit acute endocytic protein uptake by most proximal kidney tubular cells. C57BL/6J WT male mice were adapted to inverted 24-h light cycles (so that feeding ad libitum is reprogrammed during day light, to ensure maximal plasma L-lysine level during tracer uptake) and supplemented or not by 5-fold excess L-lysine in their dietary pellets. After 3 weeks, mice were deeply anesthetized, injected i.v. with a large bolus (600 microg) of TexasRed-ovalbumin (TR-OVA), and euthanized after 20 min. Kidneys were perfusion-fixed and whole sections were examined by fluorescence microscopy at low magnification (A) or high magnification of cortex (B) under identical settings for TR-OVA (red), LAMP1 (green; lysosomes), and megalin (blue). At A, notice predominant uptake under CTL diet by kidney cortex with much lower signal in the outermedulla, i.e. by the most proximal S1-S2 convoluted PT segments. In L-lysine-treated mice, cortex uptake is severely damped and endocytic cargo is transferred to S3 straight segment in the outer stripe of outer medulla. At (B), notice under CTL diet significant but incomplete association of TR-OVA with LAMP1, contrasting with undetectable TR-OVA signal under L-Lysine. Boxed areas are reproduced below with TR-OVA signal only.

Taking all data above together, we can conclude that dietary supplementation by high doses of dbAA for two weeks was effective to inhibit receptor-mediated endocytosis (RME) in WT mouse PTCs. However, the underlying mechanism is not defined by this experiment. Lack of detectable megalin redistribution to the brush border at steady-state does also not exclude significant impairment of megalin trafficking, which would require kinetic studies in primary PTC cultures.

Long-term dibasic amino acid supplementation prevents albumin uptake/accumulation and could possibly protect cystinotic kidneys against cystine accumulation.

We next looked at the effect of dbAA on RME in *Ctns*$^{-/-}$ PTCs. As shown by Figure 4 left, *Ctns*$^{-/-}$ female PTCs at 6 months of age showed greatly enlarged late-endosomes/lysosomes (labeled by LAMP-1, green emission), either distorted (presumably by crystals) or filled with immunoreactive mouse albumin (red emission), consistent with recapture but defective proteolysis in secondary lysosomes.(Gaide Chevronnay et al. 2014; Raggi et al. 2014)

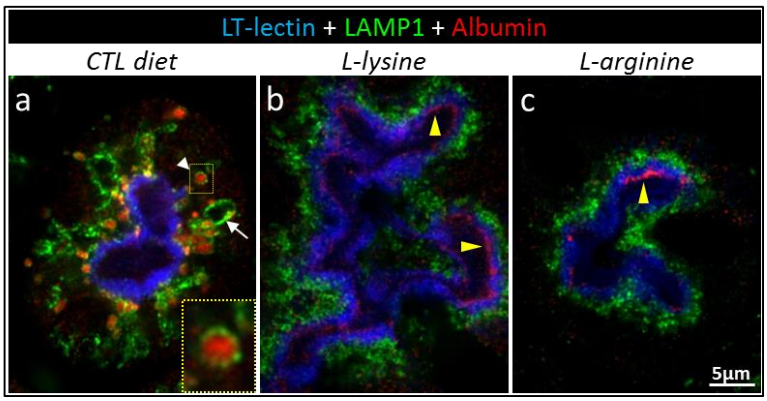

Figure 4. Effect of basic amino-acids in *Ctns* KO mice: prevention of lysosomal swelling and loss of detection of endogenous albumin labeling. Six months old *Ctns* KO female mice were either left untreated (CTL diet) or treated since 2 months of age by oral supplementation with L-lysine or L-arginine. Kidneys were perfusion-fixed with formaldehyde and processed for triple fluorescence labelling for brush border (LT-lectin, blue), lysosomes (LAMP-1, green) and endogenous mouse albumin (red). Notice in the untreated *Ctns*$^{-/-}$ mouse at left the occurrence of enlarged, distorted lysosomes (white arrow, compatible with large cystine crystal), and the easy detection of albumin immunoreactivity in secondary lysosomes (white arrowhead, red disk circumscribed by green circle, as typical "signed-ring" pattern). In contrast, both L-lysine and L-arginine appear to fully preserve lysosome size and shape. In addition, albumin is not detected within lysosomes of L-lysine- and L-arginine-treated in the same immunolabeling conditions, indicating either preserved degradation, or impaired endocytosis. Yellow arrowheads indicate linear deposits of albumin immunoreactivity, sometimes found resting on the luminal tip of brush border (not penetrating deep into the brush border layer). We interpret these deposits as albumin that escaped endocytosis and was cross-linked at the lumen: brush border interface by the perfusion-fixation procedure.

Such abnormal lysosomes extended deeper in the cytoplasm than in the narrow subapical layer as usually found in wild-type mouse PTCs. Upon treatment by either L-lysine or L-arginine pellets (Figure 4 center and right), lysosomes were limited to a well-delineated subapical layer and showed a regular small size without detectable mouse albumin (in our immunolabeling conditions). In contrast, albumin was sometimes detected as linear deposits resting on the top of the brush border (yellow arrowheads in Figure 4). We attribute this signal to albumin remaining in the lumen due to defective endocytosis and trapped onto the brush border upon perfusion-fixation.

Our data further suggest that long-term bAA oral supplementation can prevent endocytic recapture of albumin (and presumably other megalin/cubilin ligands) and normalize lysosome size, shape and subapical positioning. Since inhibition of endocytosis of disulfide-rich ultrafiltrated plasma protein into PTCs should decrease lysosomal cystine supply, thus storage in cystinosin absence, we are currently measuring cystine levels in untreated v*s* L-arginine- or L-lysine-treated kidneys of the *Ctns*$^{-/-}$ females from the same colony. As suggested by preliminary results shown by Figure 5A, there is a consistent tendency to a decrease in cystine levels of L-arginine- and especially L-lysine-treated cystinotic female kidneys as compared with untreated ones. Moreover, while I was writing my thesis, a new set of data was generated by Dr Laura Rita Rega, in Dr Emma's lab (Figure 5A'). Surprisingly, the results obtained by Dr. Mak's lab, our collaborators at UCSD (San Diego), do not converge with those obtained above. They do not show difference in cystine level between the three

groups from their mouse colony. To evaluate the possibility of secondary treatment (initiated later, when lesions are present), she treated *Ctns* KO female mice from 6 till 8 months of age and also found decrease of kidney cystine content When data of the two studies are combined (expressed as % of untreated *Ctns* KO female controls), differences upon treatment are clearly statistically significant (Figure 5A’’).

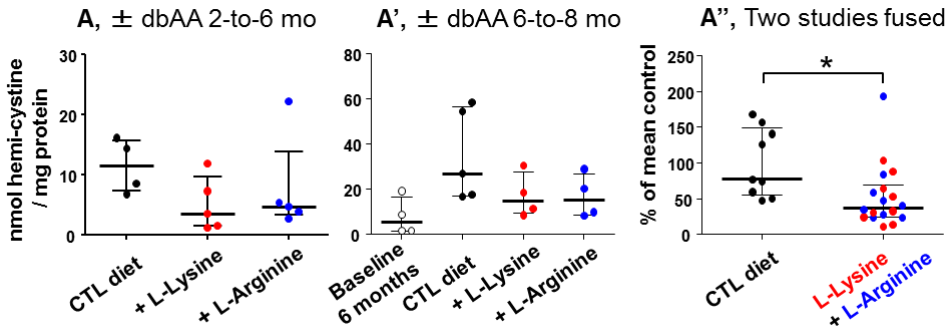

Figure 5. Dietary supplementation of Ctns KO mice with dibasic amino-acids (bAAs) tends to decrease kidney cystine accumulation in 6-months-old females (Preliminary results). Femalemice were fed from 2 till 6 months of age (A,A’’) or from 6-to-8 months of age (A’,A’’) with control, or 5-fold excess of L-lysine or L-arginine. There is a clear trend towards decrease with either bAA in two studies. Pooling studies reaches statistical significance (A’’).

In the LDL-receptor family, ligand binding domains are evolutionary conserved between megalin (also called LRP2) operating at the apical domain of polarized epithelial cells and the scavenger receptor, LRP1, extremely active in the non-polarized macrophages which are abundant in liver (Küppfer cells) and spleen and presumably account for their very high cystine values reflecting abundant crystals in cystinosis. Therefore, we also measured cystine levels in these two organs. In our limited sample collection, we found no difference upon dbAA treatment in liver and spleen, both in females at 6 months of age (4 months of treatment) and males at 9 months of age (7 months of treatment). If confirmed in larger cohorts, the difference between a probable dbAA effect in kidneys *vs* no effect in liver and spleen may be due to much higher ligand concentrations in plasma (thus poorly competable) as compared to urine (better competable).

Long-term dibasic amino acid supplementation protects cystinotic kidneys against histological lesions

Finally, we looked for kidney structural protection of dbAA-treated *Ctns*$^{-/-}$ mice by morphometry of swan-neck lesions at all glomerulo-tubular junctions (GTJs) with a recognizable tubular lumen across sagittal kidney sections. Figure 6 reports this quantitation for female *Ctns*$^{-/-}$ mice treated or not from 2 to 6 months of age with either L-lysine or L-arginine. Below the representative histology of each group, the quantitation is presented as percentages of swan-neck lesions compared to preserved GTJs across a full sagittal kidney section. Swan-necks were abundant in untreated *Ctns*$^{-/-}$

female kidneys at 6 months of age (83%), up to 100% (no remaining preserved GTJ) in one case which also exhibited the highest cystine level. The percentage of swan-necks decreased by ~ two-fold upon L-arginine treatment and by ~ four-fold upon L-lysine treatment, consistent with a higher decrease of cystine level upon L-lysine than upon L-arginine.

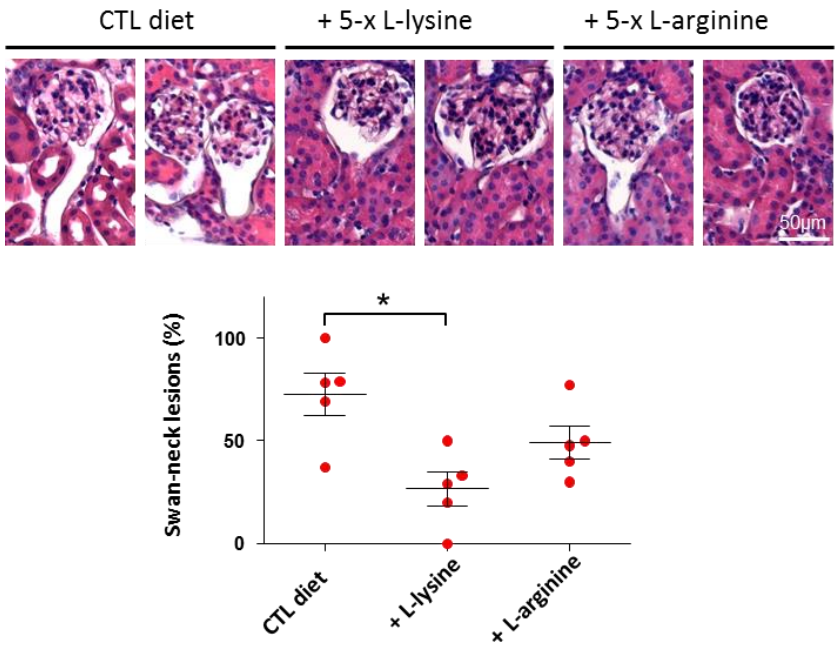

Figure 6. Preliminary results on the effects of bAAs on swan-neck lesions. **, *P*<0.01 by non-parametric Kruskal-Wallis test with correction by Dunn's comparison. From Janssens V. et al… Courtoy P.J. *Work in progress*

In conclusion, although larger numbers are obviously needed, we tentatively conclude that inhibition of RME upon dietary supplementation by L-arginine, and especially L-lysine, might significantly decrease cystine accumulation and preserve glomerulo-tubular junction. Whether these dibasic amino-acids also prevent apoptosis (caspase-3a immunolabelling) and proliferation (Ki-67) so as to normalize PTC turn-over remains to be quantified. Future studies should also address the level of macro-autophagy, based on colocalization of LAMP-1 with TOM20 (index of mitophagy). Since autophagy is repressed by an anabolic effect via mTORC1 whose recruitment and activation on lysosomes is promoted by arginine, the effect of bAAs on the colocalization of mTORC1 components with LAMP-1 deserves to be examined. An alternative approach to discriminate competition *vs* anabolic effect would be to compare L-dbAAs with their D-stereoisomers. Indeed, since competition with protein ligands for interaction with megalin and cubilin only depends on two positively charged amino-groups at the appropriate distance (Ref to Andersen/Moestrup TIBS 2014), both L- and D-dbAAs would be expected to equally compete for binding at the cell surface. In contrast, since the anabolic effect would depend on cell uptake via the *stereospecific* dbAA apical PTC transporter (rBAT-b(0,+)AT, which also serves as apical cystine transporter, Makrides, Camargo, and Verrey 2014), only L-dbAAs could activate mTORC1 signalling.

4. DISCUSSION AND PERSPECTIVES

4.1. Further discussion of the natural history on nephropathic cystinosis in the mouse model

Although symptoms are less severe than in human patients, congenic C57BL/6 cystinosin knockout mice essentially reproduce the kidney structural phenotype of nephropathic cystinosis, eventually leading to end-stage renal disease (ESRD).(Nevo et al. 2010) In contrast to untreated cystinotic children, glomerular ultra-structure is however preserved in *Ctns* knockout mice up to 9 months, thus offering a pure model of tubulopathy. As the first part of my Result Section attempts to show, this first available in *vivo* model allows to better define, from their initiation, the pathogenic time-course of nephropathic cystinosis and several adaptation mechanisms in proximal tubular cells (PTCs).

4.1.1. Signification of sequential lag phase then formation of amorphous inclusions

We have shown that structural changes in the nephron follow a longitudinal progression in which tubular lesions first appear at the glomerulo-tubular junction and then extend distally into the proximal tube leading to the typical swan-neck deformities, first described in cystinotic children as “early” lesion.(Mahoney and Striker 2000) However, the mouse model allowed to define an *earlier* sequence of PTC changes.

In the absence of cystinosin, there is first an initial silent ("lag") phase (up to ~ 3 months) before cystine starts accumulating significantly in lysosomes of the most proximal cells, forming amorphous lysosomal inclusions, indicating accumulation of undigested proteins (3-6 months). Such inclusions are also found in cystinotic blood neutrophils which are much more short-lived (a few days).(Schulman, Bradley, and Seegmiller 1969) Since net cystine accumulation is the difference between production and elimination, this difference in kinetics with a lasting lag phase in PTCs could (i) either result from a much higher rate of endocytosis of disulfide-rich proteins as cystine source in neutrophils than PTCs, which is most likely not the case since these cells are rather specialized for phagocytosis; or (ii) , since PTCs harbor a huge recycling apparatus (DATs) thus enjoy a most effective exocytosis route, the lag phase would indicate that rate of cystine production during the first months of life is almost equivalent to the rate of vesicular discharge, an explanation favored by my laboratory. Indeed, a huge cystine exocytosis in cystinotic fibroblasts has been elegantly demonstrated by Thoene and Lemons 1982 . Comparing measurements of degradation of internalized radiolabeled albumin and cystine accumulation, these authors calculated that only 1% of cystine generated by the hydrolysis of albumin was actually retained in cultured cystinotic fibroblasts, i.e. deprived of a lysosomal cystine transporter. In this acute assay, this difference suggested that 99% was disposed of by an alternative, vesicular exodus. In the *in vivo* situation during the latent phase of first months of life, i.e. when the endocytic machinery is still presumably intact, we could also estimate that 5-to-10 fold more cystine was generated from albumin endocytosis than cystine accumulation in cystinotic PTCs.(Gaide Chevronnay et al. 2014; Cherqui and Courtoy 2017) Although the latter conclusion seems reasonably solid, it remains a rough estimate as normal albumin uptake into PTCs had been deduced from its urinary loss in megalin and

cubilin KO mice; and because it ignores the additional contribution of cystine input from other LMWP proteins (1 disulfide bridge in the 14kDa beta2-microglobulin and 2 disulfides in the immunoglobulin light chain or Bence Jones protein, compared to 17 disulfides in the 67 kDa albumin).

Vesicular cystine efflux into urine might actually represent a remarkable example of spontaneous by-pass of cystinosin absence. Normally, cystinosin allows newly generated cystine to directly egress lysosomes into the cytosol where it is reduced by glutathione into cysteine, its recycled by-product. If cystine is instead secreted into the urine by recycling tubules, it should be recaptured by PTCs via the heterodimeric rBAT-b(0,+)AT apical cystine transporter (Ahmed, Dasgupta, and Khan 2006), thus also reach the cytosol and be likewise reusable if glutathione pool is preserved. Although this indirect mechanism of access to the cytosol is difficult to demonstrate, it would readily explain why cystine urinary levels are low in cystinosis, much lower than in cystinuria, when the rBAT–b(0,+)AT transporter is defective.

If a minimal cystine retention efficacy is the rule in cultured cystinotic cells and the silent phase in *Ctns*$^{-/-}$ kidneys *in vivo*, what could cause further acceleration of retention as documented by the exponential accumulation in cystinotic kidneys at later stages, even before crystals would be detected as a "concentrated, osmotically neutral storage form"?(Nevo et al. 2010) A tentative explanation is secondary uncoupling of lysosomes from the recycling pathway. Lysosomes normally actively exchange their content between themselves (homotypic fusion and fission to randomize hydrolytic equipment and digestive load, as illustrated in Figure 23, upper panel), as well as with incoming late endosomes to form hybrid organelles and - at this stage? - with the recycling pathway.

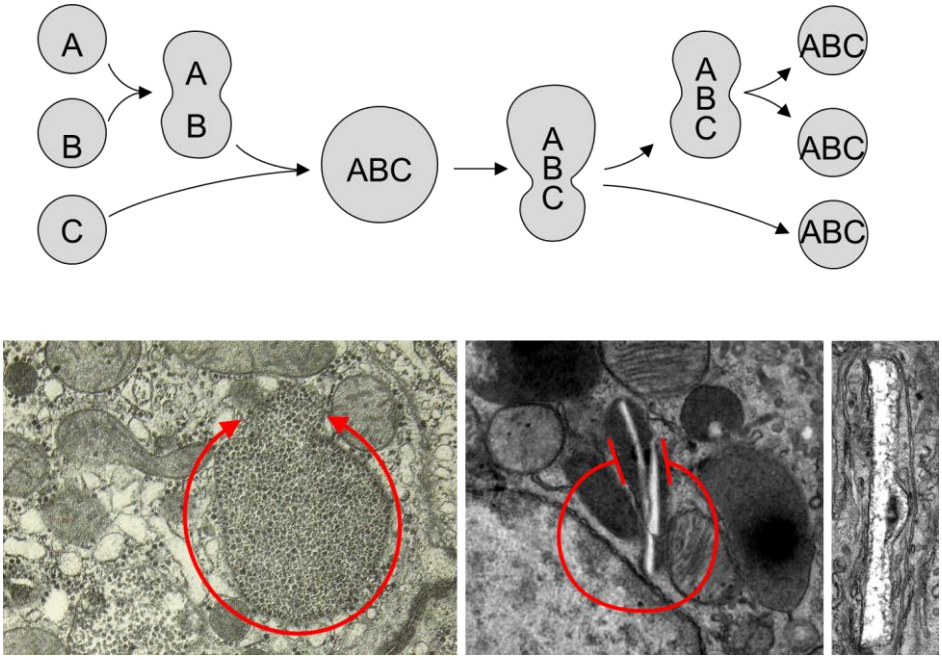

Figure 23. Normal fusion-fission dynamics in normal lysosomes or lysosomes overladed by flexible, segmentable content contrasts with late lysosomal distorsion by rigid cystine crystals which prevents fission, thus load sharing. The upper panel symbolizes homeostatic dynamics of lysosomes by continuous fusion and fission. At lower left, this dynamic is preserved in glycogenosis, because glycogen particles can be distributed upon fission (double arrowed circle). At lower right, fission is blocked when long cystine crystals develop (double-blocked circle). *From de Duve (upper panel); ICP booklet (lower left; red symbol was added); and data collected for Gaide Chevronnay et al, 2014 (lower center and right).*

However, overloaded lysosomes, e.g. upon accumulation of undigested proteins, eventually escape this vesicular fusion-fission turmoil, and evolve into residual bodies. These are still accessible to incoming vesicles (as they can be labeled by peroxidase uptake) but do no longer connect with the recycling machinery. At this stage, cystine vesicular exodus would vanish, interrupting the early “Echternach procession” by which disulfide proteins come in and are rapidly degraded with cystine generation, immediately followed by most cystine exodus. Dynamics of the whole endocytic apparatus is characterized by maturation from endosomes to lysosomes, defined in molecular terms by change in members of Rab catalyst family and fusion partners. In this view, secondary lysosomes would evolve to senescence, e.g. due to lesser and lesser Rab7 recruitment, so that the rate of vesicular exchange decreases and efflux vanishes. This view is consistent with recent reports describing endolysosomal changes in cultured cystinotic cells, when lysosomes enlarge and move from the periphery where most rapid fusion events take place to a perinuclear location.(Ivanova et al. 2015; Festa et al. 2018)

A recent comparison at the anatomical level also revealed that cystine accumulation apparently occurs more slowly in kidneys than in bones.(Battafarano et al. 2019) However, this could possibly be explained by their respective histology. Indeed, PTCs forming lengthy tubes, distal cells could be protected by initial accumulation in most proximal ones, until sequential disease extension, whereas bone cells act in parallel units with coupled osteogenesis and osteclastic resorption.

4.1.2. **On cystine crystals**

In cystinotic PTCs, amorphous lysosomal inclusions are followed by crystals, first detected around 6 months as tiny needles, then polyhedric structures that slowly aggregate into huge vacuoles (Fig. 24).

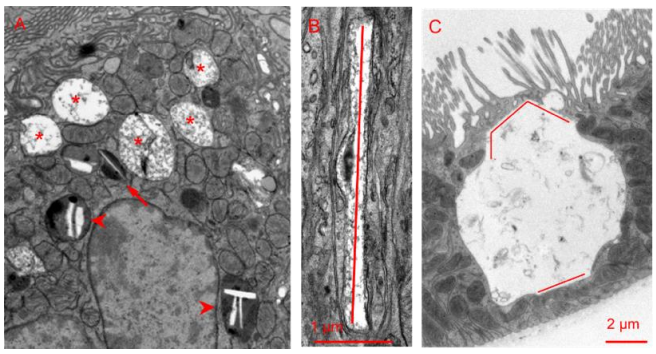

Figure 24. In PTCs, cystine crystals are heterogeneous and build-up slowly. Electron micrographs of the progression of lysosomal changes in *Ctns*$^{-/-}$ PTCs. Asterisks at A indicate amorphous lysosomal swelling. Notice progression from tiny needles (arrow and arrowheads A), to long linear lysosome distorsions (B) up to huge single vacuolar aggregates bulging into the PT lumen (C). Peripheral lines in the huge vacuole at C stress angular constraints on the limiting membrane. *From data collected for Gaide Chevronnay et al, 2014*.

In contrast to long-lived PTCs and bone marrow macrophages, the short-lived cystinotic neutrophils do not harbor crystals despite the fact that their estimated lysosomal cystine concentration exceeds the insolubility threshold at acidic pH (5 mM), suggesting that accumulation of undigested proteins in the same compartment could delay crystallization in these cells, as opposed to pure cystine solutions. The delay between lysosomal cystine accumulation in PTCs and crystal appearance also contrasts with the fast crystallization of pure cystine solutions at acidic pH and may be due to the same mechanism (Fig. 25).

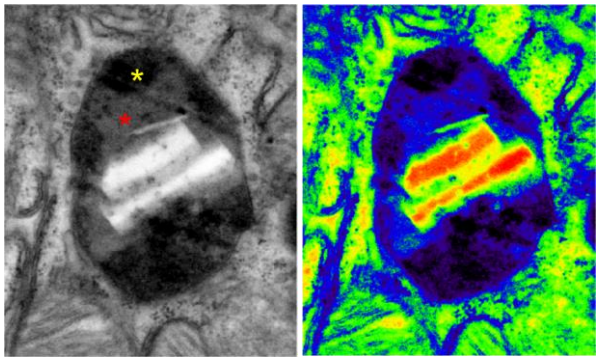

Figure 25. Crystallization is impaired in heterogeneous media. Electron micrograph showing aggregation of short crystals in a secondary lysosome. The lysosomal matrix of a dense body normally appears in black (yellow asterisk). Notice a well-defined intermediate zone between lysosomal matrix and crystals (red asterisk). This intermediate *gray* zone is tentatively interpreted as *partial* protein exclusion by cystine, yet without crystal, thus reflecting cystine supersaturation in a protein-rich matrix. Heterogeneity of lysosomal matrix is better appreciated with pseudo-colors at right.

Of note, this slow crystallization of slowly accruing cystine within a highly protein-loaded lysosomal lumen contrasts with the acute situation of phagocytosis of preformed crystals, which was shown to trigger the inflammasome in peripheral blood mononuclear cells.(Prencipe et al, 2014) Whereas this situation is clearly relevant to the abundant cystinotic macrophages infiltrating cystinotic kidneys, and even (to some extent) infiltrating transplanted WT kidneys, it remains to be shown that crystals slowly accruing in PTCs also, or to the same extent, impact on the inflammasome in the latter cells. The aggregation of crystals into a single huge apical vacuole, bulging into the lumen under a frequently partially preserved brush border, can be easily explained if longitudinal crystals prevent lysosomal fission, a requirement to maintain a large number of small lysosomes (Fig. 23, lower right). Luminal bulging could be viewed as favoring apical exocytosis with luminal crystal discharge, as could indeed be

demonstrated by immunofluorescence, with images showing continuity between the LAMP-1-labeled lysosomal membrane and apical plasma membrane markers (see Fig. 3F of Gaide Chevonnay et al, 2014 forming the basis of Results Chapter I). Crystals are eventually followed by structural apical changes such as loss of the brush border and PTC atrophy.

4.1.3. **On apical dedifferentiation**

We (Gaide Chevronnay et al. 2014) then others (Raggi et al. 2014) also observed, starting after 3 months, a progressive loss of expression of megalin, cubilin, SGLT2 and NaPi-IIa, indicating that PTCs enter a process of global apical dedifferentiation before the appearance of crystals, and explaining that the Fanconi syndrome is earlier than cystine crystals or atrophy itself. PTC differentiation depends on a transcriptional regulatory network involving, a.o, the repressor ZONAB and the activator HNF-1.

As previously shown by my laboratory, the transcription factor zonula occludens 1 (ZO-1)–associated nucleic acid binding protein (ZONAB) shuttles between tight junctions, where it is normally sequestered, and the nucleus, where it impacts on the complex transcriptional network that regulate the switch between proliferation (stimulated) and differentiation (repressed).(Lima et al. 2010) An attractive model, recently put forward by Devuyst, Festa and co-workers (Festa et al. 2018), proposes that the apical functional defect, related to increased dedifferentiation, is linked to a loss of integrity of tight junctions causing nuclear translocation of ZONAB. Indeed, lysosomal dysfunctions lead to defective autophagy-mediated clearance of damaged mitochondria related to the well-known oxidative stress in cystinotic PTCs. Oxidative stress then induces a Src-

dependent signaling pathway causing ZONAB release. Conversely, anti-oxydants and inhibition of ZONAB signaling rescue the epithelial function, leading the authors to speculate these could be new therapeutic targets for lysosomal storage disorders such as cystinosis. In the last author's view, ROS accumulate because damaged mitochondria sequestered by autophagosomes fail to fuse with lysosomes (Luciani, personal communication) yet continue to release ROS. However, ROS production requires mitochondrial activity supported by fuel supply. Pyruvate produced by glycolysis and acetyl-CoA generated from beta-oxidation of fatty acids require transporters into mitochondria. Whether they can also cross the *de novo* formed autophagosome-limiting membrane remains to be examined.

Hepatocyte nuclear factor 1α (HNF1α) is another key transcriptional factor, that instead favors PTC differentiation and in particular promotes megalin expression. Indeed, *Hnf1α*-KO mice exhibit low-molecular-weight proteinuria and decreased uptake of iodinated β2-microglobulin.(Terryn et al. 2016) Whether HNF1α signaling is impaired in cystinotic PTCs remains to be explored.

Whatever its mechanism, dedifferentiation of most proximal PTCs suppresses receptor-mediated endocytosis in these cells, thus transfers the load of disulfide-rich proteins to more distal ones, causing longitudinal disease extension up to S3. This segment is normally silent for protein endocytosis.(Schuh et al. 2018) Transfer to protein ligands into S3 *Ctns*$^{-/-}$ PTCs was documented by autoradiography in Figure 6B of Gaide Chevronnay et al. 2014 (Results Chapter I). Of note, progressive *secondary* loss of expression of endocytic receptors can be viewed as an adaptative mechanism as it minimizes the workload of suffering cells. It should not be confused with full *primary* genetic megalin ablation in the perinatal period, used as an experimental artefact in Chapter II of Results, to examine the role of the megalin pathway in the generation of lysosomal cystine.

4.1.4. **On lysosomal adaptation mechanisms**

In response to cystine overload or crystal deposition, we indeed highlighted three additional adaptation mechanisms. Firstly, in living cells, the huge lysosomes deformed by crystals can discharge their content in lumen by apical membrane fusion, as evidenced by the resulting continuity of labeling between LAMP-1 and cell surface markers, and is not a real surprise considering that lysosome exocytosis can correct patchy defects in the plasma membrane. Secondly, upon cell death, luminal shedding is an alternative way to eliminate crystals. Of note, shedding does not lead to the interstitium, since this route is barred by the tubular basement membrane, normally quite rigid and furthermore thicker in cystinosis. And thirdly, to compensate the cellular loss, we showed increased PTC proliferation that correlates with increased apoptosis in a coupled functional mechanism. In addition to ensuring epithelial continuity, proliferation provides fresh lysosomes, synthesized during cell division, that may partially slow the cystinosis progression.

4.1.5. **Tentative reinterpretation of swan-necks: the sliding metaplasia hypothesis**

In swan-neck deformities, the typical lesions in cystinosis, residual proximal tubule-lining cells, thus still named “PTCs” *by topography but not by structure or function*, are extremely flat, without organelle and any crystal.(Mahoney and Striker, 2000) Their classical view suggests that this “tubular” atrophy is the ultimate consequence of cystine-crystal induced “degeneration processes” of cystinotic PTCs. However, the flattened epithelium in the first tubular space at the

glomerulo-tubular junction more closely resembles that of Bowman's capsule and their border is even indistinguishable. Another explanation for swan-neck lesions could thus be a metaplasia by extension from Bowman's squamous epithelium into the segment S1. This hypothesis is supported by the similarity of very thick basement membrane surrounding swan-neck lesion and Bowman's capsule (our unpublished results). Unfortunately, there is no tool (such as specific antibodies against Bowman's capsule cells) that would allow to easily testing this hypothesis. An alternative is cell fate mapping upon tag expression in glomerular parietal cells. The position of the "neck" of the glomerulo-tubular junction itself is somehow preserved and its later closure increases pressure in the urinary space, eventually leading to glomerulo-tubular disconnection, evidenced by enlarged, atubular glomeruli.(Larsen, Walker, and Thoene 2010)

4.2. Mechanisms of cystine accumulation and its role in pathophysiology

4.2.1. Vesicular cystine supply into PTCs: receptor-mediated *vs* fluid-phase endocytosis

Although attention has so far focused on apical receptor-mediated endocytosis of disulfide-rich proteins as source of cystine upon proteolysis, all cells also capture AAs by a content-undiscriminant mechanism named fluid-phase endocytosis (Fig. 26). This phenomenon has initially been demonstrated by identical uptake of L- and D-alanine and PVP (Thoene, Forster, and Lloyd 1985) thus necessarily predicted for all amino-acids including plasma and urine cystine.

It was thus necessary to envisage whether pinocytosis of free cystine into PTCs could possibly contribute to its accumulation in lysosomes.

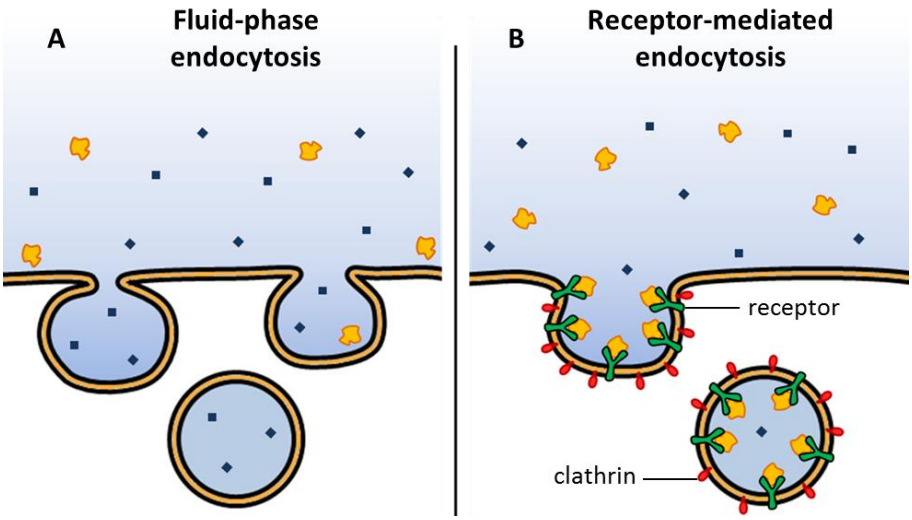

Figure 26. Comparison of efficacy between fluid-phase endocytosis and receptor-mediated endocytosis. A. Fluid-phase endocytosis captures extracellular constituents in proportion of their extracellular concentration (blue squares). B. Endocytic receptors concentrate extracellular ligands (orange "birds"). Hence, cells should achieve comparable fluid-phase uptake of free cystine occurring at 40 µM as when concentrating 100-fold by RME albumin if presented at 24 nM [24 nM multiplied by 100 (concentration factor) x 17 (number of disulfide as cystine precursor per albumin molecule = 40.000 nM)]. For more elaboration on very rough estimates, see footnote 3.

A priori, this explanation did not seem attractive, since the efficiency of receptor-mediated endocytosis into PTCs is between 2 and 3 orders of magnitude higher than fluid-phase endocytosis, as shown in Figure 27.(Lima et al. 2010) However, calculations[3] based on available measurements or reasonable estimates indicate that the much higher concentration of free over protein-bound cystine in the primary ultrafiltrate (~ >2 orders of magnitude higher) may balance the much lower efficiency of fluid-phase versus receptor-mediated endocytosis (~ >2 orders of magnitude lower).(Christensen and Maunsbach 1979; Schiller and Taugner 1980) The contribution of fluid-phase endocytosis to free cystine supply (Thoene, Forster, and Lloyd 1985) into normal PTCs should thus not be a *priori* neglected.

[3] Albumin permselectivity rate in man (35 microg/min in man: Mogensen and Soelling, Scand J Clin Lab Invest, 1977) can be translated into 1.6 nM albumin or 30 nM albumin-bound "cystine" (17 disulfide bonds/albumin molecule) in the primary ultrafiltrate presented to receptor-mediated endocytosis. Of note, this is an underestimate as it ignores disulfide bridges carried by the more readily ultrafiltrated low-molecular weight proteins. Let us assume equivalent protein-bound cystine supply by LMWP being more abundant, yet with 3-times lower intrinsic abundance of disulfide bonds (albumin, 68 kDa, 17 S-S; Ig light chain, 24 kDa, 2 S-S; beta2-microglobulin, 14 kDa, 1 S-S). This would bring our estimate to *60 nM LMW "protein-bound cystine"*. This estimate value would seem negligible be compared with *40 microM free cystine* in plasma thus primary ultrafiltrate cystine, presented to fluid-phase endocytosis! However, the outstanding efficiency of the abundant cystine transporter rBAT-b(0,+)AT along the entire brush border should strongly decrease free cystine content reaching primary endocytic pits at the base of the brush border. Arguably, if final free cystine concentration would drop down to 6 microM when entering endocytic pits and assuming that receptor-mediated endocytosis is 100-fold more effective than fluid-phase pinocytosis, both processes would contribute equally. As shown by Fig. 27, my laboratory determined that, in well-polarized kidney proximal tubular cells in culture, receptor-mediated endocytosis was indeed about 100-fold more efficient than fluid-phase endocytosis, and higher efficiency might even be expected *in vivo*. Altogether, in view of all uncertainties behind each assumption, the question as to whether receptor-mediated endocytosis *vs* fluid-hase pinocytosis is the main endocytic source of cystine to PTCs thus remains open. Yet, since megalin drives also the formation of endocytic pits, thus fluid-phase endocytosis, the key role of the megalin pathway as source of PTC cystine endocytosis remains a valid conclusion.

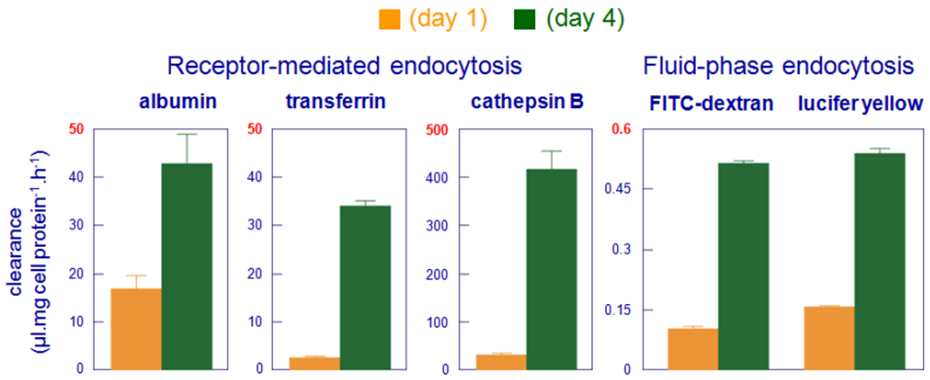

Figure 27. Quantitative comparison of clearance efficiency by fluid-phase *vs* receptor-mediated endocytosis in cultured PTC cells and effect of polarity on endocytic activity. At day 1 after plating OK cells at high density in Petri dishes (low trans-epithelial resistance) or day 4 after plating (maximal transepithelial resistance), dishes were washed then incubated for 1 h at 37°C in medium without serum and supplemented with 150 nM ^{125}I-albumin, 150 nM ^{125}I-transferrin or 1.8 nM ^{125}I-cathepsin B to study receptor-mediated endocytosis; together with 100 µM FITC-dextran (10 kDa) or 4 mM Lucifer yellow, to assess fluid-phase endocytosis. Intracellular accumulation is expressed in clearance units (values are means ± s.e.m of n=3 or 4). Please note difference of scale in the ordinates. The following conclusions were derived: (i) almost identical values for the two fluid-phase tracers indicate validity of the estimation of fluid-phase activity (non-discriminant); (ii) one-log difference in the clearance of albumin and transferrin *viz* cathepsin B underlines that efficacy of receptor-mediated endocytosis depends on intrinsic ligand affinity, or reflect a partial saturation at 150 nM albumin and transferrin; (iii) the lower value for transferrin (a cubilin ligand) as compared to albumin (a shared megalin+cubilin ligand) at 1 day may reflect slower maturation of cubilin than megalin; (iv) overall, efficiency of receptor-mediated endocytosis is between 2 (albumin) and 3 orders of magnitude (cathepsin B) higher than fluid-phase endocytosis. *Unpublished data by W.R. Lima & P.J. Courtoy. Reproduced from PhD thesis of Dr Lima, 2010. For details on methodology, see Lima et al, JASN, 2010.*

Moreover, whereas we reported that megalin ablation, to abrogate receptor-mediated endocytosis, provided spectacular protection to cystinotic kidneys, this ablation also causes, by unknown mechanism, a marked atrophy of the apical endocytic apparatus and impairment of fluid-phase endocytosis.(Bachmann et al. 2004) Pinocytosis being also impaired in our double knockout model, our experiments on megalin ablation cannot formally distinguish between a direct effect of suppression of receptor-mediated endocytic reuptake of disulfide-rich plasma proteins (highly effective mechanism for ligands present at low concentration) *versus* indirect effect of the likely decreased fluid-phase pinocytosis of all solutes including free cystine (a much less efficient mechanism but quantitatively relevant at the much higher concentration of cystine in plasma and primary ultrafiltrate). We therefore moved to the terminology “megalin pathway” to cover both mechanisms as far as they depend on megalin. The respective role of receptor-mediated *vs* fluid-phase endocytosis could however be addressed by competition, as discussed below.

4.2.2. **Net cystine accumulation in cystinotic lysosomes: vesicular inflow vs vesicular exodus**

As stated above, cystine accumulation in cystinotic fibroblasts is proportional to the extracellular concentration of albumin but after lysosomal degradation, only a small fraction of free cystine is retained in cystinotic lysosomes, the difference being attributed to cystine exocytosis.(Thoene and Lemons 1980) Lysosomal exocytosis is a Ca^{2+}-regulated process in which lysosomes reach the cell surface to fuse with the plasma membrane and release their content outside the cell. In cystinotic fibroblasts and the early stages of PTCs, this output pathway is

considered as a relatively effective mechanism of delaying lysosomal cystine overload (long regarded as the primary cause of cell damage).

Almost absent in urine, albumin, the major ultrafiltrated protein containing 17 disulfide bonds and therefore as many released cystine molecules, is expected to be virtually completely reabsorbed in proximal tubule. In PTCs from *Ctns*$^{-/-}$ mice, it has been estimated that receptor-mediated endocytosis of ultrafiltrated plasma proteins represents a cystine supply more than sufficient for PTC accumulation and actually exceeds the amount being stored.(Cherqui and Courtoy 2017) This suggests that, also in PTCs, cystine can be efficiently discharged by vesicular efflux (exocytosis). Accordingly, from a cell biological perspective, blocking megalin-mediated endocytosis as well as promoting clearance mechanisms such as vesicular exocytosis are both interesting pathways to slow down cystine accumulation in PTCs.

4.2.3. **Regulation of vesicular exodus**

In *Ctns*$^{-/-}$ cells, TFEB expression is reduced while its nuclear translocation is promoted by structural abnormalities of lysosomes because of the cystinosin defect.(Rega et al. 2016) Decreased expression in cystinosis is unexplained as TFEB system is normally activated by the lysosomal swelling itself, such as accumulation of undigestible sucrose! Moreover, the observed decrease of TFEB expression in cystinotic cells despite lysosomal enlargement is paradoxical as this transcription factor induces its own expression. A possible explanation lies in defective mTORC1 signalling in the absence of cystinosin.(Andrzejewska et al. 2016) Once dephosphorylated, TFEB normally activates the transcription of genes involved in cellular clearance, such as lysosomal biogenesis and autophagy but also

exocytosis. Indeed, lysosomal exocytosis is regulated by TFEB which activates MCOLN1 and thus leads to increased local cytosolic Ca^{2+}, resulting in lysosomal translocation and membrane fusion. TFEB activation is thus another possible target to amplify cellular clearance in cystinosis as in other lysosomal storage diseases.(Medina et al. 2011) Indeed, clearance of cystine load, and probably correction of other lysosomal defects resulting from cystinosis, could be triggered by restoring TFEB activity. Of great interest, TFEB can be stimulated in cultured cells by genistein.(Rega et al. 2016)

Additional key effectors of exocytosis are Rab proteins, a family of small GTPases which act at specific levels in the cell to control vesicular trafficking, in particular Rab27a and its receptors. In fibroblasts from *Ctns*$^{-/-}$ mice, Rab27a is downregulated, possibly because of TFEB dysfunction, lysosomal trafficking is impaired and ER stress is upregulated. However, upregulation of Rab27a in these cells rescues lysosomal transport leading to increased cystine exocytosis and decreased cystine accumulation and thus contributes to correct ER stress.(Johnson et al. 2013) Another Rab protein, Rab11, is involved in vesicular trafficking regulating exocytosis and recycling vesicles at the plasma membrane.(Takahashi et al. 2012) In a human-derived cystinotic PTC line, expression of LAMP2A, the receptor for chaperone-mediated autophagy (CMA), is decreased. Furthermore, LAMP2A accumulates on Rab11-coated vesicles leading to CMA defects. It has been demonstrated that treatment with CMA enhancers corrects Rab11 trafficking, defective in this cell line, allowing Rab11 to re-localize LAMP2A to the lysosomal membrane. Since Rab11 is also involved in megalin localization and recycling, these data suggest that Rab11 defect in cystinosis is a link between CMA impairment and dedifferentiation program which characterizes cystinotic PTCs. In cystinosis, CMA upregulation thus could protect from Fanconi syndrome independently of lysosomal overload.(Zhang et al. 2019)

4.2.4. **Signification of impaired proteolysis**

Amorphous lysosomal content of cystinotic lysosomes in neutrophils and PTCs at an early stage of the disease results from protein accumulation due to impaired proteolysis, as demonstrated in primary PTC cultures from cystinotic mice (Raggi et al. 2014) and in human cystinotic cells.(Ivanova et al. 2015) The extracellular compartment provides an oxidative environment (thus preservation of disulfide bonds). In contrast, in the reducing environment of normal lysosomes, upon capture of cysteine from the cytosol into these organelles by a still unknown mechanism, accumulating cysteine can reduce disulfide bonds. This leads to protein unfolding providing access to lysosomal endoproteases. Moreover, several cathepsins are only active in a reducing environment. For example, the cysteine (or thiol) protease, cathepsin B, contains a free thiol in its catalytic site which is protected by the reducing lysosomal lumen. Conversely, in the absence of cystinosin, cystine accumulates in lysosomes thus should prevent protein unfolding and cause oxidation of cysteine in thiol-proteases, thus their inactivation. Finally, impaired exposure of the internal peptide bond between pro- and mature enzyme in pro-cathepsins would prevent their maturation, thus activity. Impaired activation of pro-cathepsin D has been demonstrated in cystinotic cells, although the authors attributed this observation to impaired endolysosomal trafficking.(Raggi et al, 2014) Amazingly, impaired proteolysis should also slow down free cystine generation.

Defective proteolysis, the primary function of lysosomes, translates into decreased release of free amino acids and should thus lead to the inhibition of mTORC1, overcoming its expected activation by lysosomal enlargement. Therefore, TFEB should be dephosphorylated and translocated to the nucleus where it normally activates its own transcription as well as transcription of genes

promoting autophagy. However, as stated above, TFEB level and autophagy are decreased in cystinotic cells. TFEB is not known to impact on apical differentiation.

4.2.5. **Role of cystine accumulation *vs* non-transport cystinosin function(s)**

4.2.5.1 Evidence for non-transport function of cystinosin

We so far discussed the causes and consequences of lysosomal cystine accumulation. However, the concept that cystine accumulation is the starting point for all cellular and functional alterations in cystinosis is no longer accepted. Indeed, cysteamine treatment, which effectively purges lysosomal overload, does not cure cystinosis. Several other cellular defects in cystinotic cells such as lysosome enlargement and mispositioning are also not corrected by cysteamine. Thus, the absence of cystinosin itself is now recognized as responsible for cellular disturbances that are refractory to the cystine depletion by cysteamine, highlighting its non-transport function. Interestingly, Dr. Antignac's group has shown, *in vitro*, that the fifth loop of cystinosin interacts with the v-ATPase-Ragulator-Rags complex, essential components of the mTORC1 signaling pathway, and that mTORC1 response to changes in AA supply are damped in cystinotic cells. Cystinosin should thus be considered a component of LYNUS machinery and is essential for mTORC1 localization and regulation by nutrients.(Andrzejewska et al. 2016) That transport-independent function of cystinosin is abolished in the absence of the protein, as in the 57kb large deletion in the cystinosin locus, or upon mutations causing a premature stop codon or protein instability is easy to understand. However, there are point mutations compatible with expression of full cystinosin, yet inactive as transporter. These subtle mutations would suggest

that the so-called “transport-independent” function would affect sensing of transport in the LYNUS machinery.

4.2.5.2 Role of non-transport functions of cystinosin in cystinosis progression

Thus, the key question arises on the respective responsibility of cystine accumulation *vs* transport-independent function of cystinosin. Most likely both contribute, since early compliant cysteamine efficiently delays most cystinosis complications and extends average life expectancy by more than one decade, but is ineffective on the Fanconi syndrome. In the laboratory, the current way to distinguish transport-independent functions is to look for resistance to cystine accumulation upon downstream cysteamine purging. We took another approach by looking upstream, based on preventing cystine supply by suppression of the megalin pathway as we shall now discuss.

4.3. Cystine accumulation in PTCs depends on apical endocytosis. Suppression of apical endocytosis protects kidneys against swan-neck lesions

While the genetic and molecular bases of lysosomal overload are well known, the source of cystine accumulation in cystinotic kidneys had not yet been established. We thus hypothesized that the main source of cystine in PTCs originated from the endocytosis of disulfide-rich proteins, with megalin as key transporter. Therefore, I generated a new “double KO-triple transgenic” mouse model in which the two floxed megalin alleles were specifically excised in the kidney of cystinotic mice by a single copy of *Wnt4*-driven Cre-recombinase. This ablation worked exceedingly well (Fig. 1 from Janssens et al, 2019). I then

demonstrated that abrogation of the megalin pathway in cystinotic PTCs prevented cystine accumulation, thus crystal deposition. Except for some grossly remodeled areas due to a not yet fully understood inflammatory reaction related to *Wnt4*-CRE-driven megalin excision, the structure of proximal tubules in double knockout kidneys was preserved, i.e. without PTC dedifferentiation. In contrast to cystinotic mice where almost all glomerulo-tubular junctions exhibited a typical swan-neck profile, I showed that double KO kidneys contain only 20% of such lesions. This low percentage of residual lesions could be attributed to the loss of non-transport functions of cystinosin or to possible effects related to suppressed endocytic supply. For example, absence of potential nephroprotective proteins such as iron siderophore neutrophil gelatinase-associated lipocalin (NGAL) (Mori et al. 2005) or survivin (Jobst-Schwan et al. 2013) could be critical for PTCs homeostasis. We also showed that megalin ablation in cystinotic kidneys preserved the apical expression of NaPi-IIa and SGLT-2 in PTCs. Because of the loss of Fanconi syndrome phenotype in our *Ctns*$^{-/-}$ colony, urinalysis was not relevant but immunofluorescence and RT-qPCR results suggested that the megalin pathway inactivation also protects against the Fanconi syndrome of nephropathic cystinosis which makes it a potential therapeutic target. Moreover, apoptosis and proliferation rates were normal in double knockout kidneys, reflecting the absence of PTC turn-over. We thus concluded that the megalin pathway is the major route leading to lysosomal cystine overload, and that suppression of this pathway preserves cystinotic kidneys.

4.4. The megalin pathway could be targeted by oral supplementation with dibasic amino-acids

Despite remarkably slowing down progression of nephropathic cystinosis and reducing the frequency of other organ failures (Emma et al, NDT 2014), cysteamine does not provide a cure. Several investigators are thus actively looking at alternative drugs: either targeting specific defects such as free radical effects (Galaretta et al, 2015; Festa et al, 2018), TFEB via genistein (Rega et al. 2016), or CMA via CMA enhancers (Zhang et al. 2019); or using a non-biased screening approach.(Bellomo et al. 2017) Could the megalin pathway represent a novel target in cystinosis? In view of its major health issue of antibiotic nephrotoxicity, various laboratories have attempted to block PTC reuptake of gentamicin, which depends on megalin. Early attempts to compete by lysine for gentamicin uptake in rat kidneys failed due to toxicity related to high doses required.(Gilbert et al. 1982) In the frame of the european network, EuReGene, the group of Thomas Willnow then developed a patent to screen using Biacore polypeptides that could achieve this goal, but none went to the market, presumably because competitors were also accumulating in lysosomes and became toxic themselves.(Willnow, personal communication) However, low-molecular weight compounds have been recently shown to protect the kidney against massive reuptake of nephrotoxic molecules via megalin interference.(Hori et al, 2017) Despite the failure of lysine to protect kidneys from gentamicin nephrotoxicity, we thought of using dibasic amino-acids as megalin competitors for protein uptake, since lysine and arginine are essential in the protein-binding pockets of megalin and cubilin.(Andersen and Moestrup, 2014) Moreover, whereas it is indeed obviously more difficult to block the 60-to-100 gentamicin binding sites on each megalin molecule, it could be more feasible for its few protein binding sites which presumably depend on

multiple interactions.(Nagai and Takano, 2004) Furthermore, oral administration of dibasic amino acids is already used therapeutically (Peltola et al. 2000; Elpeleg and Korman 2001) and body-builders also often use basic amino acids (mostly arginine) to improve their muscular appearance and performance. Dibasic amino acids have shown the ability to inhibit megalin pathway in cultured epithelial cells (Barone et al, 2005; Thelle et al, 2006) and, *in vivo,* upon acute (max 30 h) lysine gavage to rats.(Thelle et al. 2006) In a preliminary study, I showed that 5x- oral supplementation with lysine or arginine in the drinking water during two-weeks was well tolerated by WT mice and that arginine induced a dose-dependent LMW proteinuria (lysine remains to be tested for this effect). I also showed that dbAA supplementation as solid diet can block endocytic recapture of injected fluorescent protein tracer by WT PTCs if mice were adapted to inverted daylight so as to eat during the day period of acute challenge by injected fluorescent protein tracer. I then moved to long-term study with solid diet supplementation in cystinotic mice. My preliminary results, to be complemented by a large-cohort study at UCSD (ongoing analysis, see below), indicate that the bAA-enriched diet protects cystinotic kidneys function (highly significant) and prevents structural lesions such as swan-neck deformities and PTC atrophy (significant). Of note, although these results were encouraging, I was not able to explore the Fanconi syndrome in our colony, which lost this phenotype presumably because of inbreeding. Therefore, before firmly concluding that dietary supplementation by arginine, and especially lysine, significantly decreases cystine accumulation and protects from Fanconi syndrome, we must wait for the results of the large cohort studied by our UCSD collaborators, who will be further interested in potential muscular benefits. This perspective is developed in details later.

4.5. Translational perspective: a new, dietary therapy for nephropathic cystinosis?

Data collected so far in the mouse model of cystinosis thus indicate that receptor-mediated endocytosis is a major pathway leading to cystine accumulation in kidney proximal tubules, which itself causes structural and functional alterations. Conversely, preliminary results also suggest that inhibition of this pathway by dbAAs might be beneficial to prevent kidney cystine accumulation and protect kidneys against swan-neck lesions. Assuming that the ongoing analysis of large mouse cohorts confirms the benefit of dietary supplementation by well-tolerated dibasic amino-acids, translational studies to cystinotic patients should thus be considered and even turn as a moral obligation. Indeed, long-term supplementation of patients by arginine, for metabolic deficits along the urea cycle, and by lysine, for patients with ornithinemia, underlines the acceptance and safety of this approach. A dbAA-supplemented diet would also be a flexible and very inexpensive adjuvant approach, complementary to cysteamine as current gold standard.

However, a full picture of such long-term therapy is largely missing. As stated above, *acute* competition for protein uptake has been demonstrated *in vivo* by high doses of lysine, arginine and related compounds in healthy human “volunteers” (Mogensen and Solling 1977) and by oral lysine gavage in WT mice (Thelle et al. 2006), as well as *in vitro* using purified brush border preparations (Ottosen et al. 1985) and most elegantly by the ongoing study of competition by lysine or arginine for binding of equimolar concentrations (as low as 1 microM) of pure fatty-acid-free albumin on chip-immobilized megalin and cubilin using surface plasmon resonance (Fig. 28, Moestrup and Graversen, personal communication). These very promising preliminary data indicate that both dbAAs,

used alone at clinically relevant concentrations, are direct competitive inhibitors of the binding of albumin to both immobilized megalin and cubilin, L-lysine seeming more potent than L-arginine. Since both megalin and cubilin act in tandem for receptor-mediated endocytosis of ultrafiltrated albumin by kidney proximal tubular cells (PTCs), these promising data further predict an *in vivo* synergistic effect of L-lysine, and to a lesser extent of L-arginine, to inhibit albumin uptake into PTCs, thus cystine generation therefrom. Incidentally, the observed micromolar competition in this assay is in sharp contrast with millimolar range of lysine and submillimolar range of arginine plasma thus primary urine levels. Thus dbAAs qualify as *upstream substrate depletion mechanism*, *possibly complementary to cysteamine, as downstream substrate depletion.*

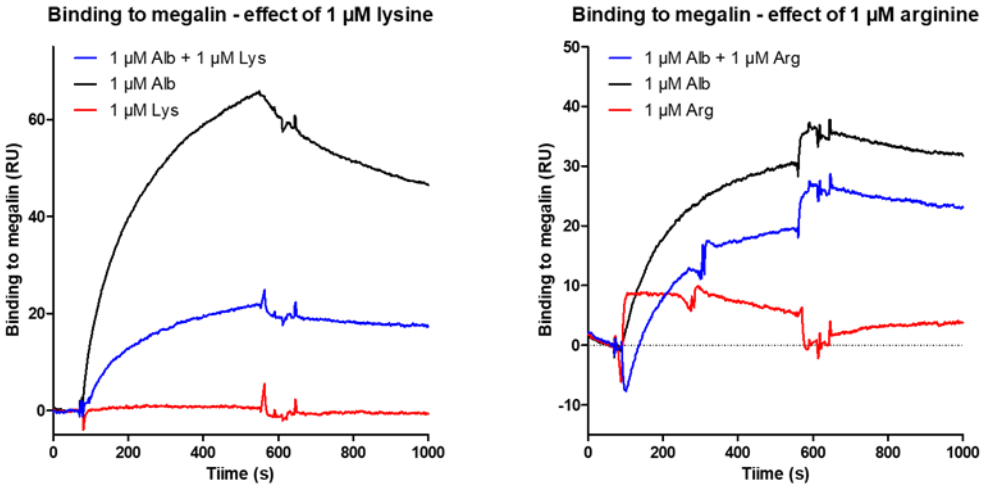

Figure 28. Evidence for direct competition by 1 microM dbAAs for 1 microM albumin binding to megalin biochips in Biacore assays. Whereas lysine alone, and presumably arginine alone, do not bind to the biochips, combination of equimolar dbAAs compete for albumin binding. Similar data were obtained on immobilized cubilin. At 100 microM dbAAs, no more albumin binding can be detected. *Preliminary data from Moestrup and Graversen, personal communication.*

However, dietary supply is by definition *discontinuous,* whereas ultrafiltration of plasma proteins is a continuous process. I indeed observed that, whereas PTC uptake of injected fluorescent protein during daytime was abolished when mice were fully adapted to inverse circadian rhythm so as to eat pellets during daytime, no protection was found without such full adaptation. This indicates postprandial competition for uptake when plasma (and urinary) dbAA levels are high, but loss of inhibition when levels decline. Thus, the question arises: would intermittent, reversible arrest of endocytic protein-driven cystine supply procure lasting benefits downstream. One possible mechanism that the constitutive lysosomal exocytosis allowing for significant vesicular efflux of cystine is not sufficient by itself to prevent cystine accumulation in the absence of transmembrane export, yet is helping doing the job when combined with discontinuous purge by cysteamine or discontinuous interruption of endocytosis-based supply. Alternatively, whether cysteamine or dbAAs promote lysosomal exocytosis has not been fully considered.

It is also unclear whether the regimen proposed has lasting impact on mTORC1 signalling, thereby switching cell preference from autophagy in favor of anabolism. Autophagy is generally considered detrimental, but was recently proposed as a beneficial process allowing to dispose of altered mitochondria and reduce ROS production.(Festa et al. 2018) I hope to tackle this complex issue after completing my PhD. Our plans are to look by immunofluorescence at the recruitment onto lysosomes of mTORC1 components (in one perfusion-fixed kidney compared to S6-kinase

phosphorylation level in extracts of the other unfixed kidney as described by Andrzejewska et al. 2016) in WT mice sacrificed during daytime after being (ia,b) untreated or (iia,b) provided with dbAA in pellets (for clinical relevance) or (iiia,b) in drinking water (to attenuate supply discontinuity); each without (a) or after established inversion of circadian rhythm (b). In parallel, I shall look at autophagy by combined immunofluorescence for p62/sequestosome, TOM20 and LAMP1, using a protocol validated in our lab for mouse kidney.(Grieco et al. 2018)

Moreover, in parallel to kidney protection, other benefits may be expected. Indeed, muscle fortification is the primary goal by the many body-builders who take arginine over the counter to accrue on muscle mass, as widely advertised in the internet. Comparable benefit on lean mass accretion is predicted for pig farms, but we could not retrieve pertinent long-term evidence. Our laboratory has suggested that a similar study on muscle in cystinotic mice should be conducted by a group combining expertise in muscle structure, anabolism/catabolism ratio including protection against apoptosis, transcriptional regulatory networks and overall strength and performance, together with genuine interest on cystinosis.(Cheung et al. 2016) The recent study on cystinotic bones by Battafarano et al, 2019, stresses that besides secondary defects due to phosphaturia, metabolic acidosis and impaired production of mature vitamin D (calcitriol), cystinotic osteoblasts and osteoclasts show primary intrinsic defects. Possible reversal by cysteamine was not included in that

study. Whether these defects can be corrected by dbAAs deserves to be examined.

There is also a crucial difference between *a priori* prevention of tissue damage by early dbAA protection, *vs* secondary stabilization (if not reversal) of lesions that necessarily already exist when diagnosis is made in cystinotic babies. Thus, another important study will address whether later supplementation by dbAAs of cystinotic mice, e.g. at 6 months of age, could prevent the exponential increase of kidney cystine content usually recorded afterwards (from 8 to 12 months of age). Additional blood, urine and tissue parameters will be analysed.

If this is effective, a pilot clinical project will be initiated to study a limited number of cystinotic children without renal insufficiency, recruited at two or three different centers (multicentric study). Each patient would serve as his/her own control, so as to reach statistical significance despite low numbers. They would be monitored every two-weeks in 5 successive periods: (i) upon base-line with all current medications including cysteamine; (ii) during two-months supplementation with either one of the dbAAs, assigned randomly, and administered at distant times from cysteamine to prevent interference on intestinal transport systems; (iii) during two-months reversal to normal diet; (iv) during two-months supplementation with the other dbAA; and (v) during second reversal to normal diet. Read-out is of course more limited, but would include (i) clinical survey (compliance and tolerance, subjective well-being including muscle strength); (ii) plasma assays for urea, creatinine, glucose,

phosphate and bicarbonate (acidosis level), (iii) and 24h urinary collections for the same constituents (change in diuresis and phosphate or glucose Tm as indicators of Fanconi syndrome?).

I would consider my duty as completed when the first clinical trial on patients will be conducted.

5. ANNEXES :

5.1. A Mouse Model Suggests Two Mechanisms for Thyroid Alterations in Infantile Cystinosis: Decreased Thyroglobulin Synthesis Due to Endoplasmic Reticulum Stress/Unfolded Protein Response and Impaired Lysosomal Processing

Gaide Chevronnay, H. P., **V. Janssens**, P. Van Der Smissen, X. H. Liao, Y. Abid, N. Nevo, C. Antignac, S. Refetoff, S. Cherqui, C. E. Pierreux, and P. J. Courtoy

Endocrinology. 2015 Jun;156(6):2349-64

5.2. Hematopoietic Stem Cells Transplantation Can Normalize Thyroid Function in a Cystinosis Mouse Model

Gaide Chevronnay, H. P.*, **V. Janssens***, P. Van Der Smissen, C. J. Rocca, X. H. Liao, S. Refetoff, C. E. Pierreux, S. Cherqui, and P. J. Courtoy

Endocrinology. 2016 Apr;157(4):1363-71
*, equal first authors

5.3. Cellular uptake of proMMP-2:TIMP-2 complexes by the endocytic receptor megalin/LRP-2

Johanns, M., P. Lemoine, **V. Janssens**, G. Grieco, S. K. Moestrup, R. Nielsen, E. I. Christensen, P. J. Courtoy, H. Emonard, E. Marbaix, and P. Henriet

Sci Rep. 2017 Jun 28;7(1):4328

5.4. Class III Phosphoinositide 3-Kinase/VPS34 and Dynamin are Critical for Apical Endocytic Recycling

Carpentier, S., F. N'Kuli, G. Grieco, P. Van Der Smissen, **V. Janssens,** H. Emonard, B. Bilanges, B. Vanhaesebroeck, H. P. Gaide Chevronnay, C. E. Pierreux, D. Tyteca, and P. J. Courtoy

Traffic. 2013 Aug;14(8):933-48

5.5. Vps34/PI3KC3 deletion in kidney proximal tubules impairs apical trafficking and blocks autophagic flux, causing a Fanconi-like syndrome and renal insufficiency

Grieco, G., **V. Janssens,** H. P. Gaide Chevronnay, F. N'Kuli, P. Van Der Smissen, T. Wang, J. Shan, S. Vainio, B. Bilanges, F. Jouret, B. Vanhaesebroeck, C. E. Pierreux[#], and P. J. Courtoy[#]

Sci Rep. 2018 Sep 20;8(1):14133
[#,] equal last authors

5.6. Vps34/PI 3-kinase type III controls thyroid hormone production by regulating thyroglobulin iodination, lysosomal proteolysis and tissue homeostasis

Grieco G.*, TS. Wang1*, O. Delcorte*, C. Spourquet*, **V. Janssens**, A. Strickaert, HP. Gaide Chevronnay, XH Liao, B. Bilanges4, S. Refetoff, B. Vanhaesebroeck, C. Maenhaut, PJ. Courtoy[#], CE. Pierreux[#]

Thyroid *"in press"*
*, equal first authors; [#,] equal last authors

ORIGINAL RESEARCH

A Mouse Model Suggests Two Mechanisms for Thyroid Alterations in Infantile Cystinosis: Decreased Thyroglobulin Synthesis Due to Endoplasmic Reticulum Stress/Unfolded Protein Response and Impaired Lysosomal Processing

H. P. Gaide Chevronnay, V. Janssens, P. Van Der Smissen, X. H. Liao, Y. Abid, N. Nevo, C. Antignac, S. Refetoff, S. Cherqui, C. E. Pierreux,* and P. J. Courtoy*

Cell Biology Unit (H.P.G.C., V.J., P.V.D.S., Y.A., C.E.P., P.J.C.), de Duve Institute and Université Catholique de Louvain, 1200 Brussels, Belgium; Departments of Medicine (X.H.L., S.R.) and Pediatrics and Genetics (S.R), The University of Chicago, Chicago, Illinois 60637; INSERM, Unité 1163 (N.N., C.A.), Hôpital Necker-Enfants Malades and Université Paris Descartes, Sorbonne Paris Cité, Institut Imagine, 75015 Paris, France; and Department of Pediatrics (S.C.), Division of Genetics, University of California, San Diego, San Diego, California 92161

Thyroid hormones are released from thyroglobulin (Tg) in lysosomes, which are impaired in infantile/nephropathic cystinosis. Cystinosis is a lysosomal cystine storage disease due to defective cystine exporter, cystinosin. Cystinotic children develop subclinical and then overt hypothyroidism. Why hypothyroidism is the most frequent and earliest endocrine complication of cystinosis is unknown. We here defined early alterations in *Ctns*$^{-/-}$ mice thyroid and identified subcellular and molecular mechanisms. At 9 months, T_4 and T_3 plasma levels were normal and TSH was moderately increased (~4-fold). By histology, hyperplasia and hypertrophy of most follicles preceded colloid exhaustion. Increased immunolabeling for thyrocyte proliferation and apoptotic shedding indicated accelerated cell turnover. Electron microscopy revealed endoplasmic reticulum (ER) dilation, apical lamellipodia indicating macropinocytic colloid uptake, and lysosomal cystine crystals. Tg accumulation in dilated ER contrasted with mRNA down-regulation. Increased expression of ER chaperones, glucose-regulated protein of 78 kDa and protein disulfide isomerase, associated with alternative X-box binding protein-1 splicing, revealed unfolded protein response (UPR) activation by ER stress. Decreased Tg mRNA and ER stress suggested reduced Tg synthesis. Coordinated increase of UPR markers, activating transcription factor-4 and C/EBP homologous protein, linked ER stress to apoptosis. Hormonogenic cathepsins were not altered, but lysosome-associated membrane protein-1 immunolabeling disclosed enlarged vesicles containing iodo-Tg and impaired lysosomal fusion. Isopycnic fractionation showed iodo-Tg accumulation in denser lysosomes, suggesting defective lysosomal processing and hormone release. In conclusion, *Ctns*$^{-/-}$ mice showed the following alterations: 1) compensated primary hypothyroidism and accelerated thyrocyte turnover; 2) impaired Tg production linked to ER stress/UPR response; and 3) altered endolysosomal trafficking and iodo-Tg processing. The *Ctns*$^{-/-}$ thyroid is useful to study disease progression and evaluate novel therapies. (***Endocrinology*** **156: 2349–2364, 2015)**

ISSN Print 0013-7227 ISSN Online 1945-7170
Printed in U.S.A.

Received August 11, 2014. Accepted March 23, 2015.
First Published Online March 26, 2015

* C.E.P. and P.J.C. contributed equally to this work.

Abbreviations: ATF, activating transcription factor; CHOP, C/EBP homologous protein; ΔCt, difference of cycle threshold; DEHAL1, dehalogenase 1; DTT, dithiothreitol; DUOX, dual oxidase; EM, electron microscopy; ER, endoplasmic reticulum; GAPDH, glyceraldehyde-3 phosphate deshydrogenase; GRP78, glucose-regulated protein of 78 kDa; LAMP-1, lysosome-associated membrane protein-1; Mct-8, monocarboxylate transporter-8; PDI, protein disulfide isomerase; PECAM-1, platelet endothelial cell adhesion molecule-1; PTC, proximal tubular cell; RT-qPCR, real-time quantitative PCR; Tg, thyroglobulin; TH, thyroid hormone; UPR, unfolded protein response; XBP-1, X-box binding protein-1; WT, wild type.

The function of individual molecular events in the thyroid gland has been unraveled by the study of monogenic defects, occurring spontaneously in human or engineered in mice (for reviews see references 1 and 2). We here address the effects in mouse thyroid of genetic ablation of the lysosomal membrane cystine exporter, cystinosin, which is absent in a rare multisystemic autosomal recessive lysosomal cystine storage disease, named infantile cystinosis (in short, cystinosis) (for reviews see references 3 and 4). Cystinosis leads almost invariably to primary hypothyroidism during the first years of life, whereas other endocrine organs are later affected (4–6).

Cystinosin, a seven-transmembrane protein of 367 amino acids displaying two strong lysosomal targeting motives (7), is the only known lysosomal membrane cystine exporter, driven by coupled proton efflux (8). Cystine is an obligatory end-degradation product of disulfide-bearing proteins. Once exported out of lysosomes, cystine is rapidly reduced into cysteine by cytosolic reducing systems. Cysteine together with glutamate participates in glutathione synthesis and thus cell redox homeostasis. The accumulation of lysosomal cystine in cystinosis can be corrected by substrate depletion therapy based on oral cysteamine, but compliance is very demanding. Cysteamine rearranges in lysosomes with cystine to a mixed disulfide that egresses via the lysine transporter (9).

The earliest manifestation of cystinosis, usually during the first year of life, is a kidney Fanconi syndrome, recognized by high urinary loss of solutes including water, salts, glucose, and phosphate together with ultrafiltrated plasma proteins. Infantile cystinosis usually leads to renal failure, even under compliant cysteamine treatment. During the first decade of life, most cystinotic children further develop subclinical and then overt hypothyroidism (5, 10). Although early compliant cysteamine treatment improves body growth and can avoid thyroid hormone replacement (11), eventually about half of treated cystinotic adults require thyroid hormones. Overall, kidney and thyroid dysfunctions are the less cysteamine-preventable complications of cystinosis (12, 13). Thus, better understanding of cellular and tissular pathogenic mechanisms in kidneys and thyroid are mandatory.

The exact causative link between cystinosis and hypothyroidism remains unexplained. As for the kidneys, defective thyroid function was originally attributed to atrophy with pathognomonic cystine crystals (5). However, the pathogenic role of crystals is questioned, and early impairment of proteolysis in cystinotic lysosomes has been evidenced and attributed to lysosomal redox imbalance (14). Thyroid hormones (THs) are released in lysosomes by proteolytic cleavage of engulfed thyroglobulin (Tg), although proteolysis may be initiated in the follicular lumen (15, 16). Tg is an oligomer of 330-kDa monomers, which assume a compact globular form stabilized by a huge number of disulfide bonds (>100/monomer) (17). Tg is dimerized in the endoplasmic reticulum (ER) and then undergoes compaction in the follicular lumen by intermolecular disulfide cross-linking to form insoluble thyroid globules for maximal storage (18, 19). Luminal compaction is attributed to extrinsic [secreted protein disulfide isomerase (PDI)] and intrinsic disulfide bond exchange mechanisms [via well preserved thioredoxin (CXXC) motives] (20). The extent of luminal Tg cross-linking varies among species and is related to age and follicle activation state (18, 19, 21). Tg unfolding via disulfide bond reduction by lysosomal reducing equivalents thus appears necessary to expose cryptic peptides targeted by lysosomal proteases (22). Stepwise Tg proteolytic processing depends on synergistic endo- and then exopeptidases, including the aspartyl protease, cathepsin D, and cysteine proteases, eg, cathepsin B (23–27). Cysteine proteases also require a reducing environment. These requirements would predict that Tg unfolding and cysteine protease attack are impaired when lysosomal cystine accumulation causes redox imbalance.

At low TSH, basal TH production is supported by endocytosis of Tg from the colloid via small endocytic pits (ie, micropinocytosis, reviewed in reference 28). This is regulated by expression and activation of tandem rate-limiting GTPase catalysts, Rab5 and Rab7, driving together vesicular transfer to lysosomes (29, 30). In some species such as mice, acute stimulation with high TSH dose triggers micrometric colloid uptake by protrusion of actin-dependent lamellipodia followed by macropinocytosis [also named phagocytosis; (31)], which brings large amounts of Tg to lysosomes in the form of colloid droplets. How released THs cross the lysosomal membrane remains unknown. This step could involve a similar transporter as monocarboxylate transporter-8 (Mct-8) (32) operating at the basolateral membrane for secretion into blood capillaries. However, a Mct-8 defect is unlikely in a monogenic disorder such as cystinosis.

We and others recently reported on the early kidney lesions and adaptations (33, 34) in a cystinosin-knockout mice strain of congenic C57BL/6 background (*Ctns*$^{-/-}$ mice), which mimics human cystinosis (35, 36). After a 3-month lag phase without detectable lesion, proximal tubular cells (PTCs) of *Ctns*$^{-/-}$ mice showed defective endolysosomal trafficking and lysosomal proteolysis, resulting into amorphous lysosomal inclusions and then cystine crystals. At the lesional stage, apoptosis and proportional proliferation revealed accelerated PTC turnover (33). We here extended our study of *Ctns*$^{-/-}$ mice to the thyroid gland, on the premise of shared high apical endo-

doi: 10.1210/en.2014-1672

cytic activity of disulfide-rich proteins and early defects in cystinotic children.

We first hypothesized that cystine accumulation in lysosomes of *Ctns*$^{-/-}$ thyrocytes would primarily affect thyroid function by delaying TH generation due to impaired Tg transfer to lysosomes, combined with defective unfolding and cysteine protease activity. As an additional hypothesis, nonmutually exclusive upstream mechanism, cystinosis causes ER stress (37) to which thyrocytes are particularly prone (38) so that ER stress would impair Tg synthesis and its supply to lysosomes. ER stress triggers the complex adaptive unfolded protein response (UPR) (for review see reference 39). UPR is initiated by transmembrane ER sensors/receptors, inositol-requiring kinase-1, protein kinase RNA-like endoplasmic reticulum kinase, and/or activating transcription factor (ATF)-6. Inositol-requiring kinase-1 activation results from high substrate competition, causing a dissociation of ER resident chaperones such as glucose-regulated protein of 78 kDa (GRP78). Downstream in the UPR pathway, activation of X-box binding protein-1 (XBP-1) by alternative mRNA splicing results in multiple structural and molecular adaptive mechanisms. These include the following: 1) expansion of the ER membrane and thus ER dilatation to accommodate protein overload; 2) increased transcription of ER chaperones (GRP78) and foldases (eg, PDI) and thus protein maturation capacity; and 3) decreased translation of secreted proteins (here Tg), which together attenuate ER stress. If stress persists or adaptive response fails, cell death is triggered via transcriptional activation of proapoptotic C/EBP homologous protein (CHOP) in response to protein kinase RNA-like endoplasmic reticulum kinase-ATF-4 axis activation (for reviews, see references 39 and 40).

We found that, after a lag phase of approximately 6 months, all *Ctns*$^{-/-}$ mice developed subclinical hypothyroidism with increased TSH, thyrocyte hyperplasia/hypertrophy, and accelerated turnover as well as angioproliferative response. Relative TSH refractoriness and colloid exhaustion could be explained by the combination of impaired Tg production due to UPR response with defective endolysosomal trafficking and Tg processing. UPR response to ER stress likely links TSH stimulation to thyrocyte apoptosis and accelerated turnover.

Materials and Methods

Mice

Congenic C57BL/6 *Ctns*$^{-/-}$ mice have been described (36). Mice were treated according to the National Institutes of Health Guide for Care and Use of Laboratory Animals. Mice were fed ad libitum with pellets containing 4.30 mg/kg iodine (Carfil Quality).

TSH, T_4, and T_3 plasma concentrations

Plasma TSH concentrations were measured by a sensitive, heterologous, disequilibrium, double-antibody precipitation RIA as described (41). T_4 and T_3 concentrations were measured by coated-tube RIA (Siemens Medical Solution Diagnostics).

Histology, multiplex immunofluorescence, and morphometry

Mice thyroids were fixed in situ by whole-body perfusion-fixation as described (33). Thyroids were dissected, postfixed overnight with 4% neutral-buffered formaldehyde, and processed for paraffin embedding. Four-micrometer-thick sections were stained with hematoxylin/eosin. Immunofluorescence was performed after antigen retrieval as described (33). Appropriate combinations of the following primary antibodies were used (Table 1): mouse anti-E-cadherin (0.25 μg/mL, 610182; DB Biosci-

Table 1. List of Antibodies

Peptide/Protein Target	Antigen Sequence (if Known)	Name of Antibody	Manufacturer, Catalog Number, and/or Name of Individual Providing the Antibody	Species Raised (Monoclonal or Polyclonal)	Dilution Used (IF;WB)
E-cadherin	—	Purified mouse anti-E-cadherin	DB Bioscience, number 610182	Mouse monoclonal (clone 36)	0.25 μg/mL
Ki-67	—	Purified mouse anti-human Ki-67	DB Pharmingen, number 556003	Mouse monoclonal (clone B56)	2 μg/mL
Active-caspase 3	—	Cleaved caspase-3 (Asp175) antibody	Cell Signaling, number 9661	Rabbit polyclonal	1:200
PECAM-1	—	Rat monoclonal anti-mouse endothelial cell marker CD31 (PECAM-1)	Dianova, number DIA310	Rat monoclonal (clone SZ31)	1:20
Ezrin	aa 362–585	Ezrin/p81/80K/cytovillin Ab-1, mouse monoclonal antibody	Thermo Scientific, number MS-661-P1	Mouse monoclonal (clone 3C12)	2 μg/mL
LAMP-1	—	Anti-LAMP-1 1D4B antibody	Hybridoma Bank, number 1D4B	Rat monoclonal (clone 1D4B)	1:100
KDEL	—	Anti-KDEL [MAC256] antibody	Abcam, number ab50601	Rat monoclonal (clone MAC256)	1:300
Tg	—	Monoclonal mouse anti-human thyroglobulin	Dako, number M0781	Mouse monoclonal (clone DAK-Tg6)	1:200; 1:1000
Iodo-Tg	—	Anti-iodo-thyroglobulin antibody	Provided by Dr Ris-Stalpers	Mouse monoclonal	1:100; 1:1000
GRP78	CT (643)GEEDTSEKDEL (654)	GRP78/BiP antibody	Thermo Scientific, number PAI-014A	Rabbit polyclonal	2 μg/mL
Cathepsin D	—	Cathepsin D antibody	Santa Cruz Biotechnology, number sc-6486	Goat polyclonal	0.2 μg/mL
GAPDH		GAPDH antibody	Ambion, number AM4300	Mouse monoclonal (clone 6C5)	0.5 μg/mL

ence), -ezrin (2 μg/mL, MS-661-P1; Thermo Scientific), -Ki-67 (2 μg/mL, 556003; DB Pharmingen), -Tg (1:200, M0781; Dako), and -iodo-Tg (1:100; kindly donated by Dr Ris-Stalpers, Laboratory of Pediatric Endocrinology, Academic Medical Center, Amsterdam, The Netherlands); rat anti-platelet endothelial cell adhesion molecule-1 (PECAM-1; 1:20, DIA310; Dianova), -lysosome-associated membrane protein-1 (LAMP-1; 1:100, 1D4B; Hybridoma Bank), and -KDEL (1:300, ab50601; Abcam); and rabbit anti-active caspase-3 (1:200, 9661; Cell Signaling). Immunolabeled sections were imaged with a spinning disk confocal microscope using EC Plan-NeoFluar ×40/1.3 or Plan Apochromat ×100/1.4 oil differential interference contrast objectives (cell observer spinning disk; Zeiss). Morphometric analyses were performed using Axiovision 4.8.2. software (Zeiss). Binary mask were prepared using fixed interactive thresholding. Thyrocytes, colloid, and interstitium were filled and areas were measured.

Electron microscopy

Thyroids were perfusion-fixed in situ with 4% neutral-buffered formaldehyde supplemented by 0.1% glutaraldehyde and then immersion fixed in 1.5% (vol/vol) glutaraldehyde overnight, postfixed with 1% (wt/vol) OsO_4 in 0.1 M cacodylate buffer for 1 hour, rinsed in veronal buffer (4 × 5 min), and stained overnight en bloc in 1% neutral uranyl acetate, all at 4°C. After extensive washing in veronal, blocks were dehydrated in graded ethanol and embedded in Spurr. Ultrathin sections were obtained (Reichert ultramicrotome), collected on 400-mesh rhodanium grids, and contrasted with 3% uranyl acetate and then lead citrate, 10 minutes each. Grids were washed with water, dried, and examined in a FEI CM12 electron microscope operating at 80 kV.

In situ hybridization

Vegf-a antisense RNA probes spanning nucleotides 94–429 of the mouse coding sequence for Vegf-a (42) were produced by RT-PCR followed by in vitro transcription with T7 RNA polymerase in the presence of digoxigenin-labeled uridine 5-triphosphate (Roche). In situ hybridization was performed on 8-μm sections as described (33).

PCR and real-time quantitative PCR (RT-qPCR)

Total RNA was extracted (TRIzol reagent; Invitrogen) and 150 ng RNA was reverse transcribed by Moloney murine leukemia virus reverse transcriptase (Invitrogen) using random hexamers. Primer sequences are described in Supplemental Table 1. PCR was performed under standard conditions with GoTaq DNA polymerase (Promega). RT-qPCR was performed as described (33) in the presence of 250 nM specific primers with Kappa SYBR Fast qPCR master mix (Kapa Biosystems) on a CFX96 touch real-time PCR detection system (Bio-Rad Laboratories). Results are presented as difference of cycle threshold (ΔCt) values normalized to actin, used as internal standard.

Western and lectin blotting

Thyroid glands were dissected and homogenized in Western blot lysis buffer (150 mM NaCl, 1% Triton X-100, 0.5% sodium deoxycholate, 0.1% sodium dodecyl sulfate, 50 mM Tris, pH 8.0) or in subcellular fractionation buffer 250 mM sucrose, 3 mM imidazole, and 1 mM EDTA (pH 7.0) buffer supplemented with Complete protease inhibitors (Roche) and phosphatase inhibitors (sodium orthovanadate, pyrophosphate, and fluoride, all 2 mM). Loading was normalized to protein concentration, measured by bicinchoninic acid method (Sigma-Aldrich). Samples were reduced or not, as indicated, with 50 or 100 mM dithiothreitol (DTT) for 10 minutes and denatured by boiling for 5 minutes. Western blotting was performed as described (43) using mouse anti-Tg (1:1000, M0781; Dako), or -glyceraldehyde-3 phosphate dehydrogenase (GAPDH; 0.5 μg/mL, AM4300; Ambion); rat anti-KDEL (2.5 μg/mL, ab50601; Abcam); rabbit anti-GRP78 (2 μg/mL, PA1–014A; Thermo Scientific); or goat anti-cathespin D (0.2 μg/mL, sc-6486; Santa Cruz Biotechnology). Lectin blotting was performed with wheat germ agglutinin lectin (10 μg/mL; Vector Biolabs) after electrophoresis under reducing conditions as described (44). Specificity of lectin signal was demonstrated by neuraminidase digestion at 37°C for 18 hours, following the manufacturer's instructions (New England BioLabs).

Cathepsin B assay

Thyroid glands were dissected and homogenized in 250 mM sucrose, 3 mM imidazole, and 1 mM EDTA (pH 7.0). Cathepsin B activity was measured as total minus 100 μM CA-074-resistant fraction (Sigma-Aldrich) in a fluorimetric assay using benzyloxycarbonyl-L-phenylalanyl-L-arginine 4-methylcoumaryl-7-amide (45), or Nα-benzoyl-DL-arginine-β-naphthylamide hydrochloride, with undistinguishable results. Activity was normalized to protein concentration measured by the bicinchoninic acid method (Sigma-Aldrich).

Analytical subcellular fractionation

Excised thyroid glands from three to four wild-type (WT) or *Ctns*$^{-/-}$ mice, aged 9–11 months, were pooled in 250 mM sucrose, 3 mM imidazole, and 1 mM EDTA (pH 7.0), supplemented with Complete protease inhibitors (Roche), and homogenized therein with a Polytron (3 × 5 sec, nominal 8500 speed). Homogenates were cleared through 40 μm BD falcon filters and first resolved by crude differential sedimentation to isolate cell debris and nuclei (1.5 10^4 g × min), postnuclear particles (6.3 10^6 g × min), and a final supernatant. Postnuclear particles were washed once by resuspension and resedimentation to minimize colloid contamination and then equilibrated by sedimentation into 1.10–1.30 (grams per milliliter) linear sucrose gradients in a SW55Ti rotor (57 10^6 g × min). Ten fractions were collected from the bottom and assayed for density (weight) and β-hexosaminidase activity as described (33). Aliquots of equal volume were analyzed by Western blotting for iodo-Tg (1:1000). Compared blots were transferred and revealed in the same membrane and then quantified using ImageJ software (National Institutes of Health, Bethesda, Maryland).

Statistical analyses

Statistical significance was tested using a Mann-Whitney U test (see Figures 1A, 3A and B, 5A and B, 6C, and 7B and C; and Supplemental Figure 4), Student's t test (Figures 1D and 2B) or χ^2 (Figure 6B). Differences were considered significant for $P < .05$. Except for specific thyroid weight, there was no significant difference between males and females in each group and for each comparison; thus, genders were not discriminated on scatter plots.

doi: 10.1210/en.2014-1672

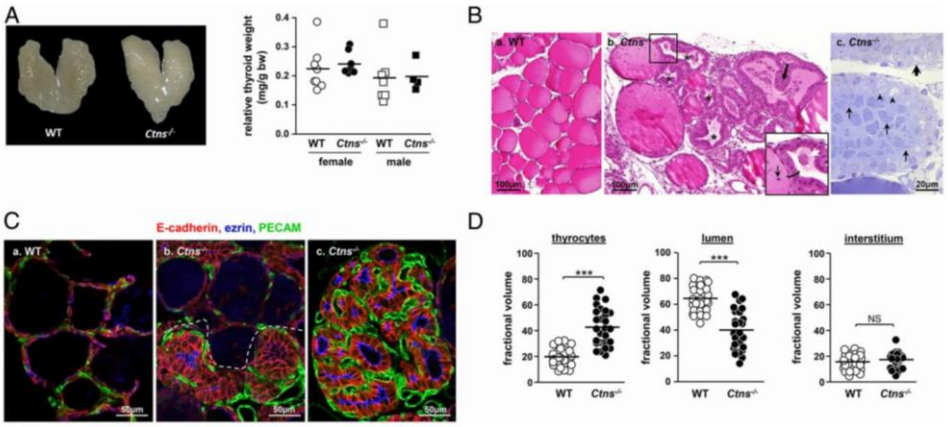

Figure 1. *Ctns*$^{-/-}$ mice develop thyroid hyperplasia and hypertrophy associated with colloid exhaustion. A, Anatomy. Left panel, Thyroid gland from control (WT) and *Ctns*$^{-/-}$ female mice at 11 months. Right panel, Thyroid glands weight normalized to body weight in WT and *Ctns*$^{-/-}$ females and males at 9–12 months. Cystinotic mice do not develop goiter. B, Histology. Paraffin sections with hematoxylin-eosin staining (a and b) and semithin plastic section with toluidine blue staining (c), all at 9 months, are shown. a, WT thyroid is made of uniform follicles filled with homogenous colloid and delimited by flat thyrocytes. b, In *Ctns*$^{-/-}$ mice, most follicles show exhausted colloid (asterisks) surrounded by thyrocytes that are both hypertrophic (insert bracket) and hyperplastic, frequently projecting into papillae (thick arrow). Boxed area at panel b is enlarged below to emphasize the contrast between the few resting follicles (flat epithelium) with colloid bearing several cell remnants (thin arrow) and an adjacent hypertrophic/hyperplastic follicle (bracket) with almost vanished colloid (white arrow suggests dissolution of a thyroid globule). c, In the plastic section of *Ctns*$^{-/-}$ thyroid, the two upper follicles with hypertrophic thyrocytes and exhausted colloid contrast with a resting follicle below with dense colloid and flat thyrocytes. Arrowheads point to apical thyrocyte vacuolation, suggesting macropinocytosis/phagocytosis; the thick arrow points to irregular basal thyrocyte clarifications aligned along the basoapical axis, suggesting dilation of endoplasmic reticulum. In the central follicle, shed cell remnants almost fill the follicular lumen (thin arrows indicate variety of shapes). Scale bars, a and b, 100 μm; c, 20 μm. For histological time course, see Supplemental Figure 1. C and D, Immunofluorescence: multifocal activation of the angiofollicular system in *Ctns*$^{-/-}$ mice thyroids and colloid exhaustion. C, Follicular hyperplasia and hypertrophy are coupled to expansion of associated blood capillary basket. Multiplex immunofluorescence for E-cadherin (red, thyrocyte basolateral membrane), ezrin (blue, thyrocyte apical membrane), and PECAM (green, blood capillaries) in the thyroid of WT (a) and *Ctns*$^{-/-}$ (b and c) mice at 9 months, performed strictly in parallel. a, WT follicles are surrounded by a blood capillary network weakly discernible by PECAM immunolabeling. b, In this intermediate *Ctns*$^{-/-}$ pattern, notice abrupt boundary (dotted line) between resting follicles (top panel) and hyperplastic follicles (bottom panel) showing microvasculature expansion associated with much stronger PECAM signal. c, In most remodeled *Ctns*$^{-/-}$ hyperplastic foci, lumina have almost vanished and microvasculature is greatly expanded. All scale bars, 50 μm. For in situ hybridization of Vegf-a, see Supplemental Figure 2. D, Follicular hyperplasia/hypertrophy is associated with colloid exhaustion. Morphometric assessment of the fractional volume of thyrocytes, colloid, and interstitial compartment (mesenchyme and blood capillaries) in WT and *Ctns*$^{-/-}$ mice (n = 3; each analyzed in nine random fields spanning the entire thyroid section, cumulative area of 3.4 10^5 μm^2 for each mouse). Note doubling of *Ctns*$^{-/-}$ thyrocyte fractional volume, at the expense of the lumen, but no significant change of interstitial fractional volume. ***, $P < .001$. NS, not significant.

Results

Ctns$^{-/-}$ thyroids develop multifocal hyperplasia/hypertrophy with colloid exhaustion and proportional vascular expansion

There was neither macroscopic change nor goiter at 9 and 12 months (Figure 1A). Thyroid glands were analyzed by conventional histopathology at 3, 6, 9, and 15 months (Figure 1B and Supplemental Figure 1). There were no detectable lesions at 3 months. Between 6 and 9 months, *Ctns*$^{-/-}$ mice consistently developed multifocal thyrocyte hypertrophy and hyperplasia with pseudostratification up to papillary lesions, luminal cell remnants (Figure 1B, b and c), and colloid exhaustion (Figure 1Bb). As better seen with 1-μm plastic sections, hypertrophic thyrocytes exhibited apical vacuolation, suggesting (TSH)-induced macropinocytosis/phagocytosis, and irregular basal cytoplasm clarification, suggesting ER dilatation (Figure 1Bc). As disease progressed, luminal cell remnants accumulated (Figure 1Bc) and colloid vanished (Supplemental Figure 1). At 15 months, most *Ctns*$^{-/-}$ follicles were hyperplastic or dedifferentiated, with few resting follicles remaining visible. In 15-month WT thyroids, most follicles remained quiescent and few peripheral follicles were activated. To focus on consistent early physiopathological mechanisms, mice were further analyzed at approximately 9 months.

The importance of thyroid capillaries as integrated part of autonomous angiofollicular units has emerged (46). Because blood capillaries are barely visible by conventional

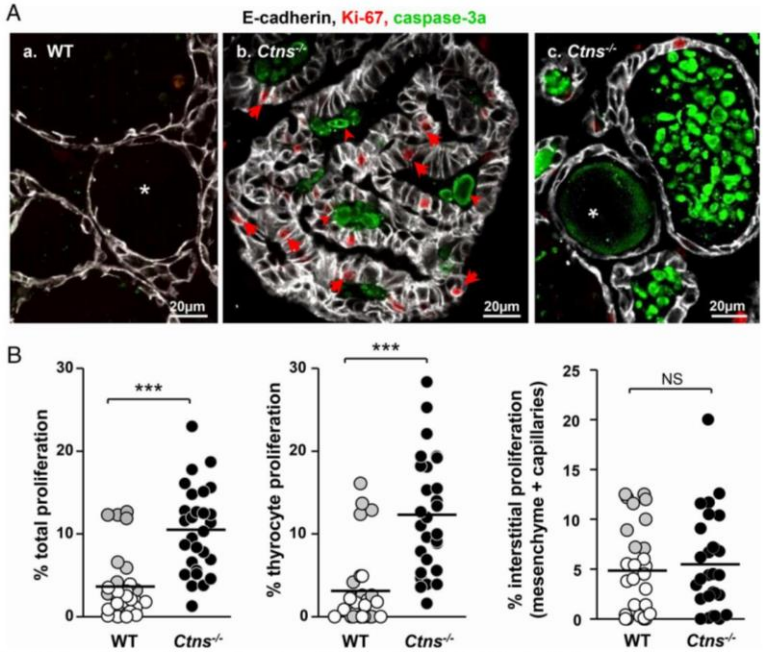

Figure 2. Cystinosis induces follicle-autonomous thyrocyte proliferation and apoptosis. A, Confocal microscopy. Immunofluorescence for E-cadherin (white; thyrocyte basolateral membrane), Ki-67 (red; cell proliferation marker), and activated caspase-3 (green, apoptosis marker) in 9-month WT (a) and $Ctns^{-/-}$ (b, c) thyroids. Notice numerous proliferating cells (arrows) in $Ctns^{-/-}$ hyperplastic follicles, pointing to autonomous follicular response, whereas Ki-67 labeling in WT thyrocytes is very rare. At panel c, large collections of apoptotic bodies in the follicular lumen of $Ctns^{-/-}$ thyroid (arrowheads) indicate accelerated cell turnover. All scale bars, 20 μm. B, Quantification of proliferation. Percentage of total nuclei area stained for Ki-67 in whole tissue (total proliferation) or associated with E-cadherin (thyrocyte proliferation) as estimated by morphometric analysis in 9-month WT (open and gray symbols; gray identifies a special WT individual) and $Ctns^{-/-}$ thyroids (filled symbols) (n = 3). For each mice, 3.4 10^5 μm^2 of area corresponding to nine fields spanning the entire thyroid section were analyzed. Proliferation is specifically increased in $Ctns^{-/-}$ thyrocytes. ***, $P < .001$.

histology, we looked for vascular changes by triple immunofluorescence confocal imaging, using E-cadherin and ezrin as markers of thyrocyte membrane domains, together with PECAM for blood capillaries. $Ctns^{-/-}$ hyperplastic follicles were consistently associated with prominent dilated capillaries as compared with resting follicles, indicating synchronous activation of the angiofollicular system (Figure 1C). Proangiogenic Vegf-a was up-regulated in hypertrophic thyrocytes, mostly in papillary projections, in full agreement with recruitment/expansion of blood capillaries (Supplemental Figure 2). Thus, $Ctns^{-/-}$ mice exhibited integrated angiofollicular activation.

To quantitate tissue changes by taking into account disease-induced heterogeneity between mice and between follicles, we exploited E-cadherin immunofluorescence. As shown by Figure 1D, thyrocyte fractional volume was increased by 2.2-fold in $Ctns^{-/-}$ mice (19.9% in WT vs 42.9% in $Ctns^{-/-}$ mice) with a concomitant decrease of fractional luminal volume (64.5% in WT vs 39.9% in $Ctns^{-/-}$ mice). Both parameters showed strong negative correlation ($r = 0.93$; $P < .0001$; data not illustrated). No significant difference was observed between WT and $Ctns^{-/-}$ mice for interstitial area (combined mesenchyme and blood capillaries). We thus focused on thyrocytes for further structural studies.

Increased proliferation and apoptosis in $Ctns^{-/-}$ thyrocytes reveals accelerated cell turnover

Cell division is rare in normal adult thyrocytes (47) but was expected to increase to support hyperplasia in $Ctns^{-/-}$ thyroids. Conversely, the striking abundance of luminal remnants was reminiscent of in vitro and in vivo evidence that cystinosis triggers apoptosis in other cells/tissues (33, 48, 49). To define the impact of cystinosis on

doi: 10.1210/en.2014-1672

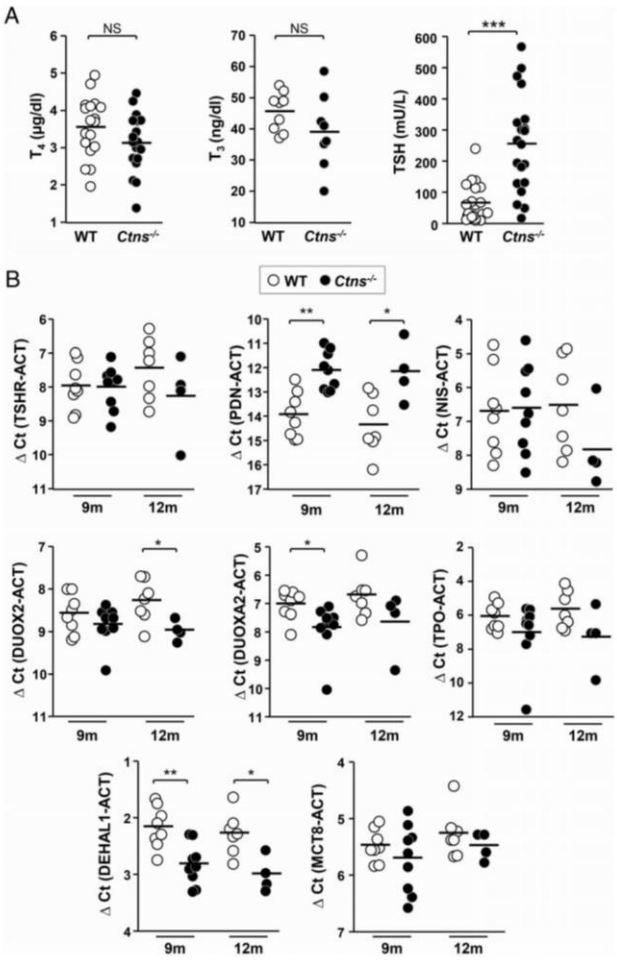

Figure 3. Compensated primary hypothyroidism and mRNA expression of thyroid hormone synthesis machinery in *Ctns*$^{-/-}$ mice. A, *Ctns*$^{-/-}$ mice elicit a compensatory TSH increase. T_4, T_3, and TSH plasma concentrations were measured in 9- to 10-month WT mice (open symbols) and *Ctns*$^{-/-}$ littermates (filled symbols) (n = 18 for T_4; n = 9 = WT and 8 *Ctns*$^{-/-}$ for T_3; n = 20 for TSH). *Ctns*$^{-/-}$ mice show an average 4-fold increase in plasma TSH level but still normal thyroid hormone plasma levels, indicating effective thyroid compensation. B, Expression of thyroid-specific genes involved in hormone synthesis. Quantification by RT-qPCR of TSH receptor (TSHR), Na/I symporter (NIS), pendrin (PDN), DUOX2, DUOXA2, thyroperoxidase (TPO), DEHAL1 and MCT8 mRNAs in WT and *Ctns*$^{-/-}$ thyroids collected at 9 and 12 months, normalized to actin mRNA (ACT) and presented as ΔCt values (difference of cycle threshold).

thyrocyte turnover, we analyzed the proliferation and apoptosis (Figure 2, A and B). Thyrocyte proliferation, monitored by Ki-67 immunolabeling, was barely detected in WT (<3%) but significantly increased in *Ctns*$^{-/-}$ mice (by 4.5-fold). Interstitial cell proliferation did not reach a significant difference between WT and *Ctns*$^{-/-}$ mice (Figure 3B, except if values of one outlier WT mouse were excluded; $P < .01$). Likewise, in WT thyroids, apoptotic events (monitored by active caspase-3 immunolabeling) were very rare (Figure 2Aa), consistent with a resting cell population. In contrast, caspase-3a-labeled apoptotic bodies accumulated in *Ctns*$^{-/-}$ follicular lumen, confirming accelerated cell turnover (Figure 2A, b and c). The distribution of apoptotic cells among follicles was much more heterogeneous than proliferative events, probably due to follicle heterogeneity in disease progression and unequal long-term retention of apoptotic bodies in follicular lumina [in contrast to continuous shedding in kidney proximal tubules; (33)].

Ctns$^{-/-}$ mice develop subclinical hypothyroidism

Because histological alterations of *Ctns*$^{-/-}$ thyroid suggested TSH activation and because cystinotic children develop subclinical hypothyroidism, we next evaluated the thyroid hormonal status in *Ctns*$^{-/-}$ mice and analyzed the expression of critical genes involved in thyroid hormone synthesis. As shown in Figure 3A, plasma TSH concentrations of *Ctns*$^{-/-}$ mice at 9–10 months were significantly increased (by 4.4-fold) as compared with WT mice, a feedback response sufficient to maintain normal plasma T_4 and T_3 concentrations. Although mRNA of some components of thyroid hormone biosynthetic machinery were moderately altered [pendrin, dual oxidase (DUOX)-2, DUOXA2, dehalogenase 1 (DEHAL1)], none (including the basolateral transporter of TH, Mct-8) was really defective in *Ctns*$^{-/-}$ mice (Figure 3B). We concluded that *Ctns*$^{-/-}$ mice mimic subclinical hypothyroidism of cystinotic children.

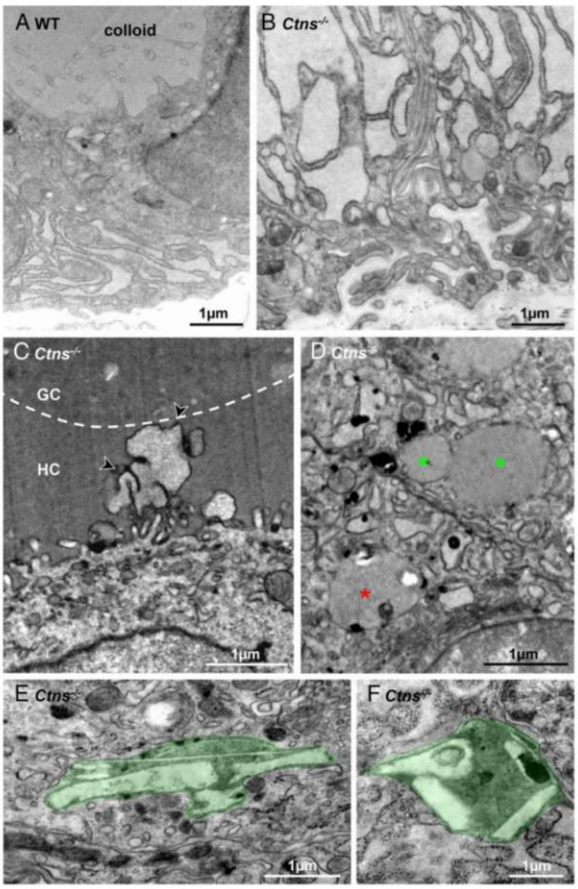

Figure 4. Ultrastructural alterations in *Ctns*$^{-/-}$ thyrocytes. Representative EM views of resting WT (A) and activated *Ctns*$^{-/-}$ thyrocytes (B–F). A, In this resting WT thyrocyte at 12 months, notice limited ER expansion and thin apical projections. B, Hyperplastic *Ctns*$^{-/-}$ thyrocyte at 12 months showing strong dilation of endoplasmic reticulum lumen. Notice characteristic tortuous basal plasma membrane and basal lamina. C, This activated *Ctns*$^{-/-}$ thyrocyte at 8 months projects a lamellipodium, characteristic of macropinocytosis (arrowheads) across a homogenous peripheral colloid ring (HC) up to central granular colloid (GC), indicated by the broken line. D, Asterisks indicate colloid droplets in two adjacent activated thyrocytes, two with homogenous colloid content and undergoing homotypic fusion (green asterisks), one bearing additional luminal structures indicating fusion with lysosomes (red asterisk). E and F, Cystine crystals-bearing lysosomes in *Ctns*$^{-/-}$ thyrocytes at 12 months.

Tg synthesis is quantitatively but not qualitatively altered in *Ctns*$^{-/-}$ mice

As an explanation for colloid exhaustion observed in *Ctns*$^{-/-}$ thyroids, we first looked at Tg biosynthetic machinery, including ER structure, disulfide-bonding, and N-glycosylation. Electron microscopy revealed prominent ER dilatation in the hypertrophic *Ctns*$^{-/-}$ thyrocytes, contrasting with normal Golgi complex (Figure 4, A vs B). Also by confocal microscopy, immunolabeling for the C-terminal ER-retention motive, KDEL, confirmed that basolateral dilations seen in semithin plastic sections of hypertrophic thyrocytes (Figure 1C), reflected a major enlargement of this compartment (Figure 5A, b and c). Simultaneous Tg immunolabeling disclosed its accumulation in the dilated ER, compatible with either increased synthesis upon TSH stimulation or defective export, eg, upon ER stress (50) (Figure 5A, b and c). To discriminate between these two hypotheses, we quantified Tg mRNA expression in thyroids at 9 and 12 months and found a significant decrease in *Ctns*$^{-/-}$ as compared with WT mice (Figure 5B). Western blotting on thyroid lysates confirmed a decreased total Tg content and revealed a decreased proportion of high-molecular-weight Tg (ie, cross-linked) in *Ctns*$^{-/-}$ thyroids (Figure 5C). Irrespectively of the cystinosin status, Tg could be completely reduced by DTT into 330-kDa monomers (Figure 5C) by as low as 0.3 mM DTT (not shown). These data indicated that Tg could still oligomerize in *Ctns*$^{-/-}$ follicle lumina and suggested accelerated colloid turnover. Of note, the extent of cross-linking differed between mice studied here (low) and young human adults (higher) (21): species differences should be kept in mind when extrapolating conclusions from cystinotic mice to patients. Analysis of Tg terminal N-glycosylation by sialic acid lectin blotting of thyroid lysates revealed no major difference between WT and *Ctns*$^{-/-}$ mice (Figure 5D). We thus concluded that Tg processing was qualitatively preserved in *Ctns*$^{-/-}$ mice and that ER enlargement was not due to increased Tg synthesis, pointing instead to quantitative defect in export, possibly upon ER stress.

doi: 10.1210/en.2014-1672

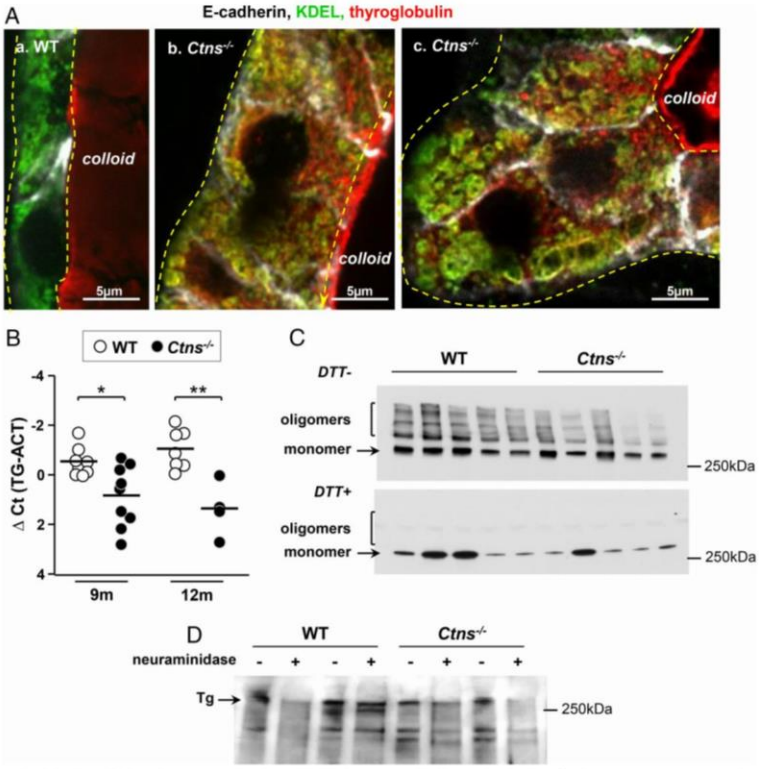

Figure 5. Tg synthesis is slowed down but maturation is qualitatively preserved in hyperplastic *Ctns*$^{-/-}$ thyrocytes. A, Tg accumulates in the ER of *Ctns*$^{-/-}$ thyrocytes. Comparison of WT (a) and *Ctns*$^{-/-}$ mice (b, c) at 9–10 months for E-cadherin (white), KDEL (green, retention motive used as marker of ER), and Tg (red). Yellow broken lines indicate thyrocyte profiles. Tg labeling of colloid is out of focus because of artifactual colloid stickiness to the coverslip. In WT thyrocytes (a), the ER is usually localized to the basolateral cytoplasm, without resolution of the reticulum at the confocal level and shows barely visible Tg signal in our labeling conditions. In contrast, *Ctns*$^{-/-}$ hyperplastic thyrocytes (b and c) show ER dilatations, resolved at the confocal level (KDEL, green), containing detected Tg (red), resulting in yellow signal, and expanding up to the apical pole. B, Decreased levels of Tg mRNA in *Ctns*$^{-/-}$ mice thyroid. Quantification of thyroglobulin (TG) mRNA by RT-qPCR in WT and *Ctns*$^{-/-}$ thyroids collected at 9 and 12 months, normalized to actin mRNA (ACT), and presented as ΔCt values. *, $P < .05$; **, $P < .01$. C and D, Preserved thyroglobulin maturation. C, Disulfide bonding. Thyroid extracts of five WT and five *Ctns*$^{-/-}$ thyroids were analyzed by Western blotting for Tg, without or after reduction of disulfide bonds by 100 mM DTT. Notice that total Tg is decreased in *Ctns*$^{-/-}$ thyroid and that Tg oligomers remain detectable in *Ctns*$^{-/-}$ thyroids, although their proportion is decreased as compared with WT. These effects are attributed to accelerated colloid turnover. Oligomers are fully reduced into 330-kDa monomers upon DTT. Decreasing DTT concentration to 0.3 mM yielded identical results (not shown). D, Terminal N-glycosylation. Thyroid extracts from two WT and two *Ctns*$^{-/-}$ mice were analyzed by lectin blotting after reduction by DTT, without or with pretreatment with neuraminidase as lectin-specificity control. Notice comparable terminal Tg sialylation. This blot is representative of two experiments.

Ctns$^{-/-}$ thyrocytes develop the unfolded protein response to ER stress

Secretory cells are particularly prone to ER stress, previously documented in activated thyrocytes (38, 50). Moreover, cystinosis has been associated with ER stress (51). We thus evaluated whether the UPR was activated in response to ER stress in *Ctns*$^{-/-}$ thyroid by looking at UPR-target genes and products (52, 53). The ER-resident chaperone GRP78 and PDI, both bearing the KDEL ER-retention motive, were increased at the protein level in *Ctns*$^{-/-}$ thyroid homogenates (Figure 6A). Downstream in the UPR pathway, unconventional splicing of transcription factor XBP-1 mRNA, yielding the spliced XBP-1 form, was detected in almost all *Ctns*$^{-/-}$ thyroids but only in a minority of WT thyroids. As illustrated by Figure 6B, at 9 months, 10 of 13 *Ctns*$^{-/-}$ vs 3 of 9 WT mice thyroids

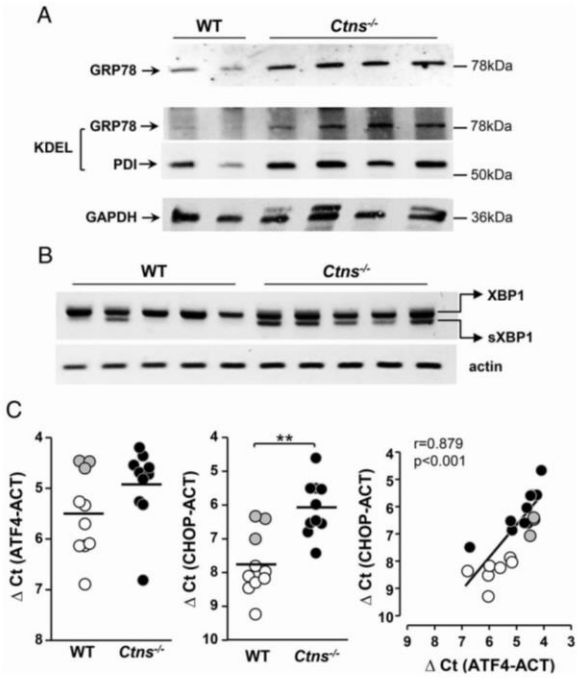

Figure 6. ER stress is triggered in *Ctns*$^{-/-}$ thyroid. A, Increased expression of GRP78 and PDI in *Ctns*$^{-/-}$ mice thyroid. Thyroid lysates from WT and *Ctns*$^{-/-}$ at 11–12 months were analyzed by Western blotting with antibodies to GRP78 (upper panel) or KDEL (the latter identifies both GRP78 and PDI; medium panel) and to GAPDH (stripped reprobed blot, lower panel). B, Unconventional splicing of XBP-1 mRNA is triggered in *Ctns*$^{-/-}$ mice thyroid. RT-PCR analysis of XBP-1 mRNA maturation in thyroid of five WT and five *Ctns*$^{-/-}$ mice at 9 months. Notice the alternative spliced XBP1 lower band in all *Ctns*$^{-/-}$ samples and only one WT sample. C, Induction of ATF-4 expression triggers CHOP mRNA expression. Quantification of ATF-4 and CHOP mRNAs by RT-qPCR in WT and *Ctns*$^{-/-}$ thyroids collected at 9 months, normalized to actin mRNA (ACT), and presented as ΔCt values. **, $P < .01$. Gray dots correspond to outlier WT mice for which both ATF-4 and CHOP mRNAs were increased. At right, increased expression of ATF-4 strongly correlates with increased expression of CHOP.

exhibited nonconventional XBP-1 mRNA splicing ($P <$ .001); at 12 months, the proportion were 8 of 9 *Ctns*$^{-/-}$ vs 2 of 8 WT ($P < .01$; not shown). Further in the UPR pathway, induction of ATF-4 expression strongly correlated with increased expression of its downstream effector, the transcription factor CHOP (Figure 6C). These data together supported the hypothesis that activation of ER stress/UPR pathway in *Ctns*$^{-/-}$ thyrocytes not only leads to defective Tg synthesis and secretion, thus colloid exhaustion, but also contributes to apoptosis triggering.

Lysosomal Tg processing is altered in *Ctns*$^{-/-}$ mice

In addition to UPR effects, our alternative working hypothesis for primary hypothyroidism was the defective release of thyroid hormones from iodo-Tg. To this aim, we looked for ultrastructural alterations of the endocytic apparatus (Figure 4) and at LAMP-1 immunofluorescence for late endosomes/lysosomes (Figure 7). By EM, although the apical surface of resting WT thyrocytes showed only sparse thin microvilli (Figure 4A), *Ctns*$^{-/-}$ thyrocytes in activated follicles frequently showed apical lamellipodia (Figure 4C), sequestration of primary colloid droplets, and their fusion into phagolysosomes (Figure 4D). These are characteristic of TSH-induced macropinocytosis, the structural equivalent of accelerated endocytosis. In contrast, we detected no change in the abundance of Rab5 and Rab7 mRNAs, which finely tune micropinocytosis (Supplemental Figure 4). By immunofluorescence, induced macropinocytosis correlated with enlarged LAMP-1-labeled apical structures (Figure 7Ab), absent in resting WT thyrocytes (Figure 7Aa). In addition, LAMP-1 labeled some distorted structures (Figure 7Ac), either strongly elongated or showing angular membranes, reminiscent of the abundant lysosome-bearing crystals in *Ctns*$^{-/-}$ kidney proximal tubular cells (33). Electron microscopy of *Ctns*$^{-/-}$ thyrocytes yielded several examples of severely distorted secondary lysosomes, identified by a limiting membrane and heterogeneous content and containing characteristic electron-lucent needles or long polyhedric objects, ie, bona fide cystine crystals (Figure 4, E and F). Remarkably, small LAMP-1-labeled vesicles appeared closely apposed to distorted LAMP-1-labeled structures, suggesting lysosomal docking but impaired fusion (Figure 7Ac) as seen in *Ctns*$^{-/-}$ PTCs in which a late endocytic trafficking defect has been evidenced.

Because late endocytic trafficking seemed affected in *Ctns*$^{-/-}$ thyrocytes, we looked for a functional impact on iodo-Tg processing to explain TSH feedback and partial TSH refractoriness. By immunofluorescence, we frequently found iodo-Tg retained in LAMP-1-labeled lysosomes selectively in *Ctns*$^{-/-}$ hypertrophic thyrocytes, suggesting defective prohormone processing (Figure 7B, b–e,

doi: 10.1210/en.2014-1672

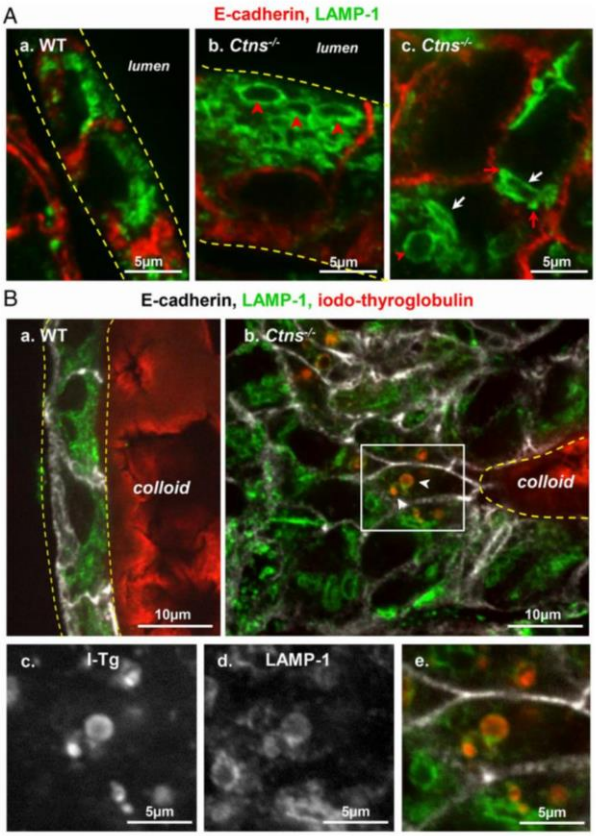

Figure 7. Alterations of the late endocytic apparatus in hyperplastic *Ctns*$^{-/-}$ thyrocytes. A, Identification of large apical vacuoles and crystal-bearing structures as lysosomes. Comparison of WT (a) and *Ctns*$^{-/-}$ mice (b and c) at 9 months for immunolabeling of E-cadherin (red) and LAMP-1 (green; late endosome/lysosome membrane). a, In this resting WT follicle, flat thyrocytes show at their apical pole packed lysosomes of uniform small size and round shape. b and c, In activated *Ctns*$^{-/-}$ thyrocytes, late endosomes-lysosomes are frequently dilated (red arrowheads) and distorted (better seen at panel c, white arrows). Red arrows at panel c suggest docked but not fused late endosomes/lysosomes. For levels of Rab5 and Rab7 mRNAs, see Supplemental Figure 4. B, Iodo-Tg is retained in lysosomes. Comparison of WT (a) and *Ctns*$^{-/-}$ mice (b–e) at 9–10 months for E-cadherin (white), LAMP-1 (green), and iodo-Tg (red). In resting WT follicles (a), iodo-Tg is stored in the colloid and is never detected within thyrocytes. In activated *Ctns*$^{-/-}$ thyrocytes (b), vesicles filled with iodo-Tg and labeled by LAMP-1 (thus not primary colloid droplets) are frequently found at the apical pole of hyperplasic thyrocytes. Enlargements of the boxed field (c–e) first show single-channel images of iodo-Tg and LAMP-1 in black and white for optimal resolution and easier pattern comparison and then merged back with E-cadherin in triple colors as above. The apparent defect of (iodo-)Tg labeling of the central lumen is due to artifactual sticking of the colloid to the coverslip, thus out of focus by confocal imaging. For a gallery of representative images of iodo-Tg retained in lysosomes, see Supplemental Figure 3.

and Supplemental Figure 3). This was never observed in WT thyrocytes. Furthermore, by subcellular fractionation using isopycnic centrifugation combined with Western blotting, we demonstrated that *Ctns*$^{-/-}$ thyroid lysosomes were denser and contained more iodo-Tg as compared with WT (Figure 8A and Supplemental Figure 5). To examine whether accumulation of iodo-Tg in lysosomes could be due to impaired lysosomal enzymatic machinery, we also looked at the expression and activity of cathepsin B and D. Both cathepsins were actually increased at the mRNA level, but cathepsin B activity and cathepsin D protein level were not appreciably affected in *Ctns*$^{-/-}$ thyrocytes. We concluded that TH release from Tg in lysosomes is further impaired in *Ctns*$^{-/-}$ thyrocytes, whereas major cathepsins are preserved, pointing instead to a defect in the lysosomal milieu, likely its redox status.

Discussion

In this study, we report for the first time that C57BL/6 *Ctns*$^{-/-}$ mice recapitulate the earliest and almost obligatory endocrine complication of cystinotic children, namely primary hypothyroidism. The longitudinal study of knockout mice thus allowed to delineate the early events of thyroid changes, presumably also occurring in affected children before the end-stage atrophy mostly documented in pathological samples. Two complementary pathogenic mechanisms were found to operate in *Ctns*$^{-/-}$ mice: 1) impaired Tg biosynthesis involving the unfolded protein response to ER stress and contributing to progressive colloid exhaustion; and 2) impaired lysosomal iodo-Tg proteolytic processing, thus defective TH release. Adaptation mechanisms include TSH increase, accelerated colloid uptake by macropinocytosis, thyrocyte hyperplasia/hyperthrophy combined with microvascular basket expansion, and accelerated cell turnover/apoptosis.

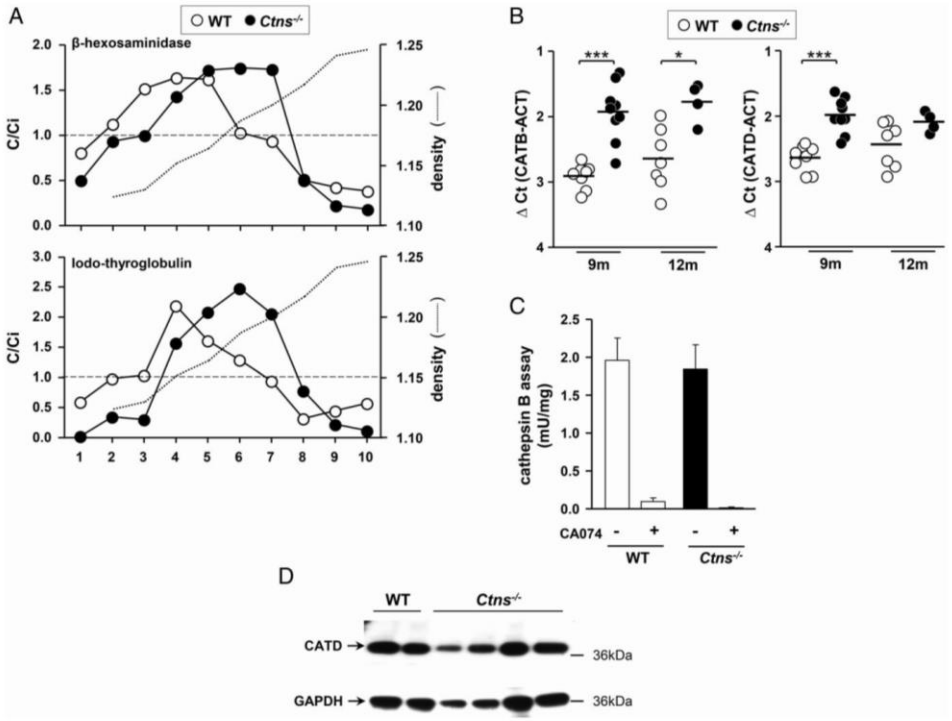

Figure 8. Subcellular fractionation of iodo-thyroglobulin distribution and assessment of hormonogenic cathepsins. A, Sucrose density gradients. Thyroids glands pooled from four WT (open symbols) or four *Ctns*$^{-/-}$ mice (filled symbols) were homogenized and postnuclear particles were resolved by isopycnic centrifugation into linear sucrose gradients. Ten fractions were collected from the bottom and analyzed for density (dotted lines), β-Hexosaminidase activity as lysosomal marker (upper panel), and iodo-Tg (lower panel; densitometry of Western blot bands with molecular weight >250 kDa, ie, the sum of monomer and oligomers). Results are expressed by reference to the sum of all fractions so that C/Ci indices greater than 1 indicate enrichment level over initial concentration (broken lines). Corresponding Western blots are shown in Supplemental Figure 5. In *Ctns*$^{-/-}$ mice, iodo-Tg accumulates in fractions corresponding to lysosomes, equilibrating at higher density as compared with WT mice. Representative experiment of two is shown. B–D, Cathepsins B/D expression and activity are not defective in *Ctns*$^{-/-}$ thyroid glands. B, Expression of cathepsin B and D mRNAs. Quantification by RT-qPCR of cathepsin B (CATB) and cathepsin D (CATD) mRNAs in WT and *Ctns*$^{-/-}$ thyroids collected at 9 and 12 months, normalized to actin mRNA (ACT) and presented as ΔCt values. C, Cathepsin B activity. Cathepsin B activity, assayed using benzyloxycarbonyl-L-phenylalanyl-L-arginine 4-methylcoumaryl-7-amide, is given by the difference in absence or presence of the specific inhibitor, CA-074; data normalized to protein concentration. D, Western blot for cathepsin D. Thyroid extracts from two WT and four *Ctns*$^{-/-}$ individual mice at 11–12 months were analyzed by Western blotting with antibodies to cathepsin D (CATD), using GAPDH for normalization in parallel blots.

In 9-month *Ctns*$^{-/-}$ mice, TSH was moderately increased with T_4 and T_3 values remaining normal. Increased TSH induced follicle-autonomous hyperplasia/hypertrophy and microvascular basket expansion but was not associated with significant decrease in global expression of iodo-Tg synthesis-related genes except Tg itself, nor cathepsins B and D or of the thyroid hormone transporter, Mct-8. Thus, primary hypothyroidism was adequately compensated at this age (subclinical) and originated from a more subtle mechanism. Immunofluorescence proved particularly useful to demonstrate proliferation, apoptosis, and microvasculature changes. In the integrated angiofollicular units, capillaries not only serve to passively feed thyrocytes and to collect TH but also take part in an active, bidirectional paracrine cross-talk that instructs follicular embryological differentiation (54). Furthermore, follicular changes upon iodine deficiency/goitrogenesis are closely associated with increased thyroid blood flow and vascular expansion (55, 56). Thus, expansion of follicular capillaries not only reflects increased tissue

doi: 10.1210/en.2014-1672

demands but also can be a useful independent functional marker of follicle activation.

The first key pathogenic finding of this study was activation of the UPR. Newly synthesized Tg accounts for greater than 50% of normal thyrocyte protein content (57) and can be further increased by TSH (58, 59). Professional secretory cells such as thyrocytes have a well-developed pathway for protein export and rely on a sophisticated quality control machinery to escape ER stress when overstimulated. However, when ER folding capacity is exceeded or fully abrogated by Tg point mutations (38, 60), UPR is triggered to attenuate protein synthesis, up-regulate folding capacity, and increase protein degradation by proteasomes. We here demonstrate that Tg accumulates in the dilated ER of *Ctns*$^{-/-}$ thyrocytes yet with decreased mRNA level despite higher TSH stimulation. Folding of core-glycosylated Tg necessitates the simultaneous assistance of a variety of ER-resident chaperones (eg, GRP78) and foldase (PDI), both of which were strongly increased in *Ctns*$^{-/-}$ thyroids. GRP78 is a major quality-control monitor of Tg folding status (61, 62). Formation of mixed-disulfide folding intermediates between Tg and the ER oxidoreductase, PDI, is crucial for Tg maturation and export (63). These chaperones functionally depend on ER redox homeostasis and high ATP levels, both of which are impaired in cystinosis (51, 64, 65). Combined with general concepts from literature, our data on *Ctns*$^{-/-}$ thyrocytes are thus consistent with the following hypotheses: 1) correct Tg disulfide bonding is slower due to impaired luminal redox, which results in misfolded/unfolded Tg accumulation in ER, triggering the UPR response; 2) consequently, slower ER exit/impaired secretion leads to ER dilatation and contributes to colloid exhaustion.

Activation of ER-resident chaperones associated with UPR has been analyzed in detail in a congenital hypothyroidism goiter due to a mutated Tg trafficking defect (38, 66, 67). In contrast, immortalized FRTL5 cells showed increased expression of ER chaperones upon activation of Tg synthesis by TSH independently of UPR (no alternative XBP-1 splicing or CHOP expression) (68). In most 9- and 12-month-old *Ctns*$^{-/-}$ thyroids, we here report the alternative splicing of XBP-1 as well as coordinated increased expression of ATF-4 and CHOP, strongly supporting activation of UPR in response to ER stress. This conclusion has several implications. XBP-1 transcriptional activation triggers ER expansion (69, 70), as we observed in *Ctns*$^{-/-}$ thyrocytes, but also promotes gene transcription of ER resident chaperones (71) and of proteins involved in ER-associated degradation of misfolded/unfolded protein by proteasome. Moreover, induced CHOP expression triggers apoptosis, in particular via the down-regulation of the major antiapoptotic regulator, Bcl-2 (for a review, see reference 40). This mechanism likely contributes to apoptotic thyrocyte shedding, as evidenced by the accumulation of cell remnants immunolabeled for cleaved caspase-3 in the *Ctns*$^{-/-}$ colloid.

Also consistent with a role for UPR in cystinotic thyroid physiopathology, activation of UPR has been demonstrated in cystinotic proximal tubular cells (37, 51, 72) and in several noncystinotic lysosomal storage diseases (72). Interestingly, rescue of Rab27a-dependent vesicular trafficking alleviated defective lysosomal transport and reduced ER stress in cystinotic proximal tubular cells (37). Rab27a is a Ras-related small GTPase that regulates vesicular transport and exocytosis in a variety of secretory cells, including thyrocytes. We therefore raise the possibility that, in the thyroid gland, lysosomal vesicular transport defect due to cystine overload may be linked to ER stress and UPR activation.

Our second key pathogenic observations in *Ctns*$^{-/-}$ thyrocytes relate to structural and functional endocytic alterations. These include the following: 1) induced macropinocytosis as expected for TSH stimulation; 2) retention of undigested iodo-Tg in enlarged (LAMP-1 immunolabeling) and denser endosomes/lysosomes (fractionation data), indicating defective Tg lysosomal degradation without alteration of lysosomal cathepsin expression and activity; and 3) progressive build-up of lysosomal cystine needles and exclusion of cystine-crystal bearing lysosomes from endocytic trafficking. Increased lysosomal density is better accounted for by protein (density 1.33 g/mL) than cystine crystal accumulation [1.73 g/mL (73)]. Similar alterations in the apical endocytic pathway have recently been demonstrated in *Ctns*$^{-/-}$ kidney PTCs, but lesions appeared earlier on and crystals were more prominent than in thyrocytes (33, 34). Although kidney PTCs and thyrocytes are both specialized for apical endocytosis, the constitutive endocytic rate is faster in PTCs, and the sequence of kidney then thyroid lesions in *Ctns*$^{-/-}$ mice also mimics the order of appearance of clinical signs in cystinotic children (4).

Lysosomal cargo retention despite conservation of hydrolytic equipment implies an altered lysosomal milieu, probably an impaired redox environment as immediate consequence of cystine sequestration. Alteration of intracellular redox potential due to defective lysosomal cystine export has been broadly associated to cystinosis physiopathology (64). Thyroid hormone release from Tg requires stepwise proteolytic processing by synergistic endopeptidases acting at specific sites around conserved N-terminal and C-terminal hormonogenic residues, allowing for final pruning by exopeptidases (23–27). However, the crucial endopeptidases cathepsin B and D were not appreciably affected in *Ctns*$^{-/-}$ thyrocytes. The need for a lysosomal supply of reducing equivalents to expose buried cathepsin-sensitive peptide is supported by the ac-

celeration of Tg degradation by lysosomal proteinases in a reducing environment (22, 74). In vitro, the addition of reduced glutathione boosted degradation of Tg by a thyroid phagolysosome-enriched fraction (22). This effect was originally attributed to substrate unfolding, a conclusion confirmed with highly purified cathepsin D and ^{125}I-thyroglobulin, supporting the concept that Tg unfolding by disulfide bond reduction renders it more susceptible to proteolysis (75). However, a combined effect on activation of cysteine proteinases is now well accepted (15, 23). A lysosomal cysteine import system has been demonstrated (14), but associated gene(s) remain to be identified. We thus propose that, in *Ctns*$^{-/-}$ thyrocytes, alteration of lysosomal redox status upon cystine accumulation impairs cathepsin action. In turn, defective lysosomal processing of iodo-Tg leads to decreased TH production, thus primary hypothyroidism, eliciting a compensatory TSH response, thyrocyte hypertrophy/hyperplasia, and integrated vascular expansion as well as accelerated endocytosis by macropinocytosis.

Endocrine dysfunction related to a lysosomal storage disorder is not unique to cystinosis. Subclinical hypothyroidism with elevated TSH has been reported in patients affected by Fabry disease [lysosomal galactosidase-A deficiency (76, 77) and Hurler syndrome/mucopolysaccharidosis type IH (α-L-iduronidase deficiency (78)], which are more frequent than cystinosis. However, to the best of our knowledge, their underlying thyroid physiopathology has not been explored. Comparison of Tg synthesis and processing into TH in corresponding knockout mouse models would be interesting.

In conclusion, 9-month-old C57BL/6 *Ctns*$^{-/-}$ mice recapitulate several key features of infantile cystinosis underlying compensated/subclinical hypothyroidism, namely chronically increased TSH, follicular activation and proliferation, and eventual thyrocyte lysosomal crystals. They also disclose early pathogenic, so far unreported mechanisms, such as ER stress triggering UPR, itself contributing to apoptosis; and impaired endolysosomal trafficking associated with defective lysosomal Tg processing. Combination of impaired Tg secretion and accelerated endocytosis provide a satisfactory explanation for colloid exhaustion. We suggest that defective Tg processing following silent accumulation of Tg-derived cystine (single substrate) is the primum movens event of the other functional and structural changes. Thus, C57BL/6 *Ctns*$^{-/-}$ mice are a useful model to better understand early pathogenic vs adaptative cascades leading to eventual cystinotic thyroid atrophy and to evaluate the stage-specific benefit (and limitations) of conventional (cysteamine) or new drugs to be developed as well as novel therapies such as gene and stem cell therapy (79–81). A particularly promising generic approach for gene therapy, validated in mice, is based on hematopoietic stem cell correction, by which immunocompatible grafted cells bearing normal cystinosin (or other) genes are selectively attracted to diseased tissue areas. We recently reported that hematopoietic stem cells project expansions, known as tunneling nanotubes, whereby they physically interconnect with diseased epithelial cells across basement laminae and can bidirectionally exchange lysosomes by tubulin-based motion (82).

Acknowledgments

We thank Dr E. Marbaix for helpful advice in thyroid pathology, Dr T. Arnould for valuable suggestions on endoplasmic reticulum stress, Dr C. Ris-Stalpers for providing anti-iodo-Tg antibodies, and Mrs L. Thanh for assistance with the electron microscopy.

Address all correspondence and requests for reprints to: Pierre J. Courtoy, PhD, de Duve Institute and Université Catholique de Louvain, 75 Avenue Hippocrate, PO Box B1.75.05, 1200 Brussels, Belgium. E-mail: pierre. courtoy@uclouvain.be.

The content is solely the responsibility of the authors and does not necessarily represent the official views of the National Institutes of Health.

H.P.G.C. is Postdoctoral Researcher and C.E.P. is Senior Research Associate at Belgian Fonds de la Recherche Scientifique (Belgium).

This work was mainly supported by the Cystinosis Research Foundation, Belgian Science Policy Office-Interuniversity Attraction Poles Program Grant IAP P7/43-BeMGI, Belgian Fonds de la Recherche Scientifique and Actions de Recherche Concertées (to C.E.P. and P.J.C.), National Institutes of Health Grants RO1-DK090058, R21-DK090548, and RO1-DK099338 (to S.C.). This work was also supported in part by Grants R37-DK15070 from the National Institutes of Health (to S.R.). The Platform for Imaging Cells and Tissues was financed by National Lottery, Région Bruxelloise, Région Wallonne, Université Catholique de Louvain, and de Duve Institute (to P.J.C.).

Disclosure Summary: The authors have nothing to disclose.

References

1. **Van Vliet G.** Development of the thyroid gland: lessons from congenitally hypothyroid mice and men. *Clin Genet*. 2003;63(6):445–455.
2. **Grasberger H, Refetoff S. Congenital defects of thyroid hormone synthesis. In: Weiss RE, Refetoff S.** eds. *Genetics Diagnosis of Endocrine Disorders*. Amsterdam, The Netherlands: Academic Press, Elsevier, Inc; 2010:87–95.
3. **Gahl WA, Thoene JG, Schneider JA.** Cystinosis. *N Engl J Med*. 2002;347(2):111–121.
4. **Gahl WA, Thoene J.** Cystinosis: a disorder of lysosomal membrane transport. In: Scriver CR, Beaudet AL, Sly WS, Valle D, Childs B, Kinzler KW, Vogelstein B, eds. *The Metabolic and Molecular Basis*

of Inherited Disease. Vol 3, 8th ed. New York: McGraw-Hill Companies, Inc; 2001:5085–5108. *Online update 2013*.
5. **Chan AM, Lynch MJ, Bailey JD, Ezrin C, Fraser D.** Hypothyroidism in cystinosis. A clinical, endocrinologic and histologic study involving sixteen patients with cystinosis. *Am J Med*. 1970;48(6):678–692.
6. **Broyer M, Niaudet P.** Cystinosis. In: Saudubray JM, van den Berghe G, Walter JH, eds. *Inborn Metabolic Diseases*: Berlin Heidelberg: Springer; 2012:617–624.
7. **Cherqui S, Kalatzis V, Trugnan G, Antignac C.** The targeting of cystinosin to the lysosomal membrane requires a tyrosine-based signal and a novel sorting motif. *J Biol Chem*. 2001;276(16):13314–13321.
8. **Kalatzis V, Cherqui S, Antignac C, Gasnier B.** Cystinosin, the protein defective in cystinosis, is a H(+)-driven lysosomal cystine transporter. *EMBO J*. 2001;20(21):5940–5949.
9. **Jezegou A, Llinares E, Anne C, et al.** Heptahelical protein PQLC2 is a lysosomal cationic amino acid exporter underlying the action of cysteamine in cystinosis therapy. *Proc Natl Acad Sci USA*. 2012;109(50):E3434–E3443.
10. **Lucky AW, Howley PM, Megyesi K, Spielberg SP, Schulman JD.** Endocrine studies in cystinosis: compensated primary hypothyroidism. *J Pediatr*. 1977;91(2):204–210.
11. **Kimonis VE, Troendle J, Rose SR, Yang ML, Markello TC, Gahl WA.** Effects of early cysteamine therapy on thyroid function and growth in nephropathic cystinosis. *J Clin Endocrinol Metab*. 1995;80(11):3257–3261.
12. **Brodin-Sartorius A, Tete MJ, Niaudet P, et al.** Cysteamine therapy delays the progression of nephropathic cystinosis in late adolescents and adults. *Kidney Int*. 2012;81(2):179–189.
13. **Emma F, Nesterova G, Langman C, et al.** Nephropathic cystinosis: an international consensus document. *Nephrol Dialysis Transplant*. 2014;29(suppl 4):iv87–94.
14. **Pisoni RL, Acker TL, Lisowski KM, Lemons RM, Thoene JG.** A cysteine-specific lysosomal transport system provides a major route for the delivery of thiol to human fibroblast lysosomes: possible role in supporting lysosomal proteolysis. *J Cell Biol*. 1990;110(2):327–335.
15. **Brix K, Lemansky P, Herzog V.** Evidence for extracellularly acting cathepsins mediating thyroid hormone liberation in thyroid epithelial cells. *Endocrinology*. 1996;137(5):1963–1974.
16. **Friedrichs B, Tepel C, Reinheckel T, et al.** Thyroid functions of mouse cathepsins B, K, and L. *J Clin Invest*. 2003;111(11):1733–1745.
17. **Edelhoch H, Rall J.** The proteins and enzymes of the thyroid In: Pitt-Rivers R, Trotter W, eds. *The Thyroid Gland*. London: Butterworths; 1964:113–130.
18. **Herzog V, Berndorfer U, Saber Y.** Isolation of insoluble secretory product from bovine thyroid: extracellular storage of thyroglobulin in covalently cross-linked form. *J Cell Biol*. 1992;118(5):1071–1083.
19. **Gerard AC, Denef JF, Colin IM, van den Hove MF.** Evidence for processing of compact insoluble thyroglobulin globules in relation with follicular cell functional activity in the human and the mouse thyroid. *Eur J Endocrinol*. 2004;150(1):73–80.
20. **Klein M, Gestmann I, Berndorfer U, Schmitz A, Herzog V.** The thioredoxin boxes of thyroglobulin: possible implications for intermolecular disulfide bond formation in the follicle lumen. *Biol Chem*. 2000;381(7):593–601.
21. **Berndorfer U, Wilms H, Herzog V.** Multimerization of thyroglobulin (TG) during extracellular storage: isolation of highly cross-linked TG from human thyroids. *J Clin Endocrinol Metab*. 1996;81(5):1918–1926.
22. **Peake BL, Balasubramaniam K, Deiss WP.** Effect of reduced glutathione on the proteolysis of intraparticulate and native thyroglobulin. *Biochim Biophys Acta*. 1967;148:689–702.
23. **Yoshinari M, Taurog A.** Lysosomal digestion of thyroglobulin: role of cathepsin D and thiol proteases. *Endocrinology*. 1985;117(4):1621–1631.
24. **Dunn AD, Dunn JT.** Cysteine proteinases from human thyroids and their actions on thyroglobulin. *Endocrinology*. 1988;123(2):1089–1097.
25. **Dunn AD, Crutchfield HE, Dunn JT.** Proteolytic processing of thyroglobulin by extracts of thyroid lysosomes. *Endocrinology*. 1991;128(6):3073–3080.
26. **Dunn AD, Myers HE, Dunn JT.** The combined action of two thyroidal proteases releases T4 from the dominant hormone-forming site of thyroglobulin. *Endocrinology*. 1996;137(8):3279–3285.
27. **Nakagawa H, Ohtaki S.** Thyroxine (T4) release from thyroglobulin and its T4-containing peptide by thyroid thiol proteases. *Endocrinology*. 1985;116(4):1433–1439.
28. **Marino M, McCluskey RT.** Role of thyroglobulin endocytic pathways in the control of thyroid hormone release. *Am J Physiol Cell Physiol*. 2000;279(5):C1295–C1306.
29. **Croizet-Berger K, Daumerie C, Couvreur M, Courtoy PJ, van den Hove MF.** The endocytic catalysts, Rab5a and Rab7, are tandem regulators of thyroid hormone production. *Proc Natl Acad Sci USA*. 2002;99(12):8277–8282.
30. **van den Hove MF, Croizet-Berger K, Tyteca D, Selvais C, de Diesbach P, Courtoy PJ.** Thyrotropin activates guanosine 5′-diphosphate/guanosine 5′-triphosphate exchange on the rate-limiting endocytic catalyst, Rab5a, in human thyrocytes in vivo and in vitro. *J Clin Endocrinol Metab*. 2007;92(7):2803–2810.
31. **Fujita H.** Functional morphology of the thyroid. *Int Rev Cytol*. 1988;113:145–185.
32. **Di Cosmo C, Liao XH, Dumitrescu AM, Philp NJ, Weiss RE, Refetoff S.** Mice deficient in MCT8 reveal a mechanism regulating thyroid hormone secretion. *J Clin Invest*. 2010;120(9):3377–3388.
33. **Gaide Chevronnay HP, Janssens V, Van Der Smissen P, et al.** Time course of pathogenic and adaptation mechanisms in cystinotic mouse kidneys. *J Am Soc Nephrol*. 2014;25(6):1256–1269.
34. **Raggi C, Luciani A, Nevo N, Antignac C, Terryn S, Devuyst O.** Dedifferentiation and aberrations of the endolysosomal compartment characterize the early stage of nephropathic cystinosis. *Hum Mol Genet*. 2014;23(9):2266–2278.
35. **Cherqui S, Sevin C, Hamard G, et al.** Intralysosomal cystine accumulation in mice lacking cystinosin, the protein defective in cystinosis. *Mol Cell Biol*. 2002;22(21):7622–7632.
36. **Nevo N, Chol M, Bailleux A, et al.** Renal phenotype of the cystinosis mouse model is dependent upon genetic background. *Nephrol Dialysis Transpl*. 2010;25(4):1059–1066.
37. **Johnson JL, Napolitano G, Monfregola J, Rocca CJ, Cherqui S, Catz SD.** Upregulation of the Rab27a-dependent trafficking and secretory mechanisms improves lysosomal transport, alleviates endoplasmic reticulum stress, and reduces lysosome overload in cystinosis. *Mol Cell Biol*. 2013;33(15):2950–2962.
38. **Baryshev M, Sargsyan E, Wallin G, et al.** Unfolded protein response is involved in the pathology of human congenital hypothyroid goiter and rat non-goitrous congenital hypothyroidism. *J Mol Endocrinol*. 2004;32(3):903–920.
39. **Hetz C.** The unfolded protein response: controlling cell fate decisions under ER stress and beyond. *Nat Rev Mol Cell Bio*. 2012;13(2):89–102.
40. **Szegezdi E, Logue SE, Gorman AM, Samali A.** Mediators of endoplasmic reticulum stress-induced apoptosis. *EMBO Rep*. 2006;7(9):880–885.
41. **Pohlenz J, Maqueem A, Cua K, Weiss RE, Van Sande J, Refetoff S.** Improved radioimmunoassay for measurement of mouse thyrotropin in serum: strain differences in thyrotropin concentration and thyrotroph sensitivity to thyroid hormone. *Thyroid*. 1999;9(12):1265–1271.
42. **Pierreux CE, Cordi S, Hick AC, et al.** Epithelial: endothelial cross-talk regulates exocrine differentiation in developing pancreas. *Dev Biol*. 2010;347(1):216–227.
43. **Gaide Chevronnay HP, Cornet PB, Delvaux D, et al.** Opposite regulation of transforming growth factors-β2 and -β3 expression in the human endometrium. *Endocrinology*. 2008;149(3):1015–1025.

44. **Zachara NE, Vosseller K, Hart GW.** Detection and analysis of proteins modified by O-linked N-acetylglucosamine. *Curr Protoc Protein Sci*. 2011;Chapter 12:Unit12.8.
45. **Barrett AJ.** Fluorimetric assays for cathepsin B and cathepsin H with methylcoumarylamide substrates. *Biochem J*. 1980;187(3):909–912.
46. **Colin IM, Denef JF, Lengele B, Many MC, Gerard AC.** Recent insights into the cell biology of thyroid angiofollicular units. *Endocr Rev*. 2013;34(2):209–238.
47. **Coclet J, Foureau F, Ketelbant P, Galand P, Dumont JE.** Cell population kinetics in dog and human adult thyroid. *Clin Endocrinol (Oxf)*. 1989;31(6):655–665.
48. **Park MA, Thoene JG.** Potential role of apoptosis in development of the cystinotic phenotype. *Pediatr Nephrol*. 2005;20(4):441–446.
49. **Sansanwal P, Kambham N, Sarwal MM.** Caspase-4 may play a role in loss of proximal tubules and renal injury in nephropathic cystinosis. *Pediatr Nephrol*. 2010;25(1):105–109.
50. **Leonardi A, Vito P, Mauro C, et al.** Endoplasmic reticulum stress causes thyroglobulin retention in this organelle and triggers activation of nuclear factor-κB via tumor necrosis factor receptor-associated factor 2. *Endocrinology*. 2002;143(6):2169–2177.
51. **Sansanwal P, Li L, Hsieh SC, Sarwal MM.** Insights into novel cellular injury mechanisms by gene expression profiling in nephropathic cystinosis. *J Inherit Metab Dis*. 2010;33(6):775–786.
52. **Oslowski CM, Urano F.** Measuring ER stress and the unfolded protein response using mammalian tissue culture system. *Methods Enzymol*. 2011;490:71–92.
53. **Samali A, Fitzgerald U, Deegan S, Gupta S.** Methods for monitoring endoplasmic reticulum stress and the unfolded protein response. *Int J Cell Biol*. 2010;2010:830307.
54. **Hick AC, Delmarcelle AS, Bouquet M, et al.** Reciprocal epithelial: endothelial paracrine interactions during thyroid development govern follicular organization and C-cells differentiation. *Dev Biol*. 2013;381(1):227–240.
55. **Ramsden JD, Buchanan MA, Egginton S, Watkinson JC, Mautner V, Eggo MC.** Complete inhibition of goiter in mice requires combined gene therapy modification of angiopoietin, vascular endothelial growth factor, and fibroblast growth factor signaling. *Endocrinology*. 2005;146(7):2895–2902.
56. **Imada M, Kurosumi M, Fujita H.** Three-dimensional aspects of blood vessels in thyroids from normal, low iodine diet-treated, TSH-treated, and PTU-treated rats. *Cell Tissue Res*. 1986;245(2):291–296.
57. **Van Herle AJ, Vassart G, Dumont JE.** Control of thyroglobulin synthesis and secretion (first of two parts). *N Engl J Med*. 1979; 301(5):239–249.
58. **Van Heuverswyn B, Streydio C, Brocas H, Refetoff S, Dumont J, Vassart G.** Thyrotropin controls transcription of the thyroglobulin gene. *Proc Natl Acad Sci USA*. 1984;81(19):5941–5945.
59. **Van Heuverswyn B, Leriche A, Van Sande J, Dumont JE, Vassart G.** Transcriptional control of thyroglobulin gene expression by cyclic AMP. *FEBS Lett*. 1985;188(2):192–196.
60. **Kim PS, Lee J, Jongsamak P, et al.** Defective protein folding and intracellular retention of thyroglobulin-R19K mutant as a cause of human congenital goiter. *Mol Endocrinol*. 2008;22(2):477–484.
61. **Kim PS, Bole D, Arvan P.** Transient aggregation of nascent thyroglobulin in the endoplasmic reticulum: relationship to the molecular chaperone, BiP. *J Cell Biol*. 1992;118(3):541–549.
62. **Kim PS, Arvan P.** Calnexin and BiP act as sequential molecular chaperones during thyroglobulin folding in the endoplasmic reticulum. *J Cell Biol*. 1995;128(1–2):29–38.
63. **Di Jeso B, Park YN, Ulianich L, et al.** Mixed-disulfide folding intermediates between thyroglobulin and endoplasmic reticulum resident oxidoreductases ERp57 and protein disulfide isomerase. *Mol Cell Biol*. 2005;25(22):9793–9805.
64. **Levtchenko E, de Graaf-Hess A, Wilmer M, van den Heuvel L, Monnens L, Blom H.** Altered status of glutathione and its metabolites in cystinotic cells. *Nephrol Dialysis Transpl*. 2005;20(9): 1828–1832.
65. **Levtchenko EN, Wilmer MJ, Janssen AJ, et al.** Decreased intracellular ATP content and intact mitochondrial energy generating capacity in human cystinotic fibroblasts. *Pediatr Res*. 2006;59(2): 287–292.
66. **Medeiros-Neto G, Kim PS, Yoo SE, et al.** Congenital hypothyroid goiter with deficient thyroglobulin. Identification of an endoplasmic reticulum storage disease with induction of molecular chaperones. *J Clin Invest*. 1996;98(12):2838–2844.
67. **Kim PS, Kwon OY, Arvan P.** An endoplasmic reticulum storage disease causing congenital goiter with hypothyroidism. *J Cell Biol*. 1996;133(3):517–527.
68. **Christis C, Fullaondo A, Schildknegt D, Mkrtchian S, Heck AJ, Braakman I.** Regulated increase in folding capacity prevents unfolded protein stress in the ER. *J Cell Sci*. 2010;123(Pt 5):787–794.
69. **Sriburi R, Jackowski S, Mori K, Brewer JW.** XBP1: a link between the unfolded protein response, lipid biosynthesis, and biogenesis of the endoplasmic reticulum. *J Cell Biol*. 2004;167(1):35–41.
70. **Shaffer AL, Shapiro-Shelef M, Iwakoshi NN, et al.** XBP1, downstream of Blimp-1, expands the secretory apparatus and other organelles, and increases protein synthesis in plasma cell differentiation. *Immunity*. 2004;21(1):81–93.
71. **Lee AH, Iwakoshi NN, Glimcher LH.** XBP-1 regulates a subset of endoplasmic reticulum resident chaperone genes in the unfolded protein response. *Mol Cell Biol*. 2003;23(21):7448–7459.
72. **Wei H, Kim SJ, Zhang Z, Tsai PC, Wisniewski KE, Mukherjee AB.** ER and oxidative stresses are common mediators of apoptosis in both neurodegenerative and non-neurodegenerative lysosomal storage disorders and are alleviated by chemical chaperones. *Hum Mol Genet*. 2008;17(4):469–477.
73. **Schulman JD, Bradley KH, Seegmiller JE.** Cystine: compartmentalization within lysosomes in cystinotic leukocytes. *Science*. 1969; 166(3909):1152–1154.
74. **Pisarev MA, Dumont JE.** The role of reduced glutathione in thyroglobulin proteolysis iv vitro. *Acta Endocrinol*. 1975;79(1):76–85.
75. **Dunn AD, Dunn JT.** Thyroglobulin degradation by thyroidal proteases: action of purified cathepsin D. *Endocrinology*. 1982;111(1): 280–289.
76. **Faggiano A, Pisani A, Milone F, et al.** Endocrine dysfunction in patients with Fabry disease. *J Clin Endocrinol Metab*. 2006;91(11): 4319–4325.
77. **Hauser AC, Gessl A, Lorenz M, Voigtlander T, Fodinger M, Sunder-Plassmann G.** High prevalence of subclinical hypothyroidism in patients with Anderson-Fabry disease. *J Inherit Metab Dis*. 2005; 28(5):715–722.
78. **Polgreen LE, Tolar J, Plog M, et al.** Growth and endocrine function in patients with Hurler syndrome after hematopoietic stem cell transplantation. *Bone Marrow Transpl*. 2008;41(12):1005–1011.
79. **Syres K, Harrison F, Tadlock M, et al.** Successful treatment of the murine model of cystinosis using bone marrow cell transplantation. *Blood*. 2009;114(12):2542–2552.
80. **Yeagy BA, Harrison F, Gubler MC, Koziol JA, Salomon DR, Cherqui S.** Kidney preservation by bone marrow cell transplantation in hereditary nephropathy. *Kidney Int*. 2011;79(11):1198–1206.
81. **Harrison F, Yeagy BA, Rocca CJ, Kohn DB, Salomon DR, Cherqui S.** Hematopoietic stem cell gene therapy for the multisystemic lysosomal storage disorder cystinosis. *Mol Ther*. 2013;21(2):433–444.
82. **Naphade S, Sharma J, Gaide Chevronnay HP, et al.** Brief reports: lysosomal cross-correction by hematopoietic stem cell-derived macrophages via tunneling nanotubes. *Stem Cells*. 2015;33(1):301–309.

Supplemental Table . List of primer sequences.

gene	forward primer (5' → 3')	reverse primer (5' →3')
Tg	TGGGACGTGAAAGGGGAATGGTGC	GTGAGCTTTTGGAATGGCAGGCGA
Tpo	TGCCAACAGAAGCATGGGCAAC	GCACAAAGTTCCCATTGTCCAC
TSHr	CTGCGGGGCAAAGAGTGTGC	AGGGGAGCTCTGTCAAGGCA
Nis	AGCAGGCTTAGCTGTATCCC	AGCCCCGTAGTAGAGATAGGAG
Pdn	GACTGTAAAGACCCTCTTGATCTGA	GGAAGCAAGTCTACGCATGG
Duox2	TCCAGAAGGCGCTGAACAG	GCGACCAAAGTGGGTGATG
Duoxa2	CGTTAACATTACACTCCGAGGAACA	CAGAATGCCACCCACAGTGT
Dehal1	ACACCGCCCCAGTTCTGAT	ACCGTCACTAGCCCTGCATT
Mct8	GTGCTCTTGGTGTGCATTGG	CCGAAGTCCCGGCATAGG
Catb	AGCCATTTCTGACCGAACCT	TTGTCCAGAAGCTCCATGCT
Catd	GTCGGACTATGACGGAGGT	TCGCCATAGTACTGGGCATC
Rab5	GACTTAGCAAATAAAAGAGC	TCACTAAGGTCTACTCCTCG
Rab7	TCAATATGCGTCCCTCCTC	TGGAGTTTCTTTTGGCAGC
Xbp1	GAACCAGGAGTTAAGAACACG	GGGTCCAAGTTGTCCAGAATGC
Atf-4	GGGTTCTGTCTTCCACTCCA	AAGCAGCAGAGTCAGGCTTTC
Chop	CCACCACACCTGAAAGCAGAA	AGGTGAAAGGCAGGGACTCA
Actin	TCCTGAGCGCAAGTACTCTGT	CTGATCCACATCTGCTGGAAG

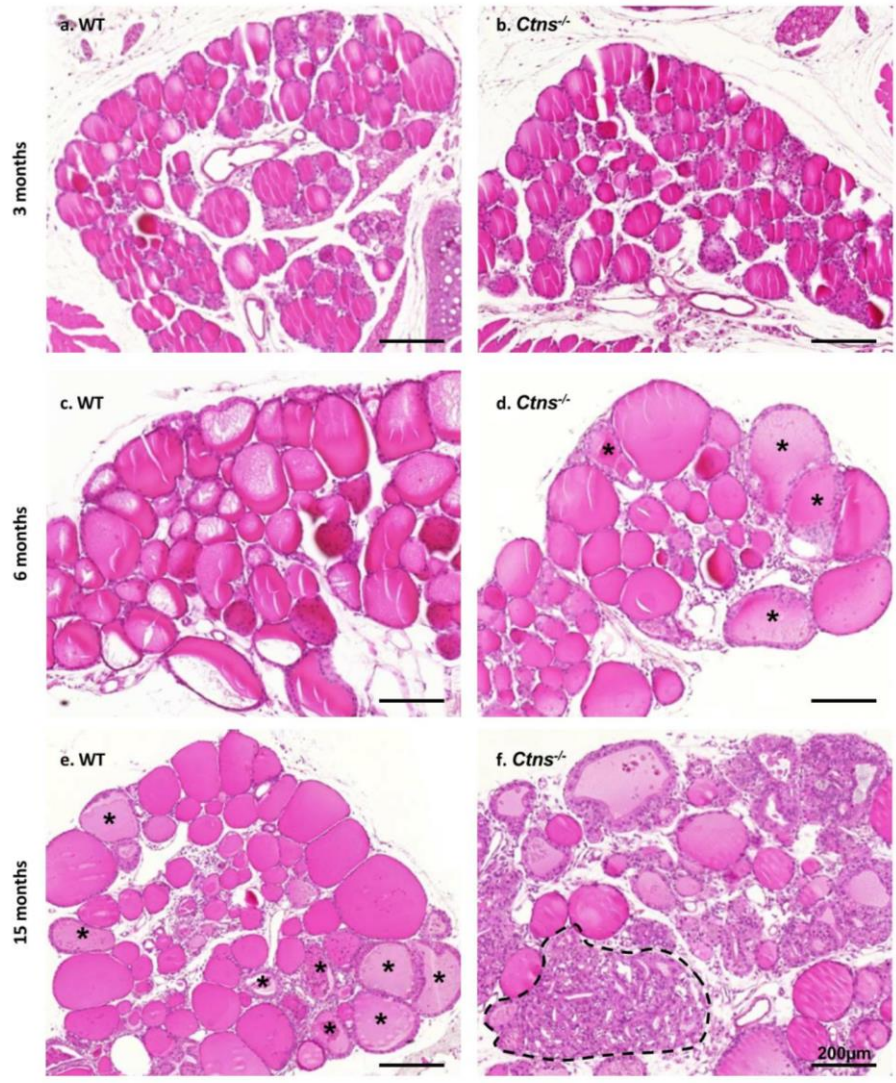

Supplemental Figure 1 (complements Fig1B). Earlier and later time course of histological lesions. Hematoxylin-eosin staining of paraffin sections from WT (a,c,e) and *Ctns*$^{-/-}$ (b,d,f) thyroids at 3 (a-b), 6 (c,d) and 15 months (e,f). At 3 months, no difference is detected between WT and *Ctns*$^{-/-}$ thyroid follicles. At 6 months, a few *Ctns*$^{-/-}$ follicles are becoming hyperplastic and their colloid is paler (asterisks at d), but most of the tissue appears histologically normal. At 15 months, WT mice also present a limited number of hyperplastic follicles (asterisks at e). In contrast, most *Ctns*$^{-/-}$ follicles are abnormal and some areas are barely recognizable (example enclosed by broken line) yet a few follicles still appear resting and retain a dense colloid. All scale bars, 200 µm.

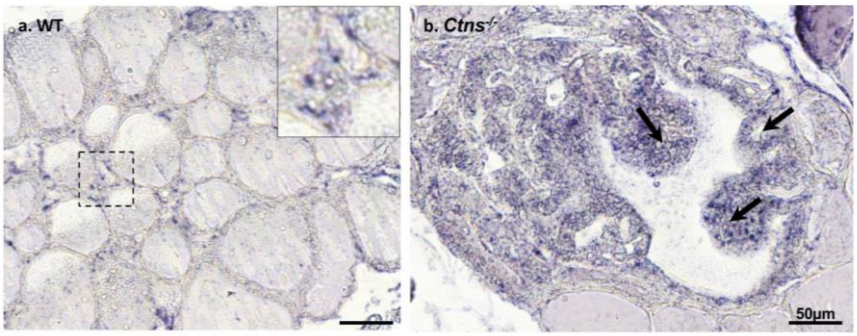

Supplemental Figure 2 (complements Fig1C). Hyperplastic thyrocytes strongly express vascular endothelial growth factor-a (Vegfa). mRNA localization by *in situ* hybridization in WT **(a)** and *Ctns*$^{-/-}$ thyroid **(b)** at 9 months. Increased Vegf-a expression in hyperplastic thyrocytes correlates with blood capillaries recruitment/expansion, especially in papillary projections (arrows). All scale bars, 50 µm.

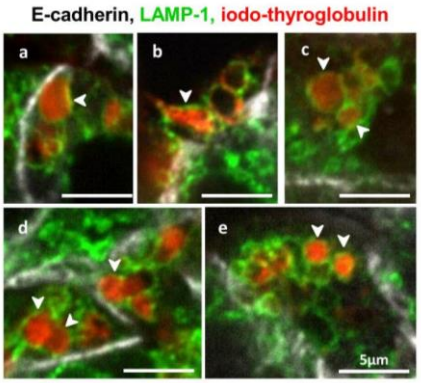

Supplemental Figure 3 (complements Fig7). Iodo-Tg is retained in lysosomes. Representative images by confocal immunofluorescence of vesicles filled with iodo-Tg (red) and labeled at their membrane by LAMP-1 (green) in hypertrophic *Ctns*$^{-/-}$ thyrocytes (E-cadherin, white).

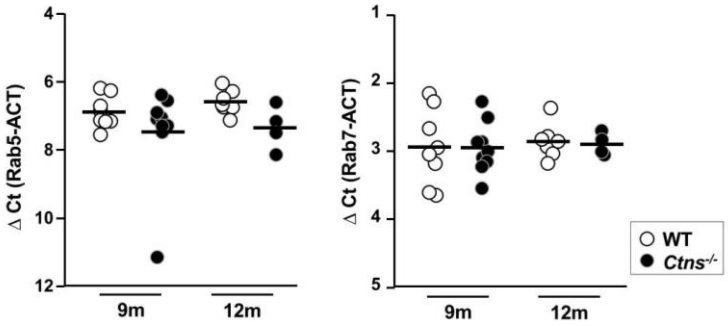

Supplemental Figure 4. Rab5 and Rab7 mRNA expression is not affected in *Ctns*$^{-/-}$ thyroid (complements Fig4). Quantification by RT-qPCR of Rab5 and Rab7 mRNAs in WT and *Ctns*$^{-/-}$ thyroids collected at 9 and 12 months, normalized to actin (ACT) and presented as ΔCt values. No difference is statistically significant.

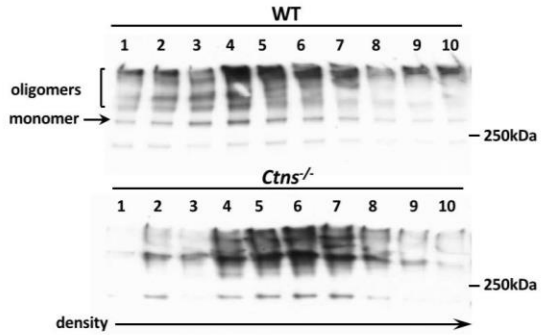

Supplemental Figure 5. Subcellular fractionation of iodo-thyroglobulin distribution Thyroids glands from 4 WT or *Ctns*$^{-/-}$ mice were homogenized and postnuclear supernatants were resolved in sucrose gradient. Ten fractions were collected and analysed for iodo-thyroglobulin by western blotting In *Ctns*$^{-/-}$ mice, iodo-thyroglobulin equilibrates in fractions corresponding to lysosomes with higher density compared to WT mice.

BRIEF RESEARCH REPORT

Hematopoietic stem cells transplantation can normalize thyroid function in a cystinosis mouse model

H.P. Gaide Chevronnay[1,*], V. Janssens[1,*], P. Van Der Smissen[1], C. Rocca[2], X.H. Liao[3], S. Refetoff[3], C.E. Pierreux[1], S. Cherqui[3,#], and P.J. Courtoy[1,#]

1, Cell Biology Unit, de Duve Institute & Université catholique de Louvain, Brussels, Belgium (H.P.G.C., V.J., C.E.P., P.J.C.); 2, Department of Pediatrics, Division of Genetics, University of California San Diego, CA, USA (C.R, SC); 3, Department of Medicine (X.H.L., S.R.), Pediatrics and Genetics (S.R), The University of Chicago, Chicago, IL, USA

Hypothyroidism is the most frequent and earliest endocrine complication in cystinosis, a multisystemic lysosomal storage disease caused by defective transmembrane cystine transporter, cystinosin (*CTNS* gene). We recently demonstrated in *Ctns*$^{-/-}$ mice that altered thyroglobulin biosynthesis associated with endoplasmic reticulum stress, combined with defective lysosomal processing, caused hypothyroidism. In *Ctns*$^{-/-}$ kidney, hematopoietic stem cell (HSC) transplantation provides long-term functional and structural protection. Tissue repair involves transfer of cystinosin-bearing lysosomes from HSCs differentiated as F4/80 macrophages into deficient kidney tubular cells, via tunnelling nanotubes (TNTs) that cross basement laminae. Here, we evaluated the benefit of HSCs transplantation for cystinotic thyroid and investigated underlying mechanisms. HSC engraftment in *Ctns*$^{-/-}$ thyroid drastically decreased cystine accumulation, normalized TSH level and corrected the structure of a large fraction of thyrocytes. In the thyroid microenvironment, HSCs differentiated into a distinct, mixed macrophage/dendritic cell lineage expressing CD45 and MHCII but low CD11b and F4/80. Grafted HSCs closely apposed to follicles and produced TNT-like extensions that crossed follicular basement laminae. HSCs themselves further squeezed into follicles, allowing extensive contact with thyrocytes, but did not transdifferentiate into Nkx2.1-expressing cells. Our observations revealed significant differences of basement lamina porosity between thyroid and kidney, and/or intrinsic macrophage invasive properties once in the thyroid microenvironment. The contrast between extensive thyrocyte protection and low HSC abundance at steady state suggests multiple sequential encounters and/or remnant impact. This is the first report demonstrating the potential of HSCs transplantation to correct thyroid disease, and supports a major multisystemic benefit of stem cells therapy for cystinosis.

Infantile cystinosis is an inherited multisystem lysosomal storage disease, where cystine, an obligatory degradation product of disulphide-bounded proteins, fails to exit lysosome due to genetic inactivation of its transmembrane transporter, cystinosin (*CTNS* gene) (1). Additional roles of cystinosin, such as mTORC1 regulation, have recently been demonstrated (2). Cystinosis typically manifests itself before one year of age as renal Fanconi syndrome, ie, generalized proximal tubular cell (PTC) dysfunction, and inevitably evolves to renal insufficiency. Primary ("TSH-compensated") hypothyroidism is the earliest and almost obligatory endocrine dysfunction in cystinotic children (3, 4).

Cystinosin-deficient mice in a strict congenic C57/BL6 background (*Ctns*$^{-/-}$ mice) mimic human cystinosis (5) and proved informative to unravel early pathogenic and adaptive mechanisms in kidneys and thyroid (6–9). In *Ctns*$^{-/-}$ kidneys, impaired apical receptor-mediated endocytosis, endolysosomal trafficking and lysosomal proteolysis are associated to PTC dedifferentiation (7). In *Ctns*$^{-/-}$ thyroid,

ISSN Print 0013-7227 ISSN Online 1945-7170
Printed in USA

Received August 28, 2015. Accepted January 20, 2016.

Abbreviations:

altered thyroglobulin biosynthesis with endoplasmic reticulum (ER) stress, combined with defective lysosomal processing of iodothyroglobulin, lead to impaired thyroid hormone production, resulting in subclinical hypothyroidism (increased TSH), thyrocyte hyperplasia/hypertrophy and accelerated cell turnover (8).

Lysosomal cystine accumulation can be corrected by substrate depletion therapy with cysteamine, the only current approved drug. Cysteamine reacts with lysosomal cystine to form mixed cysteamine/cysteine disulphide that exits lysosomes by the lysine transporter system (10). However, cysteamine therapy is very demanding and even early implementation in compliant patients fails to prevent renal insufficiency and thyroid dysfunction (11, 12). Alternative therapies are thus needed. Recent reports demonstrated a major benefit of hematopoietic stem cell (HSC) transplantation to prevent kidney disease progression and corneal defects in *Ctns*$^{-/-}$ mice, as evidenced by decreased cystine level and long-term functional protection (13–16). Engrafted HSC-derived cells mostly expressed the common macrophage markers F4/80 and MHCII and did not fuse with kidney epithelial cells or keratocytes (15–17). In coculture experiments, bone marrow-derived macrophages generated tunnelling nanotubes (TNTs) whereby cystinosin bearing-lysosomes were transported into Ctns-deficient fibroblasts (17). Conversely, cystine-loaded lysosomes of Ctns-deficient fibroblasts used the same physical connection towards WT macrophages, to fuse with the competent lysosomal pool (17). In vivo, HSCs grafted in *Ctns*$^{-/-}$ kidney also generated TNT-like structures that crossed basement laminae and connected with epithelial cells which acquired cystinosin (17). These data provided the first demonstration of cross-correction of a genetic lysosomal storage disease. The same mechanism was recently documented in the cornea (16). We here document the remarkable benefits of HSC transplantation in *Ctns*$^{-/-}$ thyroid and define structural protective mechanisms.

Materials and Methods

Mice

Wild-type *Ctns*$^{+/+}$ (WT) eGFP-transgenic mice (C57BL/6-Tg(ACTB-EGFP)1Osb/J) were from Jackson Laboratory. Cross-breeding of DsRed-transgenic mice (B6.Cg-Tg(CAG-DsRed*MST)1Nagy/J; Jackson Laboratory) with C57BL/6 *Ctns*$^{-/-}$ mice generated by Dr. C. Antignac (5) produced transgenic DsRed *Ctns*$^{-/-}$ mice, ubiquitously expressing the DsRed fluorescent protein (15). Protocols were approved by UCSD Animal Care and Use Committee. Mice were fed ad libitum with pellets containing 3 mg/kg iodine (Harlan Laboratories).

HSCs isolation and transplantation

Bone marrow cells were collected from WT eGFP-transgenic mice. Sca1^{+} HSCs selected by immunomagnetic separation (Miltenyi Biotec) were transplanted i.v. into 2-months old DsRed *Ctns*$^{-/-}$ mice, irradiated (8Gy) on the previous day (17). Since histological changes appeared in *Ctns*$^{-/-}$ thyroid around 6 months and became prominent 2–3 months thereafter (8), *Ctns*$^{-/-}$ mice transplanted with WT-eGFP HSCs ("grafted *Ctns*$^{-/-}$ mice") were analyzed at 8 months of age/6 months post-transplant and compared to age-matched WT and *Ctns*$^{-/-}$ mice. Older mice were occasionally examined. We studied 10 wild-type (4 males; 6 females), 15 *Ctns*$^{-/-}$ mice (4 males; 11 females) and 16 grafted *Ctns*$^{-/-}$ mice (6 males; 10 females).

Biochemical assays

Thyroid cystine and plasma TSH, T3 and T4 were measured as described (14, 18).

Microscopy

Perfusion-fixed thyroids were dissected, postfixed overnight with 4% neutral-buffered formaldehyde (4%F). Thyroid lobes were either equilibrated in 20% sucrose, embedded in Tissue-Tek/O.C.T. and snap-frozen in isopentane or processed for paraffin embedding. For histological analysis, 4 μm-thick paraffin sections were stained with hematoxylin/eosin. Immunofluorescence was performed as described, using antibodies listed in Table 1 (7). HSCs were identified by immunofluorescence instead of intrinsic GFP fluorescence, because of its inactivation during tissue paraffin processing and rapid photobleaching in frozen sections; and to amplify detection sensitivity in cytoplasmic extensions. For detection of inflammatory cell markers, blocking solution with 10% normal goat serum and 2% milk was used. Alexa-fluor antibodies were selected, at the exclusion of red fluorophores for frozen sections, to avoid confusion with DsRed endogenous emission. Antigen retrieval in citrate buffer pH 6.0 was performed for E-cadherin, LAMP-1, KDEL, ZO-1, F4/80 and NKx2.1. Sections were imaged with a spinning disk confocal microscope using EC Plan-NeoFluar 40X/1.3 or Plan Apochromat 100x/1.4 Oil DIC objectives (Cell Observer Spinning Disk; Zeiss) and pseudocolors were assigned afterwards using Axio-

Table 1. Antibody table

Peptide/protein target	Antigen sequence (if known)	Name of Antibody	Manufacturer, catalog #, and/or name of individual providing the antibody	Species raised in; monoclonal or polyclonal	Dilution used
E-cadherin		Purified Mouse Anti-E-cadherin	DB Bioscience, 610 182	mouse monoclonal (clone 36)	0.25 µg/ml
Nkx2–1		Purified Mouse Anti-Human Ki-67	DB Pharmingen, 556 003	mouse monoclonal (clone B56)	2 µg/ml
TTF1		Mouse Anti-Thyroid Transcription Factor	Dako, M3575	mouse monoclonal (clone 8G7G3/1)	1/500
GFP		GFP (D5.1) XP Rabbit mAb	Cell signaling, 2956	rabbit polyclonal	1/200
GFP	aa1–246	Anti-GFP antibody	Abcam, ab6673	goat polyclonal	1/250
ZO-1	aa463–1109	Rabbit anto ZO-1	Invitrogen, 61–7300	rabbit polyclonal	2.5 µg/ml
laminin		Anti-laminin antibody	Sigma, L9393	rabbit polyclonal	5 µg/ml
F4/80		Anti-F4/80 antibody	Abcam, ab6640	rat monoclonal (clone C1:A3–1)	3.4 µg/ml
F4/80		Anti-mouse F4/80 antigen purified	eBioscience, 14–4801	rat monoclonal (clone BM8)	5 µg/ml

doi: 10.1210/en.2015-1762

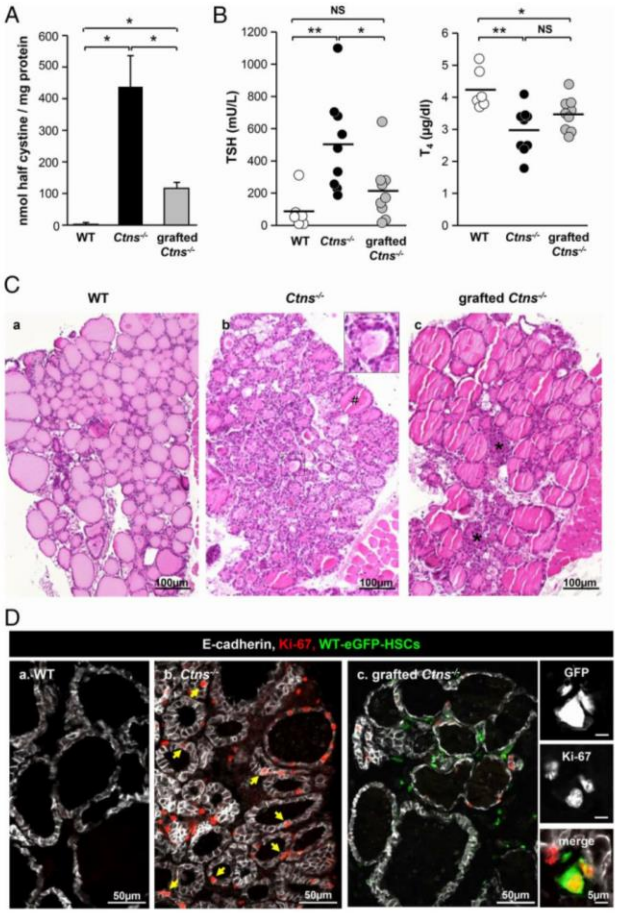

Figure 1. WT HSC transplantation into *Ctns*$^{-/-}$ mice can normalize thyroid function and prevents thyrocyte hyperplasia and hypertrophy. Eight months-old/6-months post-transplant *Ctns*$^{-/-}$ mice were compared to age-matched WT and *Ctns*$^{-/-}$ mice. Since there was no significant difference between males and females, combined values are presented. **A. Normalization of cystine accumulation.** Cystine levels were assayed in thyroid lysates of WT, *Ctns*$^{-/-}$ and grafted *Ctns*$^{-/-}$ mice and were normalized to protein concentration. * $P < .05$; ** $P < .01$; NS, non significant. **B. Protection against against primary hypothyroidism.** TSH and T4 plasma concentrations were measured in WT, *Ctns*$^{-/-}$ and grafted *Ctns*$^{-/-}$ mice. In about half treated *Ctns*$^{-/-}$ mice, TSH and T4 plasma concentration are within normal range. **C, Prevention of thyrocyte hyperplasia and hypertrophy.** Hematoxylin and eosin staining of thyroid paraffin sections from WT (a), *Ctns*$^{-/-}$ (b) and grafted *Ctns*$^{-/-}$ mice (c). (a) WT thyroid is made of uniform follicles filled with homogenous colloid and mostly delineated by flat thyrocytes. (b) In *Ctns*$^{-/-}$ thyroid, sustained TSH response causes thyrocytes hypertrophy and hyperplasia associated to colloid exhaustion (insert); # indicates a rare normal follicle. (c) In grafted *Ctns*$^{-/-}$ mice, follicular activation is suppressed, except at the gland center (asterisks). **D. Normalization of thyrocyte proliferation.** Triple immunostaining for E-cadherin (white, thyrocyte basolateral membrane), Ki-67 (red, proliferation marker) and GFP (green, HSCs) in WT (a), *Ctns*$^{-/-}$ (b) and grafted *Ctns*$^{-/-}$ mice thyroid (c). Notice in nongrafted *Ctns*$^{-/-}$ numerous proliferating cells, mostly thyrocytes (arrows), as compared to WT and grafted

Vision Rel. 4.8 software. Electron microscopy was performed exactly as described (8).

Statistical analysis

Statistical significance was tested using Mann-Whitney test. Differences were considered significant for $P < .05$.

Results

HSC transplantation into *Ctns*$^{-/-}$ mice normalizes thyroid function and protects follicular structures

We recently reported that *Ctns*$^{-/-}$ mice develop between 6–9 months subclinical hypothyroidism with multifocal thyrocyte hyperplasia/hypertrophy and colloid exhaustion, as cystinotic patients. Increased *Ctns*$^{-/-}$ thyrocyte apoptosis and proliferative repair revealed accelerated cell turnover (8). Clinical benefit of early WT-eGFP-HSCs transplantation was first assessed by measuring thyroid cystine and plasma hormone levels. Grafting of WT-eGFP-HSCs decreased by ~75% cystine accumulation in 8-months old *Ctns*$^{-/-}$ thyroid (Figure 1A), half of them showing normal plasma T4 and TSH levels (Figure 1B). By conventional histopathology, grafted *Ctns*$^{-/-}$ thyroids showed striking overall improvement over nongrafted controls, as evidenced by predominantly normal thyrocyte height and homogeneous colloid filling (Fig 1Cc). Thyrocyte proliferation, as measured by Ki-67 immunolabeling, was decreased by ~60% upon transplantation, in agreement with hyperplasia correction (Figure 1D; Supplemental Figure 1). This analysis also revealed proliferation of WT-eGFP-HSCs, indicating local graft expansion in cystinotic thyroid (Fig 1Dc and insert). Altogether, these data demonstrated a remarkable benefit of early engraftment of WT-eGFP-HSCs to correct thyroid disease progression in *Ctns*$^{-/-}$ mice.

Ctns$^{-/-}$ mice. *For quantification, see Supplemental Figure 1.* At right, high magnification views from grafted *Ctns*$^{-/-}$ mice show individual channels then merge images of grafted HSCs (GFP) immunolabeled for Ki-67 (red), demonstrating ongoing local graft expansion.

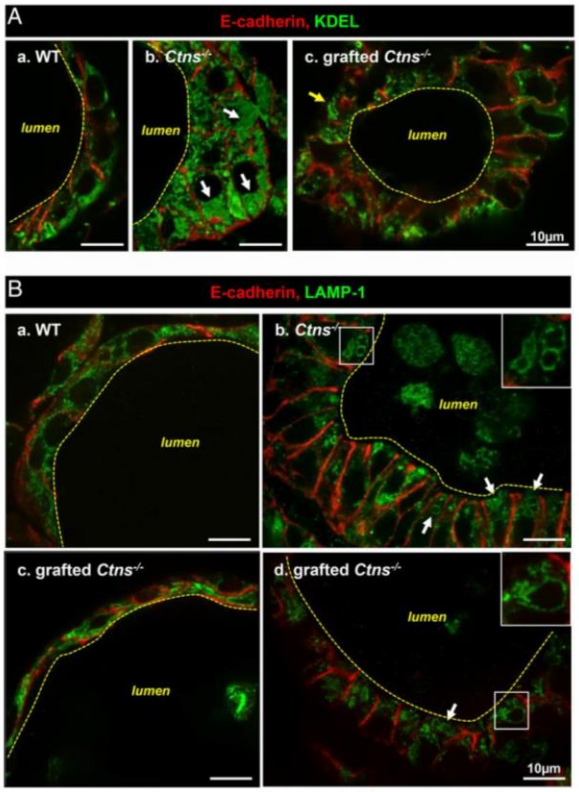

Figure 2. Improvement by HSC transplantation of biosynthetic and lysosomal overload in *Ctns*$^{-/-}$ thyroid. Eight months-old/6-months post-transplant *Ctns*$^{-/-}$ mice were compared to age-matched WT and *Ctns*$^{-/-}$ mice. Samples were analyzed by double immunofluorescence for E-cadherin (red, thyrocyte structure) and either (green) KDEL, as generic marker of endoplasmic reticulum residents (A) or LAMP-1, as lysosomal membrane marker (B). **A. Endoplasmic reticulum (ER) expansion**. In WT follicles (a), thyrocytes are flat or cuboidal and the ER mostly occupies the basal cytoplasm. In nongrafted *Ctns*$^{-/-}$ (b), thyrocytes are columnar (hypertrophic, reaching ~20 µm in height), and KDEL labeling fills the lumen of dilated ER (arrows), which is spread over the entire cytoplasm. Upon grafting (c), *Ctns*$^{-/-}$ thyrocyte height is generally decreased and the ER is overall reduced as compared to (b). However, KDEL antibodies occasionally delineate larger structures devoid of luminal signal (arrow). **(B) Lysosome abnormalities.** In WT thyrocytes (a), LAMP-1-labeled structures are dotty and sparse along the cytoplasm. In nongrafted *Ctns*$^{-/-}$ thyrocytes (b), many lysosomes are dilated and concentrated at the apical pole (arrows and enlarged in insert). LAMP-1 also labels abundant cell remnants in the follicular lumen. Panels (c) and (d) show two distinct patterns of grafted *Ctns*$^{-/-}$ thyrocytes. At (c), aspect is comparable to WT (ie, « preserved »). At (d), enlarged lysosomes are obvious, even frequently larger than at (b). *For EM, see Supplemental Figure 2* (crystals were only detected in nongrafted *Ctns*$^{-/-}$ thyrocytes).

WT-eGFP-HSCs transplantation improves biosynthetic and lysosomal overload in *Ctns*$^{-/-}$ thyroid.

We thus looked for protection by HSC transplantation against subcellular alterations induced by cystinosis (8). Upon grafting, we found a major decrease of ER expansion in most *Ctns*$^{-/-}$ thyrocytes, as monitored by KDEL immunolabeling, suggesting relief of ER stress (Figure 2A). Endolysosomal status of grafted *Ctns*$^{-/-}$ thyroids, monitored by LAMP-1 immunolabeling (Figure 2B) and electron microscopy (EM) (Suppl Figure 2), was very heterogeneous: regions apparently normal upon grafting, elsewhere very much altered, but no cystine crystal could be detected, in contrast to non-grafted *Ctns*$^{-/-}$ thyroids (Suppl Figure 2). Of note, neither cystinosis (data not shown) nor HSC engraftment and follicular infiltration (see below) disrupted thyrocyte tight junction integrity, thus epithelial barrier (Suppl Figure 2).

Thyroid-grafted WT-eGFP-HSCs emit tunneling nanotube-like expansions able to cross follicle basement lamina

We next addressed the mechanism(s) of HSCs-mediated tissue protection in a bifluorescent mouse model (17), which allows to discriminate the fate of green WT-eGFP-HSCs transplanted into DsRed mice (here identifying *Ctns*$^{-/-}$ thyrocytes). No grafted WT-eGFP-HSCs simultaneously expressed DsRed (Figure 2A, no yellow signal), thereby excluding cell fusion as protective mechanism. WT-eGFP-HSCs with dendritic-like shape frequently apposed onto follicular basement laminae (Figure 3Aa,b and Ba) which they further crossed by long cytoplasmic extensions, either very thin (stricto sensu "tunnelling nanotubes") or much thicker with budding tips (Fig 3Ba-c). Furthermore,

doi: 10.1210/en.2015-1762

several WT-eGFP-HSCs became completely inserted inside follicles, intertwined with thyrocytes (Fig 3Aa,b; Ba; Suppl Figure 3). Inserted WT-eGFP-HSCs thus enjoyed extensive close contact with adjacent *Ctns*$^{-/-}$ thyrocytes, which was never found in *Ctns*$^{-/-}$ PTC (Suppl Figure 8). Lateral extensions of individual inserted HSCs could further contact several thyrocytes (Suppl Figure 3). Follicular basement lamina porosity to invading cells could be due to tissue-specific difference between thyroid and kidneys, combined with cystinosis-related alterations (Suppl Figure 4). Indeed, follicular basement lamina in nongrafted *Ctns*$^{-/-}$ mice lost normal circularity (indicating lesser tensile strength) and disclosed large discontinuities which were not seen in grafted congeners.

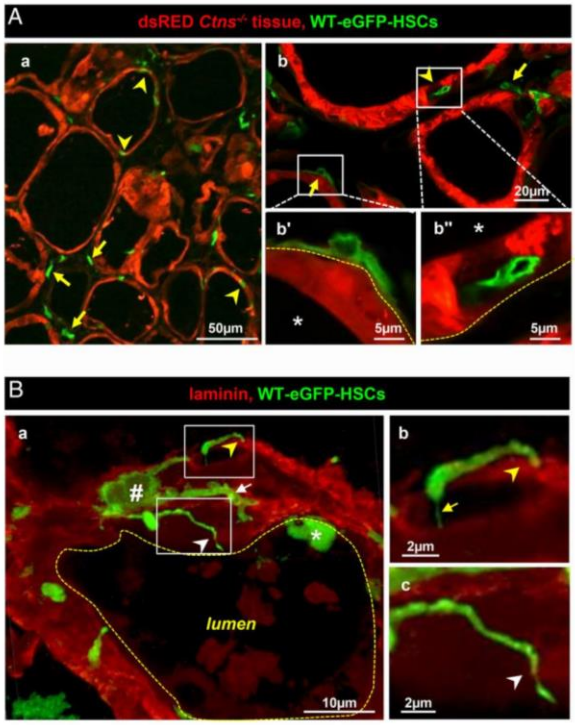

Figure 3. Grafted GFP$^+$-WT-HSCs produce tunneling nanotubes that perforate follicular basement lamina and squeeze into the thyrocyte monolayer. *Note here different use of red at A (Ctns$^{-/-}$ tissue) vs B (laminin).* A. General view of spatial relation between GFP$^+$-WT HSCs and DsRed$^+$-*Ctns*$^{-/-}$ thyrocytes. Double fluorescence confocal imaging in cryostat sections of 6 (a) and 11 months (b) post-transplant *Ctns*$^{-/-}$ mice (endogenous emission from DsRed (red, thyrocytes) and GFP (green, HSCs)). (a) Low magnification shows that HSCs either preferentially *appose* onto follicles (arrows; outside yellow dotted line at b' indicating basement lamina at (b)) or appear colinear with, ie, *integrate* within, thyrocytes (arrowheads; inside follicular space at b''). *For further views of HSCs fully incorporated into the follicle, see Supplemental Figures 3 and 5.* Colloid space is indicated by asterisks. Notice that intrafollicular HSCs do not fuse with thyrocytes (no yellow signal). **B. Extrafollicular HSCs produce tunneling nanotubes.** 3-D reconstruction of z-stack series images (0.23-μm increment, 5-μm total thickness) obtained after double immunolabeling for GFP (green, HSCs) and laminin (red, basement lamina) in frozen sections of grafted mice thyroid at 6-months post-transplantation. (a) Typical extrafollicular HSCs (#), closely apposed to the follicle basement lamina, produce slender cytoplasmic extensions some of which bend perpendicular to (yellow arrowhead) or cross the basement lamina (white arrowhead). Extensions can be very thin (yellow arrow at (b)) or irregular and varicose (white arrow at (a)). Notice local absence of laminin indicating basement lamina galleries allowing TNT passage (better seen in enlargement at (c)) and the overall mottled aspect of follicular basement lamina. Asterisk indicates another, intrafollicular HSC. *For rotating view, see Supplemental video 1. For comparison of laminin structure between WT, Ctns$^{-/-}$ vs grafted Ctns$^{-/-}$see Supplemental Figure 4.*

Despite extensive contiguity, inserted WT-eGFP-HSCs do not transdifferentiate into thyrocytes

Grafted WT-eGFP-HSCs did not simultaneously expressed DsRed, thus excluding cell *fusion* as protective mechanism. However, in response to tissue injury, engrafted HSCs may transdifferentiate into unexpected lineages, including epithelial cells (19). We thus investigated whether follicle-inserted WT-eGFP-HSCs could instead *transdifferentiate* into thyrocytes. Although inserted WT-eGFP-HSCs were apparently circumscribed by the thyrocyte baso-lateral membrane marker, E-cadherin, (Suppl Figure 5A), they never engaged in tight junction formation with neighboring thyrocytes (Suppl Figure 5B). This indicated that HSCs did not transdifferentiated into polarized thyrocytes and suggested that circumscribing E-cadherin signal originated from a single, adjacent epithelial cell, thus arguing against transdifferentiation. Furthermore, none of the inserted WT-eGFP-HSCs nuclei were labeled for the thyrocyte-specific transcription factor, Nkx2–1, excluding transdifferentiation into thyrocytes (Suppl Figure 5C). No WT-eGFP-HSCs expressed calcitonin (not shown), thereby excluding transdifferentiation into epithelial C-cells.

Distinct phenotype of thyroid-engrafted WT-eGFP-HSCs

Macrophages form a plastic population (20), yet poorly characterized in thyroid disease. In *Ctns*$^{-/-}$ liver, brain and kidneys, HSC-derived cells mainly differentiate into F4/80^{high} macrophages (13–15, 17)(Suppl Figure 8). We thus looked at macrophage abundance and differentiation markers in WT, *Ctns*$^{-/-}$ and grafted *Ctns*$^{-/-}$ thyroid. In WT thyroid, F4/80^{+} macrophages were extremely rare but became massively recruited in *Ctns*$^{-/-}$ mice between 6 and 9 months of age, concomitant with histoarchitectural alterations (Suppl Figure 6). Most such endogenous macrophages further inserted into *Ctns*$^{-/-}$ follicles, like WT-eGFP-HSCs described above (Fig 4Ab and Suppl Figure 6f). In grafted *Ctns*$^{-/-}$ thyroid, much fewer endogenous F4/80^{+} macrophages were observed, probably due to considerable correction of tissue injury (for full thyroid section, see Suppl Figure 7). We next attempted to better define the status of engrafted WT-eGFP-HSC-derived cells. CD45 confirmed hematopoietic cell lineage origin (Figure 4B) but F4/80 was rarely detected, arguing against conventional macrophages (Fig 4Ac and B). This differed from other cystinotic tissues such as kidneys, indicating a unique role of the thyroid microenvironment (Suppl Figure 8). Most engrafted WT-eGFP-HSC-derived cells expressed MHCII, consistent with "healing" differentiation (16). The signal for CD11b macrophage marker was weak and neither Ly6c nor CD11c were detected (Figure 4B). These data indicated that HSC-derived cells grafted into *Ctns*$^{-/-}$ thyroid apparently replaced typical endogenous F4/80^{+} macrophages recruited in nongrafted congeners and acquired in this particular tissue microenvironment a distinct combination of macrophage/dendritic differentiation markers. Of note, steady-state abundance of grafted, particularly follicle-apposed and inserted HSCs was very low as compared to most apparently protected thyrocytes (Suppl Figure 7).

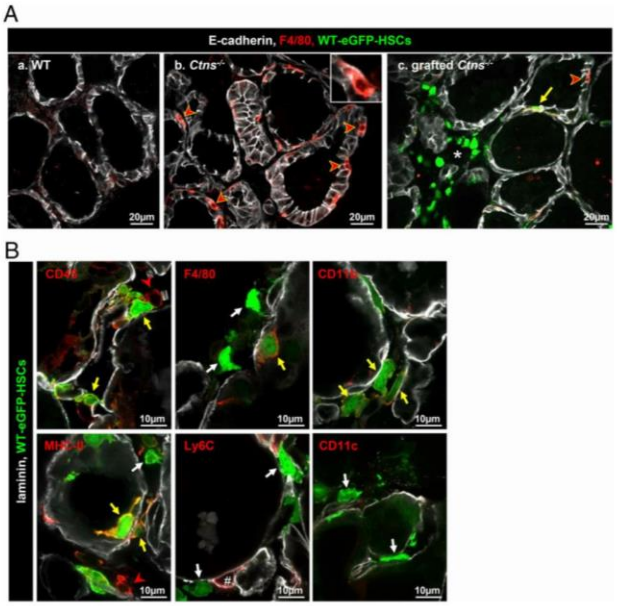

Figure 4. Grafted WT-HSCs replace endogenous *Ctns*$^{-/-}$ macrophages and differentiate into macrophage/dendritic cell lineages. A. GFP^{+}-WT HSCs grafted into *Ctns*$^{-/-}$ mice thyroid replace endogenous macrophages recruitment. Triple immunofluorescence for E-cadherin (white), F4/80 (red, common macrophage marker) and GFP (green, HSCs) on thyroids of WT (a) *Ctns*$^{-/-}$ (b) and grafted *Ctns*$^{-/-}$ mice (c). (a) In WT mice, macrophages are rare. (b) In *Ctns*$^{-/-}$ mice, macrophages are abundant around and within follicles. (red arrowheads and insert). (c) In grafted *Ctns*$^{-/-}$ mice, much fewer endogenous F4/80^{+} macrophages (red arrowhead) are seen. Whereas some grafted HSCs also express detectable F4/80 marker (yellow arrow), most do not (interstitial cluster around the white asterisk). **B. Phenotype of grafted HSCs.** Multiplex immunofluorescence for laminin (white), GFP (green, HSCs) and specific markers of macrophages/dendritic cells (red): the common leukocyte marker (CD45); two common macrophages makers (F4/80 or CD11b); a dendritic cells and macrophage marker (MHCII); a monocytes and endothelial cell marker (Ly6C); and a macrophage and dendritic cells marker (CD11c). Most grafted HSCs are labeled for CD45 and some also express F4/80, CD11b and MHCII markers (yellow arrow). In our conditions, Ly6C antibodies did not label HSCs, but endothelium (#). HSCs that do not express specific marker tested are indicated by white arrow. Endogenous inflammatory cells expressing CD45 and MHCII are indicated by a red arrowhead.

Discussion

We here report that HSC transplantation can protect thyroid structure and normalize function in a mouse model of cystinosis (*Ctns*$^{-/-}$), a lysosomal storage disease due to defective membrane transporter. Thyroid-engrafted HSCs generate extensions that cross follicular basal lamina and fully squeeze into the thyrocyte monolayer, thus providing extensive close contact with target cells. HSCs neither fuse with, nor transdifferentiate into, thyrocytes but mostly differentiate into MHCII-positive macrophage/dendritic lin-

doi: 10.1210/en.2015-1762

eage instead of homogenous F4/80-labeling found in engrafted kidneys and eye, pointing to a unique role of thyroid microenvironment in macrophage differentiation.

Stem cell transplantation is now a therapeutic option for a broad range of congenital or acquired disorders (21) but has never been validated for thyroid disorders. To the opposite, case reports suggested that HSCs may trigger auto-immune thyroiditis and favor thyroid cancer, although indirect effects of myeloablation are unclear (22, 23). However, in a mouse model of Hashimoto's disease, *mesenchymal stem cells* efficiently reduced inflammation and improved clinical outcome (24, 25). We here demonstrate that *bone marrow-derived HSCs* can partially protect *Ctns*$^{-/-}$ thyroid structure and normalize function. These data further support a major multisystemic benefit of stem cells therapy for cystinosis, in particular thyroid protection, and suggest it may represent a generic treatment for membrane protein defects. A clinical trial is currently being developed for human cystinosis based on autologous transplantation of ex vivo lentivirus-transduced HSCs combined with myeloablation by chemotherapy.

In *Ctns*$^{-/-}$ kidneys and cornea, tissue repair by transplanted HSCs involves TNT formation and transfer into deficient cells of cystinosin-bearing lysosomes as correcting factor, ie, cross-correction (16, 17). HSC recruitment thus cannot be primarily related to the altered thyroid state but to the general disease (13, 16). However, the thyroid seems so far unique, as HSCs not only emit TNT-like structures able to cross (damaged?) follicular basement lamina, but fully squeeze into the epithelial monolayer and simultaneously contact several thyrocytes. Thus, inserted HSCs adopt optimal membrane disposition to interact closely and promiscuously with diseased thyrocytes. In nongrafted *Ctns*$^{-/-}$ thyroid, infiltrating endogenous (cystinosin-deficient, F4/80^{+}) macrophages can also squeeze across follicular basement lamina, but are obviously inefficient to prevent disease progression since they are unable to provide gene- or protein-associated correcting factor. Dendritic cells, commonly infiltrating follicles in auto-immune thyroiditis, Graves disease and iododeficiency goitre (26, 27), also strongly adhere to basement membrane, extend cytoplasmic extensions in-between thyrocytes and even cross apical tight junctions (26). Furthermore, mutual interactions between invading lymphocytes and thyrocytes, rendering possible transfer of material, have been evidenced in Hashimoto's thyroiditis (28). Altogether, these observations suggest that (i) thyroid is more prone to full HSCs infiltration across basement lamina as compared to the kidney where HSC bodies are restricted around tubules (13, 14, 17); and (ii) HSCs, once fully infiltrated within the epithelial monolayer, enjoy close vicinity with cystinotic thyrocytes, which allows for efficient correction as testified by the normalization of thyroid function in most *Ctns*$^{-/-}$ mice.

A striking discrepancy was further noted between the low abundance of thyrocyte-contacting HSCs at steady-state and the remarkable extent of tissue protection. This discrepancy favors the view of multiple cross-corrective interactions, ie, (i) the ability of individual *dendritic-shaped* HSCs to simultaneously interact with several adjacent disease cells; and (ii) HSC *mobility* allowing iterative exchange of correcting organelles at each new location over time.

Overall histological and functional protection was however not matched by comprehensive general subcellular preservation. Tissue heterogeneity, between and within follicles, is not really surprising if protection depends on local physical connections. A deleterious effect of irradiation can also not be excluded, although not supported by previous investigations (13). Considering the thyroid functional reserve whereby independent follicles contribute in parallel to total thyroid hormone production, incomplete structural protection may still support adequate functional correction.

In *Ctns*$^{-/-}$ thyroid, engrafted WT-HSCs alleviates afflux of endogenous cystinotic F4/80^{+} macrophages, as also observed in kidney (14), probably due to the correction of tissue injury. Most WT-HSC-derived cells in cystinotic thyroid expressed CD45 and MHCII as opposed to conventional F4/80^{+} macrophages suggesting a distinct differentiation in *Ctns*$^{-/-}$ thyroid vs kidneys and cornea, likely due to the cystinotic thyroid microenvironment. Remarkably, although proinflammatory cytokines are known modifiers of thyroid epithelial barrier function (eg, (29)), the inflammatory component of either cystinosis itself, or linked to HSC engraftment and infiltration, was apparently not sufficient to disrupt thyrocyte tight junction integrity, thus epithelial barrier. Whether cytokines specify the tissue-specific cystinotic landscape and whether macrophage specification influences their ability to fully cross basement laminae deserve to be studied.

Acknowledgments

We gratefully acknowledge Dr. Corinne Antignac (Inserm U983, Paris, France) for providing the original *Ctns*$^{-/-}$ mice. This work was supported mainly by the Cystinosis Research Foundation, Belgian Science Policy Office-Interuniversity Attraction Poles program IAP P7/43-BeMGI, Belgian Fonds de la Recherche Scientifique (F.R.S-FNRS) and Actions de Recherche concertées (to PJC and CEP), National Institutes of Health RO1-DK090058, RO1-DK099338 and R21-NS090066 (to SC). This work was also supported in part by Grant R37-DK15070 from the National Institutes of Health (to SR). The content is solely the re-

sponsibility of the authors and does not necessarily represent the official NIH views. The Platform for Imaging Cells and Tissues (PICT) was financed by National Lottery, Région bruxelloise, Région wallonne, Université catholique de Louvain and de Duve Institute (to PC). HGC is Postdoctoral Researcher and CEP is Research Associate at F.R.S-FNRS (Belgium). We thank Dr. A. Cominelli for comments as well as Y. Abid and T. Lac for experimental help.

Address all correspondence and requests for reprints to: Héloïse P. Gaide Chevronnay, de Duve Institute and Université catholique de Louvain, 75, avenue Hippocrate, PO Box B1.75.05, 1200-Brussels, Belgium, Phone +32 2 764.75.55, FAX +32 2 764.75.41, e-mail : heloise.gaidechevronnay@uclouvain.be; Pierre J. Courtoy, MD, PhD, de Duve Institute and Université catholique de Louvain, 75, avenue Hippocrate, PO Box B1.75.05, 1200-Brussels, Belgium, Phone +32 2 764.75.43, FAX +32 2 764.75.41, e-mail : pierre.courtoy@uclouvain.be

This work was supported by .

(*, equal first authors; #, equal last authors)

Disclosure Statement: The authors have nothing to disclose

References

1. **Gahl WA, Thoene J, Schneider JA.** Cystinosis: A Disorder of Lysosomal Membrane Transport. In: Scriver CR, Beaudet AL, Sly WS, Valle D, Childs B, Kinzler KW, Vogelstein B, eds. *The Metabolic and Molecular Basis of Inherited Disease*. Vol 3. Eight Edition ed: McGraw-Hill Companies, Inc.;2001: 5085–5108. *Online update 2013*.
2. **Andrzejewska Z, Nevo N, Thomas L, Chhuon C, Bailleux A, Chauvet V, Courtoy P, Chol M, Guerrera IC, Antignac C.** Cystinosin is a component of the v-ATPase-Ragulator-Rag complex controlling mTORC1. *Journal of the American Society of Nephrology*. 2015;in press.
3. **Chan AM, Lynch MJ, Bailey JD, Ezrin C, Fraser D.** Hypothyroidism in cystinosis. A clinical, endocrinologic and histologic study involving sixteen patients with cystinosis. *The American journal of medicine*. 1970;48(6):678–692.
4. **Lucky AW, Howley PM, Megyesi K, Spielberg SP, Schulman JD.** Endocrine studies in cystinosis: compensated primary hypothyroidism. *The Journal of pediatrics*. 1977;91(2):204–210.
5. **Nevo N, Chol M, Bailleux A, Kalatzis V, Morisset L, Devuyst O, Gubler MC, Antignac C.** Renal phenotype of the cystinosis mouse model is dependent upon genetic background. *Nephrology, dialysis, transplantation : official publication of the European Dialysis and Transplant Association - European Renal Association*. 2010;25(4):1059–1066.
6. **Raggi C, Luciani A, Nevo N, Antignac C, Terryn S, Devuyst O.** Dedifferentiation and aberrations of the endolysosomal compartment characterize the early stage of nephropathic cystinosis. *Human molecular genetics*. 2014.
7. **Gaide Chevronnay HP, Janssens V, Van Der Smissen P, N'Kuli F, Nevo N, Guiot Y, Levtchenko E, Marbaix E, Pierreux CE, Cherqui S, Antignac C, Courtoy PJ.** Time course of pathogenic and adaptation mechanisms in cystinotic mouse kidneys. *Journal of the American Society of Nephrology : JASN*. 2014;25(6):1256–1269.
8. **Gaide Chevronnay HP, Janssens V, Van Der Smissen P, Liao XH, Abid Y, Nevo N, Antignac C, Refetoff S, Cherqui S, Pierreux CE, Courtoy PJ.** A mouse model suggests two mechanisms for thyroid alterations in infantile cystinosis: decreased thyroglobulin synthesis due to endoplasmic reticulum stress/unfolded protein response and impaired lysosomal processing. *Endocrinology*. 2015;156(6):2349–2364.
9. **Ivanova EA, De Leo MG, Van Den Heuvel L, Pastore A, Dijkman H, De Matteis MA, Levtchenko EN.** Endo-lysosomal dysfunction in human proximal tubular epithelial cells deficient for lysosomal cystine transporter cystinosin. *PloS one*. 2015;10(3):e0120998.
10. **Jezegou A, Llinares E, Anne C, Kieffer-Jaquinod S, O'Regan S, Aupetit J, Chabli A, Sagne C, Debacker C, Chadefaux-Vekemans B, Journet A, Andre B, Gasnier B.** Heptahelical protein PQLC2 is a lysosomal cationic amino acid exporter underlying the action of cysteamine in cystinosis therapy. *Proceedings of the National Academy of Sciences of the United States of America*. 2012;109(50):E3434–3443.
11. **Brodin-Sartorius A, Tete MJ, Niaudet P, Antignac C, Guest G, Ottolenghi C, Charbit M, Moyse D, Legendre C, Lesavre P, Cochat P, Servais A.** Cysteamine therapy delays the progression of nephropathic cystinosis in late adolescents and adults. *Kidney international*. 2012;81(2):179–189.
12. **Emma F, Nesterova G, Langman C, Labbe A, Cherqui S, Goodyer P, Janssen MC, Greco M, Topaloglu R, Elenberg E, Dohil R, Trauner D, Antignac C, Cochat P, Kaskel F, Servais A, Wuhl E, Niaudet P, Van't Hoff W, Gahl W, Levtchenko E.** Nephropathic cystinosis: an international consensus document. *Nephrology, dialysis, transplantation : official publication of the European Dialysis and Transplant Association - European Renal Association*. 2014;29 Suppl 4:iv87–94.
13. **Syres K, Harrison F, Tadlock M, Jester JV, Simpson J, Roy S, Salomon DR, Cherqui S.** Successful treatment of the murine model of cystinosis using bone marrow cell transplantation. *Blood*. 2009;114(12):2542–2552.
14. **Yeagy BA, Harrison F, Gubler MC, Koziol JA, Salomon DR, Cherqui S.** Kidney preservation by bone marrow cell transplantation in hereditary nephropathy. *Kidney international*. 2011;79(11):1198–1206.
15. **Harrison F, Yeagy BA, Rocca CJ, Kohn DB, Salomon DR, Cherqui S.** Hematopoietic stem cell gene therapy for the multisystemic lysosomal storage disorder cystinosis. *Molecular therapy : the journal of the American Society of Gene Therapy*. 2013;21(2):433–444.
16. **Rocca CJ, Kreymerman A, Ur SN, Frizzi KE, Naphade S, Lau A, Tran T, Calcutt NA, Goldberg JL, Cherqui S.** Treatment of Inherited Eye Defects by Systemic Hematopoietic Stem Cell Transplantation. *Investigative ophthalmology, visual science*. 2015;56(12):7214–7223.
17. **Naphade S, Sharma J, Gaide Chevronnay HP, Shook MA, Yeagy BA, Rocca CJ, Ur SN, Lau AJ, Courtoy PJ, Cherqui S.** Brief reports: Lysosomal cross-correction by hematopoietic stem cell-derived macrophages via tunneling nanotubes. *Stem cells*. 2015;33(1):301–309.
18. **Pohlenz J, Maqueem A, Cua K, Weiss RE, Van Sande J, Refetoff S.** Improved radioimmunoassay for measurement of mouse thyrotropin in serum: strain differences in thyrotropin concentration and thyrotroph sensitivity to thyroid hormone. *Thyroid : official journal of the American Thyroid Association*. 1999;9(12):1265–1271.
19. **Lagasse E, Connors H, Al-Dhalimy M, Reitsma M, Dohse M, Osborne L, Wang X, Finegold M, Weissman IL, Grompe M.** Purified hematopoietic stem cells can differentiate into hepatocytes in vivo. *Nature medicine*. 2000;6(11):1229–1234.
20. **Murray PJ, Allen JE, Biswas SK, Fisher EA, Gilroy DW, Goerdt S, Gordon S, Hamilton JA, Ivashkiv LB, Lawrence T, Locati M, Mantovani A, Martinez FO, Mege JL, Mosser DM, Natoli G, Saeij JP, Schultze JL, Shirey KA, Sica A, Suttles J, Udalova I, van Ginderachter JA, Vogel SN, Wynn TA.** Macrophage activation and polarization: nomenclature and experimental guidelines. *Immunity*. 2014;41(1):14–20.
21. **Gratwohl A, Baldomero H, Gratwohl M, Aljurf M, Bouzas LF,**

Horowitz M, Kodera Y, Lipton J, Iida M, Pasquini MC, Passweg J, Szer J, Madrigal A, Frauendorfer K, Niederwieser D, Worldwide Network of B, Marrow T. Quantitative and qualitative differences in use and trends of hematopoietic stem cell transplantation: a Global Observational Study. *Haematologica*. 2013;98(8):1282–1290.

22. **Milenkovic T, Vujic D, Vukovic R, Zecevic Z, Soldatovic I, Mitrovic K, Todorovic S, Zdravkovic D.** Subclinical hypothyroidism in children and adolescents after hematopoietic stem cells transplantation without irradiation. *Vojnosanitetski pregled*. 2014;71(12):1123–1127.
23. **Vantyghem MC, Cornillon J, Decanter C, Defrance F, Karrouz W, Leroy C, Le Mapihan K, Couturier MA, De Berranger E, Hermet E, Maillard N, Marcais A, Francois S, Tabrizi R, Yakoub-Agha I, Societe Francaise de Therapie C.** Management of endocrino-metabolic dysfunctions after allogeneic hematopoietic stem cell transplantation. *Orphanet journal of rare diseases*. 2014;9:162.
24. **Choi EW, Shin IS, Lee HW, Park SY, Park JH, Nam MH, Kim JS, Woo SK, Yoon EJ, Kang SK, Ra JC, Youn HY, Hong SH.** Transplantation of CTLA4Ig gene-transduced adipose tissue-derived mesenchymal stem cells reduces inflammatory immune response and improves Th1/Th2 balance in experimental autoimmune thyroiditis. *The journal of gene medicine*. 2011;13(1):3–16.
25. **Choi EW, Shin IS, Park SY, Yoon EJ, Kang SK, Ra JC, Hong SH.** Characteristics of mouse adipose tissue-derived stem cells and therapeutic comparisons between syngeneic and allogeneic adipose tissue-derived stem cell transplantation in experimental autoimmune thyroiditis. *Cell transplantation*. 2014;23(7):873–887.
26. **Molne J, Jansson S, Ericson LE, Nilsson M.** Adherence of RFD-1 positive dendritic cells to the basal surface of thyroid follicular cells in Graves' disease. *Autoimmunity*. 1994;17(1):59–71.
27. **Wilders-Truschnig MM, Kabel PJ, Drexhage HA, Beham A, Leb G, Eber O, Hebenstreit J, Loidolt D, Dohr G, Lanzer G, et al.** Intrathyroidal dendritic cells, epitheloid cells, and giant cells in iodine deficient goiter. *The American journal of pathology*. 1989;135(1):219–225.
28. **Irvine WJ, Muir AR.** An electron microscopic study of Hashimoto thyroiditis. *Quarterly journal of experimental physiology and cognate medical sciences*. 1963;48:13–26.
29. **Tedelind S, Ericson LE, Karlsson JO, Nilsson M.** Interferon-gamma down-regulates claudin-1 and impairs the epithelial barrier function in primary cultured human thyrocytes. *European journal of endocrinology / European Federation of Endocrine Societies*. 2003;149(3):215–221.

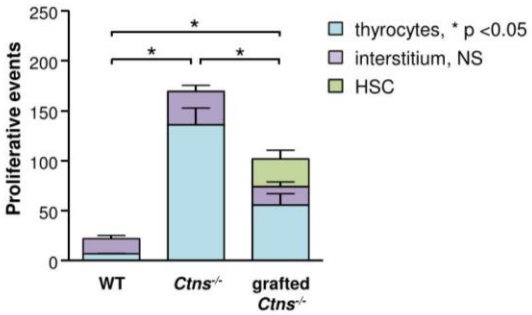

Supplemental Figure 1. Quantification of proliferation in thyroid of WT, *Ctns*$^{-/-}$ and grafted *Ctns*$^{-/-}$ mice. Cells immunolabeled for the proliferation marker (Ki-67) were counted in sections (n=3 WT, n=4 *Ctns*$^{-/-}$, n=4 grafted *Ctns*$^{-/-}$ mice); 7 representative fields spanning each entire thyroid and corresponding to 2.6 10^5 μm^2 were analyzed. Notice significant decrease of proliferation in thyrocytes of grafted compared to non-grafted *Ctns*$^{-/-}$ mice.* $p<0.05$ for comparison of thyrocytes.

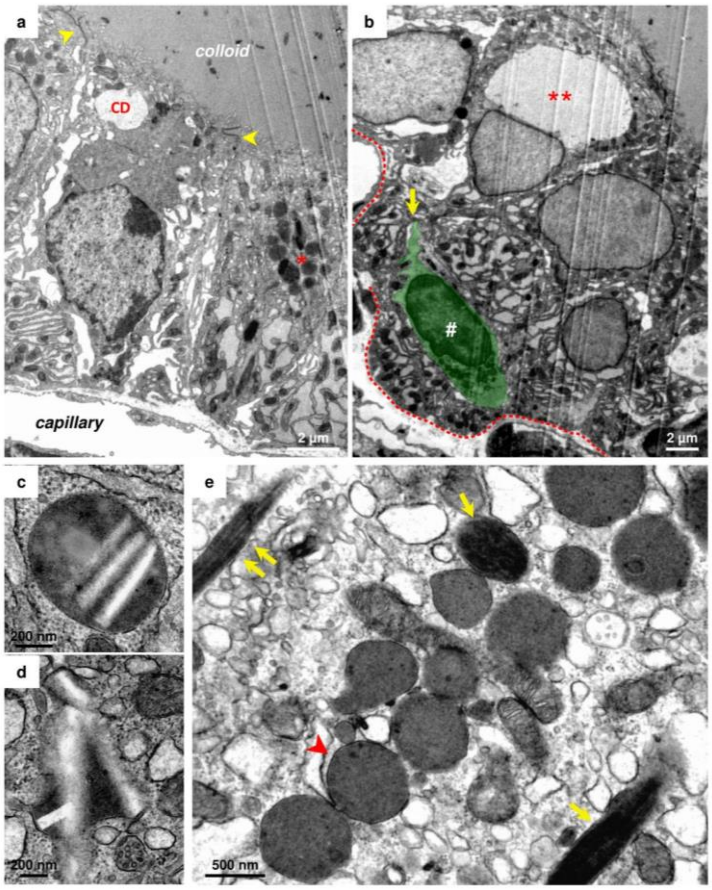
a
colloid
CD
capillary
2 µm
b
**
#
2 µm
c
200 nm
d
200 nm
e
500 nm

Supplemental Figure 2. Electron microscopy. Upper panel. Two low-magnification views of grafted *Ctns*$^{-/-}$ thyroid at 8 months / 6 months post-transplant. For comparison with non-grafted *Ctns*$^{-/-}$ thyroid, see (Gaide Chevronnay et al. Endocrinology 2015). At (a), three preserved columnar thyrocytes (activated) with well-defined apical junctions (yellow arrowheads). CD, colloid droplet; asterisk, cluster of normal lysosomes. At (b), cluster of thyrocytes with pale chromatin (suggesting proliferation). Double asterisk denotes a huge apical vesicle filled with finely granular material, of comparable structure as colloid droplet identified at (a). At lower left, # indicates a cell body with electron-dense elongated nucleus, infiltrated within basement lamina boundaries (red dotted line) and extending a cone penetrating between thyrocytes (yellow arrow), suggesting an HSC with projecting radial TNT. **Lower panel, lysosomes.** c,d. Two thyrocytes in non-grafted *Ctns*$^{-/-}$ mice with crystal-bearing lysosomes of normal size (~400nm sectioned diameter) within preserved cytoplasm. e. Grafted *Ctns*$^{-/-}$ thyrocyte showing a cluster of normal lysosomes (~500nm sectioned diameter, arrowhead points to single limiting membrane with pale halo wrapping homogenous electron-dense matrix). Note the vicinity with longitudinal sections of TNTs (yellow arrows); filamentous core is best seen at double arrow.

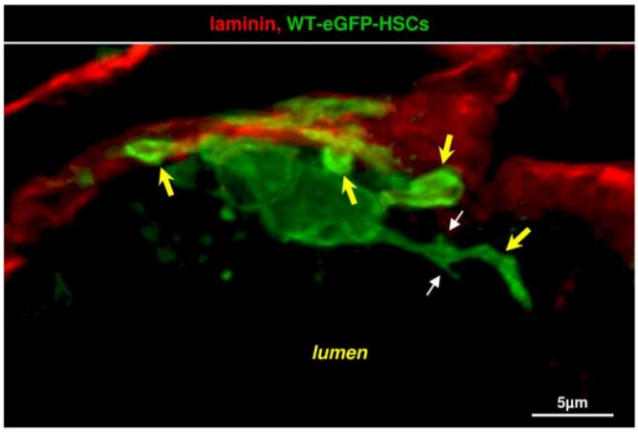

Supplemental Figure 3. Inserted WT-eGFP-HSC emits thin and thick cytoplasmic extensions, allowing contacting several thyrocytes. 3-D reconstruction of z-stack series images (0.23 µm increment, 5 µm total thickness) after double immunolabelling for laminin (red, basement lamina) and GFP (green, HSCs). This inserted HSC with dendritic shape emits both thin (white arrows) and thick (yellow arrows) cytoplasmic extensions.

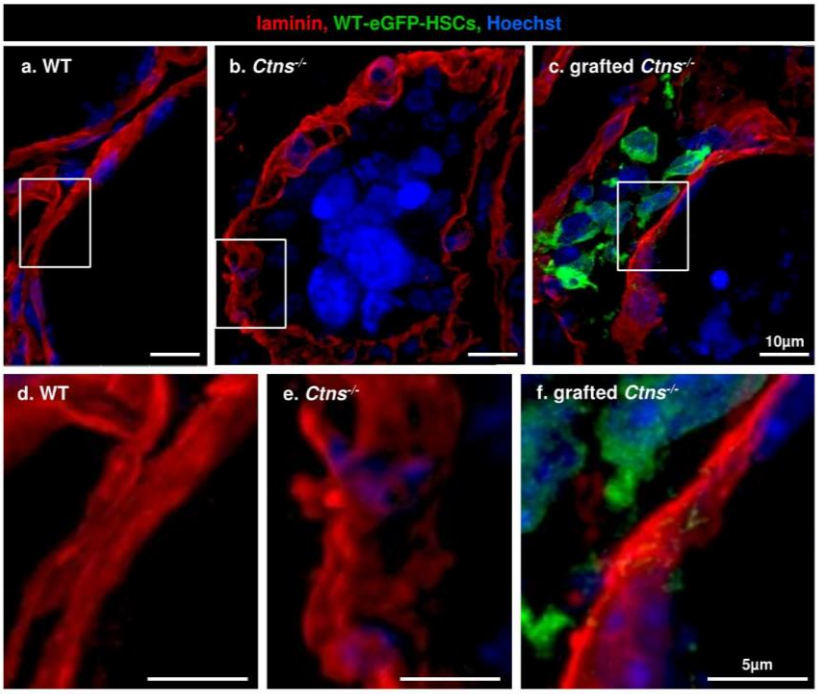

Supplemental Figure 4. Fine structure of basal lamina. Grazing views in WT (a,d), *Ctns*$^{-/-}$ (b,e), and grafted *Ctns*$^{-/-}$ (c,f). Lower panels are enlargements of areas boxed above. Notice homogenous structure and regular circular orientation of laminin in WT thyroid, contrasting with scalloped contour and enclosures/cavities in *Ctns*$^{-/-}$. HSCs grafting largely preserves circularity and homogeneity of follicle basement lamina, except at small discontinuities frequently occupied by HSC projections.

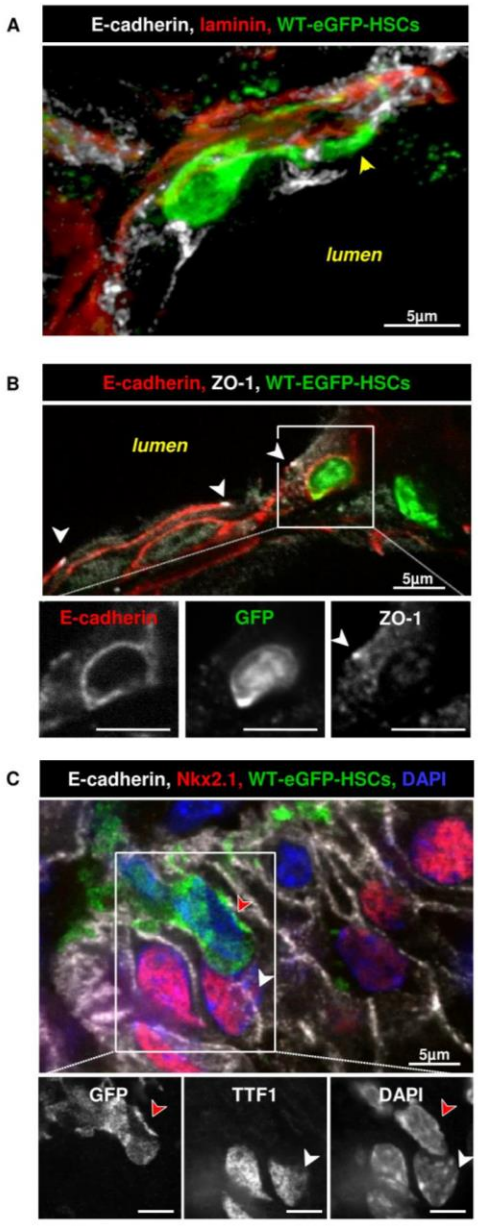
A
E-cadherin, laminin, WT-eGFP-HSCs
lumen
5µm
B
E-cadherin, ZO-1, WT-EGFP-HSCs
lumen
5µm
E-cadherin
GFP
ZO-1
C
E-cadherin, Nkx2.1, WT-eGFP-HSCs, DAPI
5µm
GFP
TTF1
DAPI

Supplemental Figure 5. Follicle inserted GFP$^+$-WT HSCs do not transdifferentiate into thyrocytes. A. GFP$^+$-WT HSCs insert between follicular basement and thyrocytes. 3-D reconstruction of z-stack series images (0.23 µm increment, 5 µm total thickness) obtained after triple immunolabelling for E-cadherin (white, thyrocytes baso-lateral membrane), laminin (red, basement lamina) and GFP (green, HSCs). DsRed signal is not shown here, for clarity. A HSC has passed through the follicle basement lamina and is intertwined within the thyrocyte monolayer (at least two thyrocytes are contacted, one by the cell body at left, and the second by a large extension (yellow arrowhead) **B. Follicle-inserted HSC do not form tight junction with thyrocytes.** Triple immunostaining for E-cadherin (red), ZO-1 (white, thyrocyte tight junctions) and GFP (green, HSCs). The boxed HSC is inserted into the thyrocyte monolayer and appears circumscribed by E-cadherin but does not engage into apical tight junction, nor reaches the lumen. **C. Follicle-inserted HSC do not transdifferentiate in thyrocytes.** Triple immunolabelling for E-cadherin (white), Nkx2.1 (red, thyroid-specific transcription factor) and GFP (green, HSCs). All nuclei are further stained with DAPI (blue). In contrast to thyrocyte nuclei (white arrowhead), the nucleus of inserted HSCs (red arrowhead) is not labelled for Nkx2.1. Boxed areas at B and C are split below into black/white images for the three indicated channels.

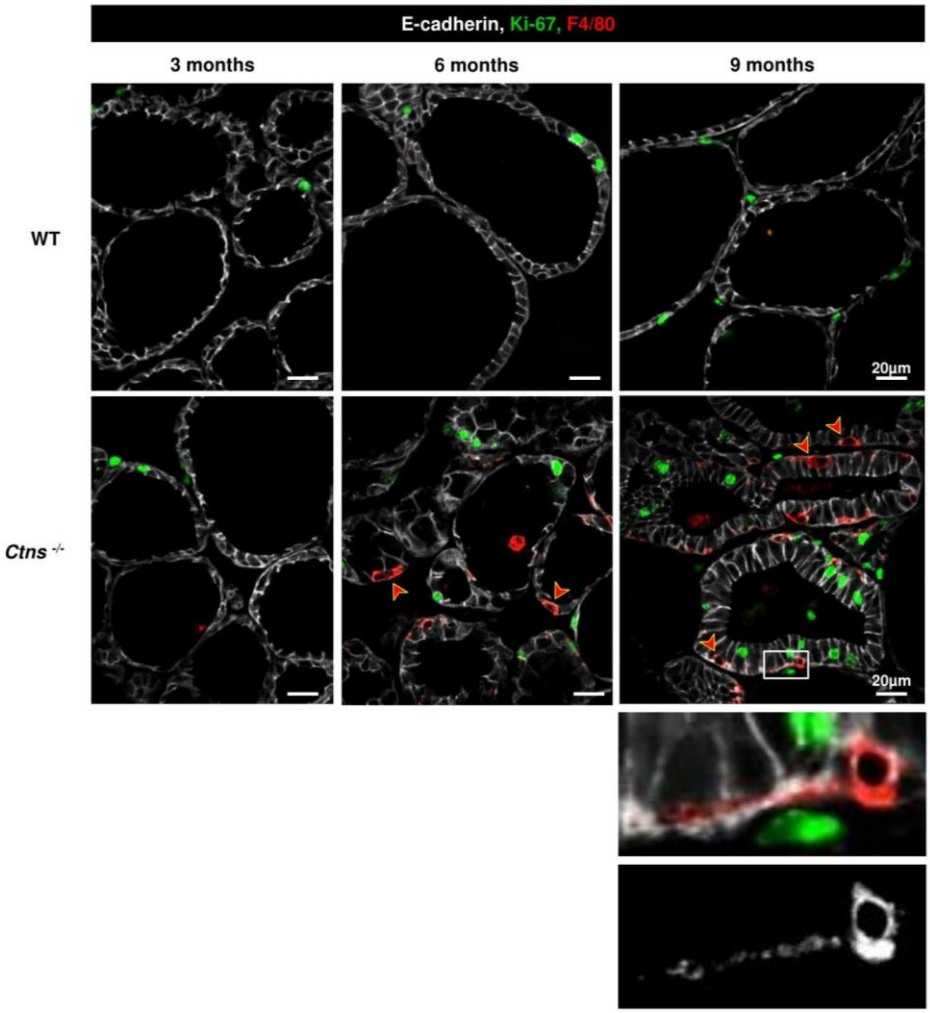
E-cadherin, Ki-67, F4/80
3 months
6 months
9 months
WT
Ctns -/-
20µm
20µm

Supplemental Figure 6. Endogenous macrophage recruitment in *Ctns*$^{-/-}$ thyroid correlates with thyrocyte proliferation and structural alterations. Time-course of endogenous macrophage infiltration was analyzed by immunolabelling (F4/80, red) and compared to proliferative repair (Ki-67, green) in thyroid of WT or *Ctns*$^{-/-}$ mice at 3, 6 and 9 months. Macrophages invade the cystinotic tissue between 6 and 9 months, concomitant with structural tissue alterations (E-cadherin; white) and increased cell proliferation (Ki67; green). As in *Ctns*$^{-/-}$ kidney (Gaide Chevronnay et al. JASN 2014), notice silent phase for at least 3 months. Starting around 6 months and maximal at ~9 months of age, endogenous, cystinosin-deficient macrophages insert within cystinotic follicles (red arrowheads, best seen in enlarged box), exactly as GFP^{+}-WT HSCs bearing normal cystinosin, but fail to provide protection.

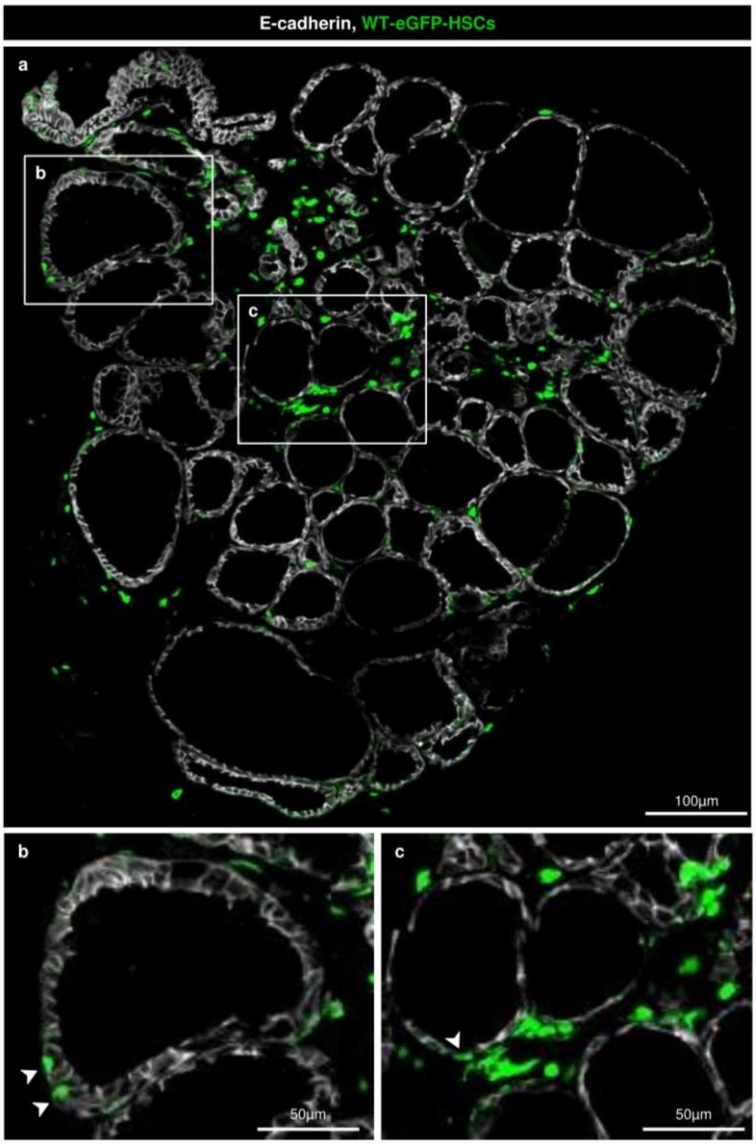

Supplemental Figure 7. Pattern of GFP⁺-WT HSC infiltration in the thyroid of grafted *Ctns*$^{-/-}$ mice. (a) Immunolabelling of grafted WT-eGFP-HSCs (GFP, green) in one representative mouse out of 5 reveals the pattern of infiltrating HSCs in the entire cystinotic thyroid. Thyroid full view was obtained using MosaiX module of AxioVision Software allowing tilling and stitching of images captured across the thyroid section. Enlargement (b) shows individual HSCs (white arrowheads), inserted within the epithelium (E-cadherin, white); enlargement (c) shows 3 foci of HSC clusters mainly in the interstitium of the center of the gland.

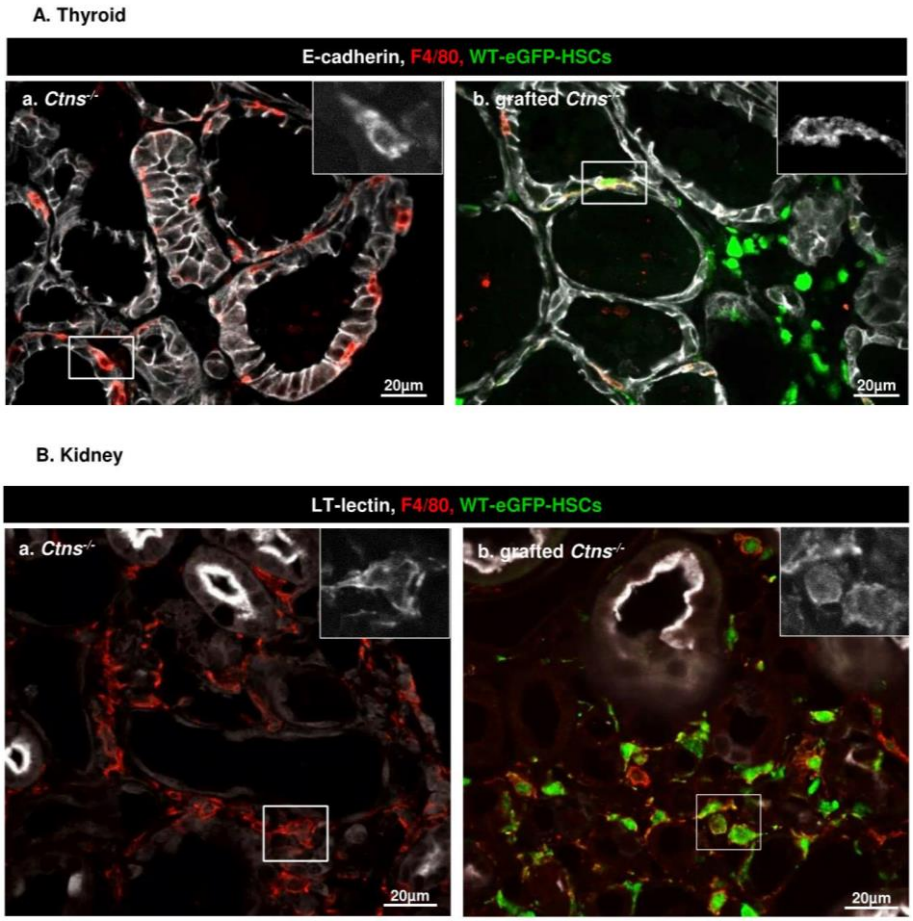

Supplemental Figure 8. In contrast to kidney, only few WT-eGFP-HSCs grafted in the thyroid express F4/80 differentiation marker. Multiplex fluorescence labeling for GFP (green, HSC), F4/80 (red, macrophages) and E-cadherin (white, thyrocyte basolateral membrane) or by LT-lectin (white, kidney proximal tubule cells apical membrane). In contrast to endogenous macrophages, few WT-eGFP-HSCs grafted in the thyroid express detectable F4/80 marker. In kidney, both endogenous macrophages and grafted HSCs show strong comparable F4/80 signal. Boxed fields point to cells clearly immunolabelled for F4/80, enlarged in the insets as black/white.

www.nature.com/scientificreports

SCIENTIFIC REPORTS

OPEN

Cellular uptake of proMMP-2:TIMP-2 complexes by the endocytic receptor megalin/LRP-2

Received: 19 July 2016
Accepted: 18 May 2017
Published online: 28 June 2017

Manuel Johanns[1], Pascale Lemoine[1], Virginie Janssens[1], Giuseppina Grieco[1], Soren K. Moestrup[2], Rikke Nielsen[2], Erik I. Christensen[2], Pierre J. Courtoy[1], Hervé Emonard[3], Etienne Marbaix[1] & Patrick Henriet[1]

Matrix metalloproteinases (MMPs) are regulated at multiple transcriptional and post-transcriptional levels, among which receptor-mediated endocytic clearance. We previously showed that low-density lipoprotein receptor-related protein-1 (LRP-1) mediates the clearance of a complex between the zymogen form of MMP-2 (proMMP-2) and tissue inhibitor of metalloproteinases, TIMP-2, in HT1080 human fibrosarcoma cells. Here we show that, in BN16 rat yolk sac cells, proMMP-2:TIMP-2 complex is endocytosed through a distinct LRP member, megalin/LRP-2. Addition of receptor-associated protein (RAP), a natural LRP antagonist, caused accumulation of endogenous proMMP-2 and TIMP-2 in conditioned media. Incubation with RAP also inhibited membrane binding and cellular uptake of exogenous iodinated proMMP-2:TIMP-2. Moreover, antibodies against megalin/LRP-2, but not against LRP-1, inhibited binding of proMMP-2:TIMP-2 to BN16 cell surface. BIAcore analysis confirmed direct interaction between the complex and megalin/LRP-2. Conditional renal invalidation of megalin/LRP-2 in mice resulted in accumulation of proMMP-2 and TIMP-2 in their urine, highlighting the physiological relevance of the binding. We conclude that megalin/LRP-2 can efficiently mediate cell-surface binding and endocytosis of proMMP-2:TIMP-2 complex. Therefore megalin/LRP-2 can be considered as a new actor in regulation of MMP-2 activity, an enzyme crucially involved in many pathological processes.

Matrix metalloproteinases (MMPs) compose a family of Zn^{2+}-dependent endoproteases that display a large variety of substrates including extracellular matrix macromolecules, cell-surface receptors, growth factors, cytokines and chemokines[1]. These proteinases play important roles in physiological processes, such as wound repair[2] and cyclic endometrial remodeling[3], as well as in the development of various pathologies including cancer[4].

Matrix metalloproteinases are regulated at both transcriptional and post-transcriptional levels. Mechanisms of activity regulation common to all members of the MMP family include activating cleavage of the latent proenzyme form and inhibition of the active enzyme by tissue inhibitors of metalloproteinases (TIMPs)[5]. In addition, extracellular levels of certain MMPs are regulated by selective internalization and intracellular degradation. In this regard, low-density lipoprotein receptor-related proteins (LRPs) compose a family of endocytic and signaling receptors that exert their activities on a large variety of molecules including proteolytic enzymes[6]. Particularly, LRP-1 regulates the extracellular levels of MMPs and serine-proteinases[7,8].

Megalin/LRP-2 shares numerous common ligands with LRP-1, notably the complexes between the plasminogen activator (PA) inhibitor type-1 (PAI-1) with either tissue-type PA (tPA)[9], pro-urokinase-type PA (pro-uPA) or mature uPA[10,11]. Moreover, a member of the MMP family, MMP-9 also binds to both LRP-1 and -2[12]. In addition, we previously reported that LRP-1 mediates endocytic clearance of the proMMP-2:TIMP-2 complex[13], which represents the major form of MMP-2 in biological tissues[14].

In the present study, we investigated the ability of megalin/LRP-2 to control extracellular levels of MMP-2 and TIMP-2 by endocytosis of the proMMP-2:TIMP-2 complex. For this purpose, we used Brown Norway rat yolk sac carcinoma cells (BN16) that express megalin/LRP-2 but not LRP-1[15,16]. We also evaluated the physiological relevance of proMMP-2 and TIMP-2 uptake in transgenic mice undergoing renal invalidation of megalin/LRP-2[17].

[1]de Duve Institute, Université catholique de Louvain, 1200, Brussels, Belgium. [2]Department of Biomedicine, Aarhus University, 8000, Aarhus, Denmark. [3]CNRS UMR 7369, Matrice Extracellulaire et Dynamique Cellulaire, Université de Reims Champagne-Ardenne, 51687, Reims, France. Etienne Marbaix and Patrick Henriet contributed equally to this work. Correspondence and requests for materials should be addressed to P.H. (email: patrick.henriet@uclouvain.be)

Class III phosphoinositide 3-kinase/VPS34 and dynamin are critical for apical endocytic recycling

PI3K-III/ VPS34 and dynamin in apical endocytic recycling

Carpentier S.[1], N'Kuli F.[1], Grieco P.[1], Van Der Smissen P.[1], Janssens V.[1], Emonard H.[2], Bilanges B.[3], Vanhaesebroeck B.[3], Gaide Chevronnay H.P.[1], Pierreux C.E.[1,*], Tyteca D.[1,*], Courtoy P.J.[1,*]

[1]*CELL Unit, Université catholique de Louvain & de Duve Institute, Brussels, Belgium*
[2]*URCA/CNRS FRE 3481, Reims, France*
[3]*Centre for Cell Signalling, Barts Cancer Institute, Queen Mary, University London, UK*
**These authors contributed equally to this work*

Corresponding author: Tyteca D., CELL Unit, de Duve Institute & Université Catholique de Louvain, UCL B1.75.02, avenue Hippocrate, 75, B-1200 Brussels, Belgium. Phone: +32-2-764.75.91; Fax: +32-2-764.75.43; e-mail: donatienne.tyteca@uclouvain.be

Recycling is a limiting step for receptor-mediated endocytosis. We first report three *in vitro* or *in vivo* evidences that class III PI3K/VPS34 is the key PI3K isoform regulating apical recycling. A substractive approach, comparing in OK cells a pan-class I/II/III PI3K inhibitor (LY294002) with a class I/II PI3K inhibitor (ZSTK474), suggested that class III PI3K/VPS34 inhibition induced selective apical endosome swelling and sequestration of the endocytic receptor, megalin/LRP-2, causing surface down-regulation. GFP-(FYVE)x2 overexpression to sequester PI(3)P caused undistinguishable apical endosome swelling. In mouse kidney proximal tubular cells, conditional *Vps34* inactivation also led to vacuolation and intracellular megalin redistribution. We next report that removal of LY294002 from LY294002-treated OK cells induced a spectacular burst of recycling tubules and restoration of megalin surface pool. Acute triggering of recycling tubules revealed recruitment of dynamin-GFP and dependence of dynamin-GTPase, guidance directionality by microtubules, and suggested that a microfilamentous net constrained endosomal swelling. We conclude that (i) besides its role in endosome fusion, PI3K-III is essential for endosome fission/recycling; and (ii) besides its role in endocytic entry, dynamin also supports tubulation of recycling endosomes. The unleashing of recycling upon acute reversal of PI3K inhibition may help study its dynamics and associated machineries.

Key words: megalin, kidney tubules, recycling, tubulation, PI3K class III, VPS34, LY294002, wortmannin, ZSTK474, dynamin

Apical receptor-mediated endocytosis (ARME) plays a central role in the biogenesis and maintenance of polarized epithelia (1) and is essential for embryonic development (e.g. holoprosencephaly`, 2, 3) and for vitamin metabolism and homeostasy (4, 5). Polarized membrane trafficking which uses endocytic machineries for sorting and delivery of plasma membrane proteins to apical and basolateral domains can be perturbed in cancer (6) and mendelian trafficking disorders, such as Dent's disease and Lowe syndrome that impact on recycling (7).

Kidney proximal tubular cells (PTC) use the multivalent tandem endocytic receptors, megalin and cubilin, to support full reabsorption of ultrafiltrated low-molecular weight (LMW) proteins (8, 9). The exceptionally high endocytic activity of PTC is due to the combination of a strong expression of the endocytic receptors with a particularly fast endocytic cycle (T1/2 ~90sec`, 10), thus offering a model of choice to identify rate-limiting regulators of ARME.

Megalin, first identified as the large target antigen of experimental Heyman glomerulonephritis (11), is also known as LRP-2 for its high similarity to the scavenger receptor LRP-1, but is targeted instead to the apical membrane (12). As a consequence of defective PTC endocytosis, megalin-KO mice suffer from impaired vitamin D kidney activation leading to rickets (4), and impaired lysosomal biogenesis due to failure to recapture ultrafiltrated lysosomal enzymes (13). A dual, endocytic and signalling, function of megalin has been suggested (14) but the latter is not essential, as shown by lack of phenotype in transgenic mice with deleted megalin cytoplasmic domain (15). Megalin trafficking involves (i) rapid internalization thanks to its three NPXY-like motives, membrane; (ii) fusion with the apical recycling endosome (ARE); and (iii) recycling via tubules known as "dense apical tubules" in kidney PTC, where extremely dense immunolabelling identifies a major fraction of total receptor pool (16).

Both small (Rabs) and large (dynamin) GTPases are involved in endocytic trafficking. Extensive studies based on *in vitro* (acellular) vesicle fusion assays established that homotypic membrane docking and fusion at the early endosome compartment is triggered by Rab5-dependent activation of class III phosphoinositide 3-kinase (PI3K-III), the only PI3K able to generate phosphatidylinositol 3-phosphate [PI(3)P], which in turn recruits the bivalent adaptator EEA1 thanks to its FYVE domains (17, 18). Rapid recycling occurs from Rab5/Rab4 interconnected domains on the same early endosome compartment, while slow recycling is under the control of Rab5 and Rab11 on endosome recycling compartment (19). Dynamin GTPase, essential for coated-pits internalization (20) and involved in endosome recycling (21), can promote tubulation *in vitro* (22) and could be

www.nature.com/scientificreports

SCIENTIFIC REPORTS

OPEN

Vps34/PI3KC3 deletion in kidney proximal tubules impairs apical trafficking and blocks autophagic flux, causing a Fanconi-like syndrome and renal insufficiency

Received: 10 January 2018
Accepted: 1 July 2018
Published online: 20 September 2018

Giuseppina Grieco[1], Virginie Janssens[1], Héloïse P. Gaide Chevronnay[1], Francisca N'Kuli[1], Patrick Van Der Smissen[1], Tongsong Wang[1], Jingdong Shan[2], Seppo Vainio[2], Benoit Bilanges[3], François Jouret[4], Bart Vanhaesebroeck[3], Christophe E. Pierreux[1] & Pierre J. Courtoy[1]

Kidney proximal tubular cells (PTCs) are highly specialized for ultrafiltrate reabsorption and serve as paradigm of apical epithelial differentiation. Vps34/PI3-kinase type III (PI3KC3) regulates endosomal dynamics, macroautophagy and lysosomal function. However, its *in vivo* role in PTCs has not been evaluated. Conditional deletion of Vps34/PI3KC3 in PTCs by Pax8-Cre resulted in early (P7) PTC dysfunction, manifested by Fanconi-like syndrome, followed by kidney failure (P14) and death. By confocal microscopy, $Vps34^{\Delta/\Delta}$ PTCs showed preserved apico-basal specification (brush border, NHERF-1 *versus* Na^+/K^+-ATPase, ankyrin-G) but basal redistribution of late-endosomes/lysosomes (LAMP-1) and mis-localization to lysosomes of apical recycling endocytic receptors (megalin, cubilin) and apical non-recycling solute carriers (NaPi-IIa, SGLT-2). Defective endocytosis was confirmed by Texas-red-ovalbumin tracing and reduced albumin content. Disruption of Rab-11 and perinuclear galectin-3 compartments suggested mechanistic clues for defective receptor recycling and apical biosynthetic trafficking. p62-dependent autophagy was triggered yet abortive (p62 co-localization with LC3 but not LAMP-1) and PTCs became vacuolated. Impaired lysosomal positioning and blocked autophagy are known causes of cell stress. Thus, early trafficking defects show that Vps34 is a key *in vivo* component of molecular machineries governing apical vesicular trafficking, thus absorptive function in PTCs. Functional defects underline the essential role of Vps34 for PTC homeostasis and kidney survival.

Kidney proximal tubular cells (PTCs) show exquisite structural differentiation that supports their huge reabsorption activity and serve as paradigm for apical polarity[1]. Efficient reabsorption of water and solutes from the ultrafiltrate is ensured by abundance of channels and transporters (NaPi-IIa for phosphate, SGLT-2 for glucose) at the highly developed apical brush border membrane. These transporters are anchored by ezrin and by multi-PDZ scaffold proteins including Na^+/H^+-exchanger regulatory factor-1 (NHERF-1)[2–5]. Transepithelial transport is achieved by complementary sets of channels and transporters inserted into infolded basolateral membrane and complemented by Na^+/K^+-ATPase as primary transport driving force, itself stabilized by ankyrin-G scaffold. Full reabsorption of ultrafiltrated proteins by apical receptor-mediated endocytosis is no less remarkable, considering the brief contact of PTCs with rapidly passing urine. Full reabsorption is made possible by high expression of multiligand tandem receptors, megalin and cubilin[6], combined with extremely fast apical endocytic recycling rate[7].

[1]Cell Biology Unit, de Duve Institute, Université catholique de Louvain, Brussels, Belgium. [2]Laboratory of Developmental Biology, Oulu Center for Cell-Matrix Research, Biocenter Oulu and Faculty of Biochemistry and Molecular Medicine, University of Oulu, Oulu, Finland. [3]UCL Cancer Institute, University College London, 72 Huntley Street, London, WC1E 6DD, UK. [4]Groupe Interdisciplinaire de Génoprotéomique Appliquée (GIGA), Cardiovascular Sciences, University of Liège, Liège, Belgium. Christophe E. Pierreux and Pierre J. Courtoy jointly supervised this work. Correspondence and requests for materials should be addressed to C.E.P. (email: christophe.pierreux@uclouvain.be)

Vps34/PIK3C3 controls thyroid hormone production by regulating thyroglobulin iodination, lysosomal proteolysis and tissue homeostasis

Grieco G.*, TS. Wang1*, O. Delcorte*, C. Spourquet*, **V. Janssens**, A. Strickaert, HP. Gaide Chevronnay, XH Liao, B. Bilanges4, S. Refetoff, B. Vanhaesebroeck, C. Maenhaut, PJ. Courtoy[#], CE. Pierreux[#]

Thyroid. *2019 Oct 25. doi: 10.1089/thy.2019.0182. [Epub ahead of print]*
*, equal first authors; [#,] equal last authors

Abstract

BACKGROUND: The production of thyroid hormones (T_3, T_4) depends on thyroid organization in follicles, lined by a monolayer of thyrocytes with strict apico-basal polarity. Polarization supports vectorial transport of thyroglobulin for storage into, and recapture from, the colloid. It also allows selective addressing of channels, transporters, pumps and enzymes to their appropriate basolateral (NIS, SLC26A7 and Na^+/K^+-ATPase) or apical membrane domain (Anoctamin, SLC26A4, DUOX2, DUOXA2 and TPO). How these actors of T_3/T_4 synthesis reach their final destination remains poorly understood. Vps34/PIK3C3 is now recognized as a main component in the general control of vesicular trafficking and of cell homeostasis via autophagy. We recently reported that conditional Vps34 inactivation in kidney proximal tubular cells by Pax8-driven excision prevents normal addressing of apical membrane proteins and causes abortive macroautophagy.

METHODS: Vps34 was inactivated using a Pax8-driven Cre recombinase system. The impact of Vps34 inactivation in thyrocytes was analyzed by histological, immunolocalization and mRNA expression profiling. Thyroid hormone synthesis was assayed by ^{125}I injection and by serum plasma analysis.

RESULTS: Vps34^{cKO} mice were born at the expected Mendelian ratio and showed normal growth until postnatal day 14, then stopped growing and died at around 1 month of age. We therefore analyzed thyroid Vps34^{cKO} at postnatal day 14. We found that loss of Vps34 in thyrocytes causes: (i) disorganization of thyroid parenchyma with abnormal thyrocyte and follicular shape and reduced PAS^{+} colloidal spaces; (ii) severe non-compensated hypothyroidism with extremely low T_4 levels (0.75 ± 0.62 μg/dL) and huge TSH plasma levels (19,300 ± 10,500 mU/L); (iii) impaired ^{125}I organification at comparable uptake and frequent occurrence of follicles with luminal thyroglobulin but non-detectable T4-bearing thyroglobulin; (iv) intense signal in thyrocytes for the lysosomal membrane marker, LAMP-1, as well as thyroglobulin and the autophagy marker, p62, indicating defective lysosomal proteolysis, and (v) presence of macrophages in the colloidal space.

CONCLUSIONS: We conclude that Vps34 is crucial for thyroid hormonogenesis, at least by controlling epithelial organization, Tg iodination as well as proteolytic T_3/T_4 excision in lysosomes.

REFERENCES

Ahmed, K., P. Dasgupta, and M. S. Khan. 2006. 'Cystine calculi: challenging group of stones', *Postgrad Med J*, 82: 799-801.

Amsellem, S., J. Gburek, G. Hamard, R. Nielsen, T. E. Willnow, O. Devuyst, E. Nexo, P. J. Verroust, E. I. Christensen, and R. Kozyraki. 2010. 'Cubilin is essential for albumin reabsorption in the renal proximal tubule', *J Am Soc Nephrol*, 21: 1859-67.

Andersen, C. B., and S. K. Moestrup. 2014. 'How calcium makes endocytic receptors attractive', *Trends Biochem Sci*, 39: 82-90.

Andrews, N. W., and M. Corrotte. 2018. 'Plasma membrane repair', *Curr Biol*, 28: R392-R97.

Andrzejewska, Z., N. Nevo, L. Thomas, A. Bailleux, V. Chauvet, A. Benmerah, and C. Antignac. 2015. 'Lysosomal Targeting of Cystinosin Requires AP-3', *Traffic*, 16: 712-26.

Andrzejewska, Z., N. Nevo, L. Thomas, C. Chhuon, A. Bailleux, V. Chauvet, P. J. Courtoy, M. Chol, I. C. Guerrera, and C. Antignac. 2016. 'Cystinosin is a Component of the Vacuolar H+-ATPase-Ragulator-Rag Complex Controlling Mammalian Target of Rapamycin Complex 1 Signaling', *J Am Soc Nephrol*, 27: 1678-88.

Bachmann, S., U. Schlichting, B. Geist, K. Mutig, T. Petsch, D. Bacic, C. A. Wagner, B. Kaissling, J. Biber, H. Murer, and T. E. Willnow. 2004. 'Kidney-specific inactivation of the megalin gene impairs trafficking of renal inorganic sodium phosphate cotransporter (NaPi-IIa)', *J Am Soc Nephrol*, 15: 892-900.

Bakris, G. L., V. A. Fonseca, K. Sharma, and E. M. Wright. 2009. 'Renal sodium-glucose transport: role in diabetes mellitus and potential clinical implications', *Kidney Int*, 75: 1272-77.

Barone, R., P. Van Der Smissen, O. Devuyst, V. Beaujean, S. Pauwels, P. J. Courtoy, and F. Jamar. 2005. 'Endocytosis of the somatostatin analogue, octreotide, by the proximal tubule-derived opossum kidney (OK) cell line', *Kidney Int*, 67: 969-76.

Batshaw, M. L., R. B. MacArthur, and M. Tuchman. 2001. 'Alternative pathway therapy for urea cycle disorders: twenty years later', *J Pediatr*, 138: S46-54; discussion S54-5.

Battafarano, G., M. Rossi, L. R. Rega, G. Di Giovamberardino, A. Pastore, M. D'Agostini, O. Porzio, N. Nevo, F. Emma, A. Taranta, and A. Del Fattore. 2019. 'Intrinsic Bone Defects in Cystinotic Mice', *Am J Pathol*, 189: 1053-64.

Baum, M. 1998. 'The Fanconi syndrome of cystinosis: insights into the pathophysiology', *Pediatr Nephrol*, 12: 492-7.

Baumner, S., and L. T. Weber. 2018. 'Nephropathic Cystinosis: Symptoms, Treatment, and Perspectives of a Systemic Disease', *Front Pediatr*, 6: 58.

Behr, T. M., R. M. Sharkey, G. Sgouros, R. D. Blumenthal, R. M. Dunn, K. Kolbert, G. L. Griffiths, J. A. Siegel, W. S. Becker, and D. M. Goldenberg. 1997. 'Overcoming the nephrotoxicity of radiometal-labeled immunoconjugates: improved cancer therapy administered to a nude mouse model in relation to the internal radiation dosimetry', *Cancer*, 80: 2591-610.

Bellomo, F., D. L. Medina, E. De Leo, A. Panarella, and F. Emma. 2017. 'High-content drug screening for rare diseases', *J Inherit Metab Dis*, 40: 601-07.

Bellomo, F., A. Taranta, S. Petrini, R. Venditti, M. T. Rocchetti, L. R. Rega, S. Corallini, L. Gesualdo, M. A. De Matteis, and F. Emma. 2016. 'Carboxyl-Terminal SSLKG Motif of the Human Cystinosin-LKG Plays an Important Role in Plasma Membrane Sorting', *PLoS One*, 11: e0154805.

Benevenga, N. J., and K. P. Blemings. 2007. 'Unique aspects of lysine nutrition and metabolism', *J Nutr*, 137: 1610S-15S.

Besouw, M. T., R. Bowker, J. P. Dutertre, F. Emma, W. A. Gahl, M. Greco, M. R. Lilien, J. McKiernan, F. Nobili, J. A. Schneider, F. Skovby, L. P. van den Heuvel, W. G. Van't Hoff, and E. N. Levtchenko. 2011. 'Cysteamine toxicity in patients with cystinosis', *J Pediatr*, 159: 1004-11.

Besouw, M. T., J. Schneider, M. C. Janssen, M. Greco, F. Emma, E. A. Cornelissen, K. Desmet, F. Skovby, F. Nobili, M. R. Lilien, A. De Paepe, F. Malfait, S. Symoens, L. P. van den Heuvel, and E. N. Levtchenko. 2013. 'Copper deficiency in patients with cystinosis with cysteamine toxicity', *J Pediatr*, 163: 754-60.

Besouw, M., L. van den Heuvel, R. van Eijsden, I. Bongaers, L. Kluijtmans, M. Dewerchin, and E. Levtchenko. 2013. 'Increased human dermal microvascular endothelial cell survival induced by cysteamine', *J Inherit Metab Dis*, 36: 1073-7.

Bishop, R. 2017. 'Ocular Complications of Infantile Nephropathic Cystinosis', *J Pediatr*, 183S: S19-S21.

Bois, E., J. Feingold, P. Frenay, and M. L. Briard. 1976. 'Infantile cystinosis in France: genetics, incidence, geographic distribution', *J Med Genet*, 13: 434-8.

Boustany, R. M. 2013. 'Lysosomal storage diseases--the horizon expands', *Nat Rev Neurol*, 9: 583-98.

Braun, M., A. Waheed, and K. von Figura. 1989. 'Lysosomal acid phosphatase is transported to lysosomes via the cell surface', *EMBO J*, 8: 3633-40.

Brodin-Sartorius, A., M. J. Tete, P. Niaudet, C. Antignac, G. Guest, C. Ottolenghi, M. Charbit, D. Moyse, C. Legendre, P. Lesavre, P. Cochat, and A. Servais.

2012. 'Cysteamine therapy delays the progression of nephropathic cystinosis in late adolescents and adults', *Kidney Int*, 81: 179-89.

Carpentier, S., F. N'Kuli, G. Grieco, P. Van Der Smissen, V. Janssens, H. Emonard, B. Bilanges, B. Vanhaesebroeck, H. P. Gaide Chevronnay, C. E. Pierreux, D. Tyteca, and P. J. Courtoy. 2013. 'Class III phosphoinositide 3-kinase/VPS34 and dynamin are critical for apical endocytic recycling', *Traffic*, 14: 933-48.

Charlton, J. R., M. W. Harer, C. Swan, and R. Nielsen. 2019. 'Immature megalin expression in the preterm neonatal kidney is associated with urinary loss of vitamin carrier proteins', *Pediatr Res*, 85: 405-11.

Cherqui, S. 2012. 'Cysteamine therapy: a treatment for cystinosis, not a cure', *Kidney Int*, 81: 127-9.

Cherqui, S., and P. J. Courtoy. 2017. 'The renal Fanconi syndrome in cystinosis: pathogenic insights and therapeutic perspectives', *Nat Rev Nephrol*, 13: 115-31.

Cherqui, S., C. Sevin, G. Hamard, V. Kalatzis, M. Sich, M. O. Pequignot, K. Gogat, M. Abitbol, M. Broyer, M. C. Gubler, and C. Antignac. 2002. 'Intralysosomal cystine accumulation in mice lacking cystinosin, the protein defective in cystinosis', *Mol Cell Biol*, 22: 7622-32.

Cheung, W. W., S. Cherqui, W. Ding, M. Esparza, P. Zhou, J. Shao, R. L. Lieber, and R. H. Mak. 2016. 'Muscle wasting and adipose tissue browning in infantile nephropathic cystinosis', *J Cachexia Sarcopenia Muscle*, 7: 152-64.

Christensen, E. I., and H. Birn. 2002. 'Megalin and cubilin: multifunctional endocytic receptors', *Nat Rev Mol Cell Biol*, 3: 256-66.

Christensen, E. I., and A. B. Maunsbach. 1979. 'Effects of dextran on lysosomal ultrastructure and protein digestion in renal proximal tubule', *Kidney Int*, 16: 301-11.

Christensen, E. I., P. J. Verroust, and R. Nielsen. 2009. 'Receptor-mediated endocytosis in renal proximal tubule', *Pflugers Arch*, 458: 1039-48.

Christensen, E. I., C. A. Wagner, and B. Kaissling. 2012. 'Uriniferous tubule: structural and functional organization', *Compr Physiol*, 2: 805-61.

Coppens, I., P. Baudhuin, F. R. Opperdoes, and P. J. Courtoy. 1993. 'Role of acidic compartments in Trypanosoma brucei, with special reference to low-density lipoprotein processing', *Mol Biochem Parasitol*, 58: 223-32.

Courtoy, P.J. 1991. 'Dissection of endosomes. In Intracellular trafficking of proteins (C Steer, J Hanover, eds), Cambridge University Press (1991) pp.103-56'.

Crawley, S. W., M. S. Mooseker, and M. J. Tyska. 2014. 'Shaping the intestinal brush border', *J Cell Biol*, 207: 441-51.

Custer, M., M. Lotscher, J. Biber, H. Murer, and B. Kaissling. 1994. 'Expression of Na-P(i) cotransport in rat kidney: localization by RT-PCR and immunohistochemistry', *Am J Physiol*, 266: F767-74.

Dikic, I., and Z. Elazar. 2018. 'Mechanism and medical implications of mammalian autophagy', *Nat Rev Mol Cell Biol*, 19: 349-64.

Dohil, R., M. Fidler, J. A. Gangoiti, F. Kaskel, J. A. Schneider, and B. A. Barshop. 2010. 'Twice-daily cysteamine bitartrate therapy for children with cystinosis', *J Pediatr*, 156: 71-75 e1-3.

Efeyan, A., W. C. Comb, and D. M. Sabatini. 2015. 'Nutrient-sensing mechanisms and pathways', *Nature*, 517: 302-10.

Elmonem, M. A., K. R. Veys, N. A. Soliman, M. van Dyck, L. P. van den Heuvel, and E. Levtchenko. 2016. 'Cystinosis: a review', *Orphanet J Rare Dis*, 11: 47.

Elpeleg, N., and S. H. Korman. 2001. 'Sustained oral lysine supplementation in ornithine delta-aminotransferase deficiency', *J Inherit Metab Dis*, 24: 423-4.

Emma, F., G. Nesterova, C. Langman, A. Labbe, S. Cherqui, P. Goodyer, M. C. Janssen, M. Greco, R. Topaloglu, E. Elenberg, R. Dohil, D. Trauner, C. Antignac, P. Cochat, F. Kaskel, A. Servais, E. Wuhl, P. Niaudet, W. Van't Hoff, W. Gahl, and E. Levtchenko. 2014. 'Nephropathic cystinosis: an international consensus document', *Nephrol Dial Transplant*, 29 Suppl 4: iv87-94.

Festa, B. P., Z. Chen, M. Berquez, H. Debaix, N. Tokonami, J. A. Prange, G. V. Hoek, C. Alessio, A. Raimondi, N. Nevo, R. H. Giles, O. Devuyst, and A. Luciani. 2018. 'Impaired autophagy bridges lysosomal storage disease and epithelial dysfunction in the kidney', *Nat Commun*, 9: 161.

Futerman, A. H., and G. van Meer. 2004. 'The cell biology of lysosomal storage disorders', *Nat Rev Mol Cell Biol*, 5: 554-65.

Gahl, W. A., J. G. Thoene, and J. A. Schneider. 2002. 'Cystinosis', *N Engl J Med*, 347: 111-21.

Gaide Chevronnay, H. P., V. Janssens, P. Van Der Smissen, X. H. Liao, Y. Abid, N. Nevo, C. Antignac, S. Refetoff, S. Cherqui, C. E. Pierreux, and P. J. Courtoy. 2015. 'A mouse model suggests two mechanisms for thyroid alterations in infantile cystinosis: decreased thyroglobulin synthesis due to endoplasmic reticulum stress/unfolded protein response and impaired lysosomal processing', *Endocrinology*, 156: 2349-64.

Gaide Chevronnay, H. P., V. Janssens, P. Van Der Smissen, F. N'Kuli, N. Nevo, Y. Guiot, E. Levtchenko, E. Marbaix, C. E. Pierreux, S. Cherqui, C. Antignac, and P. J. Courtoy. 2014. 'Time course of pathogenic and adaptation mechanisms in cystinotic mouse kidneys', *J Am Soc Nephrol*, 25: 1256-69.

Gaide Chevronnay, H. P., V. Janssens, P. Van Der Smissen, C. J. Rocca, X. H. Liao, S. Refetoff, C. E. Pierreux, S. Cherqui, and P. J. Courtoy. 2016. 'Hematopoietic Stem Cells Transplantation Can Normalize Thyroid Function in a Cystinosis Mouse Model', *Endocrinology*, 157: 1363-71.

Galarreta, C. I., M. S. Forbes, B. A. Thornhill, C. Antignac, M. C. Gubler, N. Nevo, M. P. Murphy, and R. L. Chevalier. 2015. 'The swan-neck lesion: proximal tubular adaptation to oxidative stress in nephropathic cystinosis', *Am J Physiol Renal Physiol*, 308: F1155-66.

Gerasimenko, J. V., A. V. Tepikin, O. H. Petersen, and O. V. Gerasimenko. 1998. 'Calcium uptake via endocytosis with rapid release from acidifying endosomes', *Curr Biol*, 8: 1335-8.

Ghislat, G., and E. Knecht. 2013. 'Ca(2)(+)-sensor proteins in the autophagic and endocytic traffic', *Curr Protein Pept Sci*, 14: 97-110.

Gilbert, D. N., S. J. Kohlhepp, P. W. Kohnen, W. C. Elliott, and W. M. Bennett. 1982. 'Failure of lysine to prevent experimental gentamicin nephrotoxicity', *J Infect Dis*, 145: 129.

Gisler, S. M., I. Stagljar, M. Traebert, D. Bacic, J. Biber, and H. Murer. 2001. 'Interaction of the type IIa Na/Pi cotransporter with PDZ proteins', *J Biol Chem*, 276: 9206-13.

Gleixner, E. M., G. Canaud, T. Hermle, M. C. Guida, O. Kretz, M. Helmstadter, T. B. Huber, S. Eimer, F. Terzi, and M. Simons. 2014. 'V-ATPase/mTOR signaling regulates megalin-mediated apical endocytosis', *Cell Rep*, 8: 10-9.

Gottschalk, S., A. Waheed, B. Schmidt, P. Laidler, and K. von Figura. 1989. 'Sequential processing of lysosomal acid phosphatase by a cytoplasmic thiol proteinase and a lysosomal aspartyl proteinase', *EMBO J*, 8: 3215-9.

Grieco, G., V. Janssens, H. P. Gaide Chevronnay, F. N'Kuli, P. Van Der Smissen, T. Wang, J. Shan, S. Vainio, B. Bilanges, F. Jouret, B. Vanhaesebroeck, C. E. Pierreux, and P. J. Courtoy. 2018. 'Vps34/PI3KC3 deletion in kidney proximal tubules impairs apical trafficking and blocks autophagic flux, causing a Fanconi-like syndrome and renal insufficiency', *Sci Rep*, 8: 14133.

Harrison, F., B. A. Yeagy, C. J. Rocca, D. B. Kohn, D. R. Salomon, and S. Cherqui. 2013. 'Hematopoietic stem cell gene therapy for the multisystemic lysosomal storage disorder cystinosis', *Mol Ther*, 21: 433-44.

Hediger, M. A., and D. B. Rhoads. 1994. 'Molecular physiology of sodium-glucose cotransporters', *Physiol Rev*, 74: 993-1026.

Hilfiker, H., O. Hattenhauer, M. Traebert, I. Forster, H. Murer, and J. Biber. 1998. 'Characterization of a murine type II sodium-phosphate cotransporter expressed in mammalian small intestine', *Proc Natl Acad Sci U S A*, 95: 14564-9.

Hill, C. H., G. M. Cook, S. J. Spratley, S. Fawke, S. C. Graham, and J. E. Deane. 2018. 'The mechanism of glycosphingolipid degradation revealed by a GALC-SapA complex structure', *Nat Commun*, 9: 151.

Honing, S., I. V. Sandoval, and K. von Figura. 1998. 'A di-leucine-based motif in the cytoplasmic tail of LIMP-II and tyrosinase mediates selective binding of AP-3', *EMBO J*, 17: 1304-14.

Hu, S., X. Li, R. Rezaei, C. J. Meininger, C. J. McNeal, and G. Wu. 2015. 'Safety of long-term dietary supplementation with L-arginine in pigs', *Amino Acids*, 47: 925-36.

Huynh, K. K., E. L. Eskelinen, C. C. Scott, A. Malevanets, P. Saftig, and S. Grinstein. 2007. 'LAMP proteins are required for fusion of lysosomes with phagosomes', *EMBO J*, 26: 313-24.

Iglesias, D. M., R. El-Kares, A. Taranta, F. Bellomo, F. Emma, M. Besouw, E. Levtchenko, J. Toelen, L. van den Heuvel, L. Chu, J. Zhao, Y. K. Young, N. Eliopoulos, and P. Goodyer. 2012. 'Stem cell microvesicles transfer cystinosin to human cystinotic cells and reduce cystine accumulation in vitro', *PLoS One*, 7: e42840.

Ishola, D. A., Jr., D. M. van der Giezen, B. Hahnel, R. Goldschmeding, W. Kriz, H. A. Koomans, and J. A. Joles. 2006. 'In mice, proteinuria and renal inflammatory responses to albumin overload are strain-dependent', *Nephrol Dial Transplant*, 21: 591-7.

Ivanova, E. A., M. G. De Leo, L. Van Den Heuvel, A. Pastore, H. Dijkman, M. A. De Matteis, and E. N. Levtchenko. 2015. 'Endo-lysosomal dysfunction in human proximal tubular epithelial cells deficient for lysosomal cystine transporter cystinosin', *PLoS One*, 10: e0120998.

Jentsch, T. J., and M. Pusch. 2018. 'CLC Chloride Channels and Transporters: Structure, Function, Physiology, and Disease', *Physiol Rev*, 98: 1493-590.

Jezegou, A., E. Llinares, C. Anne, S. Kieffer-Jaquinod, S. O'Regan, J. Aupetit, A. Chabli, C. Sagne, C. Debacker, B. Chadefaux-Vekemans, A. Journet, B. Andre, and B. Gasnier. 2012. 'Heptahelical protein PQLC2 is a lysosomal cationic amino acid exporter underlying the action of cysteamine in cystinosis therapy', *Proc Natl Acad Sci U S A*, 109: E3434-43.

Jobst-Schwan, T., K. X. Knaup, R. Nielsen, T. Hackenbeck, M. Buettner-Herold, P. Lechler, S. Kroening, M. Goppelt-Struebe, U. Schloetzer-Schrehardt, B. G. Furnrohr, R. E. Voll, K. Amann, K. U. Eckardt, E. I. Christensen, and M. S. Wiesener. 2013. 'Renal uptake of the antiapoptotic protein survivin is mediated by megalin at the apical membrane of the proximal tubule', *Am J Physiol Renal Physiol*, 305: F734-44.

Johnson, J. L., G. Napolitano, J. Monfregola, C. J. Rocca, S. Cherqui, and S. D. Catz. 2013. 'Upregulation of the Rab27a-dependent trafficking and secretory mechanisms improves lysosomal transport, alleviates endoplasmic reticulum stress, and reduces lysosome overload in cystinosis', *Mol Cell Biol*, 33: 2950-62.

Kalatzis, V., N. Serratrice, C. Hippert, O. Payet, C. Arndt, C. Cazevieille, T. Maurice, C. Hamel, F. Malecaze, C. Antignac, A. Muller, and E. J. Kremer. 2007. 'The ocular anomalies in a cystinosis animal model mimic disease pathogenesis', *Pediatr Res*, 62: 156-62.

Karim, Z., B. Gerard, N. Bakouh, R. Alili, C. Leroy, L. Beck, C. Silve, G. Planelles, P. Urena-Torres, B. Grandchamp, G. Friedlander, and D. Prie. 2008. 'NHERF1 mutations and responsiveness of renal parathyroid hormone', *N Engl J Med*, 359: 1128-35.

Kaushik, S., and A. M. Cuervo. 2012. 'Chaperone-mediated autophagy: a unique way to enter the lysosome world', *Trends Cell Biol*, 22: 407-17.

———. 2018. 'The coming of age of chaperone-mediated autophagy', *Nat Rev Mol Cell Biol*, 19: 365-81.

Kir'ianov, N. A., E. L. Bazhenov, and E. V. Stetsenko. 1992. '[Cystinosis in an adult]', *Arkh Patol*, 54: 34-6.

Laplante, M., and D. M. Sabatini. 2012. 'mTOR signaling in growth control and disease', *Cell*, 149: 274-93.

Larsen, C. P., P. D. Walker, and J. G. Thoene. 2010. 'The incidence of atubular glomeruli in nephropathic cystinosis renal biopsies', *Mol Genet Metab*, 101: 417-20.

Lee, K. Y., J. R. Kim, and H. C. Choi. 2016. 'Genistein-induced LKB1-AMPK activation inhibits senescence of VSMC through autophagy induction', *Vascul Pharmacol*, 81: 75-82.

Leheste, J. R., B. Rolinski, H. Vorum, J. Hilpert, A. Nykjaer, C. Jacobsen, P. Aucouturier, J. O. Moskaug, A. Otto, E. I. Christensen, and T. E. Willnow. 1999. 'Megalin knockout mice as an animal model of low molecular weight proteinuria', *Am J Pathol*, 155: 1361-70.

Lima, W. R., K. S. Parreira, O. Devuyst, A. Caplanusi, F. N'Kuli, B. Marien, P. Van Der Smissen, P. M. Alves, P. Verroust, E. I. Christensen, F. Terzi, K. Matter, M. S. Balda, C. E. Pierreux, and P. J. Courtoy. 2010. 'ZONAB promotes proliferation and represses differentiation of proximal tubule epithelial cells', *J Am Soc Nephrol*, 21: 478-88.

Lloyd, J. B. 1986. 'Disulphide reduction in lysosomes. The role of cysteine', *Biochem J*, 237: 271-2.

Lo, J. C., G. M. Chertow, H. Rennke, and J. L. Seifter. 1996. 'Fanconi's syndrome and tubulointerstitial nephritis in association with L-lysine ingestion', *Am J Kidney Dis*, 28: 614-7.

Lucky, A. W., P. M. Howley, K. Megyesi, S. P. Spielberg, and J. D. Schulman. 1977. 'Endocrine studies in cystinosis: compensated primary hypothyroidism', *J Pediatr*, 91: 204-10.

Luzio, J. P., P. R. Pryor, and N. A. Bright. 2007. 'Lysosomes: fusion and function', *Nat Rev Mol Cell Biol*, 8: 622-32.

Mahoney, C. P., and G. E. Striker. 2000. 'Early development of the renal lesions in infantile cystinosis', *Pediatr Nephrol*, 15: 50-6.

Makrides, V., S. M. Camargo, and F. Verrey. 2014. 'Transport of amino acids in the kidney', *Compr Physiol*, 4: 367-403.

Manz, F., and N. Gretz. 1985. 'Cystinosis in the Federal Republic of Germany. Coordination and analysis of the data', *J Inherit Metab Dis*, 8: 2-4.

Marcano, D. C., C. S. Shin, B. Lee, L. C. Isenhart, X. Liu, F. Li, J. V. Jester, S. C. Pflugfelder, J. Simpson, and G. Acharya. 2016. 'Synergistic Cysteamine Delivery Nanowafer as an Efficacious Treatment Modality for Corneal Cystinosis', *Mol Pharm*, 13: 3468-77.

Marzolo, M. P., and P. Farfan. 2011. 'New insights into the roles of megalin/LRP2 and the regulation of its functional expression', *Biol Res*, 44: 89-105.

Marzolo, M. P., M. I. Yuseff, C. Retamal, M. Donoso, F. Ezquer, P. Farfan, Y. Li, and G. Bu. 2003. 'Differential distribution of low-density lipoprotein-receptor-related protein (LRP) and megalin in polarized epithelial cells is determined by their cytoplasmic domains', *Traffic*, 4: 273-88.

McNeal, C. J., C. J. Meininger, D. Reddy, C. D. Wilborn, and G. Wu. 2016. 'Safety and Effectiveness of Arginine in Adults', *J Nutr*, 146: 2587S-93S.

Medina, D. L., and A. Ballabio. 2015. 'Lysosomal calcium regulates autophagy', *Autophagy*, 11: 970-1.

Medina, D. L., S. Di Paola, I. Peluso, A. Armani, D. De Stefani, R. Venditti, S. Montefusco, A. Scotto-Rosato, C. Prezioso, A. Forrester, C. Settembre, W. Wang, Q. Gao, H. Xu, M. Sandri, R. Rizzuto, M. A. De Matteis, and A. Ballabio. 2015. 'Lysosomal calcium signalling regulates autophagy through calcineurin and TFEB', *Nat Cell Biol*, 17: 288-99.

Medina, D. L., A. Fraldi, V. Bouche, F. Annunziata, G. Mansueto, C. Spampanato, C. Puri, A. Pignata, J. A. Martina, M. Sardiello, M. Palmieri, R. Polishchuk, R. Puertollano, and A. Ballabio. 2011. 'Transcriptional activation of lysosomal exocytosis promotes cellular clearance', *Dev Cell*, 21: 421-30.

Mellman, I., R. Fuchs, and A. Helenius. 1986. 'Acidification of the endocytic and exocytic pathways', *Annu Rev Biochem*, 55: 663-700.

Moestrup, S. K., S. Cui, H. Vorum, C. Bregengard, S. E. Bjorn, K. Norris, J. Gliemann, and E. I. Christensen. 1995. 'Evidence that epithelial glycoprotein 330/megalin mediates uptake of polybasic drugs', *J Clin Invest*, 96: 1404-13.

Mogensen, C. E., and Solling. 1977. 'Studies on renal tubular protein reabsorption: partial and near complete inhibition by certain amino acids', *Scand J Clin Lab Invest*, 37: 477-86.

Mori, K., H. T. Lee, D. Rapoport, I. R. Drexler, K. Foster, J. Yang, K. M. Schmidt-Ott, X. Chen, J. Y. Li, S. Weiss, J. Mishra, F. H. Cheema, G. Markowitz, T. Suganami, K. Sawai, M. Mukoyama, C. Kunis, V. D'Agati, P. Devarajan, and

J. Barasch. 2005. 'Endocytic delivery of lipocalin-siderophore-iron complex rescues the kidney from ischemia-reperfusion injury', *J Clin Invest*, 115: 610-21.

Morris, S. M., Jr. 2016. 'Arginine Metabolism Revisited', *J Nutr*, 146: 2579S-86S.

Murer, H., N. Hernando, I. Forster, and J. Biber. 2003. 'Regulation of Na/Pi transporter in the proximal tubule', *Annu Rev Physiol*, 65: 531-42.

Nagai, J., and M. Takano. 2004. 'Molecular aspects of renal handling of aminoglycosides and strategies for preventing the nephrotoxicity', *Drug Metab Pharmacokinet*, 19: 159-70.

Naphade, S., J. Sharma, H. P. Gaide Chevronnay, M. A. Shook, B. A. Yeagy, C. J. Rocca, S. N. Ur, A. J. Lau, P. J. Courtoy, and S. Cherqui. 2015. 'Brief reports: Lysosomal cross-correction by hematopoietic stem cell-derived macrophages via tunneling nanotubes', *Stem Cells*, 33: 301-9.

Nesterova, G., and W. A. Gahl. 2013. 'Cystinosis: the evolution of a treatable disease', *Pediatr Nephrol*, 28: 51-9.

Nevo, N., M. Chol, A. Bailleux, V. Kalatzis, L. Morisset, O. Devuyst, M. C. Gubler, and C. Antignac. 2010. 'Renal phenotype of the cystinosis mouse model is dependent upon genetic background', *Nephrol Dial Transplant*, 25: 1059-66.

Nielsen, R., E. I. Christensen, and H. Birn. 2016. 'Megalin and cubilin in proximal tubule protein reabsorption: from experimental models to human disease', *Kidney Int*, 89: 58-67.

Ottosen, P. D., K. M. Madsen, F. Bode, K. Baumann, and A. B. Maunsbach. 1985. 'Inhibition of protein reabsorption in the renal proximal tubule by basic amino acids', *Ren Physiol*, 8: 90-9.

Peltola, K., O. J. Heinonen, K. Nanto-Salonen, K. Pulkki, and O. Simell. 2000. 'Oral lysine feeding in gyrate atrophy with hyperornithinaemia--a pilot study', *J Inherit Metab Dis*, 23: 305-7.

Peters, C., M. Braun, B. Weber, M. Wendland, B. Schmidt, R. Pohlmann, A. Waheed, and K. von Figura. 1990. 'Targeting of a lysosomal membrane protein: a tyrosine-containing endocytosis signal in the cytoplasmic tail of lysosomal acid phosphatase is necessary and sufficient for targeting to lysosomes', *EMBO J*, 9: 3497-506.

Piwon, N., W. Gunther, M. Schwake, M. R. Bosl, and T. J. Jentsch. 2000. 'ClC-5 Cl- -channel disruption impairs endocytosis in a mouse model for Dent's disease', *Nature*, 408: 369-73.

Prencipe, G., I. Caiello, S. Cherqui, T. Whisenant, S. Petrini, F. Emma, and F. De Benedetti. 2014. 'Inflammasome activation by cystine crystals: implications for the pathogenesis of cystinosis', *J Am Soc Nephrol*, 25: 1163-9.

Prie, D., V. Huart, N. Bakouh, G. Planelles, O. Dellis, B. Gerard, P. Hulin, F. Benque-Blanchet, C. Silve, B. Grandchamp, and G. Friedlander. 2002. 'Nephrolithiasis and osteoporosis associated with hypophosphatemia caused by mutations in the type 2a sodium-phosphate cotransporter', *N Engl J Med*, 347: 983-91.

Racusen, L. C., A. Whelton, and K. Solez. 1985. 'Effects of lysine and other amino acids on kidney structure and function in the rat', *Am J Pathol*, 120: 436-42.

Raggi, C., A. Luciani, N. Nevo, C. Antignac, S. Terryn, and O. Devuyst. 2014. 'Dedifferentiation and aberrations of the endolysosomal compartment characterize the early stage of nephropathic cystinosis', *Hum Mol Genet*, 23: 2266-78.

Rega, L. R., E. Polishchuk, S. Montefusco, G. Napolitano, G. Tozzi, J. Zhang, F. Bellomo, A. Taranta, A. Pastore, R. Polishchuk, F. Piemonte, D. L. Medina, S. D. Catz, A. Ballabio, and F. Emma. 2016. 'Activation of the transcription factor EB rescues lysosomal abnormalities in cystinotic kidney cells', *Kidney Int*, 89: 862-73.

Ruivo, R., G. C. Bellenchi, X. Chen, G. Zifarelli, C. Sagne, C. Debacker, M. Pusch, S. Supplisson, and B. Gasnier. 2012. 'Mechanism of proton/substrate coupling in the heptahelical lysosomal transporter cystinosin', *Proc Natl Acad Sci U S A*, 109: E210-7.

Russell, R. C., H. X. Yuan, and K. L. Guan. 2014. 'Autophagy regulation by nutrient signaling', *Cell Res*, 24: 42-57.

Sbano, L., M. Bonora, S. Marchi, F. Baldassari, D. L. Medina, A. Ballabio, C. Giorgi, and P. Pinton. 2017. 'TFEB-mediated increase in peripheral lysosomes regulates store-operated calcium entry', *Sci Rep*, 7: 40797.

Scheepers, A., H. G. Joost, and A. Schurmann. 2004. 'The glucose transporter families SGLT and GLUT: molecular basis of normal and aberrant function', *JPEN J Parenter Enteral Nutr*, 28: 364-71.

Schiller, A., and R. Taugner. 1980. 'The renal handling of low molecular weight polyvinylpyrrolidone and inulin in rats. In: Maunsbach AB, Steen Olsen T, Christensen EI, eds. Functional Ultrastructure of the Kidney. London: Academic Press; 1980:315-26.'.

Schuh, C. D., M. Polesel, E. Platonova, D. Haenni, A. Gassama, N. Tokonami, S. Ghazi, M. Bugarski, O. Devuyst, U. Ziegler, and A. M. Hall. 2018. 'Combined Structural and Functional Imaging of the Kidney Reveals Major Axial Differences in Proximal Tubule Endocytosis', *J Am Soc Nephrol*, 29: 2696-712.

Schulman, J. D., K. H. Bradley, and J. E. Seegmiller. 1969. 'Cystine: compartmentalization within lysosomes in cystinotic leukocytes', *Science*, 166: 1152-4.

Settembre, C., A. Fraldi, D. L. Medina, and A. Ballabio. 2013. 'Signals from the lysosome: a control centre for cellular clearance and energy metabolism', *Nat Rev Mol Cell Biol*, 14: 283-96.

Settembre, C., R. Zoncu, D. L. Medina, F. Vetrini, S. Erdin, S. Erdin, T. Huynh, M. Ferron, G. Karsenty, M. C. Vellard, V. Facchinetti, D. M. Sabatini, and A. Ballabio. 2012. 'A lysosome-to-nucleus signalling mechanism senses and regulates the lysosome via mTOR and TFEB', *EMBO J*, 31: 1095-108.

Simpson, J. L., C. J. Nien, K. J. Flynn, and J. V. Jester. 2011. 'Evaluation of topical cysteamine therapy in the CTNS(-/-) knockout mouse using in vivo confocal microscopy', *Mol Vis*, 17: 2649-54.

Straus, W. 1962. 'Colorimetric investigation of the uptake of an intravenously injected protein (horseradish peroxidase) by rat kidney and effects of competition by egg white', *J Cell Biol*, 12: 231-46.

———. 1964a. 'Cytochemical Observations on the Relationship between Lysosomes and Phagosomes in Kidney and Liver by Combined Staining for Acid Phosphatase and Intravenously Injected Horseradish Peroxidase', *J Cell Biol*, 20: 497-507.

———. 1964b. 'Occurrence of Phagosomes and Phago-Lysosomes in Different Segments of the Nephron in Relation to the Reabsorption, Transport, Digestion, and Extrusion of Intravenously Injected Horseradish Peroxidase', *J Cell Biol*, 21: 295-308.

Takahashi, S., K. Kubo, S. Waguri, A. Yabashi, H. W. Shin, Y. Katoh, and K. Nakayama. 2012. 'Rab11 regulates exocytosis of recycling vesicles at the plasma membrane', *J Cell Sci*, 125: 4049-57.

Tang, S., S. Danda, M. Zoleikhaeian, M. Simon, and T. Huang. 2009. 'An Indian boy with nephropathic cystinosis: a case report and molecular analysis of CTNS mutation', *Genet Test Mol Biomarkers*, 13: 435-8.

Tanner, S. M., M. Aminoff, F. A. Wright, S. Liyanarachchi, M. Kuronen, A. Saarinen, O. Massika, H. Mandel, H. Broch, and A. de la Chapelle. 2003. 'Amnionless, essential for mouse gastrulation, is mutated in recessive hereditary megaloblastic anemia', *Nat Genet*, 33: 426-9.

Tenten, V., S. Menzel, U. Kunter, E. M. Sicking, C. R. van Roeyen, S. K. Sanden, M. Kaldenbach, P. Boor, A. Fuss, S. Uhlig, R. Lanzmich, B. Willemsen, H. Dijkman, M. Grepl, K. Wild, W. Kriz, B. Smeets, J. Floege, and M. J. Moeller. 2013. 'Albumin is recycled from the primary urine by tubular transcytosis', *J Am Soc Nephrol*, 24: 1966-80.

Terryn, S., K. Tanaka, J. P. Lengele, E. Olinger, D. Dubois-Laforgue, S. Garbay, R. Kozyraki, P. Van Der Smissen, E. I. Christensen, P. J. Courtoy, C. Bellanne-Chantelot, J. Timsit, M. Pontoglio, and O. Devuyst. 2016. 'Tubular proteinuria in patients with HNF1alpha mutations: HNF1alpha drives endocytosis in the proximal tubule', *Kidney Int*, 89: 1075-89.

Thelle, K., E. I. Christensen, H. Vorum, H. Orskov, and H. Birn. 2006. 'Characterization of proteinuria and tubular protein uptake in a new model of oral L-lysine administration in rats', *Kidney Int*, 69: 1333-40.

Thoene, J. G., S. Forster, and J. B. Lloyd. 1985. 'The role of pinocytosis in the cellular uptake of an amino acid', *Biochem Biophys Res Commun*, 127: 733-8.

Thoene, J. G., and R. Lemons. 1980. 'Modulation of the intracellular cystine content of cystinotic fibroblasts by extracellular albumin', *Pediatr Res*, 14: 785-7.

Thoene, J. G., and R. M. Lemons. 1982. 'Cystine accumulation in cystinotic fibroblasts from free and protein-linked cystine but not cysteine', *Biochem J*, 208: 823-30.

Thoene, J. G., R. G. Oshima, D. G. Ritchie, and J. A. Schneider. 1977. 'Cystinotic fibroblasts accumulate cystine from intracellular protein degradation', *Proc Natl Acad Sci U S A*, 74: 4505-7.

Thoene, J., T. Goss, M. Witcher, J. Mullet, F. N'Kuli, P. Van Der Smissen, P. Courtoy, and S. H. Hahn. 2013. 'In vitro correction of disorders of lysosomal transport by microvesicles derived from baculovirus-infected Spodoptera cells', *Mol Genet Metab*, 109: 77-85.

Tyteca, D., A. Schanck, Y. F. Dufrene, M. Deleu, P. J. Courtoy, P. M. Tulkens, and M. P. Mingeot-Leclercq. 2003. 'The macrolide antibiotic azithromycin interacts with lipids and affects membrane organization and fluidity: studies on Langmuir-Blodgett monolayers, liposomes and J774 macrophages', *J Membr Biol*, 192: 203-15.

Tyteca, D., P. Van Der Smissen, M. Mettlen, F. Van Bambeke, P. M. Tulkens, M. P. Mingeot-Leclercq, and P. J. Courtoy. 2002. 'Azithromycin, a lysosomotropic antibiotic, has distinct effects on fluid-phase and receptor-mediated endocytosis, but does not impair phagocytosis in J774 macrophages', *Exp Cell Res*, 281: 86-100.

Vallon, V., K. A. Platt, R. Cunard, J. Schroth, J. Whaley, S. C. Thomson, H. Koepsell, and T. Rieg. 2011. 'SGLT2 mediates glucose reabsorption in the early proximal tubule', *J Am Soc Nephrol*, 22: 104-12.

Verroust, P. J., and E. I. Christensen. 2002. 'Megalin and cubilin--the story of two multipurpose receptors unfolds', *Nephrol Dial Transplant*, 17: 1867-71.

Veys, K. R., M. A. Elmonem, F. O. Arcolino, L. van den Heuvel, and E. Levtchenko. 2017. 'Nephropathic cystinosis: an update', *Curr Opin Pediatr*, 29: 168-78.

Wagner, M. C., S. B. Campos-Bilderback, M. Chowdhury, B. Flores, X. Lai, J. Myslinski, S. Pandit, R. M. Sandoval, S. E. Wean, Y. Wei, L. M. Satlin, R. C. Wiggins, F. A. Witzmann, and B. A. Molitoris. 2016. 'Proximal Tubules Have the Capacity to Regulate Uptake of Albumin', *J Am Soc Nephrol*, 27: 482-94.

Weyer, K., P. K. Andersen, K. Schmidt, G. Mollet, C. Antignac, H. Birn, R. Nielsen, and E. I. Christensen. 2018. 'Abolishment of proximal tubule albumin endocytosis does not affect plasma albumin during nephrotic syndrome in mice', *Kidney Int*, 93: 335-42.

Willnow, T. E., and A. Christ. 2017. 'Endocytic receptor LRP2/megalin-of holoprosencephaly and renal Fanconi syndrome', *Pflugers Arch*, 469: 907-16.

Wilmer, M. J., F. Emma, and E. N. Levtchenko. 2010. 'The pathogenesis of cystinosis: mechanisms beyond cystine accumulation', *Am J Physiol Renal Physiol*, 299: F905-16.

Wolfson, R. L., and D. M. Sabatini. 2017. 'The Dawn of the Age of Amino Acid Sensors for the mTORC1 Pathway', *Cell Metab*, 26: 301-09.

Yang, J., S. Carra, W. G. Zhu, and H. H. Kampinga. 2013. 'The regulation of the autophagic network and its implications for human disease', *Int J Biol Sci*, 9: 1121-33.

Yang, Y. J., Y. Hu, R. Zhao, X. He, L. Zhao, M. Tu, L. Zhou, J. Guo, L. Wu, T. Zhao, and Y. M. Zhu. 2015. 'First report of CTNS mutations in a Chinese family with infantile cystinosis', *ScientificWorldJournal*, 2015: 309410.

Yang, Y., Z. Wu, S. Jia, S. Dahanayaka, S. Feng, C. J. Meininger, C. J. McNeal, and G. Wu. 2015. 'Safety of long-term dietary supplementation with L-arginine in rats', *Amino Acids*, 47: 1909-20.

Yoshioka, H., Y. Yoshiko, T. Minamizaki, S. Suzuki, Y. Koma, A. Nobukiyo, Y. Sotomaru, A. Suzuki, M. Itoh, and N. Maeda. 2011. 'Incisor enamel formation is impaired in transgenic rats overexpressing the type III NaPi transporter Slc20a1', *Calcif Tissue Int*, 89: 192-202.

Yuseff, M. I., P. Farfan, G. Bu, and M. P. Marzolo. 2007. 'A cytoplasmic PPPSP motif determines megalin's phosphorylation and regulates receptor's recycling and surface expression', *Traffic*, 8: 1215-30.

Zhang, J., J. He, J. L. Johnson, F. Rahman, E. Gavathiotis, A. M. Cuervo, and S. D. Catz. 2019. 'Chaperone-Mediated Autophagy Upregulation Rescues Megalin Expression and Localization in Cystinotic Proximal Tubule Cells', *Front Endocrinol (Lausanne)*, 10: 21.

Zhang, J., J. L. Johnson, J. He, G. Napolitano, M. Ramadass, C. Rocca, W. B. Kiosses, C. Bucci, Q. Xin, E. Gavathiotis, A. M. Cuervo, S. Cherqui, and S. D. Catz. 2017. 'Cystinosin, the small GTPase Rab11, and the Rab7 effector RILP regulate intracellular trafficking of the chaperone-mediated autophagy receptor LAMP2A', *J Biol Chem*, 292: 10328-46.

Zhuo, J. L., and X. C. Li. 2013. 'Proximal nephron', *Compr Physiol*, 3: 1079-123.